Inaugural-Dissertation

zur Erlangung der Doktorwürde

der Naturwissenschaftlich-Mathematischen

Gesamtfakultät

der Ruprecht-Karls-Universität Heidelberg

vorgelegt von

Diplom-Geologin Friederike Ursula Bauer

aus Osterburken

Tag der mündlichen Prüfung: 20. Dezember 2007

The Sabiñánigo Sandstone Succession,

Jaca Basin,

Southern Pyrenees, NE-Spain

– A Depositional Model –

Gutachter: Hochschuldozent Dr. Rainer Zühlke

Privatdozent Dr. Ulrich A. Glasmacher

Earth and Ocean seem

To sleep in one another’s arms and dream

Of waves, flowers, clouds, woods, rocks and all that we

Read in their smiles, and call reality. (Shelley, *Epipsychidion*)

Abstract

The Eocene Sabiñánigo Sandstone Succession (SSt-Succession) forms part of the sedimentary infill of the Jaca Basin, which evolved as a piggyback basin in front of the emerging Pyrenean orogeny. Foreland basins in general, and their siliciclastic deposits in particular, are not only of scientific but also of common economic interest, due to their outstanding relevance for hydrocarbon exploration. Furthermore, the SSt-Succession is of great scientific interest, as it takes over a challenging position within the Jaca Basin. It forms the transitional part from deep marine to continental deposition, promising to reveal some insights on the depositional processes affecting the Jaca Basin. Thus, the scientific research was driven by the general interest in the genesis of the SSt-Succession, and how it fits into the Pyrenean realm, e.g. how basin formation was triggered by the Pyrenean orogeny.

Therefore, the SSt-Succession was scrutinized from different points of view, integrating distinct approaches, and analytical methods, with the working process described in this case study.

The SSt-Succession is exposed within two distinct ridges, showing excellent outcrop conditions, with lateral and vertical stratigraphic surfaces, that can be traced physically and optically over large distances. But they are lacking any marker horizon between both ridges that enables to easily link-up both exposure sites situated at the northern and the southern limb of the Basa Anticline. Therefore, the sediments of the SSt-Succession have been processed in detail to get a data set that enables to construct a time-calibrated framework of each exposure site. This in turn allows connecting both exposure sites and developing a depositional model of the entire SSt-Succession.

Different techniques were applied within this study to characterize the sedimentary succession of the Sabiñánigo Sandstones. It considers gamma ray logs together with standard lithological profiles. In addition, to constrain the previous sedimentary overburden, covering the SSt-Succession, low-temperature thermochronology has been applied. Spectral gamma ray analyses were used to refine standard facies analysis and to support sequence stratigraphic correlation within the SSt-Succession. Detailed facies analyses and gamma ray spectrometry studies were combined, revealing a pattern of returning facies types, large-scale facies associations and related vertical stacking patterns. On the basis of the generated data set a scheme of facies types and corresponding facies associations was established, comprising various lithologies, ranging from argillaceous siltstones rich in *Nummulites* up to coarse-grained sandstones

and conglomerates. This allowed to deduce the depositional setting of the SSt-Succession, reaching from transitional offshore to delta plain environments, and enabled to characterize the sedimentary evolution of the Sabiñánigo Delta system, and thus, to elucidate driving mechanisms controlling the depositional processes.

This study greatly benefits from a wide data set that allows interpreting the deposits of the SSt-Succession from different points of view and to integrate the applied methods into a time calibrated model. It, therefore, was possible to identify two progradational sequences as well as to examine the depositional history of the SSt-Succession and to reveal corresponding driving mechanisms. The SSt-Succession reflects a process response system that connects the evolution of the Pyrenean Orogeny with sedimentary deposition in the southern Foreland basin (Jaca Basin). The development as a piggyback basin is stored in the sedimentary archive. The first stage of evolution clearly identifies a partly developed delta, whereas the sedimentary sequence of the second stage indicates a full-developed delta. In the early stage, the moving piggyback basin was filled from the emerging Boltaña Anticline in the east, and during the second stage from the newly uplifted Axial Zone in the north.

Zusammenfassung

Die Eozäne Sabiñánigo Sandstein Abfolge (SSt-Abfolge) stellt einen Teil der sedimentären Beckenfüllung des Jaca Beckens dar. Im Zuge der nach Süden fortschreitenden Heraushebung der Pyrenäen entwickelte sich das Jaca Becken zu einem "Huckepack-Becken" im südlichen Vorland. Vorlandbecken im Allgemeinen und deren Sedimentfüllung im Besonderen, sind auf Grund ihrer herausragenden Bedeutung als Lagerstätten für Kohlenwasserstoffe nicht nur von wissenschaftlichem, sondern ebenfalls von allgemeinem wirtschaftlichem Interesse. Die guten Aufschlussverhältnisse ermöglichen eine detaillierte Beschreibung der Entwicklung von tiefmarinen zu kontinentalen Ablagerungsbedingungen. Darüber hinaus bildet die SSt-Abfolge ein wichtiges, hochauflösendes Archiv innerhalb des Jaca Beckens, das für die geowissenschaftliche Forschung Informationen über die Geschichte der pyrenäischen Gebirgsbildung gespeichert hat.

Daher wurde die SSt-Abfolge mittels verschiedener geowissenschaftlicher analytischer Methoden untersucht und die Daten zu einem Ablagerungsmodell zusammengefügt. Dieses Ablagerungsmodell wurde dann im Spannungsfeld der pyrenäischen Gebirgsbildung interpretiert.

Die SSt-Abfolge ist entlang von zwei räumlich getrennten morphologischen Rücken, die den Nord- und Südschenkel der Basa Antiklinale repräsentieren, hervorragend aufgeschlossen. Innerhalb der Nord- und Südschenkel lassen sich die Einheiten der SSt-Abfolge sowohl rein optisch als auch durch Ablaufen einzelner Horizonte über weite Strecken verfolgen. Jedoch ist die Verknüpfung der Einheiten des Nordschenkels mit denen des Südschenkels nicht möglich, da eindeutige Markerhorizonte fehlen. Die Abfolgen, die entlang des nördlichen Schenkels der Basa Antiklinale aufgeschlossen sind, können daher nicht ohne weiteres mit jenen des südlichen Schenkels korreliert werden.

Deshalb wurden die Sedimente der SSt-Abfolge detailliert bearbeitet um einen umfassenden Datensatz zu erhalten auf dessen Basis ein zeitlich einhängbarer Rahmen für beide Aufschlussbereiche erstellt werden konnte. Diese wiederum ermöglichten eine Verknüpfung beider Bereiche und schafften damit den Grundstock für das Erstellen eines großräumigen Ablagerungsmodells der SSt-Abfolge.

Im Zuge dieser Arbeit fanden unterschiedliche Methoden Anwendung. Gammaspektrometrie wurde kombiniert mit der Aufnahme lithostratigraphischer Profile. Die Methode der Niedrig-Temperatur Thermochronologie diente zur Abschätzung der heute bereits erodierten Sedimentgesteinsmächtigkeiten. Die Daten der

Gammaspektrometrie unterstützten die Faziesanalyse und die sequenzstratigraphische Korrelation innerhalb der SSt-Abfolge sowie zwischen dem Nord- und Südschenkel der Basa Antiklinale. Die Ergebnisse der detaillierten Faziesanalyse und Gammaspektrometrie ergaben ein wiederkehrendes Muster aus verschiedenen Faziestypen, die Lithologien von Mergelsteinen bis hin zu Konglomeraten umfassen. Faziesmuster, sowie laterale und vertikale Faziesverzahnungen spiegeln verschiedene Ablagerungsbereiche eines Deltas wider, die von Prodelta bis zur Deltaebene reichen. Diese Erkenntnisse ermöglichten die Entwicklung des Ablagerungssystems zu charakterisieren und steuernde Faktoren zu erfassen.

Diese Studie profitiert von der Anwendung und Integration verschiedener Methoden, die es erlauben die Ablagerungen der SSt-Abfolge von verschiedenen Gesichtspunkten zu studieren und ein zeitlich kalibriertes Modell zu erstellen. Auf dieser Basis konnten zwei Delta-Ablagerungssequenzen identifiziert, die Ablagerungsgeschichte rekonstruiert und steuernde Faktoren erkannt werden. Die Entwicklung des Jaca Beckens repräsentiert ein typisches „Process Response System“, in dem die fortschreitende Orogenese das Jaca Becken zu einem „Huckepack Becken“ (Piggyback Basin) umformt. Dies führt zu einem sukzessiven Transport des Beckens bei gleichzeitiger Subsidenz nach Süden. Diese dynamische Entwicklung ist in dem Sedimentarchive gespeichert. Das Sedimentarchive spiegelt im ersten Stadium ein teilweise und im zweiten Stadium ein voll entwickeltes Delta wieder. Während die Boltaña Antiklinale im ersten Stadium das Liefergebiet bildet wird im zweiten Stadium die Zentrale Axial Zone der Pyrenäen das dominante Liefergebiet.

Acknowledgement

Thanks to all of my friends and colleagues who supported me during the last years.

Ich möchte all meinen Freunden und Kollegen danken für ihre Unterstützung bei dieser Arbeit und für den Rückhalt an den manchmal doch recht langen Tagen am Institut.

Mein ganz besonderer Dank gilt meinen Betreuern Hochschuldozent Dr. Rainer Zühlke, der die Arbeit überhaupt erst ermöglicht hat und ebenfalls Privatdozent Dr. Ulrich A. Glasmacher, dessen unermüdliches Engagement mich schließlich dahinbrachte wo ich nun bin – Danke!

Danken möchte ich auch der Landesgraduiertenförderung für zweieinhalb Jahre der Unterstützung, sowie dem DAAD, dem IPP und dem IAS, welche die Auslandsaufenthalte mitgetragen haben.

Dem Max-Planck Institut für Kernphysik, der Heidelberger Akademie der Wissenschaften danke ich für die Bereitstellung der Laboreinrichtungen für analytische Zwecke. Und hier auch ein großes Dankeschön an die Archäometriegruppe des MPI, allen voran Susanne Lindauer für ihren Einsatz an der “Gamma Ray Front” und der nicht klein zu bekommenden Mailbox, die all die Korrekturfahnen entgegennahm ;-)

Selbstredend gebührt dem gesamten Geologisch-Paläontologischen Institut mit all seinen Mitabeitern, vom Keller bis zum Dach, mein großer Dank. Ohne deren Unterstützung wäre manches so sicher gar nicht möglich gewesen.

Nicht zu vergessen: Danke auch an die “ehemalige 1. Stock Gruppe“ für die gute Zeit und natürlich der Arbeitsgruppe Thermochronologie und Archäometrie, allen voran René Grobe für seine Unterstützung beim Endspurt. Merci Beaucoup!

Nach dem ich hier nun sicher die Eine oder den Anderen just in diesem Moment nicht expressis verbis erwähnt habe, das meiner Dankbarkeit aber keinen Abbruch tut, entschuldige ich mich jetzt schon dafür – und danke jedesmal von neuem wenn ich an so manch stressige Stunde zurückdenke, in der gerade diese Hände, dieser Kopf oder diese Geste ein Segen waren.

Ein allumfassendes Dankeschön!

Meiner Familie gebührt das letzt Wort: Ohne meine Mutter und meinen Vater wäre nichts von alle dem möglich gewesen. Und ohne meine Geschwister, Michael, Christian, Dorothea, Andreas und Matthias schon gar nicht.

Danke Euch, dass ich immer auf Euch zählen kann!

Content

Chapter 1 – Introduction

Sediments and sedimentary rocks cover large parts of the Earth's land surface and most of the ocean floor. Information about ancient depositional processes that were acting on the land surface, and resulting paleo-environments is stored within these rocks. Therefore, they provide a challenging archive of Earth's history, allowing unique insights to past climates, oceanic environments and ecosystems, giving hints on paleogeographic configurations and on mountain systems that vanished a long time ago. Not only for scientific, but also for economic interests sedimentary rocks are a highly attractive and important group of rocks as they host large quantities of economic significant products (Boggs 2001); hydrocarbon, coal and mineral deposits as well as most of the worlds building materials like chalk and gravel, for example, are associated to sedimentary rock sequences.

The presented thesis addresses research to this important group of rocks by investigating the sedimentary deposits of the Eocene Sabiñánigo Sandstone (SSt) Succession (Puigdefàbregas 1975). Thereby, the study takes advantage of the economic interest in this type of rocks, as approaches related to subsurface geology were applied, which predominantly have their origins in petroleum geology. Since the 1970ies, new methods in the investigation of sedimentary rocks have been developed (e.g. sequence stratigraphy; Mitchum et al. 1977, Posamentier et al. 1988), which have improved the understanding of physical controls of basin fills (see Aitken & Howell 1996 for an overview). Sequence stratigraphy turned out to become a widely used method in sedimentary geology, but also tools and analysing techniques, initially used as means for borehole logging in subsurface geology, are more generally applied now, as they provide additional insights in a formation's geology.

This study ties up to 'conventional' analysing techniques with methods adopted from subsurface geology to examine the deposits of the SSt-Succession, exposed in the Southern Pyrenees. The SSt-Succession formed in Paleogene times, when foreland basin with several subbasins developed in front of the emerging Pyrenees, accumulating thick sequences of foreland basin strata. The Jaca Basin, which is located in the area of Río Gallego (Fig. 1.1), constitutes one of these subbasins. It evolved as a piggyback basin that now is incorporated in the southern fold and thrust belt of the Pyrenees (Fig. 1.2) and exposes a thick pile of foreland basin strata, including the SSt-Succession. The investigated succession is exposed in the easternmost area of the Jaca Basin, where it can be studied within two separate ridges (Fig. 1.3). The southern ridge is fairly straight, trending almost ESE-WNW, whereas the northern ridge has an arc-like shape at its

western termination. Both ridges show excellent outcrop conditions, where distinct surfaces and horizons can be followed over large distances. Although some studies on the SSt-Succession, e.g. by Puigdefàbregas (1975) and Lafont (1996), already exist, a complete record of their lithofacies, comprising the northern and the southern ridge with an adequate sequence stratigraphic interpretation were still lacking.

Fig. 1.1: Geological map of the Pyrenees stretching along the Franco-Iberian boarder; with location of the Jaca Basin, displaying Eocene-Oligocene successions (modified after Vergés et al. 2002).

Furthermore, no efforts exist to relate the northern and the southern ridge within a sequence stratigraphic framework or even to pose a depositional model for the whole succession. This is quite puzzling, as the SSt-Succession combines excellent outcrop conditions and a stratigraphically interesting position at the transition from deep marine towards continental depositional environments, within an almost complete sequence of foreland basin strata. The Sabiñánigo Sandstones, therefore, were supposed to yield great evidence on depositional processes within this foreland basin setting, revealing an either allocyclic and/or autocyclic control. Thus, the genesis of the SSt-Succession is of general interest:

How does it fit into the Pyrenean realm and the foreland basin setting?

What does it tell about the triggering mechanisms, controlling sedimentation?

But first there was the question how the two ridges relate to each other, or how they could be related to each other – as the whole succession had to be taken into account in order

to unravel the history of this specific archive. To realize this and to set an appropriate correlation scheme for the entire succession, distinct analytical techniques were applied within this study. Methods developed and applied comprise both conventional outcrop analyses and techniques adopted from subsurface geology, which enabled to generate a depositional model of the SSt-Succession.

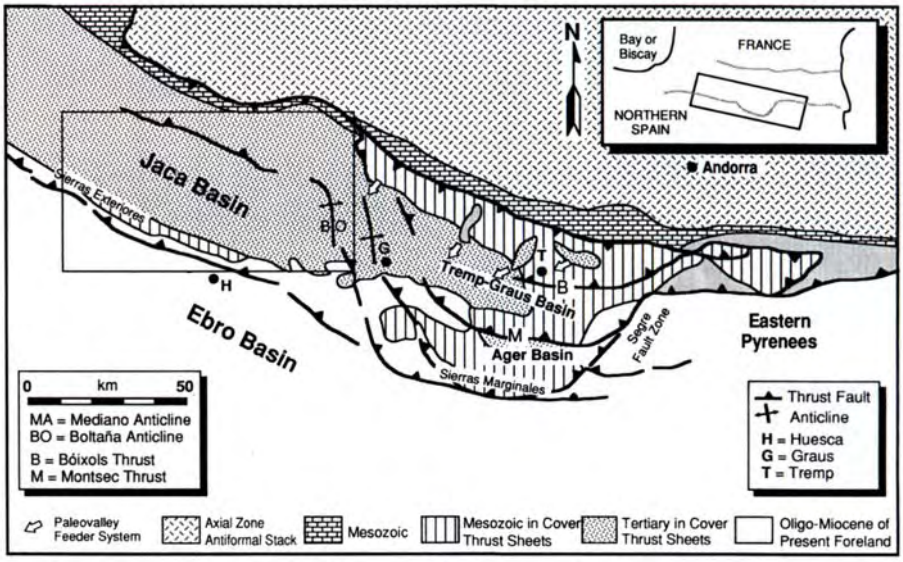

Fig. 1.2: Geological map of the Southern Pyrenees with emphasis on the large-scale tectonic elements characterizing the South-Pyrenean foreland basins, and the studying site of the Jaca Basin (modified after Hogan & Burbank 1996).

Environmental facies and geophysical properties were analysed, and interpreted following sequence stratigraphic principles. The applicability and significance of the methods used, both as individual approach and in combination, were proved and demonstrated in the course of this study. Furthermore, thermochronological evidences were scrutinized to ensure the geophysical investigations and to allow a broader understanding of the SSt-Succession in the context of the general basin evolution.

Within this framework, the aims of the presented study were:

i) To compile a detailed lithofacies analysis and decipher the depositional environments of the SSt-Succession, applying standard facies analysis methods as well as geophysical measurements, e.g. gamma ray spectrometry.

ii) To set a correlation scheme between the two ridges based on outcrop analogue studies, i.e. integrating evidences from facies analyses, spectral gamma ray investigations and sequence stratigraphic interpretations.

iii) To establish a sequence stratigraphic framework, and develop a depositional model for the entire SSt-Succession based on sequence stratigraphic

interpretation of lateral transects, that were obtained from physical/optical tracing, and log correlation.

iv) To evaluate the previous sedimentary overburden, on top of the SSt-Succession, by low-temperature thermochronology.

v) To reveal driving mechanisms, that were triggering and affecting the depositional system of the SSt-Succession within the Jaca Basin and in the Pyrenean context.

Fig. 1.3: Aerial photograph of the studying site with the two ridges of the SSt-Succession (source: Google, TerraMetrics 2007).

The conceptual framework and applied methods that form the basis to achieve the aims of this study are delineated in Tab. 1.1 and will be described in more detail in Chapter 3, while some information on the general tectonic and depositional setting of foreland basins and associated sedimentary basin filling is given in the Appendix.

Tab. 1.1: Conceptual and analytic framework of the thesis research project.

The conceptual framework for the geologic interpretation comprises:
• Facies Models
• Sequence Stratigraphy
The applied methods to achieve a comprehensive data set comprise:
• Facies Analysis
• Gamma Ray Spectrometry
• Low-Temperature Thermochronology
• Sequence Stratigraphic Interpretation

1.1 Structure of the Thesis

Chapter 1: Introduction

A brief introduction to the field of interest of this study and the according working area is provided followed by a concise illustration of the framework and intention of this thesis.

Chapter 2: Geological Setting

An overview of the geological and structural evolution of the Pyrenean realm is given, with major focus placed on the Southern Pyrenees in general and the Jaca Basin in particular.

Chapter 3: Methodology

To evaluate the implications of the SSt-Succession, the structure of the thesis is based on the concepts of facies models and sequence stratigraphy. In Chapter 3 their major terms and perceptions are introduced as well as their application in respect of this study. The distinct methods applied within this framework are described and the methodological procedure is explained. The applied methods comprise:

i) Facies Analysis: Standard analysis of lithofacies both in the field by examining vertical sections and in the laboratory by analysing thin sections and hand specimens;

ii) Gamma Ray Spectrometry: Geophysical based investigations using a portable gamma ray device to measure the natural radioactivity of the rocks along vertical sections;

iii) Sequence Stratigraphic Interpretation: Interpretation of the obtained facies data on the basis of sequence stratigraphic principles;

iv) Low-Temperature Thermochronology: (U-Th)/He-dating on detrital apatites separated from rock samples.

Chapter 4: Gamma Ray Spectrometer Calibration

Facies and sequence stratigraphic analyses were supported by gamma ray spectrometry using a hand-held gamma ray spectrometer (*GR-320enviSpec*). To define the accuracy and precision of the device used, and to assure the validity of the procedural method and obtained data, several test and calibration measurements, including calibration against international standards, were performed.

Chapter 5: Sedimentary facies of the Sabiñánigo Sandstone Succession

An illustrated description of the lithofacies of the SSt-Succession as exposed within the Jaca Basin is given. Occurring sedimentary facies and facies patterns, which were analysed within vertical profiles are listed and interpreted with respect of their depositional environments. Apart from the standard lithofacies analysis in the field (vertical sections)

and in the laboratory (thin sections) also insights obtained from gamma ray spectrometry were incorporated. Accordingly derived and defined facies types and facies associations are listed as well as the processed vertical sections.

Chapter 6: Previous Sedimentary Overburden

The minimum previous thickness of depositional strata, covering the SSt-Successions is constrained using (U-Th)/He dating. The obtained data from detrital apatites of the working area are displayed and discussed. On the basis of these data, the thermal influence affecting the rocks of the SSt-Succession was determined. This in turn enables to i) assess the previous sedimentary overburden covering the SSt-Succession, ii) to constrain the amount of subsidence and erosion within the eastern sector of the Jaca Basin, and iii) to evaluate possible diagenetic effects that might have affected the rocks under investigation. Moreover, a broad data set is given, and the thermal history of the upper Jaca Basin can be deduced from resulting age determination, which in turn provides basic parameters for further stratigraphic modelling.

Chapter 7: Depositional Model

A depositional model of the SSt-Succession is presented, using results from lithofacies analysis and spectral gamma ray measurements.

i) Two lateral transects, based on lateral correlation between the lithofacies profiles are presented. For correlation physical and optical tracing was performed (concept of real timelines).

ii) Vertical profiles measured with a portable gamma ray spectrometer are illustrated and a correlation between the gamma ray log is shown.

iii) Lithofacies transects and gamma ray log transects were synthesized and used to establish two sequence stratigraphically interpreted transects.

iv) Conventional outcrop analyses and spectral gamma ray analyses are tied in order to present a qualitative depositional model of the entire SSt-Succession

v) The reciprocal effects between the evolution of the SSt-Succession and the Pyrenean orogeny are highlighted briefly.

Chapter 8: Conclusion

A general overview of the depositional environment and the evolution of the SSt-Succession is given.

Chapter 2 – Geological Setting

2.1 The Pyrenees

The Pyrenean mountain chain is a nearly E-W trending Alpine collision belt, stretching along the European and Iberian plate boundary (Fig. 2.1). An extensive part of the complete orogenic belt, which extends from Galicia to the Alps, remains at sub sea (e.g. Muñoz 1992, Vergés et al. 2002, Bourrouilh et al. 2004), while the visible part of the mountain chain, the Pyrenees sensu strictu, forms a natural border between Spain and France (Capote et al. 2002). The Pyrenees in the narrower sense are referred to as the Eastern Pyrenees, Central Pyrenees, and West-Central Pyrenees (e.g. Muñoz 1992, Vergés et al. 2002, Bourrouilh et al. 2004), while the westernmost sector of the Pyrenean orogenic belt (Western Pyrenees), reaches as far as the Basque-Cantabrian Mountains (Fig. 2.1).

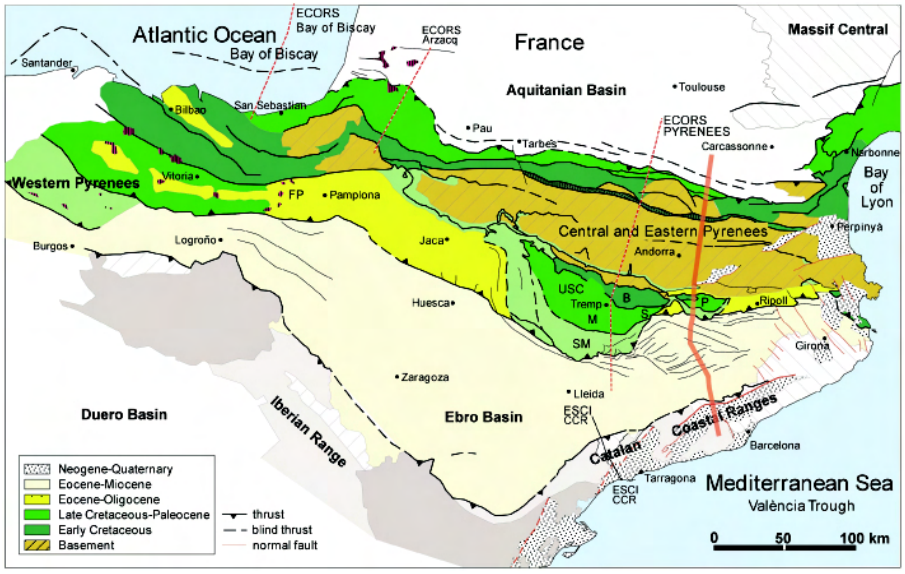

Fig. 2.1: Structural map of the Pyrenees. Locations of deep crustal-scale reflection profiles across the Pyrenees are indicated (Vergés et al. 2002); cp. Figs. 2.3, 2.6 and cited references for details.

The research interest of this study is focused on the Eocene Sabiñánigo Sandstone (SSt) Succession (e.g. Puigdefàbregas 1975, Remacha 1987), which crop out in the eastern sector of the Jaca Basin. Referring to the above-mentioned classification, the Jaca Basin belongs to the West-Central Pyrenees of the Spanish, i.e. the Southern Pyrenees (Fig. 1.1 and 2.1). The Jaca Basin impressively reflects the varying dynamic processes that affected the Pyrenean realm in Paleogene to Neogene times. Both a variety of structural elements and an almost complete sedimentary foreland basin succession, reaching from fully marine to continental, are exposed in the Jaca Basin. The SSt-Succession, thereby,

takes over a particular role, as they were deposited during the transition from fully marine towards continental environments. Due to this intermediate position within the basin infill, they reflect the depositional processes acting in the Pyrenean realm during foreland basin formation.

For a better understanding of the processes affecting the Jaca Basin and in order to analyse the implications of the SSt-Succession in the context of the Pyrenean evolution, the geological framework given below will also issue the broader studying site, as well as aspects of geodynamic and stratigraphic evolution, and the current structural configuration of the Pyrenees.

2.2 Structure of the Pyrenees

As a consequence of the Pyrenean collision and subsequent faulting and thrusting a complex system of thrust sheets and structural patterns developed (Figs. 2.2 and 2.3). In general, the structure of the Pyrenees is characterized by a double verging fold and thrust belt bordered by foreland basins on each side of the chain (Marzo et al. 1998) (Figs. 2.1 and 2.2). The North Pyrenean Fault (NPF), which separates the northern fold and thrust belt (northern thrust system, after Vergés et al. 2002) from the southern fold and thrust belt (southern thrust system, after Vergés et al. 2002), marks the suture of the two colliding plates (Iberia and Europe). Whereas the northern thrust system developed on top of the European plate, and the southern thrust system developed on top of the subducted Iberian plate (Vergés et al. 2002), Figs. 2.3 and 2.6.

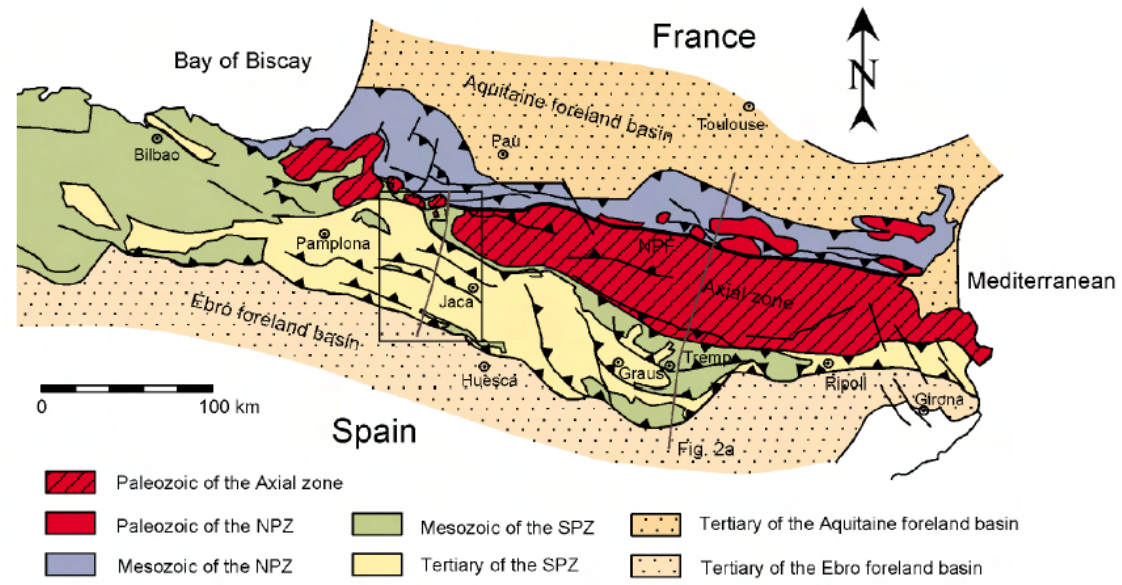

Fig. 2.2: Structure of the Pyrenees (Schellart 2002) with location of cross sections (Fig. 2.3) and Jaca Basin; NPZ: North Pyrenean Zone, SPZ: South Pyrenean Zone, NPF: North Pyrenean Fault.

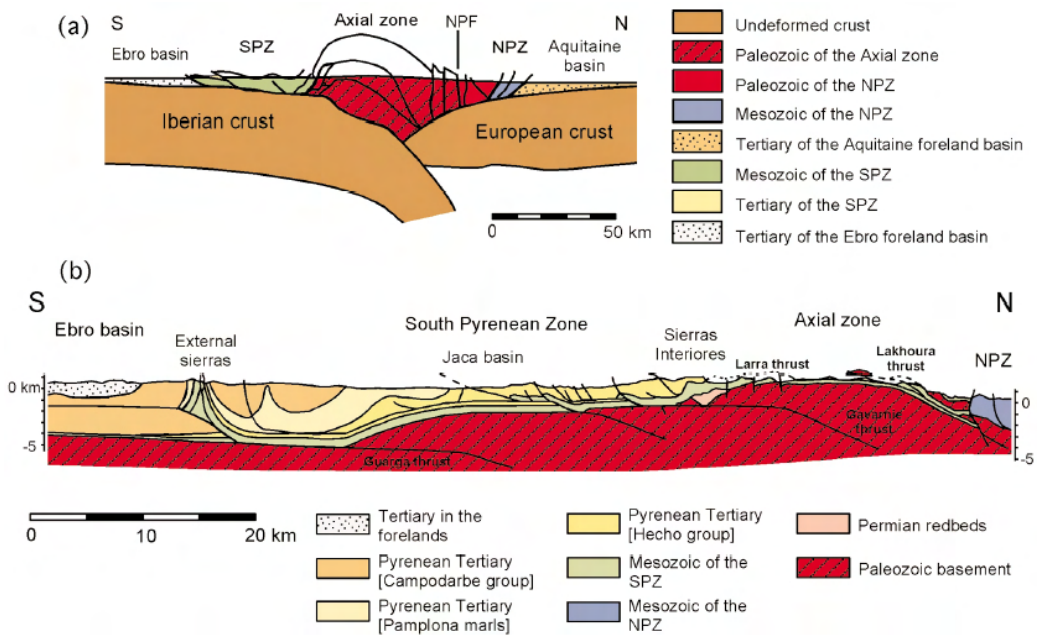

Fig. 2.3: a) Crustal scale cross-section documenting the partial subduction of the Iberian plate under the European plate, constructed on the basis of the ECORS seismic reflection data (ECORS Pyrenees Team 1988); b) Balanced N-S cross-section through the southern part of the West-Central Pyrenees (Schellart 2002); see Fig. 2.2 for location. NPZ: North Pyrenean Zone, SPZ: South Pyrenean Zone, NPF: North Pyrenean Fault.

Main geological features and structural zones of the Pyrenees can be distinguished both along strike and across strike (e.g. Séguret 1972, Muñoz 1992, Capote et al. 2002). The division along strike considers the previously mentioned lateral (E-W) variation in the geometry of the Pyrenean range that from east to west the can be divided into the:

i) Pyrenees sensu strictu (Aragonese-Catalan Pyrenees), composed of

a) Eastern Pyrenees

b) Central Pyrenees,

c) West-Central Pyrenees,

ii) Basque-Cantabrian or Western Pyrenees (e.g. Capote et al. 2002, Vergés et al. 2002, Muñoz 1992), cp. Fig. 2.1.

From north to south five structural zones can be distinguished (e.g. Vergés et al. 1995 and 2002, Schellart 2002): The 1) Aquitaine Foreland Basin, 2) North Pyrenean Thrust System, 3) Axial Zone, 4) South Pyrenean Thrust System, and 5) Ebro Foreland Basin, which are illustrated in Fig. 2.2 and described below.

(The North Pyrenean Thrust System includes the NPZ and equals the northern fold and thrust belt that developed as a consequence of the northern thrust system; AZ and SPZ or South Pyrenean Thrust System, respectively constitute the southern fold and thrust belt and developed as a consequence of the southern thrust system.)

The Aquitaine Foreland Basin

It is related to the northern Pyrenean wedge and forms a molasse basin, comprising tectonically undisturbed synorogenic sediments with maximum ages of Late Cretaceous (Schellart 2002).

The North Pyrenean Thrust System

The North Pyrenean Thrust System or northern fold and thrust belt, respectively, consists of north-vergent thrust sheets with Precambrian to Paleozoic basement-outcrops, that constitute the N-Pyrenean massifs (Bourrouilh et al. 2004). The North Pyrenean Zone (NPZ), which belongs to the northern thrust system, forms a narrow zone (1-5 km in width) of highly metamorphosed rocks and is separated from the adjacent Axial Zone by the North Pyrenean Fault (NPF), (Schellart 2002).

The Axial Zone (AZ)

The Axial Zone constitutes the northernmost part of the south Pyrenean fold and thrust belt and forms the highest part of the Pyrenees that progressively decreases westward. It is composed of a large thrust culmination, representing the orographic axis of the Pyrenees (Bourrouilh et al. 2004). Within the AZ Precambrian and Paleozoic basement rocks are exposed that still show evidence of the Hercynian orogeny (Bourrouilh et al. 2004), as they have not experienced major Alpine metamorphism (Schellart 2002). The AZ evolved into an antiformal stack; build up by three major thrust sheets, piled on top of each other (Muñoz 1992). In the Eastern and Central Pyrenees these are from bottom to top the Nogueres, Orri and Rialp thrust sheets, and in the Western-Central Pyrenees the Lakhoura, Gavernie and Guarga thrust sheets (Schellart 2002), Figs. 2.3 and 2.6.

The South Pyrenean Thrust System

The South Pyrenean Thrust System (Vergés et al. 2002) equals the South Pyrenean Zone (SPZ) of Schellart (2002). It consists of south verging thrusts and folds and is composed of a stratigraphic succession ranging from Permo-Triassic deposits up to Oligocene conglomerates (Bourrouilh et al. 2004).

The SPZ developed in the southern continuation of the Axial Zone as a southward moving crustal wedge, resulting in the tectonic delamination of the upper crust (Coney et al. 1996). Middle Triassic evaporites and siltstones constitute the detachment zone for the southward propagating thrust sheets (Muñoz 1992, Coney et al. 1996). In the course of the southward propagating thrust sheets, the South Pyrenean Foreland Basin formed, a major structural and sedimentological feature associated to the SPZ. Due to continuous

movement, the South Pyrenean Foreland Basin subsequently developed into several smaller foreland basins, which will be considered in more detail further on.

The Ebro Foreland Basin

The Ebro Foreland Basin represents the autochthonous external foreland south of the SPZ. It consists of tectonically nearly undisturbed sedimentary rocks of Cenozoic age, resting directly on top of the Hercynian basement (Schellart 2002).

2.3 Geodynamic and stratigraphic evolution

2.3.1 Pre-collisional processes – evolutionary steps

The present structure and geomorphology of the Pyrenees can be considered as a direct consequence of Mesozoic and Cenozoic tectonic activity (Capote et al. 2002). Various tectonic settings, stress regimes and geodynamic processes, esp. concerning plate configuration and paleogeography are responsible for the development of the Pyrenean mountain belt and its present-day appearance. Some of the pre-collisional processes (Vergés et al. 2002) that fundamentally affected the Pyrenean realm and paved the way for the Pyrenean orogeny were summarized after Bourrouilh et al. (2004) and Vergés et al. (2002), and are listed below:

- The break-up of Pangaea in Early Triassic (at about 250 Ma) initiated rifting in the Pyrenean realm and synchronously led to the opening of the North Atlantic.
- Two periods of rifting, lasting from Late Jurassic to Early Cretaceous and Late Barremian to Albian times, gradually thinned the crust between Iberia and Europe.
- The Late Jurassic to Late Cretaceous diachronous eastward opening of the Bay of Biscay resulted in a drift and progressive anticlockwise rotation of the Iberian plate (Figs. 2.4 and 2.5). This led to the development of pull-apart basins, with the Pyrenean rift connecting the Bay of Biscay in the west with the Tethys Ocean in the east. Oceanic crust, however, was not produced within these basins.
- The opening of both the South Atlantic and Indian Ocean, as well as the closure of the Tethys in Cretaceous times provoked the migration of the African plate towards NE and then towards N. Accordingly the free drift of the Iberian plate towards SE was stopped, while the large African plate was continuously pushing northward (Fig. 2.4).

This plate motion narrowed the open space between Europe and Africa and subsequently caused the formation of the Pyrenean-Alpine orogenic belt (Bourrouilh et al. 2004). Due to the diachronous character of the compressional regime, the collision started in Turonian

times (Upper Cretaceous) in the eastern part, to proceeded westward along the northern margin of the Iberian plate (Bourrouilh et al. 2004).

Fig. 2.4: Free drift of the Iberian Peninsula that acted as separated microplate and was pushed towards the north by the African plate, where it finally collided with the Euopean plate, followed by a continent-continent collision and associated partial subducion of the Iberian plate underneath the European plate (Teixell 2000); cp. Figs. 2.3 and 2.6, and text for further explanation.

2.3.2 Cretaceous

As already denoted, the onset of oceanic spreading in the North Atlantic area and subsequent opening of the South Atlantic Ocean caused a new paleogeographic and geodynamic situation in early Cretaceous times (Figs. 2.4 and 2.5). The Iberian microplate still moved independently, but was trapped between the continental plates of Africa and Eurasia. Iberia, therefore, was highly affected by the ongoing changes in plate configuration and underwent various phases of different tectonic stress regimes:

At the beginning of the Cretaceous, extension dominated the stress field, caused by the break-up of the Jurassic platform (Fig. 2.5a). Owing to the opening processes of the Bay of Biscay, a transtensional regime was dominant in Early to Late Cretaceous times and pull-apart basins formed (Fig. 2.5b). During this time interval first convergent movements

already affected the NW margin of Iberia, as oceanic crust of the Bay of Biscay began to be subducted beneath Iberia. The opening of the Bay of Biscay was finally accomplished during late Cretaceous time, leading to an anticlockwise rotation of Iberia, which until this point had acted as an independent microplate. After it finally got locked between Africa and Europe, the Iberian microplate was subjected to a compressional stress regime (Capote et al. 2002). The northward movement of the large African plate initiated a convergent regime between Africa and Europe, with Iberia caught in-between (Fig. 2.5c). The African plate pushed the still rotating Iberian plate towards Europe, leading to a partial subduction of Iberia beneath the Eurasian plate. These movements took place in Late Cretaceous times and resulted in a continent-continent collision, where both the subduction and the subsequent collision were of an oblique character (Fig. 2.4). This in turn led to diachronous deformation and basin inversion along the Iberian and European plate boundary: while in the western part of the Pyrenees extension was still active, the eastern part was already subjected to compression that subsequently propagated westward (Capote et al. 2002). Contemporaneously to the collision (Upper Cretaceous), two carbonate platforms developed on each side of the evolving Pyrenees; in the Aquitaine area and to the south on the Iberian plate, separated by a flysch foredeep in-between.

2.3.3 Paleogene – Neogene

In Paleogene and Neogene times, the Iberian evolution was dominated by compressional deformation that lasted for about 60 Ma until Middle Miocene times (Schellart 2002). The closure of the Tethyan Sea, and subsequent formation of the Pyrenees represent the most significant effects of the convergent movements (e.g. Vergés et al. 2002) (Figs. 2.4 and 2.5c/d). As a result, NS directed thrusting was initiated during the development of the Pyrenees (Ziegler et al. 2002). The associated crustal shortening over the entire orogen amounts to about 125 km (Vergés et al. 1995), and involves northward subduction of the Iberian lithosphere beneath Europe (Fig. 2.3). The anticlockwise rotation of the Iberian Peninsula and the earlier mentioned diachronous compression resulted in a thrust sheet emplacement that took place from North to South and from east to west (Holl & Anastasio 1995). A double vergent fold and thrust belt evolved, with associated foreland basins on each side and an Axial Zone in-between (Fig. 2.2). Of major importance for the structural evolution of the Pyrenees were the inherited tectonic elements that were created during the Mesozoic rifting and basin formation. As these previously attached structures were incorporated and reactivated during the ultimate stage of orogeny, which proceeded over the formerly thinned continental crust, giving rise to the present day configuration of the Pyrenees (Bourrouilh et al. 2004).

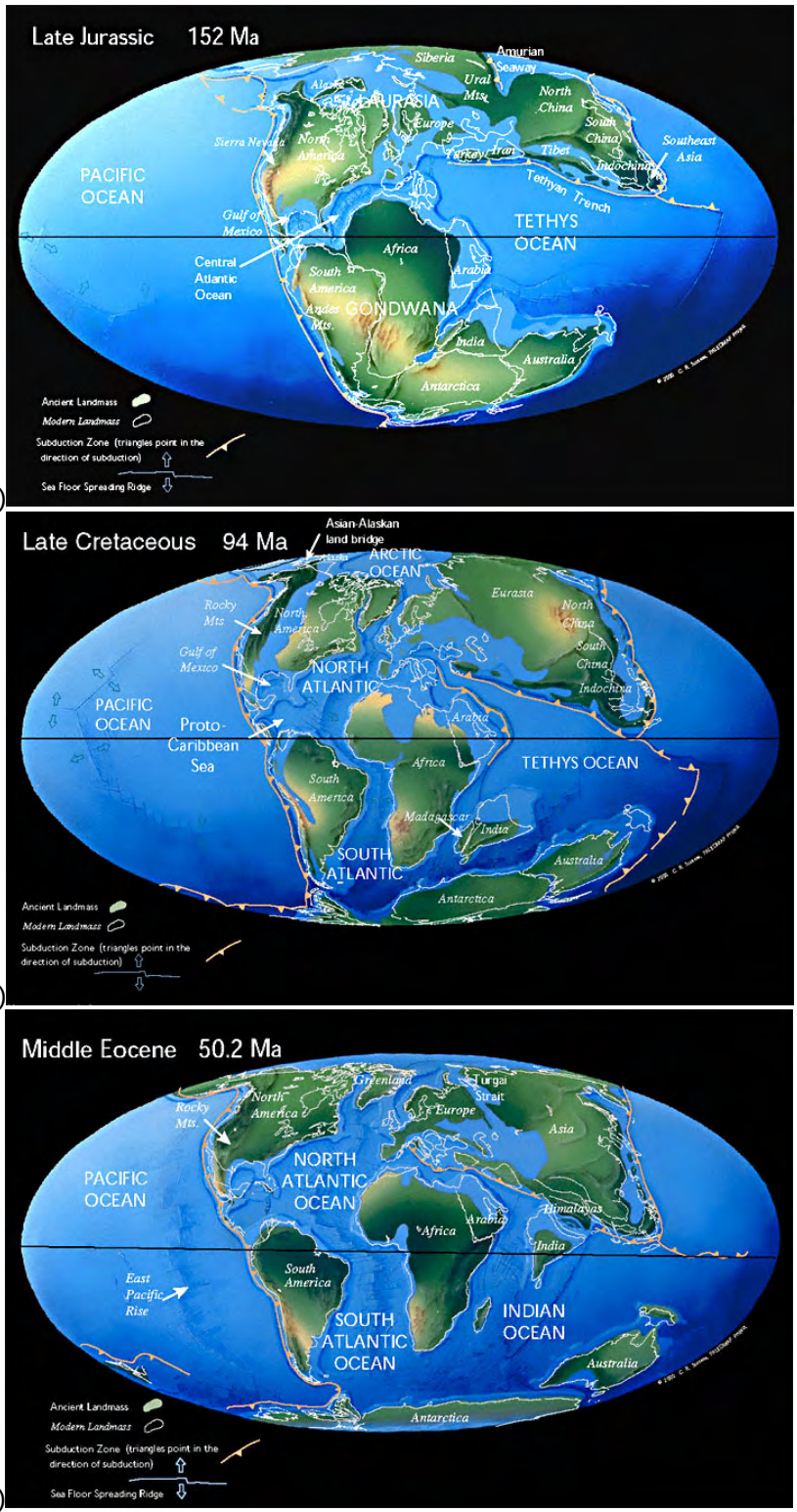

Fig. 2.5a-c: Late Jurassic – Middle Eocene: Progressive opening of North Atlantic caused several periods of different stress regimes and plate-configuration between Eurasia, Africa, and Iberia: a) Extensional stress field, break apart of Pangea, opening of the Central Atlantic;
b) transtensional regime, opening of South Atlantic and Bay of Biscay, formation of pull-apart basins, first convergent movements affect NW margin of Iberia; c) Compressional regime, Iberia locked between Africa and Eurasia, convergent movements between Iberia and Europe, partial subduction of Iberian underneath European plate (source: Scotese 2003).

d) 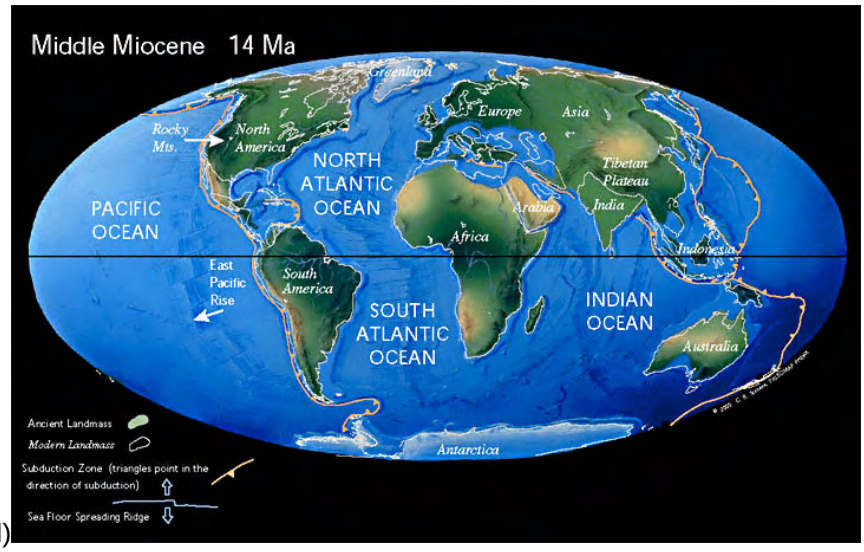

Fig. 2.5d: Plate configuration of Middle Miocene: Closure of the Tethys in Eocene times, accompanied by a series of continent-continent collisions (source: Scotese 2003).

2.4 Cenozoic uplift and sedimentation

The Cenozoic uplift of the Pyrenees was accompanied by several phases of erosion, subsidence, and coupled synorogenic deposition. Puigdefàbregas & Souquet (1986) describe the Pyrenees as a polyhistory basin, with successive stages of development recorded as tecto-sedimentary cycles (Tab. 2.1). The cycles are composed of one or more subordinate depositional sequences, in which sedimentation is controlled by the interrelations between local tectonics, subsidence, eustacy, and sediment supply (Puigdefàbregas & Souquet 1986). For higher-ranking Pyrenean cycles, however, basin-forming and basin-modifying tectonics, as listed in Tab. 2.1, pose the main controlling factors. During the transition from Mesozoic to Paleogene times for example, the Pyrenean realm is characterized by the effects of plate convergence leading to changes in basin configuration and the evolution of foreland basins. The successive exhumation of thrust sheets along major thrusts became the main tectonic control on sedimentation (Puigdefàbregas & Souquet 1986). The corresponding Paleogene to Neogene foreland-basin deposits display a synorogenic sedimentary pattern comparable to sedimentary successions described from the Alps, with an underfilled basin stage consisting of flysch deposits and an overfilled molasse stage. Deep marine turbidite sequences, which accumulated at the base of the subsiding foreland basin, gradually merge into shallow marine deposits until finally terrestrial sequences, locally expressed by evaporates, prevail (depositional sequences TE to T_O in Tab. 2.1). This also indicates progressive climatic changes that are associated to the variations in plate configuration and position during time.

Tab. 2.1: Correlation chart of basin cycles and Pyrenean tectonosedimentary events (simplified after Puigdefàbregas & Souquet 1986). The chart displays the relationship between tectonics and sedimentation in the Pyrenees. Tecto-sedimentary cycles (Pyrenean Cycles, 1-10) were controlled by basin-forming and basin-modifying tectonics and are related to different successive basin types. Tecto-sedimentary cycles include one or several depositional sequences, with sedimentation controlled by diverse mechanisms, e.g. local tectonics and sediment supply.

Pyrenean Cycles	*Depositional Sequences*		*Ages*	*Basin Types*	*Tectonics*			
10	T_O	2-1	Miocene Oligocene	Last stage foreland basins				
9	TE	6-1	Eocene	Turbidite to fluvial fill of migrating foreland basins	Convergence	Thrust sheet emplacement	Lower thrust sheets Upper thrust sheets	E-W Progr. emergence
8	TP	2-1	Paleocene	Transition to foreland basins		Initial collision at the eastern Pyrenees		
7	K_2	5-4	Maastrichtian Middle Santonian	Wrench basin including local folding, uplift with submarine and subaerial erosion	Transpression			
6	K_2	3-1	Middle Santonian Middle Cenomanian	Deeper turbidite wrench basin and related backstepping carbonate platforms		Wrenching		
5	K_1	6	Early Cenomanian Middle Albian	Strike-slip turbidite troughs along the NPFZ First flysch	Continental break-up	Sinistral wrenching	Rotation of Iberia	Transtension Heat flow
4	K_1	5-4	Early Albian Aptian	Rhombic subbasins in a NW-SE trending rift system along inherited basement directions (Parentis, Adour, Pyrenees)		Rifting of the Bay of Biscay		
3	K_1	3-1	Barremian Neocomian	Unstable platform Weald facies in Cantabrian and Iberian chains				
2	J TR	3-1 3-1	Lias-Malm Triassic	Syn-rift alluvial deposits to carbonate platform controlled by normal faulting along NE-SW inherited basement directions.		Ligurian and Atlantic rifting		
1	P		Permian	Interior fracture basins		Intra-continental rifting		

Climate variations range from tropical through humid subtropical to arid subtropical conditions and were induced (amongst other processes) by the northward movement of the Iberian plate (Capote et al. 2002). Referring to Tab. 2.1, the sedimentary deposits related to the third and fourth group of cycles are of major interest for this study. They display the development of migrating foreland basins and due to better outcrop conditions, can best be studied within the Southern Pyrenees.

2.5 South Pyrenean Foreland Basin

In the course of the earlier mentioned diachronous and oblique compression, a variety of structural units and thrust sheets evolved. Owing to the north to south and east to west directed thrust sheet emplacement, thrust sheets of the Western Pyrenees are in general younger than those of the Eastern Pyrenees (Holl & Anastasio 1995). The thrust sheets are the underlying elements of the South Pyrenean foreland and are locally carrying Cenozoic sedimentary basins atop. Along the SPZ the following major thrust sheets can be distinguished: In the **Eastern Pyrenees** the Cadí thrust sheet and the Pedraforca thrust sheet are the most important (Marzo et al. 1998). In the **Central Pyrenees** (in the literature also referred to as the South Pyrenean Central Unit after Séguret (1972)), the Cotiella-, Boixols-, Montsec- and Sierras Marginales thrust sheets can be distinguished (Marzo et al. 1998), (cp. Fig. 2.6). Whereas the Gavernie and Guarga thrust sheets belong to the **Central** and **West-Central Pyrenees** (Holl & Anastasio 1995), (Fig. 2.6).

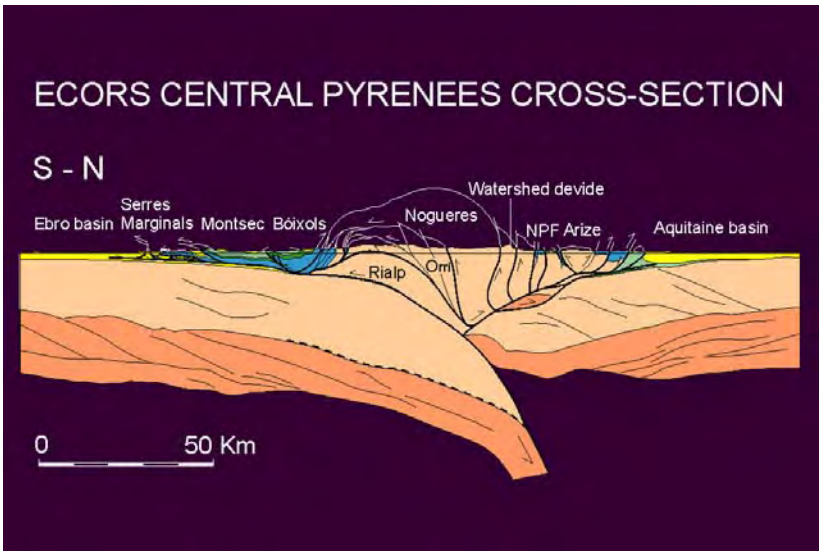

Fig. 2.6: Cross-section along the ECORS-transect (cp. Fig. 2.1), displaying piled thrust sheets of the Cenral Pyrenees, constructed on the basis of the ECORS seismic reflection data (Muñoz 2003).

In front and on top of these southward advancing thrust sheets several foreland basins developed from Early Eocene to Oligocene and were successively transported along the Triassic décollement level (Bourrouilh et al. 2004). Collectively these foreland basins are referred to as the **South Pyrenean Foreland Basin.** In the course of collision and the progressive westward-directed thrust sheet emplacement, several N-S directed anticlines developed within the SPZ. As a result the elongated South Pyrenean Foreland Basin was subdivided into several smaller ‘subbasins’, e.g. the Graus-Tremp and Aínsa Basin in the Central Pyrenees, and the Jaca Basin in the West-Central Pyrenees (Arenas et al. 2001), (cp. Fig. 2.7).

2.6 The Jaca Basin

2.6.1 Structure

The Jaca Basin is located in the southern part of the West-Central Pyrenees and is exposed within the Guarga Syncline (Figs. 2.2, 2.3 and 2.7). Now incorporated in the orogen the basin emerged in Paleogene times and shows a typical foreland basin succession composed of turbiditic and molasse sequences, while the margins are build up by ramp carbonates (Bourrouilh et al. 2004) (Tab. 2.2 and Fig. 2.9).

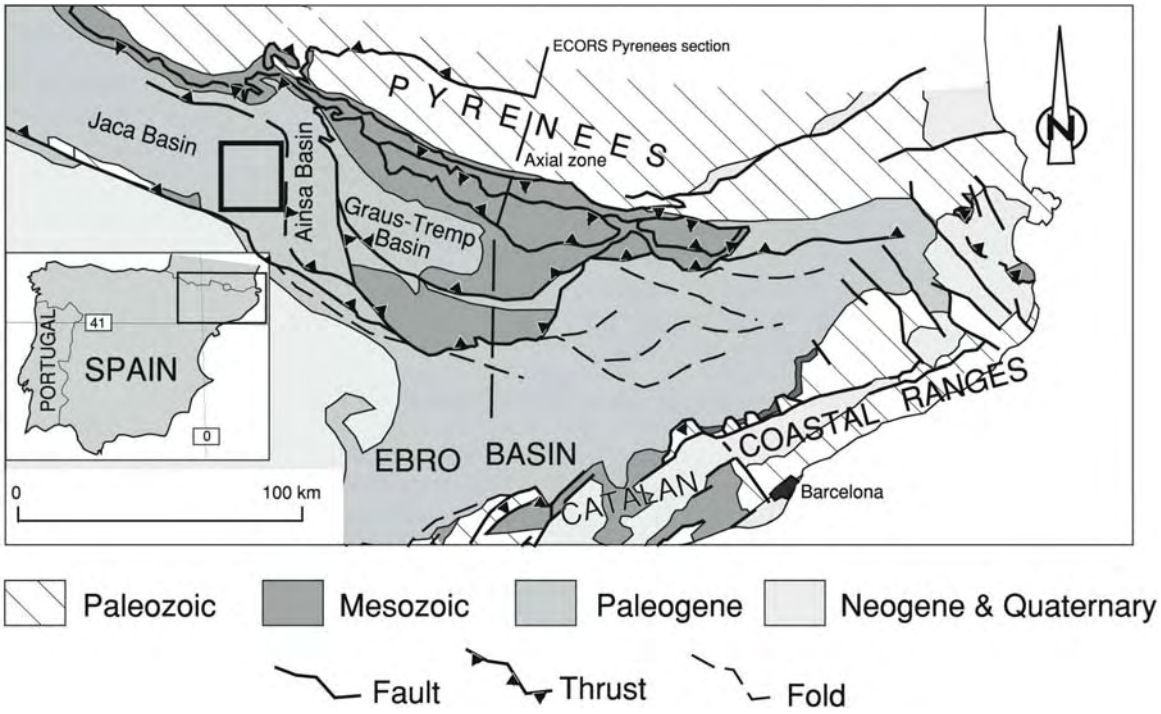

Fig. 2.7: South Pyrenean Zone with according foreland basins that evolved due to rising anticlinal structures. Location of studying site within the Jaca Basin indicated by black rectangle, (modified after López-Blanco et al. 2003)

At the northern flank of the Jaca Basin the almost E-W trending Internal Sierras crop out, representing the northernmost fold and thrust belt of the Guarga Syncline (Fig. 2.3). They expose a high relief area of intense deformation that is composed of south-vergent thrust faults and a series of steep synclines and anticlines (Capote et al. 2002): e.g. the Santa Orosía Syncline, the Peña d'Oroel and the San Juan de la Peña Syncline. The southern flank of the Jaca Basin is expressed by the External Sierras (Sierras Exteriores), which form the southern fold and thrust belt of the Guarga Syncline. The External Sierras evolved along the South Pyrenean Thrust Front and are composed of a series of N-S oriented synclines and anticlines: e.g. the Sierra de Guara Anticline and Arguis Anticline (Capote et al. 2002, Medjadj 1985). The western limitation of the Jaca Basin is lacking any significant morphological high, except for the Sangüesa ramp, which belongs to the

Foz de Binies Anticline (Camara & Klimowitz 1985). The Jaca Basin gradually plunges into the westward adjacent Pamplona Basin. At its eastern limitation, however, the Boltaña Anticline forms a striking morphological boundary towards the neighbouring Aínsa Basin (Figs. 2.7 and 2.9). The Boltaña Anticline is part of the Sobrarbe oblique fold and thrust system: a system of N-S to NW-SE trending structures in the footwall of the Montsec-Cotiella thrust sheet, which constitutes the boundary between the Central Pyrenees and the West-Central Pyrenees (Capote et al. 2002).

Due to variations in structural pattern and sedimentological composition, the Jaca Basin can be distinguished into a northern and a southern subbasin (e.g. Bentham et al. 1992, Teixell 1996):

The northern subbasin is dominated by turbiditic series of the Hecho Group that accumulated during Lower and Middle Eocene times (Tab. 2.2), and were later deformed and incorporated in the mountain chain (Bourrouilh et al. 2004). The according tectonic processes took place in Paleocene to Eocene times, and furthermore caused the formation of a set of thrust system and related folds (Puigdefàbregas & Souquet 1986, cp. Tab. 2.1), e.g. Jaca Thrust, Oturia Thrust, as well as the Basa and Atares Anticlines, which are important structures within the studying area (Fig. 2.9).

In the southern subbasin, the continental sediments of the Campodarbe Group prevail and are represented by thick siliciclastic successions of Upper Eocene to Oligocene age (Capote et al. 2002). They are exposed within the Guarga Synclinorium and accumulated during the southward propagation and emergence of the Guarga thrust sheet front. The lower Middle Eocene carbonate platform of the southern margin was partly overthrusted. In contrast to the thrust sheets of the Central Pyrenees that are piled on top of each other, the West-Central Pyrenees show an imbricate stack of basement thrust sheets with a ‘piggyback style’ (Capote et al. 2002). According to the definition of Ori & Friend (1984), the Jaca Basin can be viewed as a piggyback basin (Turner & Hancock 1990). After its detachment from the pre-Triassic basement in Middle to Late Eocene the Jaca Basin formed on top of the active Guarga thrust sheet and was carried in a southward direction. The propagation of the thrust sheet pertained until Miocene, while the ‘active’ Jaca Basin gradually was filled with synorogenic foreland strata (Turner 1990), cp. Tab. 2.2 and Tab. 2.3.

2.6.2 Stratigraphy

The pre-thrusting sequences of the Jaca Basin area are composed of Mesozoic to Paleocene shelf carbonates and siliciclastics. They overlie Triassic shales and evaporate deposits that were used as décollement level during thrust sheet emplacement (Tab. 2.2).

Tab. 2.2: Stratigraphy and stratigraphic evolution of the Jaca Basin (Barnolas & Pujalte 2004).

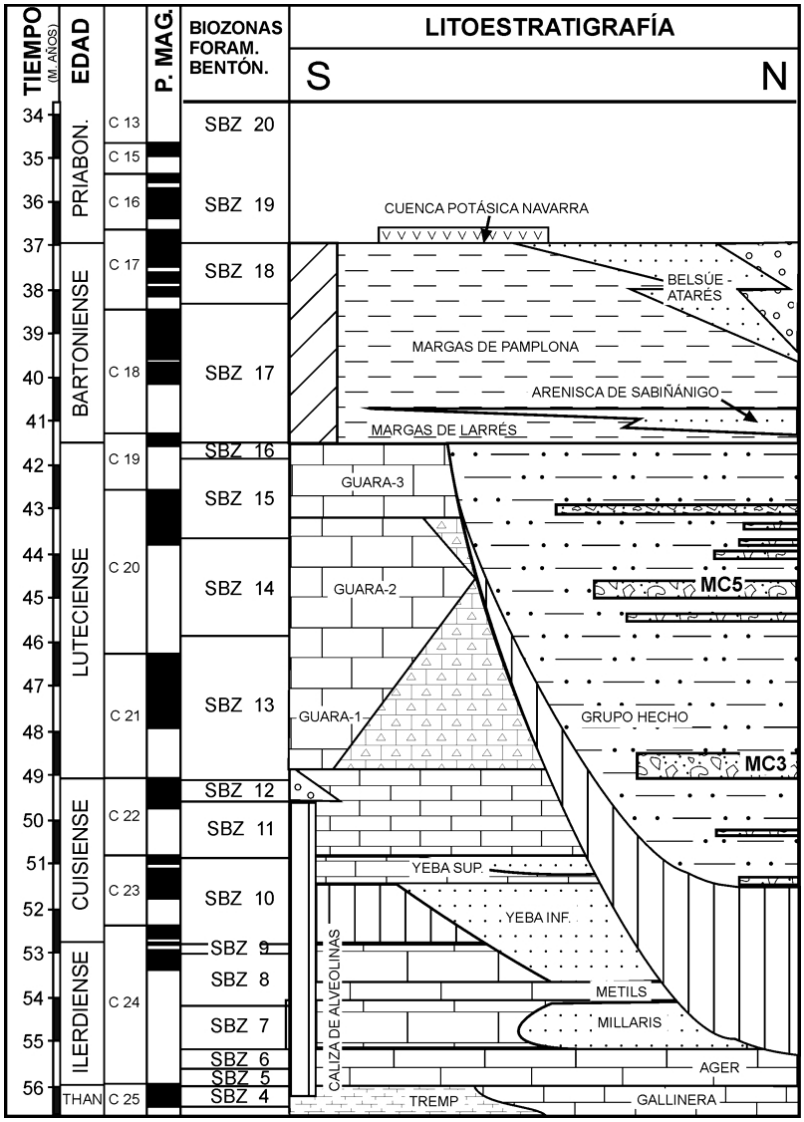

The Mesozoic and Paleocene sediments are capped by the Ypresian Alveolina limestones that were deposited in most parts of the south-central to west-central Pyrenean foreland basin, indicating a widespread transgressive episode (Fernández et al. 2004). Related to the onset of thrusting in Lower Eocene times a major change in the depositional character was initiated, and the depositional setting changed from a shallow marine platform environment to a deeper marine setting. This led to the formation of a continuously subsiding foredeep (precursor of the later South Pyrenean Foreland Basin),

an elongated trough that was gradually filled by synorogenic sediments (Barnolas & Gil-Peña 2001). Thus the infill of the Jaca Basin shows a typical foreland basin turbidite to molasse succession, while the margins are made up by ramp carbonates (Tab. 2.2 and Fig. 2.9).

The basin successions start with the deep-sea turbidites of the Hecho Group, which were deposited in Cuisian and Lutetian time (Rosell & Puigdefàbregas 1975). Their source area is assumed to be in the northeastern area of the basin with an E-W-oriented transport-direction (Fig. 2.8). The source area of the associated megaturbidite breccia sheets and olistostromes (MC3, MC5 in Tab. 2.2), which occur within the turbidite sequences, however, is supposed to be in the north (Labaume & Séguret, 1985). Coeval to the accumulation of the Hecho turbidites in the centre of the Jaca Basin, carbonate-platform sedimentation prevailed at the southern margin of the basin, while towards the western continuation a connection to the proto-Atlantic still existed (Lafont 1996).

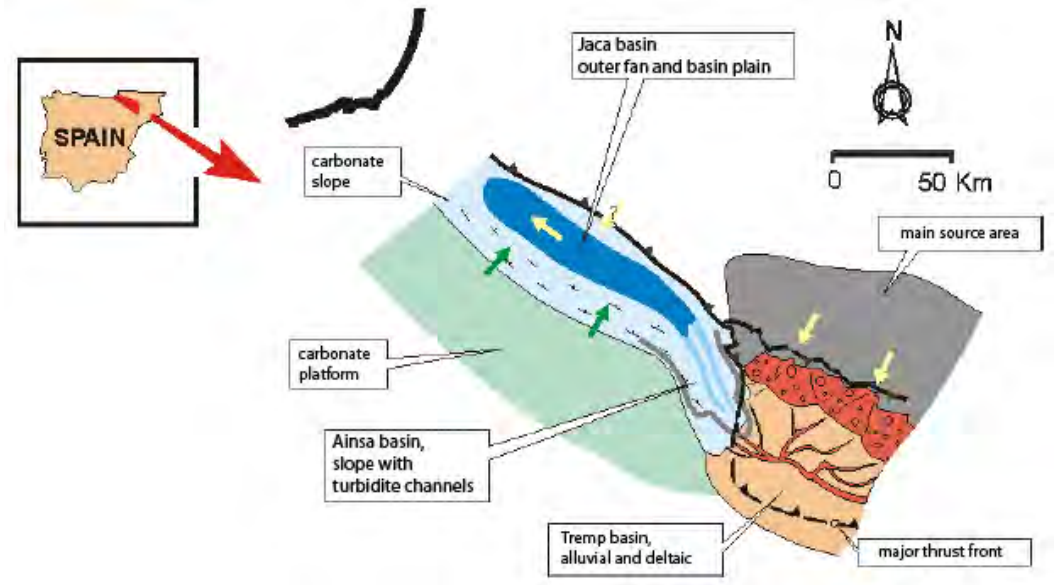

Fig 2.8: Paleogene trough of the Southern Pyrenees and deposition of deep marine turbidites in Lower to Middle Eocene times. Arrows indicate provenance (modified after Arbués et al. 2003).

Major changes regarding the paleogeographic setting and depositional conditions of the Jaca Basin are associated with the emerging Boltaña Anticline. The anticline started to rise in Middle Eocene times (Anastasio 1992) and was actively uplifted throughout the Middle and Late Eocene. In the course of this geomorphological and environmental modification, the turbiditic sedimentation of the Hecho Group ceased (Fig. 2.8). And first extensive slope-deposits of the Larrés Marls accumulated, indicating a transition from deep marine towards shallow marine environments (Tab. 2.2).

The depositional settings progressively shifted towards continental conditions, with first shallow marine deposits accumulating during Lutetian times. They are ascribed to the Sabiñánigo Sandstones (Puigdefàbregas 1975) and are represented by silt- to sand-sized siliciclastics. In Late Lutetian to Early Biarritzian time, the short-termed, but widespread Biarritzian transgression (Rosell & Puigdefàbregas 1975), led to the deposition of deeper marine marls (Pamplona Marls), which transgressively overlay the deposits of the SSt-Succession (Puigdefàbregas 1975). With the Belsué Atares Fomation, shallow marine sedimentation soon re-established in Upper Eocene times. Fluvial sandstone channels and shales characterize the deposits, grading upwards into layered massive alluvial fan conglomerates of the Oligocene Santa Orosía Formation (Bourrouilh et al. 2004).

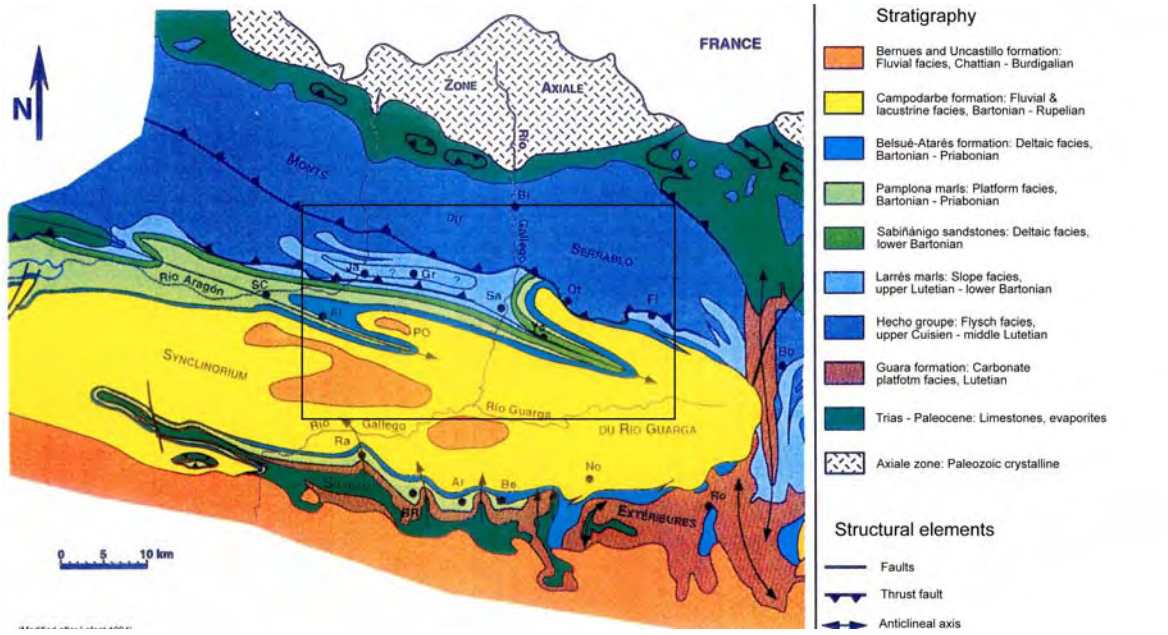

Fig. 2.9: Geological map of the Jaca Basin with location of the studying site marked by the rectangle (after Soler & Puigdefàbregas 1970, Lafont 1994).

Chapter 3 – Methodology

To evaluate the implications of the Sabiñánigo Sandstone Succession and develop the aimed depositional model a multiple approach was followed, based on conventional outcrop investigations and petrophysical analyses (cp. Tab. 1.1, Chapter 1). In order to provide a guide through the working process of this study, major terms and perceptions associated to the applied methods and the framing concepts of 'Facies Models' and 'Sequence Stratigraphy' will be outlined in this chapter.

3.1 Conceptual framework

3.1.1 Facies models

Referring to the previously mentioned '*archive of Earth's history*', the study of sedimentary rocks enables to determine the sedimentary processes, like sediment transport and deposition that were prevailing in the past. Knowing about the sedimentary processes and products in turn, allows to interpret the dynamics of the paleo-environment and thus to evaluate and reconstruct the according depositional environment.

The fundamental module for the description and interpretation of sedimentary rocks, and hence the basis for the interpretation of sedimentary environments, thereby, forms the sedimentary facies (Nichols 1999). Whereas the term 'facies' refers to the sum of the characteristics of a sedimentary unit, including: dimensions, sedimentary structures, grain sizes and types, colour and biogenic content of the sedimentary rock (Middleton 1978). The process of facies analysis, i.e. analysing and interpreting sedimentary strata in terms of their litho-, bio-, and ichnofacies enables to deduce the physical, chemical and ecological conditions that were prevailing at the time of deposition. Features like this can be combined and condensed into idealized 'facies models' that characterize particular sedimentary environments. Facies models, thereby, represent a general summary of a particular depositional system, involving many individual examples from recent sediments and ancient rocks (Walker & James 1992). To obtain an appropriate (and somehow simplified) classification scheme for the data, distinct facies models are expressed in various ways, e.g. as idealized facies successions, in descriptive forms, in geometric or statistical types etc. (Boggs 2001). At present, for most '*standard*' and also several rather '*exceptional*' sedimentary environments, facies models already exist (cp. cited literature), and commonly are used as a guideline or reference framework to interpret ancient depositional environments.

The knowledge about a former depositional environment and thus the prevailing dynamics and processes enables to constrain criteria related to critical environmental thresholds, such as sea level changes. To evaluate such lateral and temporal changes within or for a paleo-environment, however, a chronological framework is required.

3.1.2 Sequence stratigraphy

Sequence stratigraphy is the study of genetically related facies within a framework of chronostratigraphically significant surfaces (Van Wagoner et al. 1990). In the case of this thesis, sequence stratigraphic correlation techniques were used to i) establish a temporal framework of the investigated successions, ii) enable a correlation between the two ridges of the SSt-Succession, and to iii) develop a depositional model of the entire SSt-Succession. Furthermore, the sequence stratigraphic approach enables to consider the deposits of the SSt-Succession in a more regional context; i.e. once the SSt-Succession is linked to the general stratigraphic framework of the Jaca Basin, comparisons to contemporaneous successions of the Pyrenean foreland can be drawn.

General aspects

'Modern' sequence stratigraphy enables to interpret the evolution of sedimentary environments in space and time, and is based on concepts that were first presented in the mid 20th century, e.g. by Sloss et al. (1949) and Wheeler (1958, 1959). In the course of increased interest in hydrocarbons these concepts were picked up by the petroleum industry and further developed. Mainly the research group of Exxon exercised great efforts in the generation of an application tool to correlate rock units and predict hydrocarbon reserves (e.g. Vail et al. 1977). In the last few decades, sequence stratigraphy experienced an increase in prosperity and evolved from the original concepts of seismic stratigraphy to a scale above seismic resolution. Concepts developed on outcrop were successfully applied to subsurface data sets and vice versa, providing an improved understanding of facies geometries and reservoir architecture (Aitken & Howell 1996). The sequence stratigraphic technique, therefore, is now used as a powerful, predictive facies analysis tool within both hydrocarbon industry and academic research (Aitken & Howell 1996). Since the sequence stratigraphic concept got established numerous papers, reviews and books have been published on this subject (e.g. Posamentier et al. 1988, Van Wagoner et al. 1988). As the method is still improving and quite comprehensive (cp. Emery & Myers 1996, Miall 1997, Coe 2003), everything than a brief introduction to the principles and methodology of sequence stratigraphy would be too extensive. To provide an overview, the most common terms associated with the sequence

stratigraphic method are outlined shortly in Table 3.1 and illustrated in Figure 3.1; for more details please see cited literature.

Tab. 3.1: Summary of common terms and definitions related to sequence stratigraphy (after Boggs 2001, Coe 2003).

Hierarchy of Sequence-Stratigraphic Units	
Depositional sequence:	Genetically related strata bounded by surfaces of erosion or non-deposition or their correlative conformities.
	Two kinds of sequence boundaries are recognized:
Type 1 sequence boundary:	Characterized by subaerial exposure and concurrent erosion associated with stream rejuvenation, a basinward shift of facies, a downward shift in coastal onlap, and onlap of overlying strata.
Type 2 sequence boundary:	Marked by subaerial exposure and downward shift in coastal onlap landward of the depositional shoreline break; however, it lacks both subaerial erosion associated with stream rejuvenation and a basinward shift in facies.
Stratal units within sequences include:	
Depositional system:	Three-dimensional assemblage of lithofacies, genetically linked by active (modern) or inferred (ancient) processes and environments (e.g. fluvial, deltaic, barrier-island).
Systems tract:	Subdivision of a depositional system; defined by geometry and stacking pattern of depositional units, bounding surfaces, and relationship to relative sea level curve.
Parasequence set:	Succession of genetically related parasequences that form a distinctive stacking pattern, (often) bounded by major marine flooding surfaces and their correlative surfaces.
Parasequence:	Relatively conformable succession of genetically related beds or bedsets (within a parasequence set) bounded by marine flooding surfaces or their correlative surfaces.
Key surfaces and systems tracts:	
Lowstand systems tract (LST):	Lies directly on a type 1 sequence boundary; progradational to aggradational parasequence sets; onlaps the FSST.
Highstand systems tract (HST):	Upper system tract in either a type 1 or a type 2 sequence; aggradational to progradational parasequence sets; usually downlaps onto MFS and may onlap onto SB.
Falling stage systems tract (FSST):	Consequence of forced regression*, will not form during regression; progradational parasequence sets or redeposited sediments.
	*forced regression: decrease in accommodation space caused by relative sea level fall, shoreline moves basinward and downward.
Shelf-margin (SMW):	Lowermost system tract associated with a type 2 sequence boundary;
Transgressive systems tract (TST):	Middle systems tract of both type 1 and 2 sequences; increasing rate of relative sea level rise; commonly retrogradational parasequence sets.
Transgressive surface (TS):	Marks onset of pronounced relative sea level rise; it is the first significant marine flooding surface.
Marine flooding surface:	Surface that separates younger from older strata, across which there is evidence of an abrupt increase in water depth.
Maximum flooding surface (MFS):	Surface that separates a TST (below) from a HST (above). Commonly characterized by a condensed horizon reflecting very slow deposition.

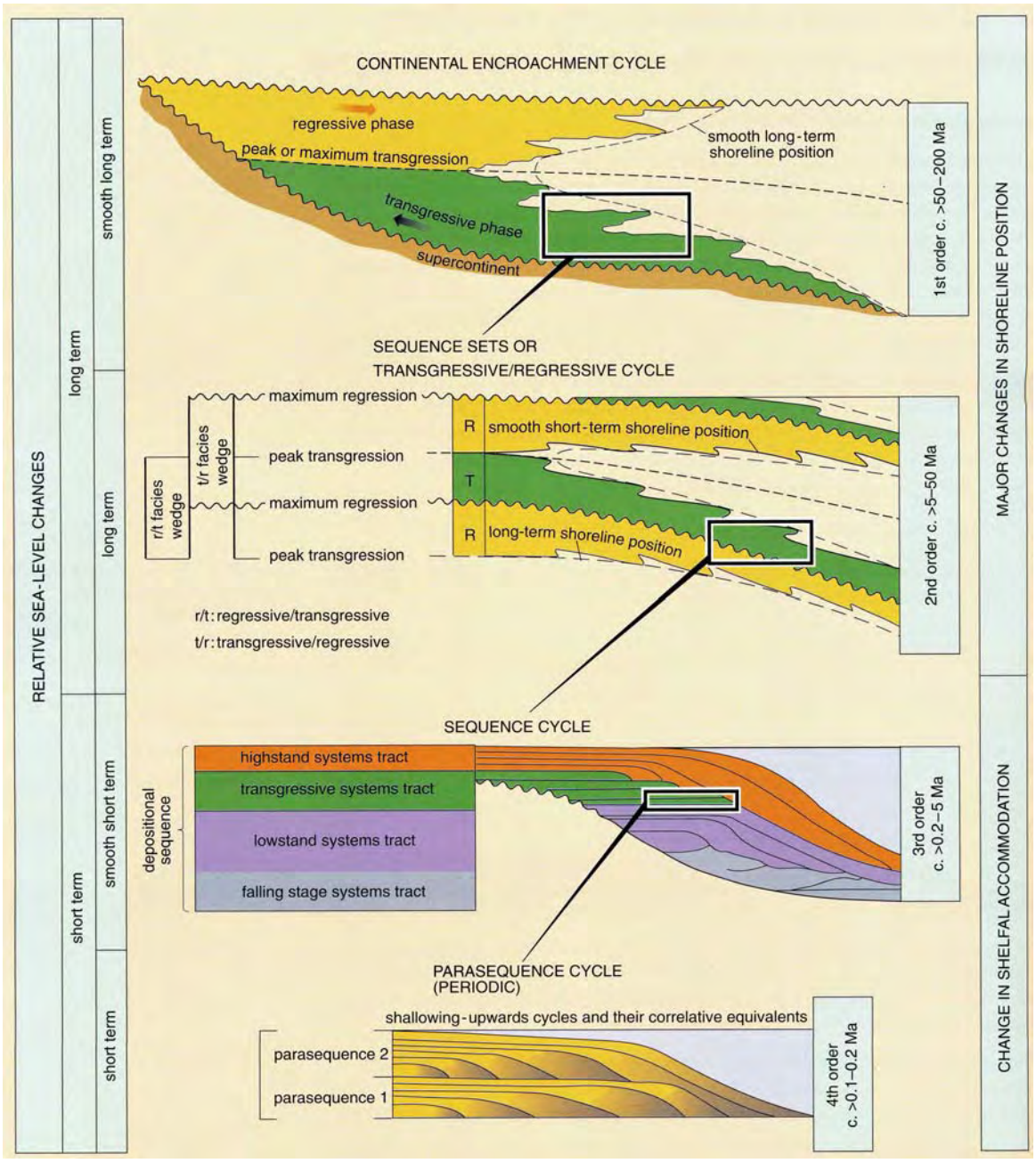

Fig. 3.1: The hierarchy of stratigraphic cycles (Coe 2003).

A general definition of the term sequence stratigraphy, as given by Posamentier et al. 1988, states that: “Sequence stratigraphy is the study of rock relationships within a chronostratigraphic framework wherein the succession of rocks is cyclic and is composed of genetically related stratal units (sequences and systems tracts)”. Whereas a “…sequence is bounded at its top and base by unconformities and their correlative conformities”. Furthermore, a sequence “…is composed of a succession of systems tracts and is interpreted to be deposited between eustatic fall inflection points” (cp. Tab. 3.1, Figs. 3.1 and 3.2).

Sequence stratigraphy, thus constitutes a means to recognize and analyse sedimentary successions by determining distinct packages of strata that were deposited during a cycle of relative sea level change and/or changing sediment supply. Where the strata packages are bounded by chronostratgraphical surfaces; including unconformities formed during relative sea level fall and flooding surfaces formed during relative sea level rise (Coe 2003).

In contrast to other stratigraphic methods and correlation techniques, e.g. lithostratigraphy and allostratigraphy, the sequence stratigraphic approach enables to establish a chronostratigraphic framework of a particular area. Individual key horizons occurring within the succession, thereby, are assumed to be isochronous and represent events of either relative or eustatic sea level changes (Fig. 3.2). Major bounding and subdividing surfaces are commonly characterized by:

- Maximum Flooding Surfaces (mfs)
- Transgressive Surfaces (TS)
- Sequence Boundaries (SB)

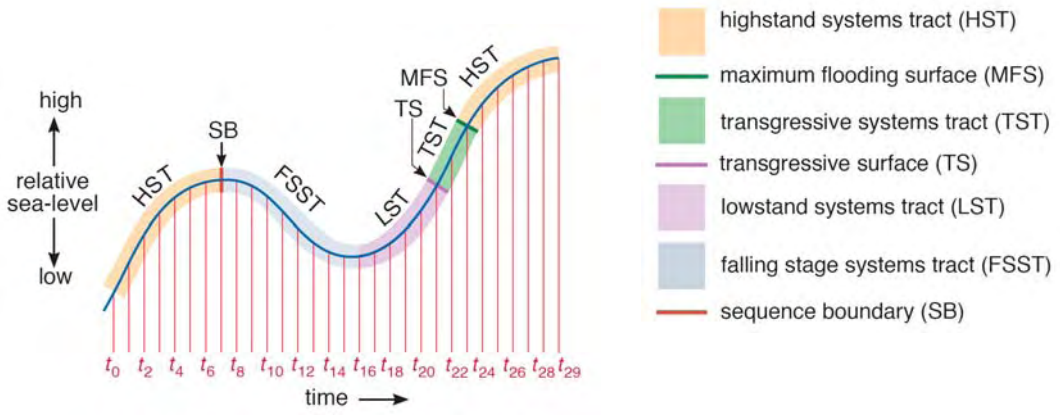

Fig. 3.2: Key surfaces, systems tracts and according inflection points as they are defined within the context of relative sea level changes (Coe 2003).

Associated with sea level changes are changes in accommodation space. The accommodation space is a crucial factor regarding the basin-filling succession and thus the formation of distinct parasequences and their stacking patterns (Nichols 1999). Depending on the balance between accommodation space and sediment supply the depositional system will show either progradational stacking pattern (parasequences build in a basinward direction), aggradational stacking pattern (parasequences remain and build vertical), or retrogradational stacking pattern (parasequences build in a landward direction) (Coe 2003).

Using the sequence stratigraphic approach, with the implicit information about lithofacies, parasequences, parasequence stacking patterns, bounding surfaces etc., allows a more decisive determination and understanding of a depositional environment, its formation and evolution in time.

3.2 Applied methods

3.2.1 Facies analysis

Information about sedimentary successions, facies properties, and facies distribution are basic parameters for evaluating a depositional environment and generating a profound depositional model. Vertical sections, their lateral connectivity and associated vertical and lateral facies shift are the key for environmental interpretation, and, therefore, the cornerstone for this study. Referring again to the general definition of the term facies as "…the characteristics of a rock unit that reflect its origin and permit its differentiation from other rock units around it…" (Walker & James 1992) shows how fundamental a solid analysis and description of the sedimentary facies is for this study. For a facies description usually all the geological features that are known and obtainable for that rock unit are considered, and commonly involve: lithology and thickness (dimensions), colour, composition, grain characteristics, bedding characteristics, sedimentary structures, nature of overlying and underlying contacts, trace and body fossils.

The characterization and description of the physical and biological properties of a facies pose the basis of an environmental interpretation. In most cases, however, it is the combination of different facies types that enables to sort a corresponding facies model as discussed earlier, and hence to reconstruct the ancient depositional environment (Nichols 1999, Reading & Levell 1996). A sandstone with wave-ripples for example indicates deposition in shallow water but only in combination with further facies types, like a herringbone cross stratified sandstone, a depositional environment influenced by tidal currents can be deduced.

Analysing sedimentary facies in terms of paleo-environment thus requires at least a two-stage process:

i) Recognition of facies types, which can be interpreted regarding the dynamics of deposition, and

ii) Establishing of facies associations, which give indications on the environment of deposition.

Facies Types can be compared to the term of facies in general, as it describes the character of a rock expressed by its composition, fossil content, sedimentary structure etc.; it can be established on the basis of a single hand specimen, a rock unit or a bed of rocks. Whereas a '*Facies Association*' represents a group of genetically related sedimentary facies, facies types respectively. In contrast to individual facies types, facies associations have much more environmental significance, as they reflect a combination of facies types, and thus a combination of acting dynamic depositional processes, which give hints on the depositional environment (Walker & James 1992, Nichols 1999). To infer the according paleo-environment from the analysed and described facies types and assigned facies associations the above-discussed facies models commonly are used as reference framework. And quite often also pose the frame for the generation of an appropriate depositional model of the processed sedimentary successions.

Within this study, the sedimentary facies of the SSt-Succession was analysed by characterizing and describing individual facies types, and grouping them into according facies associates. Therefore, a total of 16 vertical profiles were processed, and correlated to lateral transects, to enable a detailed analysis of the sedimentary facies and study of their vertical and lateral distribution. Thus, the SSt-Succession reveals a pattern of several returning facies types, large-scale facies associations and related vertical stacking patterns. As the entire facies analysis came out with quite a huge data set another important task within this study was the development of a comprehensive but straightforward classification scheme, which outlines the basic parameters, characterizing the occurring facies successions without being too confusing. On the basis of the generated data set 32 individual facies types can be distinguished within the sedimentary successions. They form the basic building blocks of the study and were described in note form within a chart (Appendix B). To obtain more indicative information on the depositional environment, the successions were scrutinized for vertical and lateral facies transitions. Due to excellent outcrop conditions within the working area both laterally connected and vertically stacked facies types could be revealed. And groups of one and more jointly occurring and genetically related facies types were grouped into 24 facies associations. They also were described in note form and outlined in a separate chart (Appendix B). Both facies types and facies associations were used for the environmental interpretation and serve as 'bricks' for the generation of the aimed depositional model. But as already denoted, the interpretation of the depositional model and generation of the according model is not only based on the outcomes of standard facies analysis, but also integrates evidences obtained from spectral gamma ray analysis.

3.2.2 Gamma ray spectrometry

The presented study demonstrates an outcrop analogue study that was worked out on the example of the SSt-Succession. Traditional facies analysis, sequence stratigraphic investigations, and spectral GR measurements were integrated to generate a depositional model of this siliciclastic succession. The proceeding Chapter 4 delineates the calibration procedure that was performed particularly for the gamma ray device used, to assure correct measurements, and to set a basis for a solid correlation between remote exposures. Chapters 5 and 7, thereafter, describe and illustrate how the spectral gamma ray tool can be used, and was used to correlate vertical profiles, derive facies indications from the GR data, and to achieve the according model. The current chapter, however, intends to introduce the reader to the topic by providing a general overview to gamma ray logging, with special emphasis on the spectral gamma ray log.

As discussed in the previous section, facies usually are described by their geological characteristics that are known and obtainable for a rock unit. In petroleum geology, and reservoir characterization, petrophysical facies properties are of great importance. Techniques like gamma ray spectrometry are often used to determine petrophysical characteristics of a rock. Thus, rock types rather than facies are more likely to be used in this context. For sedimentological issues gamma ray spectrometry, therefore, provides a supplementary application. The petrophysical facies properties can be used to derive additional data on lithological composition and to identify chronostratigraphic surfaces for sequence stratigraphic correlation more reliable. Due to these prospects gamma ray spectrometry was applied in the course of this study. The more general aspects of this method are outlined below, while the practical application and resulting outcomes are discussed in Chapter 5 and 6.

The gamma ray log in general, is a tool to measure the natural radioactivity of rocks by detecting the gamma rays that are emitted from naturally occurring radioactive elements. They predominantly comprise the isotopes of potassium (K), thorium (Th), and uranium (U). Two kinds of gamma ray (GR) ‘logging-tools’ can be distinguished: The standard gamma ray tool, which does not discriminate between the three mentioned isotopes, and the spectral gamma ray tool, which measures them separately (Coe 2003), and which was used within the scope of this study.

Both the standard and the spectral gamma ray tool generally are used in a broad range of applications, whereas the most common ones comprise (after Rider 2004):

- To derive the shale volume: as shales (or clay minerals) commonly have a relatively high gamma activity. Predominantly the standard GR is used.
- To determine the grain size distribution in a log: as coarse-grained sandstones for example tend to show low gamma ray values, usually much lower than shales.
- To correlate between distinct well logs, vertical sections respectively.
- To derive the concentration of the formations radioactive elements, and to estimate the prevailing clay mineral types using the spectral GR.

Probably all of the GR applications, or at least most of them, have their roots in subsurface geology, mainly originating from petroleum and coal production. The knowledge about the distribution of naturally occurring radioactivity is significant, as it gives indications on depositional environments, which allows identifying and localizing potential hydrocarbon source rocks. Thus, GR measurements, and particularly spectral GR measurements may constitute a very meaningful device, for sedimentological issues. But still, although it would enable a more sophisticated log interpretation regarding depositional environments, mineral content, and sequence stratigraphic pattern, the spectral GR frequently is not included in the logging suite because of some uncertainties in the accuracy of the tool itself (Rider 2004).

Gamma ray logs

The gamma ray log provides information on the radioactivity within a rock volume, by measuring the gamma ray radiation emitted from naturally occurring isotopes of uranium, thorium, and potassium. The standard GR log displays a total gamma count of these three radioactive elements, while the spectral GR log shows the quantity of the individual elements contributing to the total amount of radioactivity (cp. Appendix A for more details regarding natural gamma radiation). The common calibration unit for GR logs is the API unit (American Petroleum Institute), with a typical Midcontinent shale recording at about 100 API units (Ellis 1987, Doveton & Merriam 2004). Spectral GR measurements however are predominantly displayed by the curves of the contributing elements and their ratios, as described below.

Spectral GR measurements, GR spectrometry respectively, terms the technique of measuring the spectrum (quantity and energy) of gamma rays that are emitted during the decay of radioactive isotopes. The radioactive isotopes of potassium, thorium, and uranium, and decay products, respectively, are the main source for the natural

radioactivity. They can be detected by their specific energy levels using the scintillation detector of a gamma ray spectrometer (Schlumberger Ltd. 2006). The corresponding spectral GR data are usually presented as a total gamma ray log in counts per second (cps) and the weight fraction of potassium (wt.%), uranium (µg/g), and thorium (µg/g) (Fig. 3.3). A further log often displayed together with spectral GR logs is the computed (corrected) gamma ray log (CGR) that differs from the spectral GR log by the subtraction of the uranium content. Removing the disruptive influence of uranium provides a better match with clay mineralogy and the shale volume (Doveton & Merriam 2004).

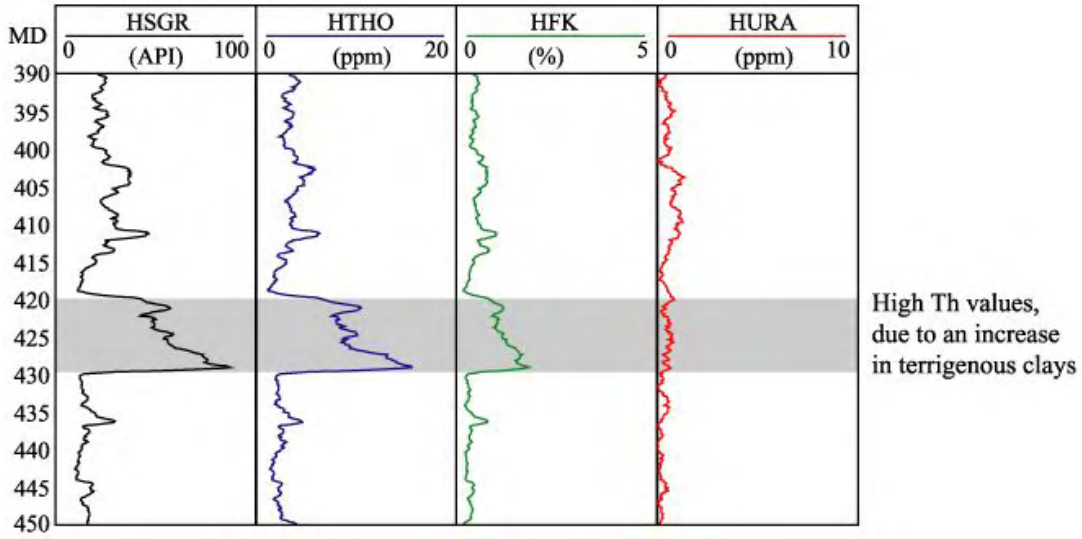

Fig. 3.3: Examples of a spectral gamma ray log; drawn from subsurface investigations and plotted against the mean depth, total counts (HSGR in API), thorium content (HTHO in ppm), potassium content (HFK in %) and uranium content (HURA in ppm). Whereas high Th contents were ascribed to an increase in terrigenous clays (source: IODP-USIO).

The standard GR log is used more qualitatively, to correlate well logs, constrain facies and sedimentary sequences or to identify lithology variations, which are mainly derived from their shale content (Tab. 3.2a). By recording the amount of the three main radioactive isotopes, however, the spectral GR tool provides additional geological information and allows for example to: i) quantify those minerals hosting the radioactive isotopes, ii) determine dominant clay mineral types, and as shown e.g. by Rider (2004) and Selley (1998), iii) to forecast potential source rock occurrences by predicting depositional environments and locating fractures in the subsurface (Tab. 3.2b).

Applications of gamma ray logs

As mentioned earlier shales tend to have a far greater concentration of naturally radioactive isotpes than other sedimentary lithologies. Therefore, GR logs traditionally are used and treated as grain size indicator. But as already denoted, the potentials of GR logs

in general, and spectral GR logs in particular, are more far-reaching and, therefore, should be used beyond the application as a 'simple' shale indicator. A comprehensive description on GR logging and its potentials can be found in Rider (2004) and the literature cited therein. Some of the GR applications that are of major importance for this study are outlined in the following section and summarized in Table 3.4.

Tab. 3.2: Principle application of the standard GR log (a), and the SGR log (b) (after Rider 2004).

a) Principle uses of the gamma ray log			
	Discipline	**Used for**	**Knowing**
Quantitative	Petrophycics	Shale volume	Gamma ray (max) Gamma ray (min)
Qualitative	Geology	Shale	Gamma ray (max) Gamma ray (min)
		Lithology	Typical radioactivity values
		Mineral identification	Mineral radioactivity
	Sedimentology Sequence Stratigraphy	Facies Parasequence & condensed sequence identification	Clay/grain size relationship Clay/grain size & organic content matter/radioactivity relationships
	Stratigraphy	Correlation	-
		Unconformity identification	-
b) Principle uses of the spectral gamma ray log			
	Discipline	**Used for**	**Knowing**
Quantitative	Petrophycics	Shale volume (V_{sh})	Th (max), Th (min) For pure shale
		Radioactive mineral volume	(V_{sh}) (Th), K (max), K (min) for shale
Semi-quantitative and qualitative	Geology	Dominant clay material	Th, K, U content of individual clay minerals
		Detrital clay mineral suite	Radioactive content of individual clay minerals
	Sedimentology & Sequence Stratigraphy	Condensed section recognition from excess uranium	Normal U and Th content or Th/U ratio of shale
		Climate changes	Th/K ratio changes in shale
	Reservoir geology	Fracture detection	Uranium contribution to radioactivity
	Geochemistry	Marine source rock identification	Uranium content of organic matter

Lithology and mineral content: Potassium, thorium, and uranium concentrations measured within a rock formation, can be used to constrain the mineral association (cp. Hurst 1990 and references therein). In a first instance, the GR log can be used to detect lithologic variations. Sandstones, carbonates, and evaporates for example generally are characterized by low or even not detectable GR values (Tab. 3.3).

Tab. 3.3: Average values of radioactive elements in lithologies (source: Schlumberger Ltd. 1972)

Lithology	*Uranium (µg/g)*	*Thorium (µg/g)*	*Potassium wt.%*
Shale	3.7	5.4	1.5
Sandstone	1.0	1.4	0.48
Limestone	1.3	0.5	0.06
Granite	4.0	5.9	1.83

Radioactivity measured within sandstones and other arenaceous rocks, indicate the presence of potassium, thorium, and uranium bearing detrital minerals, e.g. K-feldspars, micas, clay minerals, and heavy minerals. Radioactivity detected in clay mineral free carbonates, commonly indicates the presence of uranium (Rider 2004). Uranium is a trace element in carbonate minerals and can be absorbed by organic matter. Gamma radiation in marls might be dominated by potassium and thorium of clay minerals. U-bearing minerals.

Formation mineralogy: For the characterization of sandstones the thorium and potassium concentrations are the most important data set. A quantitative approach for the identification of clay minerals, using the spectral GR tool was proposed by Quirein et al. (1982): Plotting the contents of thorium and potassium against each other in a Th/K cross plot, illustrates the ratio of the elements, which is suggested to represent distinctive characteristics of clay mineral species and evaporites (Fig. 3.4). But due to the complex chemistry of shales and variable substitution within the clay lattice, however, a restrictive application of this approach turns out to be problematic (Hurst 1990).

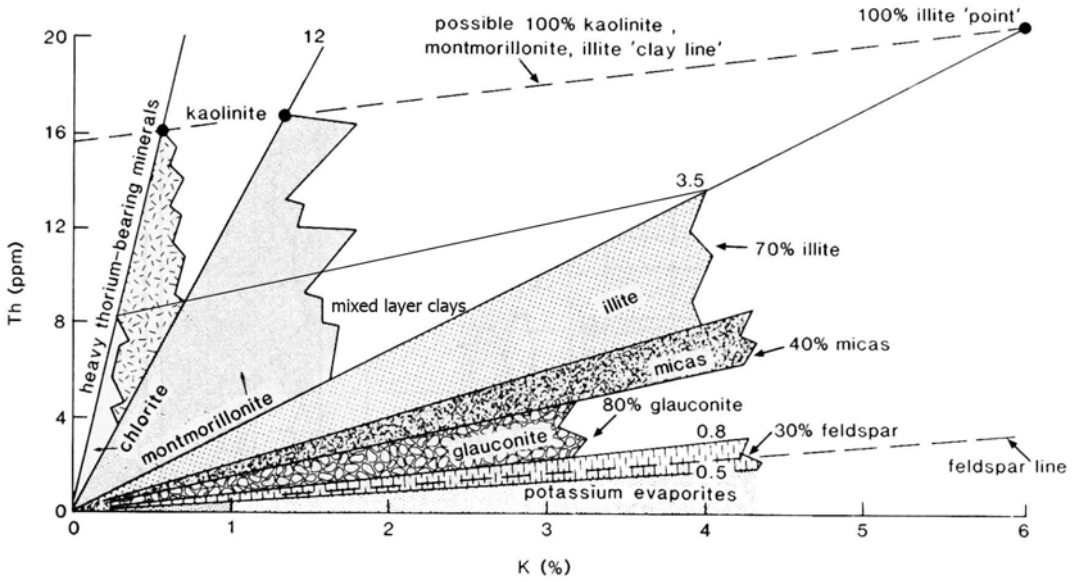

Fig. 3.4: Cross plot of thorium and potassium to identify different types of clay (and other minerals) using spectral GR data (modified after Quirein et al. 1982); displayed is the theoretical distribution of clay minerals, feldspar, heavy minerals and evaporites, in terms of potassium and thorium content.

Paleoclimate: Although the application of Th/K cross plots may be challenging, the knowledge about the Th and K content of a rock formation is particularly interesting to reveal paleoclimate variations. Schnyder et al. (2006) for example used the geochemical behaviour of thorium, potassium, and also uranium as paleoclimate indicator: K gets leached from feldspars and muscovite during kaolinite formation under hot and humid climate conditions, whereas Th commonly gets concentrated during weathering. U generally is more soluble than Th, and thus prone to mobilization during leaching and clay mineral diagenesis. Therefore, particularly the Th/K ratios might be used as paleoclimate indicator (Parkinson 1996).

Correlation: The GR log is one of the most frequently used logs for correlation. Caused by the chemical properties of uranium, thorium, and potassium and the changes in shale-composition etc., the GR value in shales remains constant laterally, but changes vertically. This reveals ideal premises for correlation purpose. Disadvantages however arise from: i) background noise (fine peaks cannot be used for correlation), ii) 'wrong' interpretation of uranium-concentrations triggering distinct signals, iii) calibration of gamma ray tools. As noted e.g. by Rider (2004), absolute values are given by the GR tool, but the logs still need to be normalized to be entirely comparable (Rider 2004). This is true especially for subsurface logging, where different conditions concerning the used tools, drilling mud etc. constitute additional sources of irritation. But also if applied for outcrop studies, the GR logs should be calibrated properly to assure a solid data set; cp. section below concerning calibration.

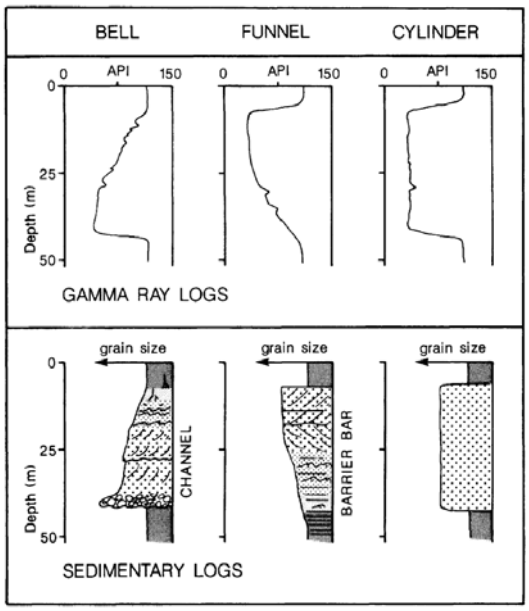

Fig. 3.5a: Basic geometrical gamma ray log shapes and their corresponding sedimentary interpretation (after Serra & Sulpice 1975).

Facies and grain size: GR log shapes, which are defined to display the relationship between grain size and shale content within sandstone bodies, are used to constrain depositional facies of detrital sediments. Funnel-, bell-, and cylinder shape can be distinguished (Fig. 3.5a). Empirically gamma ray funnel shapes mainly result from coarsening-upward succession, e.g. formed by prograding shorelines; while typical bell shapes represent fining-upward successions, e.g. fluviatile sand bodies (Rider 2004).

As this empirical approach of log shape interpretation is lacking a solid facies indicative specification, it is mainly used as an approximation to the depositional environment, but can be of great value in assisting and conforming further observations, as illustrated in Fig. 3.5b.

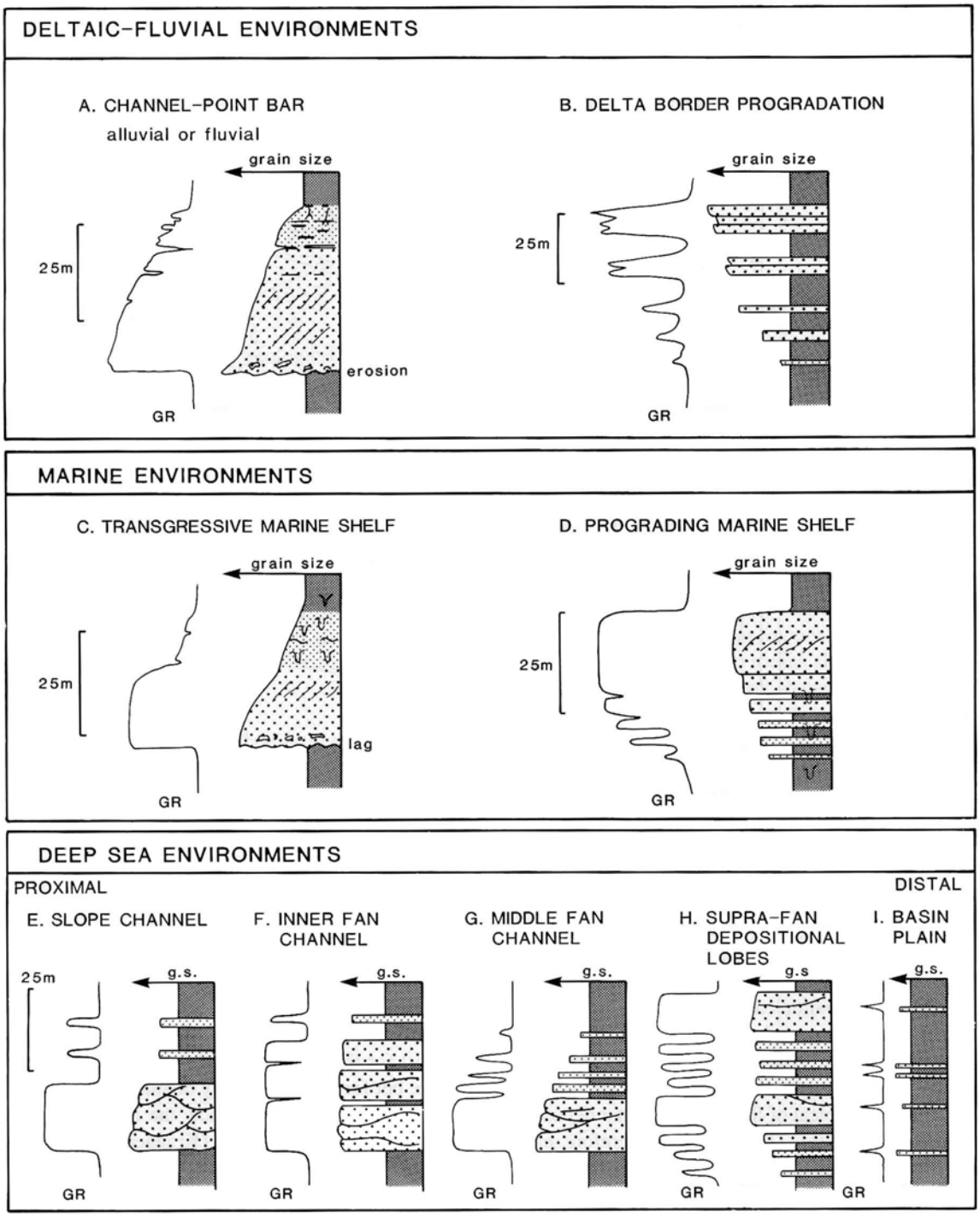

Fig. 3.5b: Gamma ray log shapes and their potential facies indication. Idealized examples of log shapes and sedimentary facies are illustrated (modified after Rider 2004).

Unconformities: Within a succession unconformities can be detected by their high GR values, displayed in the GR log as diagnostic narrow and isolated peaks. This feature can be ascribed to raised or high uranium concentrations. They indicate extreme conditions of deposition that are often associated with unconformities, resulting from starved sedimentation during long time periods.

Depositional environments: Plotting Th/U ratios constitutes an approach to decipher depositional environments and condensed sequences. Although the Th/U ratios are difficult to use as a proxy for depositional environments over a broad range, a general ratio-contrast between transgressive and regressive intervals can be determined (Doveton 1992). Owing to the geochemical behavior of the distinct elements uranium is more likely to be found within marine shales, while thorium occurs more often within terrestrial sediments (cp. Appendix A). Condensed sequences within the marine realm for example tend to show high uranium contents and associated low Th/U ratios, caused by an enrichment of organic matter within a mainly anoxic environment.

A further application for spectral GR logs as a means to constrain some properties of the depositional setting is proposed by Parkinson (1996). Observed variations in Th/K ratios are referred to corresponding proximal-distal relationships, with elevated Th/K ratios associated to more proximal environments. This implies some paleogeographic evidences for a depositional setting, as correlation of Th/K ratios along a ‘timeline’ hence can be used to acquire information about paleo-flow or progradation directions.

Gamma ray logs as sequence stratigraphic device

Considering the log features described above, and how they accomplish the criteria of sequence stratigraphy, led to ascertain that various sequence stratigraphic meaningful surfaces and sedimentary features can be detected by their specific GR response, spectral GR response respectively (Tabs. 3.2 and 3.4). The following section focuses on this approach, and outlines the applicability of gamma ray spectrometry as a means to support sequence stratigraphic analysis and interpretation. Determination of sequence stratigraphic patterns from total and spectral GR logs requires the consideration of the general hierarchy of stratigraphic surfaces and therein-evolved stacking patterns. Accordingly key stratigraphic surfaces need to be identified successively on the log data base before the stratigraphy can be further subdivided into its component systems tracts (Emery & Myers 1996), (Figs. 3.6 and 3.7).

Tab. 3.4: Summary of general features and signatures at key surfaces as observable within spectral gamma ray logs (after Davies & Elliott 1996, Doveton & Merriam 2004, Rider 2004).

General Aspects	***Remarks***
Gamma ray logs	Reading and display of natural radioactivity of rocks – gamma rays emitted by uranium (U), thorium (Th), and potassium (K).
K	K-feldspars, micas, illitic clays.
Th	Concentrated in sand- and silt-sized heavy minerals (monazite and zircon group), fine-grained fraction in association with selected clay minerals and as authigenic phosphates; affinity to terrestrial environments.
U	Occurs within heavy minerals; in anoxic sediments; organic matter; affinity to marine environments.
Th/K ratios, Th/K cross plots	Approach to identify clay minerals and detrital minerals of sandstones, to determine depositional facies, locate condensed horizons, and characterize basin-fill.
Th/U ratios	Indicator of redox potential; proxy for depositional environments and condensed sequences; e.g. low Th/U ratios indicate marine condensed sequences.
Log shapes	Display grain size variations, shale distribution; to constrain depositional facies of siliciclastics; funnel- (coarsen-upward, progradation), bell- (fining-upward, retrogradation, fluvial), cylinder shape (vertical stacking, aggradation).
Surfaces	***Identification***
Sequence boundary	Identification mainly by log response of associated lithology changes; heavy mineral bearing lag deposits may be developed, leading to high gamma ray spikes.
Maximum flooding surfaces:	*GR-spike, U peak, low Th/U ratios* Recognizable by gamma ray peaks and U peak (uranium concentrations in condensed horizons); Most terrestrial igneous rocks, from which sediments are derived, have Th/U ratios of app. 3.8. Sediments deposited in an oxidizing environment will be characterized by higher Th/U ratios (loss of U in its soluble 6+ form), whereas the low Th/U ratios encountered in marine bands result from the concentration of insoluble U^{4+}. Low Th/U ratios (3.8) are diagnostic of maximum flooding surfaces.
Transgressive surface:	Abrupt response
Erosional unconformity surface; Incised valley fills	*Low total counts and high, but variable, Th/K ratios* Decrease in total counts, increase in Th/K values; variable Th/K values, changes in K and Th content; highest Th/K ratio for incised valley fill, low amounts of K-bearing minerals, presence of heavy minerals.
Interfluve paleosol surface	*Low K and exceptionally high Th/K ratios* Low K concentrations are considered to reflect leaching of K during paleosoil formation. Above the interfluve the initial flooding surface is characterised by a return to higher total counts and low Th/K ratios. Combination of high Th/K ratios followed immediately by low Th/K ratios is a distinctive and easily recognized signature.
Successions	***Identification***
Parasequence stacking pattern:	*Th/K ratios* Parasequences are characterized by cycles of decreasing upward total counts. Th/K ratios improve the resolution of parasequences and can also be used to identify parasequence stacking pattern.
Transgressive systems tract	In successive parasequences lower Th/K ratios become predominant.
Parasequence flooding surfaces	Are characterized by a change from low total counts (low K, U, and Th) and high Th/K ratios at the bounding surface to high total counts and low Th/K ratios above.

Key Surfaces:

Sequence boundaries (SB) represent the most important surface within the hierarchy and are identified by their erosional unconformities and their correlative disconformities (Catuneanu 2002). In general they evolve directly beneath the sand-sized sediment fill of depressions on eroded and incised surfaces and over the prograding clinoforms of high stand systems tracts (HST). Thus, they commonly show an abrupt increase in grain sizes (e.g. change from distal marine shales to near shore marine sands), whereas coarse-grained, heavy mineral bearing lag deposits may be developed at the base, leading to high GR 'spikes' (Rider 2004). Although sequence boundaries are not always clear to identify by their GR response, the associated change in lithologic composition that commonly can be noticed may assist.

The **maximum flooding surface (mfs)** marks the bounding surface between coarsening- and/or fining-upward cycles, which are commonly related to deepening and shallowing upward cycles in geological sections, Fig. 3.6 (Catuneanu 2006). Associated to maximum flooding surfaces are thin, fine-grained condensed horizons of marine shelf and basinal sediments, resulting from slow sedimentation rates of pelagic-hemipelagic sediments (Mitchum 1977). These sediments in general are characterized by the presence of cemented starvation surfaces with radioactive and organic rich shales and glauconite, or hardgrounds (Baum and Vail 1988). Therefore, the GR response of maximum flooding surfaces shows a diagnostic 'spike', caused by uranium enrichment, which in turn can be identified by the spectral GR values (Rider 2004).

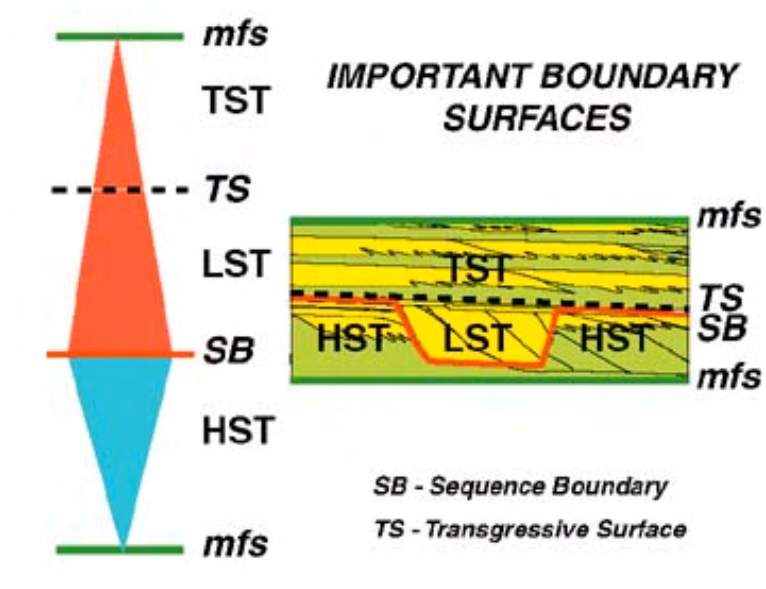

Fig. 3.6: Schematized key stratigraphic surfaces as identified from log data; they build a framework for further stratigraphic subdivision, as illustrated in Fig. 3.7 (Kendall 2003).

The **transgressive surface (TS)** forms the first significant flooding surface of a sequence. The TS commonly is characterized by consolidated muds of firmgrounds or hardgrounds (Baum & Vail 1988), and marks the transition from non-marine to marine sedimentation. As both transgressive and maximum flooding surfaces coincide and correlate with shales, the resulting log response shows similarities. Marine flooding surfaces, however, generally display a rapid but not abrupt upward increase, while transgressive surfaces are characterized by a more abrupt response (Rider 2004).

Although not fully coinciding with the sequence stratigraphic hierarchy of key surfaces, but as a matter of technique, maximum flooding surfaces (mfs) and transgressive surfaces (TS) should be identified first; as in most cases they are much more diagnostic than sequence boundaries (Galloway 1989). Referring to sequence stratigraphic predictions a sequence boundary will be developed between two of the above-mentioned surfaces, making it easier to identify and determine the SB accordingly.

Stacking pattern:

The second, but often also coincident step during the process of log interpretation is to identify vertical facies successions within the stratigraphy. Screening the vertical succession for indicative stacking patterns might reveal (parasequence) stacking pattern (coarsening-, or fining-upwards cycles), and/or distinct systems tracts. Following the sequence stratigraphic approach, the distinct building blocks of a succession are characterized by their bounding surfaces, and consequently can be recognized and defined using the key surfaces described above (Fig. 3.7). In addition, corresponding log shapes (Figs. 3.5a/b) can be used as interpretive devices to define cyclic stacking pattern, showing grain size variations that indicate either progradation, retrogradation or aggradation of a sequence.

The lowstand systems tract (LST) for example comprises progradational to aggradational parasequence sets (Coe 2003), and shows repeated stacking pattern of (Fig. 3.7):

- Cyclic fill of incised depressions that tend to fine upward.
- Cyclic sand to shale bodies of basin floor fans that tend to fine and thin upward.
- Cyclic sand to shale bodies of shelf margin clinoforms that tend to coarsen and thicken upward (Kendall 2005).

Whereas a transgressive systems tract (TST) is recognized as a retrogradational parasequence set (Emery & Myers 1996), and shows repeated stacking pattern of:

- Regressive cyclic shale to sand bodies that tend to coarsen and thin upward (Kendall 2005).

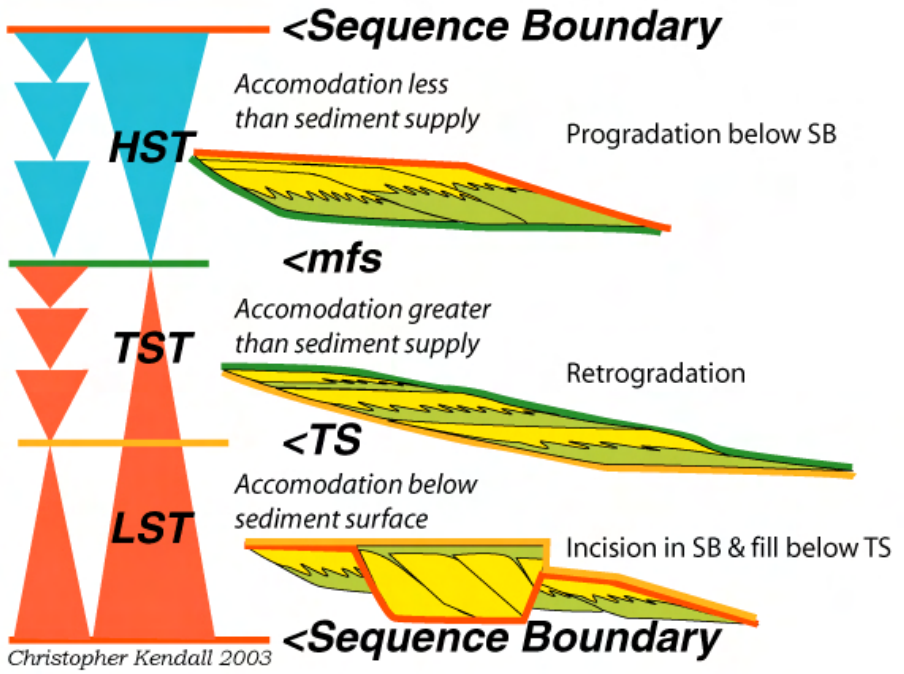

Fig. 3.7: Recognition of key surfaces (Fig. 3.6) allows further subdivision of the stratigraphy into stacking pattern and systems tracts (Emery & Myers 1996, Kendall 2003).

The highstand systems tract (HST) is characterized by progradation and is bounded at its top by a sequence boundary.

Spectral gamma ray (SGR) measurements

The SGR data of the presented study were obtained using an Exploranium GR-320 (manufactured 1996) portable gamma ray spectrometer, with a GPX-21 detector (*GR-320 enviSpec)*. During outcrop measurements, the in-situ concentrations of potassium (K), uranium (U), and thorium (Th), as well as the total radioactivity of the successions were measured with the portable GR-320 spectrometer (Fig. 3.8). The spectrometer system carries out full peak analysis to identify any isotopes in the stripped spectrum, whereas the individual isotope exposure rate is computed using an internal calibration unit (Exploranium Ltd. 2000). The internal calibration unit in combination with the inbuilt computer chip of the measuring console allows to subsequently display the spectra and to calculate the amount of K, U, and Th directly. During the measuring process in the field, data are stored by the chip of the console and afterward can be downloaded using the Exploranium software (GR-320 Explore4). To readout and plot the data from the systems memory, the software reverts to a default calibration sheet to calculate the data before they were finally plotted. There is a significant difference between the ‘raw’ data, initially

displayed on the console and the final data set, plotted by the Explore4 software (raw data for all measurements, however, are documented in the field notes and are accessible from the author). The measured concentrations, thereby, are given in counts per second (cps) for the total counts (TOT), percent for potassium (K %), and parts per million for uranium (U ppm), and thorium (Th ppm). Whereas, following the international regulations the now conventionally used units of weight percent for potassium (wt. %) and microgram per gram (µg/g) for uranium, and thorium are used within this study. The GR-320*enviSpec* is equipped with an automatic gain stabilization performed by the instrument at regular intervals. This reduces the analytical error that may arise from changing conditions in temperature and humidity as well as the risk of errors due to incorrect manual stabilization (Ahmadi & Coe 1998); (cp. Appendix A, for more technical specifications).

Fig. 3.8: Portable gamma ray spectrometer (*GR-320 enviSpec)* as used for outcrop measurements (section Latás, Spain).

Effective sample, sample geometry and area

As already denoted earlier in this section and addressed again, there are several sources of error that are associated to this technique. Thus, to assure the validity of the produced data set it is advisable to carefully frame and follow an appropriate '*measuring protocol*'. Also for the presented study a defined 'measuring protocol', as described in Chapter 4, was followed and tried to maintain. A very crucial point in keeping the analytical error as

low as possible is bounded to the precision while measuring at the rock surface. Parameters that highly affect the amount of GR counts detected by the spectrometer arise from sampling geometry and sampling region, as described e.g. by Myers & Wignall (1987), Parkinson (1996), Ahmadi & Coe (1998). The detector of the used portable device is 11.4 cm in diameter (front-side) and 39.4 cm long; the detected target rock, however, is much broader in general. The effective sample recorded by the scintillation detector can be described by a bowl shaped volume, with thickness of about 14-15 cm and surface diameter of 80-100 cm, as shown in Fig. 3.9 (Myers & Wignall 1987). Løvborg et al. (1971) calculated a volume of 49 kg as effective sample for a rock-density of 2.8 g/cm^3; whereas the exact sample volume (thickness and diameter) gathered by the detector depends on the density and the absorption coefficient of the measured material.

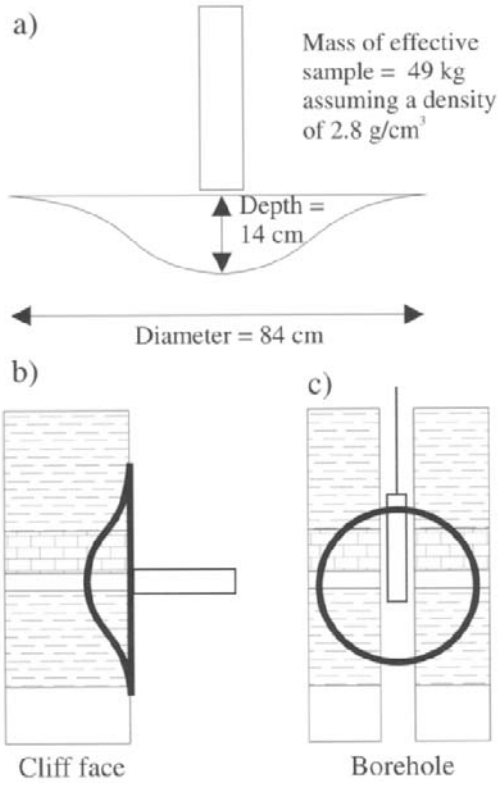

Fig. 3.9: Effective sample of gamma ray detection on the example of field and borehole measurements (after Løvborg et al. 1971, and Ahmadi 1998), illustrating the influence of adjacent beds and importance of sample geometry and area (cp. Fig. 3.10).

Within this bowl-shaped area radioactive decay is striking the detector, the measured radiation, therefore, displays a 'compound-value', instead of precise record of a specific measuring point with 11.4 cm in diameter. The bulk of measured gamma ray counts, however, is gained from a cylinder-shaped volume in straight extension of the detector. This clearly shows that measuring within too small spacing will result in smeared values, as next beds will influence the measurement, therefore, a general spacing of about one metre was maintained for this study. Furthermore, sample geometry and area decisively influence the amount of detected gamma radiation; overhangs for example should be avoided, as more radiation will be recorded, while measuring close at a cliff will give lower values in relation to general measurement.

Figure 3.10 sketches possible errors that might arise from the measuring process in relation to sample geometry and area. The following Chapter 4, which attends to the

calibration procedure, addresses the issue of effective sample, sample geometry, and area again.

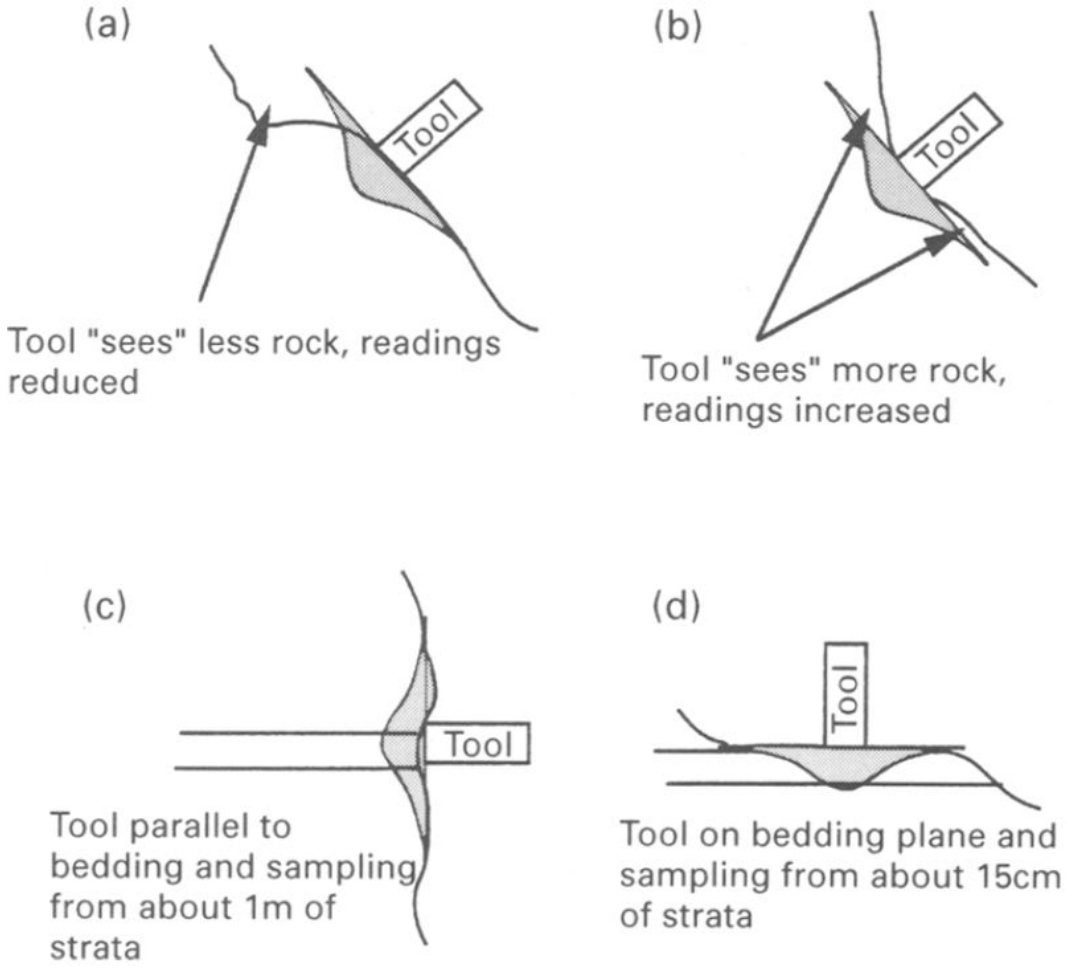

Fig. 3.10: The effects of sampling geometry and region during field spectral gamma ray measurements, with an approximation for the effective sample for a spectrometer of the type used in this study shown in grey (Parkinson 1996). (a) & (b): Uneven surfaces, cliffs and overhangs will cause either reduced or increased readings; (c) & (d): as tool resolution is ~ 1 m in diameter and ~ 0.15 m in depth, measurements parallel to bedding (c) might give a mixed value, while measurements on the bedding plane (d) will give best results (if bed thickness ≥ 0.15 m).

3.2.3 Sequence stratigraphic interpretation

The information obtained from standard facies analysis and gamma ray logs are basic parameters for this study. They provide building blocks of the aimed depositional model, and the foundation for stratigraphic correlation. As single methods they present ‘snapshots’ of the past but the comprehensive image of the past depositional setting is still lacking. The linking element forms the sequence stratigraphy, the application and interpretation of sequence stratigraphic principles respectively. Using the concept of timelines lateral transects were constructed on the basis of vertical profiles. Maximum

flooding surfaces and transgressive surfaces for example, often are expressed by well-exposed surfaces and form marker horizons, which can be followed over wide distances. As they generally separate older from younger deposits, they can be regarded as time lines. Accordant time lines, tracing horizons respectively, were achieved by physical and optical tracing of marker horizons and key stratigraphic surfaces, which in turn allows to generate a lateral transect. Owing to the good outcrop quality within the studying area, it was possible to walk out almost all of the major bounding surfaces and to correlate specified horizons between individual profiles. The main part of correlation was done in the field by physical tracing. In cases, however, where physical tracing was not possible, and as further backup, optical tracing of photo-panels and aerial photographs was executed. Two lateral transects, one along each limb of the anticline were achieved.

In a comparable approach of correlating vertical profiles, the spectral gamma ray logs were used as basis to establish lateral transects. Correlation was performed using marker beds, key surfaces respectively (cp. Tab. 3.4), and log pattern; whereas lihological boundaries were picked at the shoulder of gamma ray curves to take account of readings, which smear across bed boundaries. The correlated patterns, thereby, may represent vertical facies successions, superimposed facies successions, or unconformity-bounded units (Cant 1992). For the final link-up of remote sections further identification schemes and features, like element ratios, and facies indications (Fig. 3.5b) were used. Pattern matching, as described by Cant (1992), thereby, poses a nice technique for the correlation of logs also in difficult cases. By matching pattern, correlations are made on the basis of log shapes, comprising a succession of several beds or bedsets, rather than on individual peaks or marker horizons. Pattern matching may allow correlation even where lateral variations in lithologies, facies, and thicknesses of units have occurred. Logs can be correlated for a best overall fit, e.g. by overlying adjacent logs. Constantly shifting positions of fit may indicate lateral changes in facies or thickness, and may indicate synsedimentary tectonism (Cant 1992). Further considerations on the application of spectral gamma ray log as sequence stratigraphic device were discussed in the previous section.

The obtained lateral transects of both methods were compared, integrated, and interpreted following sequence stratigraphic principles. Based on this sequence stratigraphic approach the evolution of the depositional system in space and time can be acquired, as well as a correlation between the northern and the southern lateral transects. This conclusively allows the generation of a depositional model for the SSt-Succession, as well as a more regional consideration of the SSt-Succession in the context of the South Pyrenean Foreland.

3.2.4 Low-Temperature Thermochronology

Low-temperature thermochronology in general, and (U-Th)/He dating in particular still rank among the rather infrequently used techniques in sedimentological research, and often are affiliated with misunderstandings concerning their implications. The purpose of this section, therefore, is to introduce the principles and objectives of low-temperature thermochronology with a short excursion back to its roots, for a better understanding of the fundamental idea of this approach. After this general part, a brief description of the sample preparation process is given, followed by an outline of the (U-Th)/He dating technique, as applied in this study. A more detailed description of the preparation procedure is shown in the Appendix C.

Historical synopsis

Over the last decade one of the major advances in low-temperature thermochronology has been the development of (U-Th)/He dating techniques. Arising from the perception that the radiogenic helium isotope ^{4}He is released during alpha decay of uranium, thorium, and samarium decay chains, first attempts of radiometric dating were encouraged (cp. Reiners 2002, and references therein for more details on the historical aspects). Already in the beginning of the 20th century Ernest Rutherford used uranium, helium, and radon concentrations of U-rich minerals to calculate their ages. Another “pioneer” in radiometric age determination was Strutt (~1905), who tried to determine the age of a mineral, using its accumulated He content and thus marked the beginning of radiometric chronometry. During the first half of the 20th century the U/He method constituted the first and leading geochronologic method (Wagner 1998).

The facts that alpha decay is frequent and the analytical detection of He feasible, are preconditions for U/He dating, making it an attractive method. But as the yielded U/He ages frequently turned out to be unreliable and inexplicably low, compared to other dating methods, it was generally recognized that most minerals were extremely ‘leaky’ for He and thus the technique was essentially abandoned (Harrison & Zeitler 2005). In the cause of renewed research on the thermal diffusivity of He during the 1980ies and 1990ies (e.g. Zeitler et al. 1987) a better understanding of the basic parameters controlling the He retention in minerals was achieved, leading to a re-evaluation of the method from a thermochronological perspective. First experiments on apatite confirmed that He loss actually followed straightforward predictions of thermally activated volume diffusion, and that apatite (U-Th)/He ages effectively date the time elapsed since cooling through low temperatures (Zeitler et al. 1987). Based on this knowledge, research further on focused on the development of technical methods to better understand and characterize He

diffusion properties (Farley 2000). While the first experiments by Zeitler et al. (1987) indicated a “closure temperature” for the apatite (U-Th)/He system of about 100°C/10Myr., it is currently set at ~70-85 °C (e.g. Warnock et al. 1997; Wolf et al. 1998; Farley 2000). And the achieved (U-Th)/He ages now are interpreted as ‘cooling ages’ for very low temperatures (Lippolt et al. 1994, Wolf et al. 1996). The discussed temperature range for the apatite system, thereby, has a much wider array, as it is amongst other features highly depending on the crystal size (Reiners & Farley 2001). Due to the fast-paced research in thermochronology, owing to improved analytical techniques, and analysis of further mineral phases, specifications are subjected to permanent changes, are refined and updated. Over the past decade, (U-Th)/He dating of apatite developed to a well-established technique, and is at the point of becoming a more widely applied method in tectonic and geomorphologic studies. Apatite He-dating enables to constrain the timing and rates of cooling through a certain isotherm (T_C ~70 °C/10 Myr.) erosional and/or tectonic exhumation processes through the upper crustal part, corresponding to depths of about 1.5-3 km that can be evaluated for many settings.

The apatite He-thermochronometer, therefore, should perfectly resolve the denudation history of the working area, which still is described only allusively (e.g. Puigdefàbregas 1975, Hogan & Burbank 1996). Thus, apatite (U-Th)/He dating was used to constrain the thermal and denudation history of the upper part of the Jaca Basin. This allows to constrain the overburden on top of the SSt-Succession and, therefore, enables a better correlation with adjacent basins. And, furthermore, it allows to evaluate maximum temperatures that might have affected the succession, which is an important aspect regarding the interpretation of the spectral gamma ray logs.

The following sections concentrate on methodological and analytical aspects of the (U-Th)/He chronometry of apatite. For more detailed accounts the interested reader might refer to Reiners & Brandon (2006), Hodges (2003), Farley (2002), and references therein.

(U-Th)/He Chronometry

The (U-Th)/He method is based on the accumulation of helium ^{4}He, generated by alpha decay of the parent isotopes ^{238}U, ^{235}U, ^{232}Th decay chain, and the decay of ^{147}Sm. The vast majority of ^{4}He in most materials, however, is ultimately derived from uranium (U) and thorium (Th), because of the relatively short half-lives and greater abundance of U and Th than that of the next most important alpha producer, ^{147}Sm (Reiners & Nicolescu 2005). Radiogenic ^{4}He diffuses out of the mineral at a rate determined by the temperature and the helium (He) diffusivity of the mineral. Thus, the concentrations of ^{4}He and the parent isotopes can be used to calculate a He cooling age (Reiners & Brandon 2006).

The general age equation for the (U-Th)/He system (for rocks older ~300ka-400ka), including Sm and ignoring the potential for initial U or Th isotope disequilibrium (e.g. Farley et al. 2002) is:

$$^{4}He = 8\,^{238}U(\exp(\lambda_{238}t)-1) + 7\,^{235}U(\exp(\lambda_{235}t)-1)) + 6\,^{232}Th(\exp(\lambda_{232}t)-1)) + ^{147}Sm(\exp(\lambda_{147}t)-1)$$

^{4}He, ^{238}U, ^{235}U, ^{232}Th and ^{147}Sm refer to the present day isotopes,
λ's refer to the decay constants of the appropriate parent nuclides,
t refer to the (U-Th)/He–age (Reiners 2002, Reiners & Nicolescu 2005).

Thus, the amount of ^{4}He produced mainly depends on the half-lives of the parent isotopes involved in the decay series (Tab. 3.5).

Tab. 3.5: Half lives and decay constants for the main alpha particle producing isotopic decay systems (after Blum 1995).

System	*Decay type*	$T_{1/2}$ (10^{10} yr)	λ (10^{-10} yr^{-1})
^{238}U – ^{206}Pb	8α + 6β	0.446830	1.55130
^{235}U – ^{205}Pb	7α + 4β	0.070381	98.48500
^{232}Th – ^{208}Pb	6α + 4β	1.401000	0.49480
^{147}Sm – ^{143}Nd	1α	10.600000	0.06539

An important and somehow complicating aspect of (U-Th)/He dating is connected to the average α stopping distances. The α-stopping distance is a function of α-particle energy, as well as the composition and specific density of the mineral. The covered distance mainly depends on the parent nuclei that transmit energy to their ejected alpha particles, enabling them to pass through the crystal lattice before they run out of energy and are stopped. Each α-decay within the U and Th series has a characteristic energy and hence a characteristic and well-known stopping distance within a given material (Farley 2002). The average stopping distances of α particles in apatite range between ~15-20 µm, and therefore are, in most cases, sufficiently large relative to the size of the crystals dated (typically 100-200 µm) (Farley et al. 1996). The stopping distance can have a considerable effect on the He age, as part of the α-particles in the 15-20 µm rim of a crystal are ejected out of the crystal and will not be retained. In addition, α-particles from surrounding mineral phases potentially are implanted into the crystal of interest (Farley 2002). For a reliable α-ejection correction, the characterization of grain size and shape during the selecting process of the crystal is crucial, because the fractional alpha retention typically is determined as a function of crystal geometry and dimensions. In general, this approach is successful, but it is not feasible, or valid, for samples with known inhomogeneous U, Th distribution (Farley et al. 1996, Farley 2002, Hourigan et al. 2005), or samples subjected to extremely slow cooling (Meesters & Dunai 2002a, 2002b).

As mentioned above, He diffusion behaviour constitutes one basic aspect of the (U-Th)/He dating technique. In various laboratories, step-heating experiments have indicated that the rate of He loss can be regarded as a function of temperature and time, following the general principles of volume diffusion (Lippolt et al. 1994, Wolf et al. 1996 & 1998, Farley 2000). The diffusivity thereby, in general is described by the *closure temperature* T_C of the mineral grains accumulating radiogenic He.

The closure temperature depends on:

- the activation energy (E),
- geometric factor for the crystal form (A),
- thermal diffusivity (D_0),
- length of the average diffusion pathway from the interior to the surface of the grain (a),
- cooling rate at closure temperature (dT/dt) (Dodson 1973).

The closure temperature for the apatite (U-Th)/He system is in the range of 75 ±7 °C for a simple monotonic cooling rate of 10 °C/Ma., a subgrain domain size ~60 µm, an activation energy (E_a) of about 36 kcal/mol, and a log(D_0) of 7.7 ±0.6 cm^2/s (Wolf et al. 1996). Farley proposed E_a = 33 ±0.5 kcal/mol with log(D_0) = 1.5 ±0.6 cm^2/s for Durango apatite. The implied He closure temperature for a grain of 100 µm radius is 68°C assuming a 10°C/Myr cooling rate. The closure temperature concept is only appropriate for uniform and moderate to rapid cooling from temperatures corresponding to complete He diffusive loss to complete He retention. For such thermal histories, the calculated (U-Th)/He ages are estimates of the time elapsed since cooling through a relatively narrow temperature range, where the crystal size and chemistry does not influence the (U-Th)/He ages of apatite (Warnock et al. 1997, Wolf et al. 1998, Reiners & Farley 2001, Farley 2002, Ehlers & Farley 2003). If the cooling rate is slow relative to the He production or if He was only partially retained in the crystal for long periods of time, the He content and, therefore, the calculated (U-Th)/He ages of a crystal can be strongly dependent on variations in fractional He loss caused by crystal size variations. Wolf et al. (1998) describe solutions for the full radiogenic ingrowth-diffusion equation for different geological situations. The He production and diffusion model assumes a homogenous distribution of U and Th in secular equilibrium and that He is lost only by volume diffusion. Spherical diffusion geometry is assumed (Wolf et al. 1996).

The basic results of such simulations after Reiners & Farley (2001) are:

- The differences in age between small and large crystal size are greatest in the temperature range between ~30 to 75 °C, assuming constant reaction time.
- The difference in age with crystal size increases with time at a given depth.
- The depth (and temperature) of the maximum age difference decreases with time.

Furthermore, nowadays, a He partial retention zone between 40 and 90 °C is assumed (Wolf et al. 1998). Meesters & Dunai (2002a,b) generalized the production-diffusion equations to diffusion domains of various shapes and arbitrary cooling histories. Their set of equations allows calculating the α-ejection corrected ages and accounts for non-homogeneous distribution of uranium and thorium. The equations presented by Meesters & Dunai (2002a,b), and Dunai (2005) can be applied to all radiogenic He-bearing minerals.

More profound details of measurement techniques and general interpretations can be found in further reading literature, given e.g. by Reiners & Ehlers (2005).

Analytical work and dating procedure

As mentioned, radiogenic ^{4}He diffuses out of the mineral at a rate determined by the temperature and the He diffusivity of the mineral. Thus the concentration of ^{4}He and corresponding parent isotopes of the mineral need to be determined, to calculate the He cooling age. A two-stage analytical measurement process was accomplished to determine the particular isotope concentrations (see also Reiners & Brandon 2006):

- He-Line: Degassing of the apatite crystal by heating the crystal with a laser beam, followed by measuring of ^{4}He with a gas-source mass spectrometer.
- ICP-MS: Measuring of U, Th, and Sm on the same crystal with an inductively-coupled plasma mass spectrometer (ICP-MS).

As for all these measurements, appropriate apatite-grains are needed; apatite-bearing rock-samples have to be sampled and prepared in a first step.

Sampling and sample preparation

During the fieldwork 20 bedrock samples were collected within the siliciclastic series of the Jaca Basin, to extract heavy mineral concentrates for thermochronological analysis. As part of the accessory mineral suite, apatites commonly constitute less than 1% of the

bulk. Therefore, for each rock sample about 2-5 kg were taken, to assure a maximum likelihood for a sufficient amount of apatite crystals.

The apatite concentrates were obtained by applying standard heavy mineral separation techniques performed at the laboratory of the Research Center in Archaeometry of the Academy for Science at the Max-Planck-Institute for Nuclear Physics of Heidelberg. Further crucial minerals extracted in the course of the separation process (e.g. micas, zircons) routinely are stored separately for later investigations. For the separation process, the rock samples were cleaned from organic soiling and dirt to avoid any contamination. After drying at temperatures T < 30 °C, the rock samples were crushed successively into smaller fragments, using a jaw crusher and a rotary disc mill, until the sample was disaggregated to a sand-sized fraction. After each throughput the material was sieved with a 500 µm mesh, separating small-size fragments and mineral grains, to avoid destroying of already disaggregated mineral grains by further crushing. With the shaking table (Wilfley Table) a first separation of heavy and light components was achieved, followed by heavy liquid separation (using LST and methyl iodide) and magnetic separation. After the final separation with methyl iodide suitable apatite grains were picked for subsequent He-analyses, which were performed at Kline Lab (Yale University). The apatite concentrate, therefore, was searched through under the microscope to select appropriate apatite crystals by hand picking, using some fine tweezers. Suitable apatite crystals for (U-Th)/He dating should be (e.g. Ehlers & Farley 2003):

- large enough – at least 60 µm in diameter,
- free of inclusions,
- well shaped – preferably euhedral.

The selected grains for He analysis, therefore, were carefully inspected and from each sample at least two apatite crystals were picked, their dimensions measured, and digitally photographed (Fig. 3.11). Afterwards each crystal was loaded into a 1-mm U-free Pt-foil tube and ‘wrapped’ properly to prevent the crystal from getting lost (Mitchell & Reiners 2003). Subsequently the Pt-packages were loaded into a sample holder with 32 slots (Fig. 3.11), and set for the He-extraction (He-Line) and further analytical measurements (ICP-MS) as described by House et al. (2000); (cp. Appendix C for more details on the separation procedure).

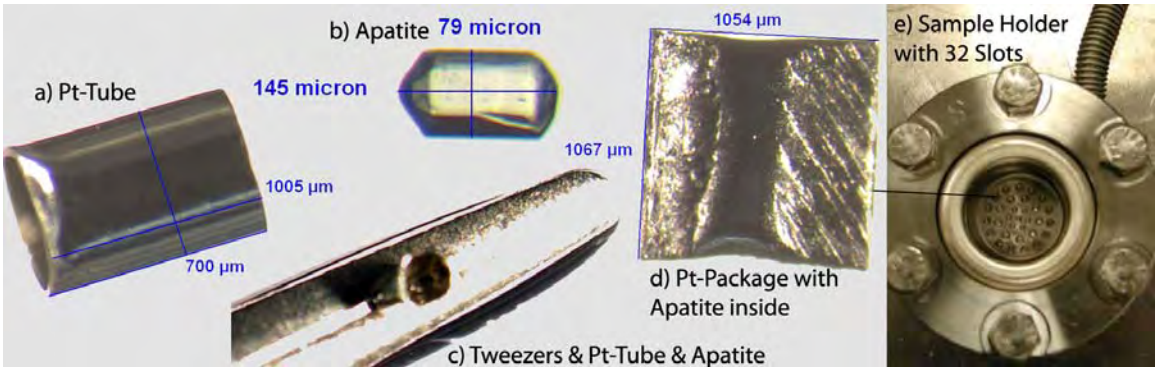

Fig. 3.11: Examples from the sample selection and preparation process: a) platinum tube; b) sub-euhedral apatite crystal with pyramidal habit; c) wrapping of the apatite; d) closed Pt-foil with apatite inside; e) sample holder with 32 sample slots for He-degassing (Kline Laboratory, Yale University).

Analytical Methods – dating procedure

The three quantities that are important for the (U-Th)/He age determination, comprising alpha-ejection, He-content, and U- and Th-content were measured on a single aliquot, i.e. a single crystal, to eliminate uncertainties that may arise from grain to grain heterogeneities, e.g. in element concentration (Farley 2002, Stockli 2005). Therefore, each package (Pt-foil) contains just one crystal (see above).

a) Measuring He-content:

To determine the He-content, the single crystal aliquots (packages) were loaded into a stainless steel sample planchet with 32 sample slots and transferred into a laser cell. After vacuum was generated the samples were heated to initiate the degassing process. The procedure of sample treatment and measuring follows the method developed and described by House et al. (2000). Each sample package was heated on the Nd-YAG laser (with about 1-5 W) for three minutes to degas He. During the heating process (degassing respectively) the foil package shows a bright white glow, which is monitored via a screen, to adjust the laser energy if necessary; the reached temperatures are not measured directly but are estimated from experiments to be at ~900-1250 °C. As reference, ^{4}He blanks were determined by heating empty foil packets, using the same procedure. After degassing the liberated gas from the sample was spiked, cryogenically concentrated, purified, and quantified (cp. Mitchell & Reiners 2003):

- Spiking with ~0.4 pmol of ^{3}He;
- Cryogenical concentration at 16K on a charcoal trap (condensation time calibrated for no significant ^{4}He/^{3}He fractionation);
- Purification by release at 37K;

- Quantification by measuring of $^{4}He/^{3}He$ ratios on a quadrupole mass spectrometer next to a cold Zr-alloy getter.

All $^{4}He/^{3}He$ sample ratios were referenced to multiple same-day measured $^{4}He/^{3}He$ ratios of ^{3}He-spiked ^{4}He standards of known volume, processed in the same way. Linearity of the $^{4}He/^{3}He$ ratio with ^{4}He pressure over the range of observed unknown $^{4}He/^{3}He$ ratios has been confirmed by spiked ^{4}He-standard gas-splitting, with varying ^{4}He pressure over more than three orders of magnitude, and age determination of Durango apatite aliquots with varying ^{4}He intensities over more than four orders of magnitude. ^{4}He standard reproducibility averages 0.2 % on a daily and long-term (tank-depletion correction) basis. Estimated 2σ analytical uncertainties on sample He determinations, including precision and accuracy from original manometric ^{4}He standard calibrations, is 1-2% (Mitchell & Reiners 2003).

This laser heating method has the advantage of significantly lower He blanks and greater sample throughput. Furthermore, applying this method offers the great advantage, at least for apatite, that the Pt-foils (U-free) after heating can be directly immersed in nitric acid and the grains inside dissolved for U-Th-Sm analysis without the often difficult task of transferring the degassed apatite crystal from the foil to another vial.

b) Measuring U-, Th-, and Sm-content:

- The parent nuclide contents were measured by isotope dilution using solution ICP-MS. The general preparation procedures used in the Yale He dating lab involve addition of isotopically distinctive U, Th, and Sm spikes to the crystal recovered and dissolved after degassing. Final solutions run on the ICP-MS are diluted to about 2-4 ml in total volume, and are ~5-10 % HNO_3, in some cases with ~0.5 % HF. Concentrations of spike isotopes in resulting solutions are ~0.1-0.2 ppb, and the vast majority of natural U and Th concentrations are within 0.5-10 times these concentrations. In detail, different minerals require very different dissolution and dilution procedures. Kline Lab uses nominally pure ^{233}U, ^{229}Th, and the enriched ^{147}Sm spike of Wasserburg (1981) for spiking (Reiners & Nicolescu 2005).

- At Kline Lab, Pt foils with degassed apatite crystals are spiked with two different spike solutions, each in 5% HNO_3 solution. The first is 25 or 50 µl of a nominally pure ^{233}U-^{229}Th spike with total U and Th concentrations of 7.57 ± 0.10 ng/ml and 12.3 ± 0.10 ng/ml respectively (uncertainties are long-term standard deviations of all concentrations determined by spiking normal solutions of assumed known U-Th concentrations). The second is 25 or 50 µl of an enriched (97 %) ^{147}Sm spike with a total Sm concentration of 10.8 ± 0.10 ng/ml. Following spiking, 200 µl of

concentrated SeaStar Baseline HNO_3 is then added to each foil, and the mixture is heated at about 90 °C for two hours. After cooling, the solutions are diluted with 2.5 ml of double-distilled 18 MΩ H_2O, for final spike isotope concentrations of ~0.1-0.2 ppb (Reiners & Nicolescu 2005).

- Following degassing, samples were retrieved from the laser cell, spiked with a calibrated ^{229}Th and ^{233}U solution, and dissolved. The apatites were dissolved in-situ from Pt-tubes in ~30% HNO_3 in Teflon vials. Each sample batch was prepared with a series of procedural blanks (Pt-foil blanks) and spiked normals to check the purity and calibration of the reagents and spikes (for more details cp. Reiners & Nicolescu 2005). Spiked solutions were analyzed as 0.5 ml of ~1-5 ppb U-Th solutions by isotope dilution on a Finnigan Element2 ICP-MS with a Teflon micro-flow nebulizer and double-pass spray chamber. Procedural U and Th blanks by this method are 1 ± 0.5 pg and 2 ± 1 pg (pg=pictogram), respectively. Routine in-run precisions and long-term reproducibilities of standard $^{232}Th/^{229}Th$ and $^{238}U/^{233}U$ are 0.1-0.4%, and estimated uncertainty on sample U-Th contents are estimated to be 1-2% (2σ) (Mitchell & Reiners, 2003).

c) Determination of α-ejection:

Alpha ejection was corrected using the method of Farley (2002). Replicate analyses of Durango apatite during the period of these analyses yielded mean ages of 32.5 ± 1.6 Ma (2σ). On the basis of reproducibility of these and other intralab standards, for this study an analytical uncertainty of 3% (1σ) was estimated for apatite age determination.

One major concern for apatite (U-Th)/He dating in general is the potential for incomplete dissolution of U-Th-bearing inclusions, which can lead to apparently unsupported He and overestimated He ages. This potential is well recognized and motivates careful screening processes during initial sample picking to exclude crystals with inclusions visible under plane-polarized and cross-polarized light at 120-160 times magnification (Reiners 2005).

In some cases, small but high-U-Th inclusions may be difficult or impossible to detect by normal picking procedures (Farley & Stockli 2002). Adoption of more aggressive dissolution procedures designed to attack refractory inclusions may recover U-Th and avoid the unsupported He problem, but in most cases resulting ages would still suffer from α-ejection correction inaccuracies caused by the inclusions. As recently demonstrated by Vermeesch et al. (2006) it is possible to avoid these problems by dissolving the apatites and their mineral inclusions, applying a complex dissolution method, using more aggressive acids such as HF.

Grain ages typically have a relative standard error (RSE) of approximately 3% to 5%, as determined by replicate measurements (Reiners & Brandon 2006). The analytical methods and apatite dating technique described above were performed at Kline Lab (Yale University). They correspond to the current technique and follow the procedures as described by House et al. (2000), Reiners & Nicolescu (2005), and Mitchell & Reiners (2003).

Chapter 4 – Gamma Ray Spectrometer Calibration

This chapter ties up to Chapter 3.2.2, and addresses the issues of outcrop gamma ray measurement and the necessary calibration of the device in detail. Despite of the general measuring process that demands the mentioned measuring protocol, another very important aspect regarding the reliability of the produced data is associated to the calibration of the system used. Although the automatic stabilization and data computing performed by the GR device, has the great advantage of reducing some pitfalls, and facilitating subsequent analysis, there are also some disadvantages connected to this system, as it reveals a kind of 'black box' with internal calibration processes. As a fundamental part of this study is based on gamma ray logs, a solid and reproducible calibration was required. Thus, a calibration scheme was set up to prove the data given by the GR-320 system and to evaluate their qualitative and quantitative use.

To monitor potential analytical drift of the used GR-320*enviSpec*, and to ascertain an accurate calibration of the obtained data, standard measurements and adequate analyses were performed. The measurements were carried out both in the field by the GR-320*enviSpec* and in the laboratory, by the Canberra spectrometer (Canberra-Spec), whereas for all field measurements (Jaca Basin, Spain, and Southern Odenwald, Germany) the basic measuring protocol described in Chapter 5 was followed routinely. Laboratory measurement were performed at the Research Centre in Archeometry of the Academy for Science at the Max-Planck-Institute for Nuclear Physics of Heidelberg (Forschungsstelle Archäometrie der Heidelberger Akademie der Wissenschaften am Max-Planck-Institut für Kernphysik), using a high purity coaxial germanium gamma spectrometer, 'FH' (Canberra-Packard Ltd.); detailed descriptions of laboratory gamma ray spectrometry and the Canberra system used, can be found in Kalchgruber (2002). The laboratory measurements were run on representative rock samples from the field and on standard reference material. As standards the intralab 'Nussi' standard (Nussloch Loess), and geochemical reference material purchased from the U.S. Geological Survey were used. Applying this approach it was possible to execute appropriate parameters for the calibration of the system, and hence to reference the data set that was obtained from field measurements to 'Nussi' and international USGS standards.

The calibration process of the GR-320 instrument comprises the following steps:

A. Field measurements by the GR-320*enviSpec*:

- System test before each measuring series, referencing to a ^{137}Cs-source (resolution < 9 % FWHM 662 keV).
- Test series of outcrop measurements on various lithologies with different time intervals.
- Outcrop measurements and subsequent sampling of representative rock specimens for laboratory measurements.

B. Laboratory measurements by the Canberra Spectrometer:

- Laboratory measurements of intralab standard, and international standards.
- Laboratory measurements of representative rock samples.

C. Resulting calibration:

- Referencing of the Canberra spectrometer to international standards and intralab 'Nussi' standard.
- Referencing of the portable GR-320 spectrometer to the Canberra spectrometer.

The main results of the experimental calibration are delineated below, followed by a short excursus, which illustrated the issues of effective sample, sample geometry and area. A record of processed measuring series is attached to Appendix A.

4.1 Field measurements

4.1.1 System Test

A system test was run on the instrument before each measuring series in the field to assure that the system was not affected in its function. During the system test, the GR-320*enviSpec* carries out automatic gain stabilization, and a check of basic system performance. Referring to the users manual (Exploranium Ltd. 2000), the performed gain stabilization is based on the following modus operandi:

"When the system test is started, a preliminary gain is computed after a 10 second (s) measurement and then the spectrum is reset and accumulation starts again. When the caesium peak exceeds the 5000 count level threshold (typically after 20 s), the system computes the correct gain using a least squares fit of a Gaussian peak shape. This is referred to as the *fine gain*. After the *fine gain* has been computed the spectrum is reset and the cycle is repeated. The *fine gain* is continuously updated every time the 5000 level

is exceeded (typically 40 s) until the system test is terminated. This ensures that System Gain is always correct."

4.1.2 Test Measurements on various lithologies with different time intervals

For the portable gamma ray spectrometer used, the time intervals of measuring can be set manually. The accessible sampling time ranges from 1 to 9999 s. Depending on the scope of the conducted measurements, the investigated rocks and the time available for the measurements, an appropriate sampling time has to be selected. The proposed time intervals for outcrop measurements of sediments using a portable gamma ray spectrometer range from 10 s (Postma 1999) up to 10 min (Myers & Wignall 1987). Before systematic field measurements on vertical sections of the working area were carried out, a series of test measurements on fine-grained marls and on coarse-grained sandstones were processed to set an appropriate count period, and to estimate the potential error that might arise from this count period. The selected coarse-grained sandstone, thereby, represents a lithology characterized by low gamma ray response and approximates the lower limit of natural radioactivity that was expected to occur within the examined successions. For the test series a specific measuring area for both lithologies was chosen and maintained. The measurements were performed twice, with measuring times set for 60, 90, 120, and 180 s, whereas for the sandstone additional measurements set for 210 and 240 s were performed (Tab. 4.1).

Tab. 4.1: Mean values for potassium (K wt. %), thorium (Th µg/g), and uranium (U µg/g) from outcrop test measurements in the working area, Jaca Basin, Spain (SSt-Succession).

Sample	*Measuring Time*		*Mean K*		*Mean Th*		*Mean U*	
	s	*Std.*	*wt. %*	*Std.*	*µg/g*	*Std.*	*µg/g*	*Std.*
Sandstone, Coarse-grained	59.19	0.02	0.35	0.05	2.87	0.32	0.97	0.14
	88.76	0.01	0.40	0.14	3.24	0.25	0.81	0.52
	118.35	0.01	0.40	0.01	3.03	0.38	0.98	0.09
	177.51	0.01	0.39	0.02	3.34	0.09	0.71	0.49
	207.09	0.06	0.39	0.01	3.02	0.31	0.63	0.06
	236.66	0.05	0.38	0.01	3.10	0.02	0.97	0.02
Marlstone Fine-grained	59.06	0.00	1.93	0.18	8.87	0.93	2.75	0.14
	88.57	0.02	1.98	0.01	9.50	0.87	2.50	0.66
	118.11	0.04	1.96	0.25	9.69	0.12	2.63	0.48
	177.18	0.08	1.92	0.01	8.85	1.26	3.40	0.12

To monitor and evaluate possible sources of error that might arise from the ultimate measuring process, further test measurements were performed. Claystone (Buntsandstein, Buchen Southern Odenwald), loess (Nussloch Loess, Nussloch Southern Odenwald), sandstone (Buntsandstein, Heidelberg), and volcanic rocks (Rhyolite,

Altenbach and Handschuhsheim, near Heidelberg) were measured ten times at the same position for 60 and 90 s (Tab. 4.2).

Tab. 4.2: Mean values for potassium (K wt. %), thorium (Th µg/g), and uranium (U µg/g) from test measurements at various lithologies, Southern Odenwald, Germany ('Nussi': Nussloch Loess, BH: Buntsandstein Heidelberg, RA: Rhyolite Altenbach, RH: Rhyolite Handschuhsheim).

Sample	*Measuring Time*		*Mean K*		*Mean Th*		*Mean U*	
	s	*Std.*	*wt. %*	*Std.*	*µg/g*	*Std.*	*µg/g*	*Std.*
Claystone	58.95	0.02	1.76	0.17	15.28	1.15	3.50	0.68
	88.43	0.03	1.69	0.09	16.51	1.27	3.35	0.71
Loess, 'Nussi'	59.03	0.02	1.49	0.17	10.42	1.29	3.88	0.91
	88.54	0.03	1.46	0.08	10.83	0.76	3.43	0.42
Sandstone, BH	59.05	0.02	3.17	0.11	5.12	0.91	0.78	0.47
	88.57	0.02	3.14	0.09	5.40	0.37	0.82	0.31
Rhyolite, RA	58.35	0.03	8.50	0.25	46.38	2.61	8.24	1.22
	87.54	0.04	8.53	0.22	45.56	2.39	8.24	0.91
Rhyolite, RH	58.25	0.04	9.50	0.47	56.71	2.17	6.29	1.69
	87.34	0.04	9.60	0.16	58.12	2.06	5.66	1.14

The mean values with standard deviation, from test measurements in the working area (Tab. 4.1) and additional test measurements in the Southern Odenwald (Tab. 4.2) show that there is no significant discrepancy in accordance to the measuring time. For all time intervals, the obtained GR readings are within the error of the standard deviation, whereas the resulting error predominantly is below 10% and does not indicate to correlate with the time period set. As longer measuring times did not reveal to lower the resulting error significantly, the time interval for each gamma ray measurement was set at 60 s. This provided enough time for the system to reach the fine gain threshold (usually after 40 s) and allowed to process each section twice within one day; this in turn enabled to keep the analytical error that might arise from changing environmental conditions as low as possible.

4.1.3 Outcrop measurements and sampling of representative rock specimens

During fieldwork in the Jaca Basin, selected vertical profiles were processed with the portable GR-320 device (cp. Chapter 5), whereas at each measuring point two readings (60 s) were taken. In the course of the field measurements, representative rock samples were taken along the vertical profiles to execute analogue laboratory measurements. The samples represent different litho-types of the SSt-Succession, with a broad grain size spectrum (Tab. 4.3). The sample number refers to the section locality and horizon the sample was taken from (e.g. F48: section Fanlillo, horizon 48). Furthermore, in the vicinity of Heidelberg (Southern Odenwald, Germany), several test series of field measurements, using the GR-320 spectrometer were performed (cp. section 4.1.2) and representative

rock samples were taken. The lithologies comprise siltstones, sandstones, and volcanic rocks of different grain sizes (Tab. 4.3).

Tab. 4.3: In-situ measured rock samples from the Jaca Basin (SSt-Succession), and from the Southern Odenwald ('Nussi': Nussloch Loess, BH: Buntsandstein Heidelberg, RA: Rhyolite Altenbach, RH: Rhyolite Handschuhsheim).

Sample		*Grain sizes*
Marly siltstone	(SSt, Y10)	Silt-sized
Marly siltstone	(SSt, Y42)	Silt-sized
Siltstone	(SSt, F48)	Silt-sized
Sandstone	(SSt, Y21)	Medium sand-sized
Sandstone	(SSt, Y66)	Medium sand-sized
Sandstone	(SSt, S45)	Coarse sand-sized
Sandstone	(SSt, L28)	Coarse sand-sized
Sandstone	(SSt, L36)	Very coarse sand-sized with granule-sized components
Loess	('Nussi')	Silt-sized
Sandstone	(BH)	Medium sand-sized
Rhyolite	(RA)	Medium graded
Rhyolite	(RH)	Coarse graded

4.2 Laboratory measurements

For laboratory measurements the sampled hand specimens from field investigations were crushed and grinded to grain sizes <63 µm, and filled into sample holder to have a well-defined geometry. The usual sample geometry can be described by a cylinder of 4.5 cm in diameter and sample heights between 2 and 14 mm. The influence of varying sample heights was simulated using the Monte Carlo technique, which enabled to derive certain geometry factors that had to be taken into account for calculating the isotope content of the sample (pers. comm. S. Lindauer). This allows to determine the content of potassium, thorium, and uranium within a small error range (< 2 %). Sample preparation and subsequent analyses with the Canberra-Spec were carried out at the laboratory of the Research Centre in Archeometry of the Academy for Science at the Max-Planck-Institute for Nuclear Physics of Heidelberg.

4.2.1 Laboratory measurements of intralab and international standards

To evaluate gamma ray counts for a particular sample, the activity of the sample and the reference standard need to be processed and calculated under consideration of the sample geometry, and afterwards compared (Kalchgruber 2002). At the laboratory of the Archeometry Research Centre, sample analyses routinely were done exclusively using Nussloch Loess ('Nussi') as current reference standard, as it has a homogeneous composition with well known contents of potassium, thorium, and uranium (Tab. 4.4).

Tab. 4.4: Content of potassium, thorium, and uranium for Nussloch Loess ('Nussi' standard, Nussloch, 'Weisse Hohl'), (Kalchgruber 2002).

Sample	*Potassium*		*Thorium*		*Uranium*	
	wt. %	*Std.*	*µg/g*	*Std.*	*µg/g*	*Std.*
Nussloch Loess, 'Nussi'	1.15	0.03	7.62	0.16	2.82	0.09

To affirm the validity of this modus operandi, i.e. using 'Nussi' as reference standard for K, Th, and U concentrations, and to warrant a proper calibration of the systems used, international standards purchased from the U.S. Geological Survey were treated as common samples and analysed (Canberra-Spec), (Tab. 4.5).

Tab. 4.5: Mean values for potassium (K), thorium (Th), and uranium (U) of USGS Geochemical Reference Material, measured with Canberra-Spec, in comparison to nominal concentrations given by the U.S. Geological Survey.

USGS Standard	*Mean K Canberra*		*Nominal K USGS*		*Deviation Canberra – USGS*
	wt. %	*Std.*	*wt. %*	*Std.*	%
Basalt, Columbia River, BCR-2	1.60	0.07	1.49	0.04	7
Carbonatite, COQ-1	0.26	0.03	0.13	0.02	50
Granodiotite, GSP-2	4.71	0.18	4.48	0.12	5
Green River Shale, SGR-1	1.70	0.07	1.38	0.10	19
Devonian Ohio Shale, SDO-1	2.73	0.13	2.79	0.06	2
Syenite, STM-1	3.84	0.22	3.56	0.07	7
USGS Standard	*Mean Th Canberra*		*Nominal Th USGS*		*Mean Canberra – USGS*
	µg/g	*Std.*	*µg/g*	*Std.*	%
Basalt, Columbia River, BCR-2	5.50	0.18	6.20	0.70	13
Carbonatite, COQ-1	10.35	0.35	10.00	1.00	3
Granodiotite, GSP-2	99.34	2.49	105.00	8.00	6
Green River Shale, SGR-1	5.34	0.18	4.80	0.21	10
Devonian Ohio Shale, SDO-1	9.49	0.51	10.50	0.55	11
Syenite, STM-1	28.34	0.92	31.00	3.00	9
USGS Standard	*Mean U Canberra*		*Nominal U USGS*		*Mean Canberra – USGS*
	µg/g	*Std.*	*µg/g*	*Std.*	%
Basalt, Columbia River, BCR-2	1.60	0.06	1.69	0.19	6
Carbonatite, COQ-1	10.43	1.09	11.00	0.60	5
Granodiotite, GSP-2	2.41	0.11	2.40	0.19	1
Green River Shale, SGR-1	5.70	0.16	5.40	0.21	5
Devonian Ohio Shale, SDO-1	41.5	1.11	48.80	6.50	18
Syenite, STM-1	8.13	0.31	9.10	0.10	12

Comparing the values given in Tab. 4.5 and plotted in Figs. 4.1a-c shows, that within the error the isotope concentration measured by the Canberra-Spec is very consistent with the concentration given by the U.S. Geological Survey.

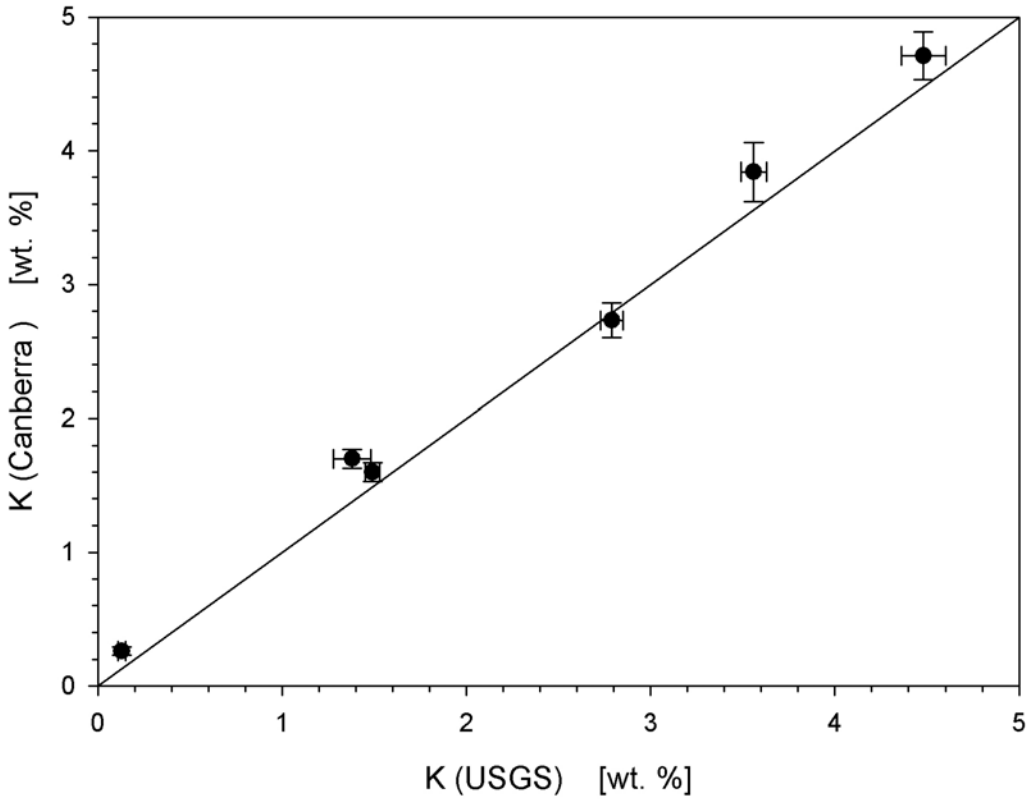

Fig.: 4.1a: Mean values for potassium (K wt. %) for USGS standards, revealed by Canberra-Spec measurements and plotted against nominal concentrations given by the U.S. Geological Survey (cp. Tab. 4.5).

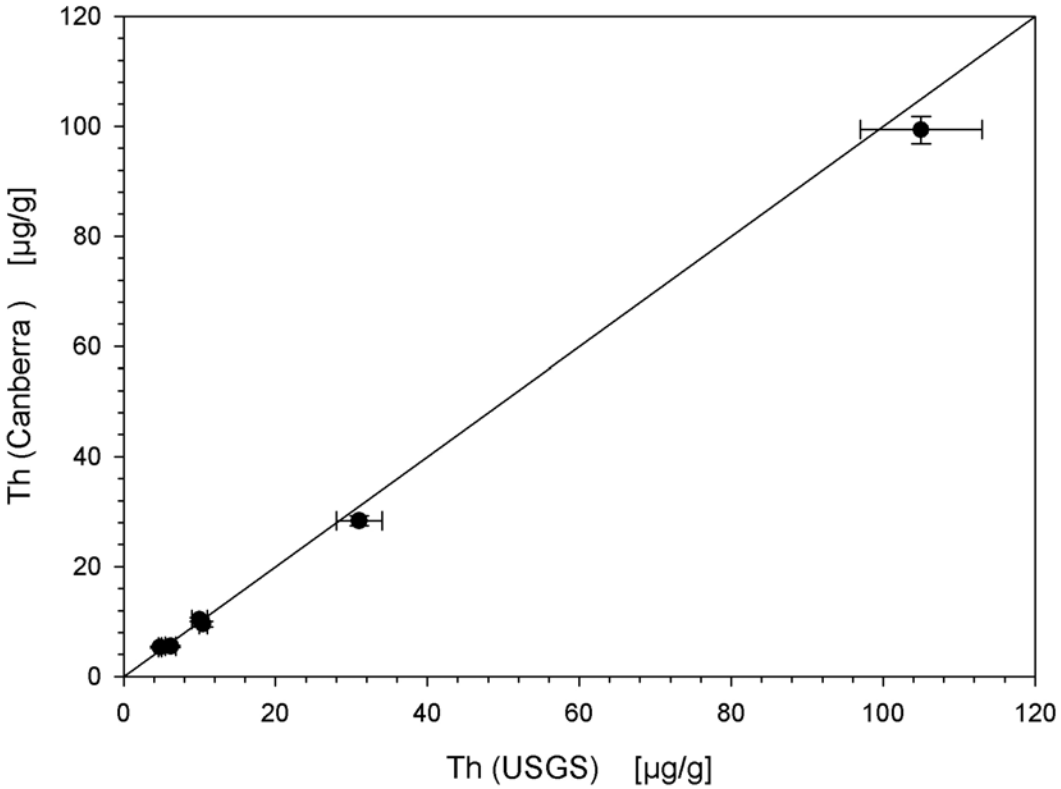

Fig. 4.1b: Mean values for thorium (Th µg/g) for USGS standards, revealed by Canberra-Spec measurements and plotted against nominal concentrations given by the U.S. Geological Survey (cp. Tab. 4.5).

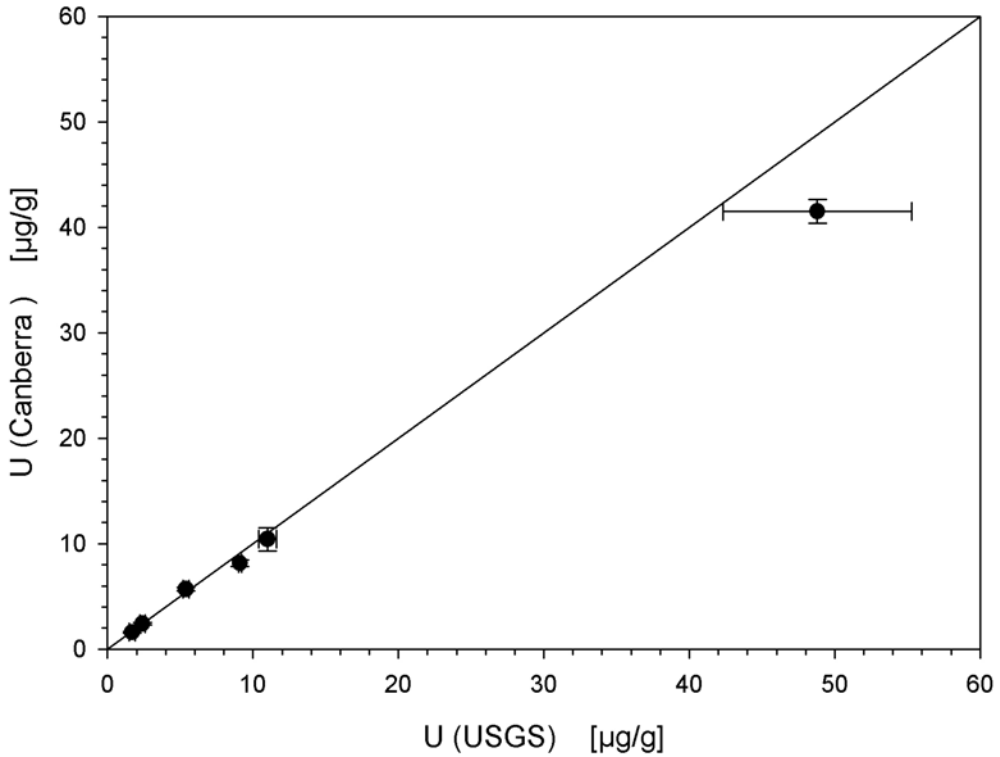

Fig. 4.1c: Mean values for uranium (U µg/g) for USGS standards, revealed by Canberra-Spec measurements and plotted against nominal concentrations given by the U.S. Geological Survey (cp. Tab. 4.5).

Observable deviations mainly occur at higher isotope concentrations, i.e. the higher the isotope concentrations of the measured USGS standards are, the higher is the resulting deviation from the calibration curve. Detector characteristics, e.g. higher susceptibility to Compton scattering below 300 keV, and decreasing efficiency in the backmost array of the spectrum may explain the deviation at high-energy ranges (pers. comm. S. Lindauer). But predominantly the Canberra-Spec and USGS nominal values are within the error. With this procedure a solid calibration for the Canberra spectrometer could be demonstrated.

4.2.2 Laboratory measurements on representative rock samples

The selected samples from outcrop measurements in the Jaca Basin and in the area of Heidelberg (cp. Tab. 4.3) were prepared as described above (crushed, grinded and filled into defined sample holder) and measured with the Canberra-Spec. The results from field- and analogue laboratory measurements are displayed in Tab. 4.6. Given are the contents of potassium, thorium, and uranium: Whereas *'Mean'* values give the element concentrations as gained from double in-situ field measurements using the portable GR-320 (59.8 ± 0.32 s); *'Nominal'* values represent analogue laboratory measurements with the Canberra-Spec. Depending on the activity of the sample measurement intervals with the Canberra-Spec vary from 2-5 days.

Tab. 4.6: Concentration of potassium (K), thorium (Th), and uranium (U) revealed from field- and analogue laboratory measurements. Displayed are '*Mean*' values from in-situ measurements with the GR-320, in comparison to '*Nominal*' values of representative rock samples taken in the field and measured with the Canberra-Spec. GR-320 measurements: 59.8 ± 0.32 s, SSt rock samples were measured twice, 'Nussi', BH, RA and RH ten times each; Canberra-Spec measurement with durations between 2-5 days.

Rock Sample		*Mean K GR-320*		*Nominal K Canberra*		*Deviation GR-320 – Canberra*
		wt. %	*Std.*	*wt. %*	*Std.*	*%*
Loess	('Nussi')	1.49	0.17	1.15	0.03	23
Sandstone	(BH)	3.17	0.11	2.05	0.08	35
Rhyolite	(RA)	8.50	0.25	7.18	0.28	15
Rhyolite	(RH)	9.50	0.47	7.18	0.28	24
Marly siltstone	(SSt, Y10)	3.28	0.06	1.40	0.06	57
Sandstone	(SSt, Y21)	1.26	0.06	0.59	0.03	53
Marly siltstone	(SSt, Y42)	3.06	0.57	1.25	0.05	59
Sandstone	(SSt, Y66)	1.91	0.24	0.90	0.04	53
Siltstone	(SSt, F48)	1.90	0.26	0.79	0.04	58
Sandstone	(SSt, S45)	1.71	0.06	0.60	0.03	65
Sandstone	(SSt, L28)	1.01	0.04	0.45	0.02	55
Sandstone	(SSt, L36)	0.54	0.05	0.37	0.02	31
Rock Sample		*Mean Th GR-320*		*Nominal Th Canberra*		*Deviation GR-320 – Canberra*
		µg/g	*Std.*	*µg/g*	*Std.*	*%*
Loess	('Nussi')	10.42	1.29	7.62	0.16	27
Sandstone	(BH)	5.12	0.91	2.06	0.09	31
Rhyolite	(RA)	46.38	2.61	33.30	0.89	45
Rhyolite	(RH)	56.71	2.17	37.90	1.00	39
Marly siltstone	(SSt, Y10)	16.32	0.94	6.42	0.20	53
Sandstone	(SSt, Y21)	8.66	1.10	2.31	0.09	38
Marly siltstone	(SSt, Y42)	15.54	2.24	5.48	0.17	58
Sandstone	(SSt, Y66)	10.00	0.32	4.10	0.13	6
Siltstone	(SSt, F48)	12.70	0.17	3.64	0.12	52
Sandstone	(SSt, S45)	10.78	1.17	2.42	0.09	38
Sandstone	(SSt, L28)	6.95	0.24	2.02	0.08	23
Sandstone	(SSt, L36)	5.18	0.54	1.57	0.07	38
Rock Sample		*Mean U GR-320*		*Nominal U Canberra*		*Deviation GR-320 – Canberra*
		µg/g	*Std.*	*µg/g*	*Std.*	*%*
Loess	('Nussi')	3.88	0.91	2.82	0.09	27
Sandstone	(BH)	0.78	0.47	0.54	0.03	60
Rhyolite	(RA)	8.24	1.22	4.53	0.15	28
Rhyolite	(RH)	6.29	1.69	3.86	0.14	33
Marly siltstone	(SSt, Y10)	4.80	1.36	2.25	0.07	61
Sandstone	(SSt, Y21)	1.66	0.94	1.03	0.04	73
Marly siltstone	(SSt, Y42)	4.13	1.29	1.72	0.06	65
Sandstone	(SSt, Y66)	1.37	0.42	1.29	0.04	59
Siltstone	(SSt, F48)	2.61	0.67	1.24	0.05	71
Sandstone	(SSt, S45)	1.96	0.52	1.22	0.04	77
Sandstone	(SSt, L28)	1.50	0.12	1.15	0.04	71
Sandstone	(SSt, L36)	1.88	0.39	1.16	0.04	70

Table 4.6 shows the results from field and analogue laboratory measurements, comprising fine- to coarse-grained siliciclastic and volcanic rock samples (cp. Tab. 4.3). The comparison of the data obtained from field and laboratory analysis, i.e. mean values obtained from GR-320 measurements in relation to nominal values obtained from Canberra-Spec measurements, allowed to calculate the deviation between both measuring procedures. The resulting deviation is given in the last column of Tab. 4.6 and plotted in Figs. 4.2a-c.

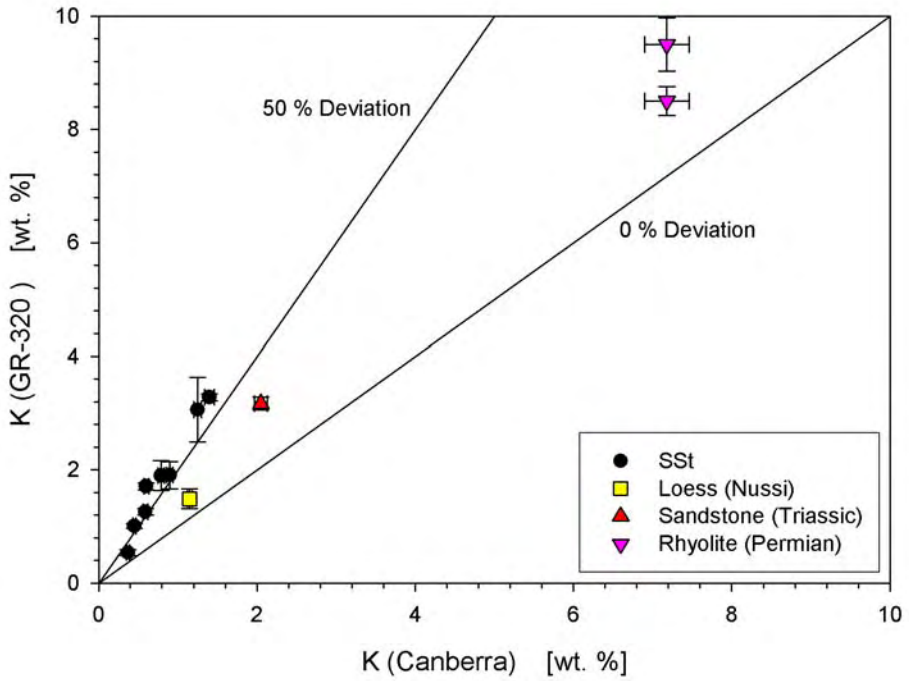

Fig. 4.2a: Potassium (K wt. %) content of representative rock samples revealed from field and analogue laboratory measurements. Plotted are '*Mean*' values from in-situ field measurements with the GR-320, against '*Nominal*' values of representative rock samples measured with the Canberra-Spec (cp. Tab. 4.6). The straight lines for '0 % Deviation' and '50 % Deviation', demonstrate the general drift of the GR-320 device, which is higher for samples from the Jaca Basin (SSt), than for the Southern Odenwald (Loess, Sandstone, Rhyolite).

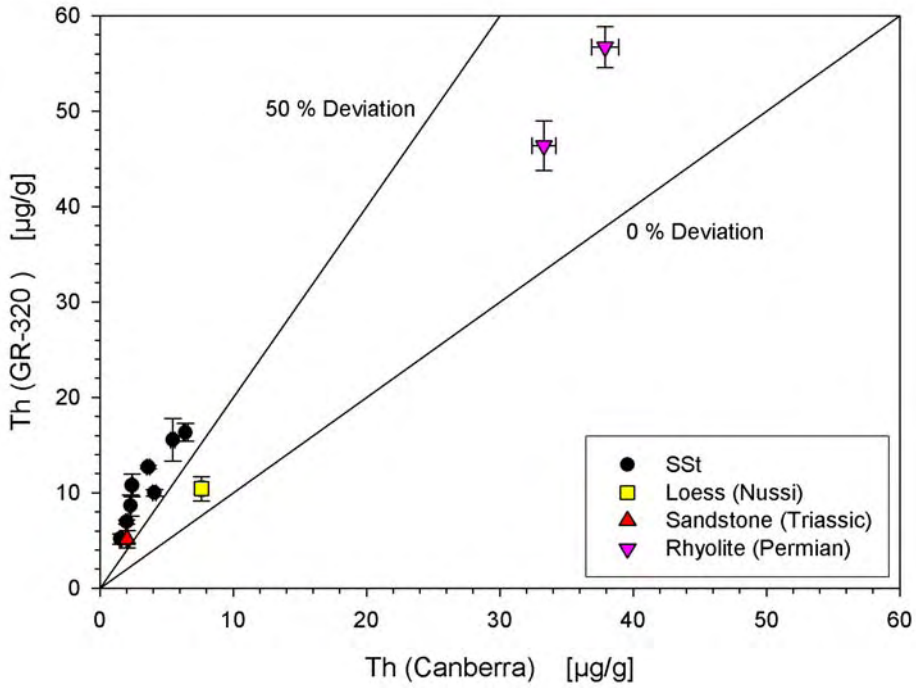

Fig. 4.2b: Thorium (Th µg/g) content of representative rock samples revealed from field and analogue laboratory measurements. Plotted are '*Mean*' values from in-situ field measurements with the GR-320, against '*Nominal*' values of representative rock samples measured with the Canberra-Spec (cp. Tab. 4.6). The straight lines for '0 % Deviation' and '50 % Deviation', demonstrate the general drift of the GR-320 device, which is higher for samples from the Jaca Basin (SSt), than for the Southern Odenwald (Loess, Sandstone, Rhyolite).

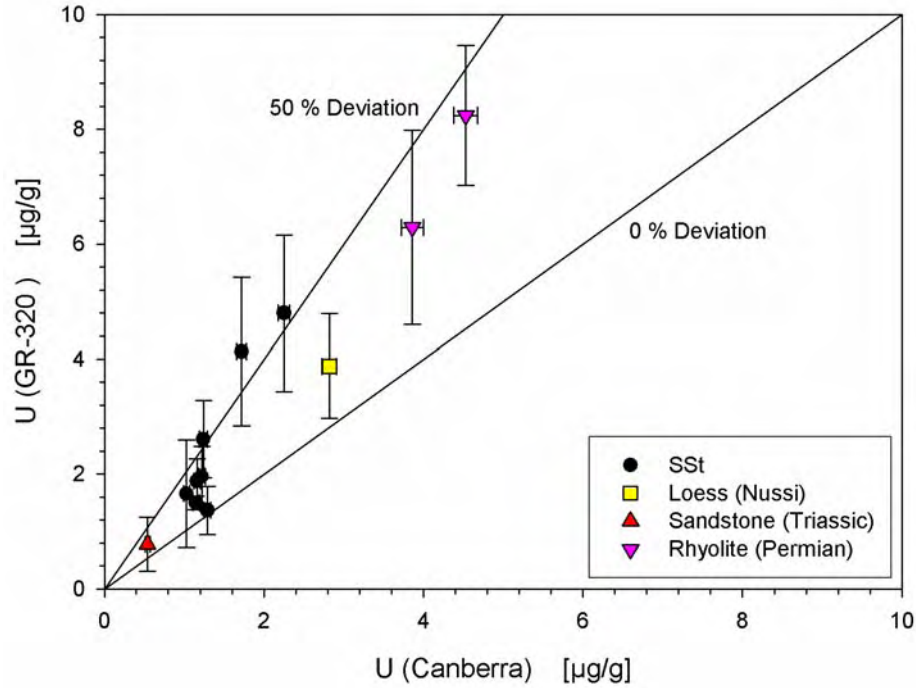

Fig. 4.2c: Uranium (U µg/g) content of representative rock samples revealed from field and analogue laboratory measurements. Plotted are '*Mean*' values from in-situ field measurements with the GR-320, against '*Nominal*' values of representative rock samples measured with the Canberra-Spec (cp. Tab. 4.6). The straight lines for '0 % Deviation' and '50 % Deviation', demonstrate the general drift of the GR-320 device, which is higher for samples from the Jaca Basin (SSt), than for the Southern Odenwald (Loess, Sandstone, Rhyolite). The plot shows much broader error for the measurements, which arises from inhomogene distribution of uranium.

The values achieved by the portable GR-spectrometer generally show a drift towards higher values, whereas following features can be recognized:

- The deviation between GR-320 measurements and analogue Canberra-Spec measurements is reproducible and, therefore, a correction factor can be computed.
- Gamma ray readings from the Jaca Basin show a larger drift than readings from the Southern Odenwald.
- Thorium and uranium values show broader scattering compared to potassium.
- Uranium values show broadest deviation.

The higher values for measurements recorded in the Jaca Basin, are referred to environmental conditions, and are assumed to represent deviations adopted from i) higher cosmic radiation affecting the measurements in the Jaca Basin due to higher elevation above sea level (Jaca Basin: ~900 m, Southern Odenwald: ~120-250 m), ii) seasonal differences, as measurements in the Jaca Basin were performed during summer time (dry rocks), while measurements in the Southern Odenwald were performed during winter time (humid rocks). Referring to the seasonal differences, a major parameter, causing the drift between measurements taken in the Jaca Basin and measurements taken in the Southern Odenwald may arise from temperature differences (Jaca Basin, summer: ~25-30°C, Southern Odenwald, winter: ~5-10°C). Kalchgruber (2002) showed, that changing temperature has a strong influence on the recorded gamma spectra by changing the sensitivity of the NaI-crystal leading to a shift of the peak positions. This behaviour of the NaI-detector can be compensated if the detection software searches for the maximum peak position and sets the window for the detection channel after finding the position. If channels are recorded just within a small window, the system will not cover the entire spectra, if a temperature related shift of the peak position occur (Fig. 4.3). The windows for the GR-320*enviSpec* used, comprise about 256 channels, whereas each isotope has a defined region of interest with a narrow array (K: 111-126, U: 134-149, Th: 193-224). The used equipment does not search for the peak position. Thus, changing temperatures will affect the gamma ray measurements of the GR-320*enviSpec*.

The broader scattering of uranium and thorium values compared to potassium is associated to their occurrence within the heavy mineral fraction. Heavy minerals commonly show an inhomogeneous distribution in a rock formation, and accordingly affect the resulting gamma ray measurements. Depending on the position of the heavy mineral grains, they are either within the effective sample, i.e. contribute to the gamma radiation or are not detected by the device. The higher deviations in uranium

measurements are attributed to the high mobility of uranium. This is a well-known issue associated to uranium, which typically shows an uneven distribution within a rock formation (Rider 2004). As the reliability of the Canberra-Spec was proved, a calibration of the data set achieved with the portable GR-320 spectrometer was feasible.

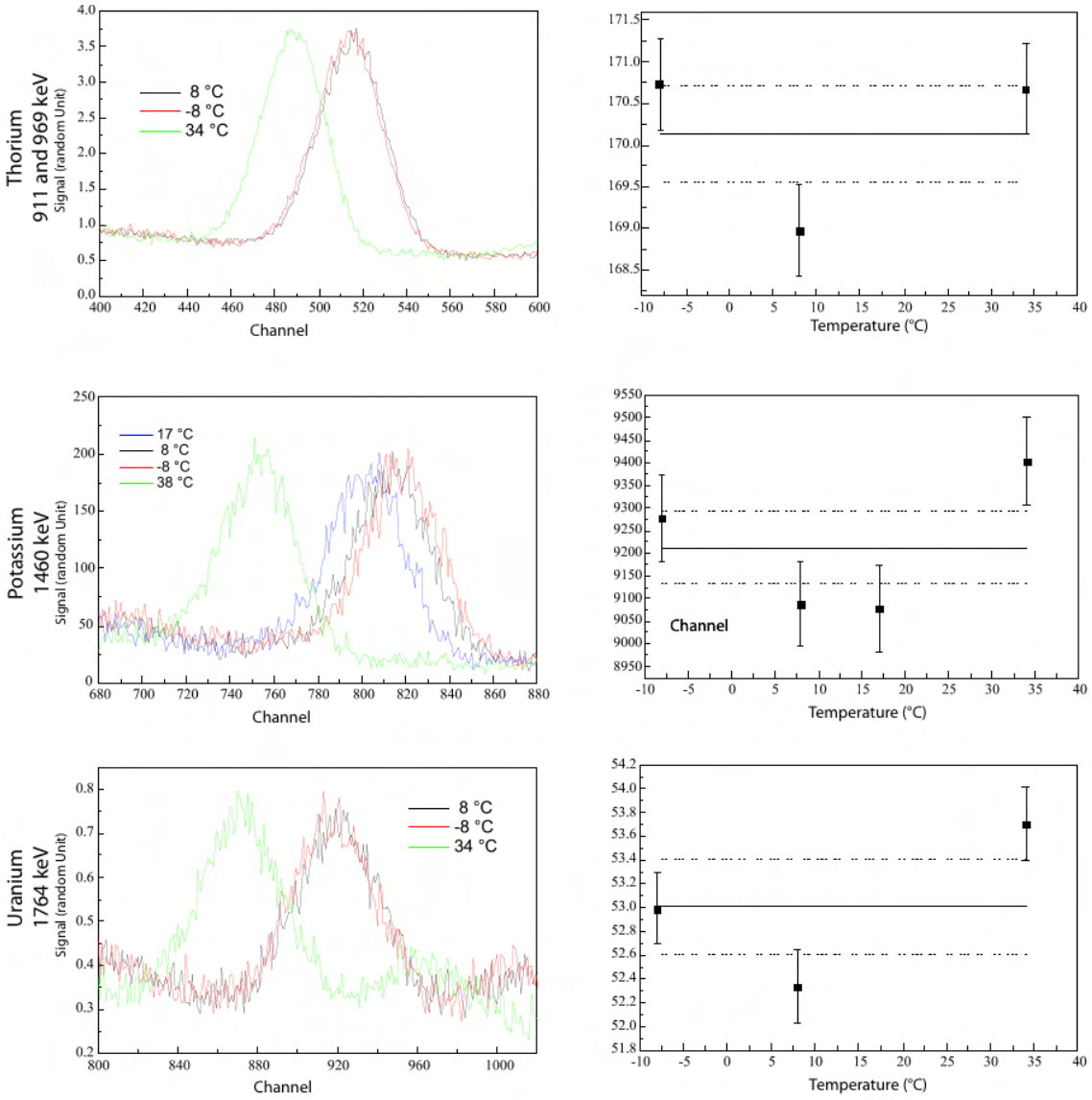

Fig. 4.3: Displayed is the shift of the gamma ray spectra at different temperatures of the NaI-detector (Kalchgruber 2002). If the channel window is too narrow, the entire spectrum might not be covered, resulting in a drift of measured data.

On the basis of the described test measurements for Nussloch Loess, Buntsandstein, Rhyolite and SSt-Samples, resulting values were evaluated statistically, and standard deviation factors for the portable GR device were computed (Tab. 4.6). The correction factors for the data set of the Jaca Basin were calculated on the basis of analogue measurements performed on the SSt samples (cp. Tab. 4.6).

The data set from field measurement in the Jaca Basin, therefore, has to be corrected about 54 % for potassium, 69 % for thorium, and 38 % for uranium:

- Potassium: 54 ± 10 %
- Thorium: 68 ± 6 %
- Uranium: 38 ± 17 %

The resulting deviation, derived from the analogue measurements refers to the total error and represents the sum of systematic and analytic errors that accumulate during the measuring process. Therein, parameters like tool precision, cosmic radiation, and individual errors associated to the measuring procedure in general are considered.

4.3 Effective sample, sample geometry and area

The issue of effective sample and sample area already was considered in Chapter 3 (cp. Figs. 3.9 and 3.10) and turned out to play an important role for spectral gamma ray measurements. This excursus addresses to this issue again and aims to illustrate their impact on the example of the Flossenbuerg Granite block (1x1 m block) and two 'Nussi' samples. The Flossenbuerg Granite block has a drill hole to evenly place the detector for stable measurements (4-pi symmetry). This simulates closely an overhang, as it might be the case during field measurements. Referring to the definition of an 'effective sample', the resulting counts, therefore, are expected to be higher, compared to a regular measurement. Ten measurements with time intervals of 60, 90, and 180 s and a single long-time measurement 3600 s were run (Tab. 4.7). Further test measurements on two 'Nussi' samples were performed. Therefore, Nussloch-Loess was filled into sample holder with 4.5 cm in diameter and sample heights of 1 cm and 3 cm. For each measurement the GR-320 scintillator was placed on the sample holder and measurements were run twice for 'Nussi' 1 cm for 60 s, and ten times for 'Nussi' 3 cm with time intervals of 60 and 90 s. The results are displayed in Tab. 4.7, whereas 'Nominal' values refer to laboratory measurements with the Canberra-Spec (Kalchgruber 2002), 'Mean Raw' values refer to the initial values measured with the GR-320 device, and 'Mean Cor' values refer to the initial GR-320 measurements corrected as followed:

For Flossenbuerg Granite: K: 20 ± 5 %, Th: 42 ± 3 %, U: 31 ± 3 %, based on Rhyolite Deviation (cp. Tab. 4.6).

For 'Nussi': K: 23 %, Th: 27 %. U: 27 %, based on Loess Deviation (cp. Tab. 4.6).

Tab. 4.7: Mean values for potassium (K), thorium (Th), and uranium (U), of Flossenbuerg Granite and 'Nussi' (varying sample geometry), as revealed from measurements with the GR-320 using time-intervals from 60 to 3600 s; and analogue nominal values obtained from laboratory measurements with the Canberra-Spec.

Sample	*Measuring Time*		*Mean Raw K GR-320*		*Nominal K Canberra*		*Mean Cor K GR-320*
	s	Std.	wt. %	Std.	wt. %	Std.	wt. %
'Nussi' < 1 cm	59.13	0.02	1.40	0.15	1.15	0.03	1.08
'Nussi' 3 cm	59.10	0.02	1.64	0.11	1.15	0.03	1.26
	88.65	0.03	1.68	0.08	1.15	0.03	1.29
Nussloch	59.03	0.02	1.49	0.17	1.15	0.03	1.15
	88.54	0.03	1.46	0.08	1.15	0.03	1.12
Flossi	57.92	0.04	8.07	0.24	3.96	0.23	6.46
	86.88	0.06	8.16	0.12	3.96	0.23	6.53
	173.76	0.07	8.25	0.22	3.96	0.23	6.60
	3475.27	---	8.12	---	3.96	0.23	6.50
Sample	*Measuring Time*		*Mean Raw Th GR-320*		*Nominal Th Canberra*		*Mean Cor U GR-320*
	s	Std.	µg/g	Std.	µg/g	Std.	µg/g
'Nussi' < 1 cm	59.13	0.02	6.71	1.58	7.62	0.16	4.90
'Nussi' 3 cm	59.10	0.02	7.11	0.94	7.62	0.16	5.20
	88.65	0.03	6.90	0.59	7.62	0.16	5.04
Nussloch	59.03	0.02	10.42	1.29	7.62	0.16	7.61
	88.54	0.03	10.83	0.76	7.62	0.16	7.91
Flossi	57.92	0.04	27.41	2.37	14.40	0.54	15.90
	86.88	0.06	27.44	1.17	14.40	0.54	15.90
	173.76	0.07	27.61	0.85	14.40	0.54	16.01
	3475.27	---	27.54	---	14.40	0.54	15.97
Sample	*Measuring Time*		*Mean Raw U GR-320*		*Nominal U Canberra*		*Mean Cor U GR-320*
	s	Std.	µg/g	Std.	µg/g	Std.	µg/g
'Nussi' < 1 cm	59.13	0.02	1.37	0.65	2.82	0.09	1.00
'Nussi' 3 cm	59.10	0.02	2.13	0.47	2.82	0.09	1.55
	88.65	0.03	2.05	0.37	2.82	0.09	1.50
Nussloch	59.03	0.02	3.88	0.91	2.82	0.09	2.83
	88.54	0.03	3.43	0.42	2.82	0.09	2.50
Flossi	57.92	0.04	33.50	1.81	20.10	0.30	23.23
	86.88	0.06	33.66	0.81	20.10	0.30	23.23
	173.76	0.07	33.47	0.73	20.10	0.30	23.09
	3475.27	---	33.72	---	20.10	0.30	23.27

The values for ‘Nussi’ < 1 cm and ‘Nussi’ 3 cm are not correlating to the nominal values; the contents for potassium are too high, while the contents for uranium and thorium are too low, with a bad reproducibility of the values. This obviously demonstrates how significant the impact of the sample geometry (volume) is. Both ‘Nussi’ samples represent a too small effective sample. Referring to Løvborg et al. 1971 the effective sample that commonly is influencing the gamma ray reading is about 80-100 cm in diameter and 14 cm depth (~49 kg). Thus the contribution of the ‘Nussi’ sample is almost negligible, while the bulk of gamma radiation that was measured results from surrounding material, causing compound and, therefore, incorrect values. For comparison Tab. 4.7 shows the outcrop measurements with the GR-320 at the type-locality of ‘Nussi’, illustrating the irreproducibility of the two ‘Nussi’ samples. The results for Flossenbuerg Granite nicely demonstrate the precision of the tool, as the obtained readings are very consistent. The values have a good reproducibility, with an error predominantly ranging below 5 %. Larger deviations in thorium and uranium concentrations can be referred to some inhomogeneity of the Flossenbuerg Granite and the radioactive decay in general. The obtained concentrations of potassium, thorium, and uranium, measured with the GR-320 spectrometer and corrected based on the deviation computed for Rhyolite (cp. Tab. 4.6), are too high compared to the nominal values. As already mentioned, the scintillation detector of the GR-device was placed in a cavity and, therefore, was surrounded by the rock, simulating an overhang situation in the field. Both examples demonstratively show, that effective sample, sample geometry and sample area are a very crucial point for the validity of data obtained from spectral gamma ray measurements.

4.4 Discussion

In conclusion during the calibration process it could be shown that the measuring stability of the used GR-320*enviSpec* is high, giving a tool precision better than 10 % error. The test-series of outcrop-measurements (Tabs. 4.1 and 4.3) and also at the Flossenbuerg Granite block (Tab. 4.7) showed that the duration of the measuring time is not a major determining factor for the measuring precision as long as the system has reached the threshold for fine gain stabilization. In fact, as can be seen in lab measurements a longer measurement interval does not change the value significantly but reduces the error due to a better counting statistic. This accounts especially towards very low and very high energies where the efficiency of the detector is either influenced by the Compton background signal, or the efficiency decreases the error and minor peaks become ‘more’ visible above the background (pers. comm. S. Lindauer). In the case of this study, repeated measuring at a vertical profile within one day would have not been possible. This would have caused an even larger error, and a minor data set would have been

possible to obtain as a matter of time available for field investigations. As it was already observed from preliminary test measurements in the working area and proved by further test-series, a measuring time of 60 s is sufficient to reach the fine gain of the system. Another factor that need to be considered carefully is associated to the sample geometry and area. This impressively is shown by the examples of 'Nussi' and Flossenbuerg Granite, with unreliable element concentrations owing to a sample geometry that was too small ('Nussi') and an effective sample that was too big (Flossenbuerg Granite).

From comparison of field and analogue laboratory measurements (Tabs. 4.6) a clear difference in the achieved values can be observed. They remarkably illustrate, that the portable GR-320 device is recording very consistently, resulting in a high instrumental precision (better than 10 %). The accuracy, however, is very bad, displaying a significant drift for potassium, thorium, and uranium, with data sets obtained from field measurements generally being too high (cp. Fig. 4.4 for precision and accuracy). The deviations between laboratory and field measurements are assumed to predominantly arise from the issue of effective sampling (Fig. 3.10a, Chapter 3). In the laboratory, a well-defined rock sample with an also well-defined geometry is measured. For field measurements, however, a much broader area is sampled, and the gamma ray reading is influenced by about 49 kg of rock (Løvborg et al. 1971), whereas about 0.5-1.0 kg of rock was subsampled for laboratory GR measurements. Mineral grains rich in uranium, like apatite and zircon, can easily be present in the non-sampled volume (subsample for laboratory measurements) but give rise to elevated uranium values from the volumetrically greater gamma ray measurements in the field.

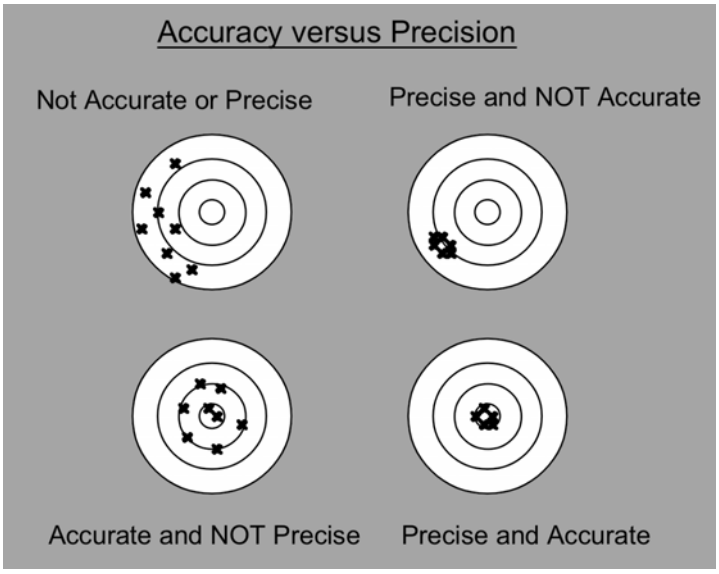

Fig. 4.4: Accuracy versus precision, to illustrate that the system may measure very precise but not necessarily accurate (source: thermochronology lecture, Glasmacher).

The differences in deviation between measurements in the Jaca Basin compared to measurements in the Southern Odenwald are predominantly assigned to changing temperature conditions, as with increasing temperatures the spectra show a drift towards lower channels and, therefore, might not be covered entirely. The element values are calculated from the spectra. Not complete detected spectra will lead to lower potassium, thorium, and uranium values. Further environmental conditions contributing to the observed drift are, e.g. humidity of rocks and different cosmic radiation.

The described test measurements highlight some pitfalls and major sources of error that are associated to measurements with a portable GR device, but can be limited if considered carefully. With the schematized calibration process, a solid calibration for the used GR-320 spectrometer could be proved; as the system enables to process reproducible and, therefore, reliable data. From field and analogue laboratory measurements a correction factor for the GR-320 device could be computed, which allows a qualitative and quantitative use of the obtained data set.

Chapter 5 – Sedimentary Facies of the Sabiñánigo Sandstone Succession

5.1 Introduction

This chapter draws together the concepts that have been recapitulated in the previous Chapter 3 in order to examine the successions of the Sabiñánigo Sandstones (SSt). As part of a thick siliciclastic basin infill the Sabiñánigo Sandstones (Puigdefàbregas 1975) were deposited at the northeastern fringe of the Jaca Basin (Figs. 5.1 and 5.2). The accumulations of the entire basin impressively portray the acting depositional and basinal processes, shifting from deep marine to continental deposition (Hogan & Burbank 1996). The sedimentology and stratigraphy of the basin infill, including the Sabiñánigo Sandstones, have been studied over the last decades, e.g. by Puigdefàbregas (1975), Remacha et al. (1987), Mutti et al. (1988), Turner (1990), and Lafont (1996), resulting in a robust sequence stratigraphic framework. The sequence stratigraphy of the SSt-Succession, however, was only covered tentatively within this framework. Although some studies on the Sabiñánigo Sandstones, e.g. by Puigdefàbregas (1975) and Lafont (1996), already exist, a complete record of the successions as exposed within the two ridges of the Basa Anticline was lacking. A consistent description of their sedimentary facies and depositional environments, as well as a sequence stratigraphic examination, comprising the northern and the southern exposures was not compiled. Furthermore, no attempt was achieved so far, to relate the northern and the southern limb within a sequence stratigraphic framework.

Due to its intermediate position within the basin succession, its excellent outcrop quality, and last but not least, its ‘two-folded’ outcropping within the two limbs of the Basa Anticline, the SSt-Succession is of particular interest for this study. It can be regarded as a key succession to study the impact of changing environmental conditions on sedimentary facies, and to evaluate the varying dynamic processes acting within a foreland basin setting. Moreover it meets the requirements for a case study to test the applicability of gamma ray spectrometry as a tool for sedimentological and sequence stratigraphic issues. To unravel the depositional processes and compose a depositional model of the SSt-Succession, a solid and consistent facies characterization needed to be done first, followed by an environmental interpretation and sequence stratigraphic examination.

5.2 Facies analysis and gamma ray spectrometry

To determine the conditions under which the SSt-Succession accumulated and how it evolved, facies analyses were conducted and a depositional model derived. The according basic data set was generated from vertical sections processed within the SSt-Succession. Therefore, standard facies analysis methods and subsurface-related geophysical analysis methods, i.e. gamma ray spectrometry, were used (cp. Chapter 3). The sedimentary facies as well as lateral and vertical facies transitions were resolved and depositional characteristics determined.

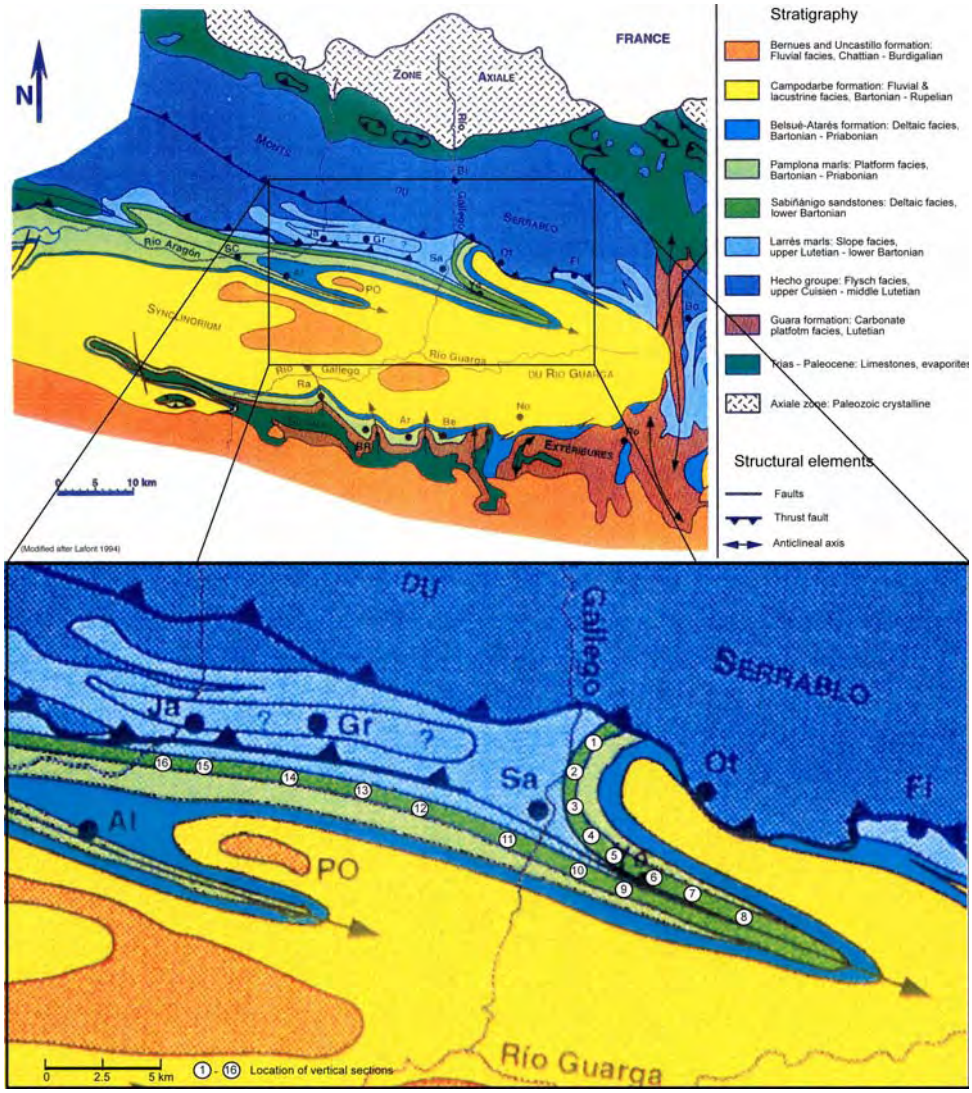

Fig. 5.1: Geological map of the Jaca Basin (modified after Puigdefàbregas 1975, Lafont 1994) with location of vertical sections along the northern and the southern limb of the Basa Anticline: 1) Larrede, 2) Javierre, 3) Latás, 4) Isún, 5) San Román, 6) Yebra, 7) Sobás, 8) Fanlillo, 9) Allué, 10) Osán, 11) Sabiñánigo Alto, 12) Sasal, 13) Jarlata, 14) Frauca, 15) Navasa, 16) Ulle. All sections were analysed regarding their lithofacies; additional gamma ray spectrometry was performed at sections 3, 4, 6-8 and 11-15.

A total of 16 vertical profiles with an average thickness of about 250 m were analysed in the standard way. The vertical profiles were set within constant spacing along the two limbs of the E-W running Basa Anticline (Figs. 5.1 and 5.2).

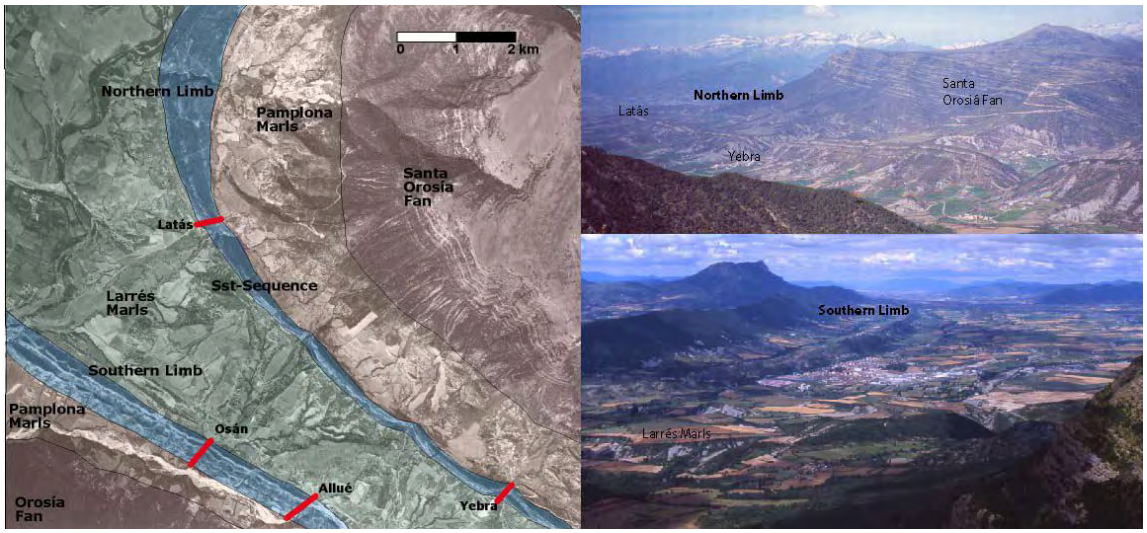

Fig. 5.2: Pictures of the studying area. Note the limbs of the Basa Anticline forming two distinct topographic ridges that can be followed over tens of kilometres, providing excellent outcrop conditions for high-resolution architectural and stratigraphic analysis. Left hand: Aerial photo of the eastern part of the studying site. Larrés Marls (green) in the core of the Basa Anticline, Sabiñánigo Sandstones (blue) exposed within the northern and southern limb, overlain by the Pamplona Marls and the deposit of the Santa Orosía Fan. Right hand, top: Picture of the northern limb, view towards N, with location of section Latás and Yebra. Below: Picture towards W, core of the Basa Anticline in the centre and the outcropping southern limb on the left side.

Most of the indications for the facies classification are based on observations made in the field. Small-scaled bed analyses (bed-resolution of dm- to cm- scale) were performed within and in-between the processed vertical sections. Thereby, lithological and paleontological characteristics, like fossil-content, grain size, sedimentary structures, lateral and vertical facies transitions were considered. Macro- and microfossils, as well as hand specimens and thin sections of selected samples were studied in the laboratory to maintain the sediment-petrographic interpretation of the field observations. In addition, 10 vertical profiles were picked and processed with a portable gamma ray spectrometer (GR-320*enviSpec*) to obtain geophysical properties of the rocks (Figs. 5.1 and 5.3). For the present case, study spectral gamma ray readings were taken within distinct spacing along the vertical profiles to obtain continuous gamma ray logs across the complete succession. According to Schlumberger Ltd. (1972), the period of time, which is required to obtain an appropriate value for gamma ray counts emitted by a rocks formation, usually averages a few seconds. Taking the difference between borehole logging and outcrop measurements, and the gained findings from test measurements (Chapter 4) into account, the measurement period for this study was set at 60 seconds for each reading,

whereas at least two readings were taken at each measuring point. Whenever possible readings were taken every 1.0 m along the section. If necessary, e.g. within alternating lithologies, shorter spacing was chosen, but due to the resolution of the GR device (~1 m diameter, cp. Chapter 3) it has to be taken in mind that compound values might be displayed by the log. The basic conditions for each profile-log were tried to keep constant by measuring each profile within one day, and by claiming to a basic measuring protocol; modified after Myers (1987), Slatt et al. (1992), and Jordan (1993). Therefore, i) planar/flat station surfaces were chosen, ii) measurements near cliffs, overhangs and in trenches were avoided, iii) altered, weathered surfaces were also avoided (leaching of K and U); iv) variable moisture contents of measured horizons were tried to avoid; v) during the measurement period a stationary position of the scintillation detector on the rock was maintained. On the basis of about 100-200 reading points per section and a total of more than 3200 measurements, a subsurface-related log pattern of the succession was generated (cp. Chapter 3 for details on GR-measurements).

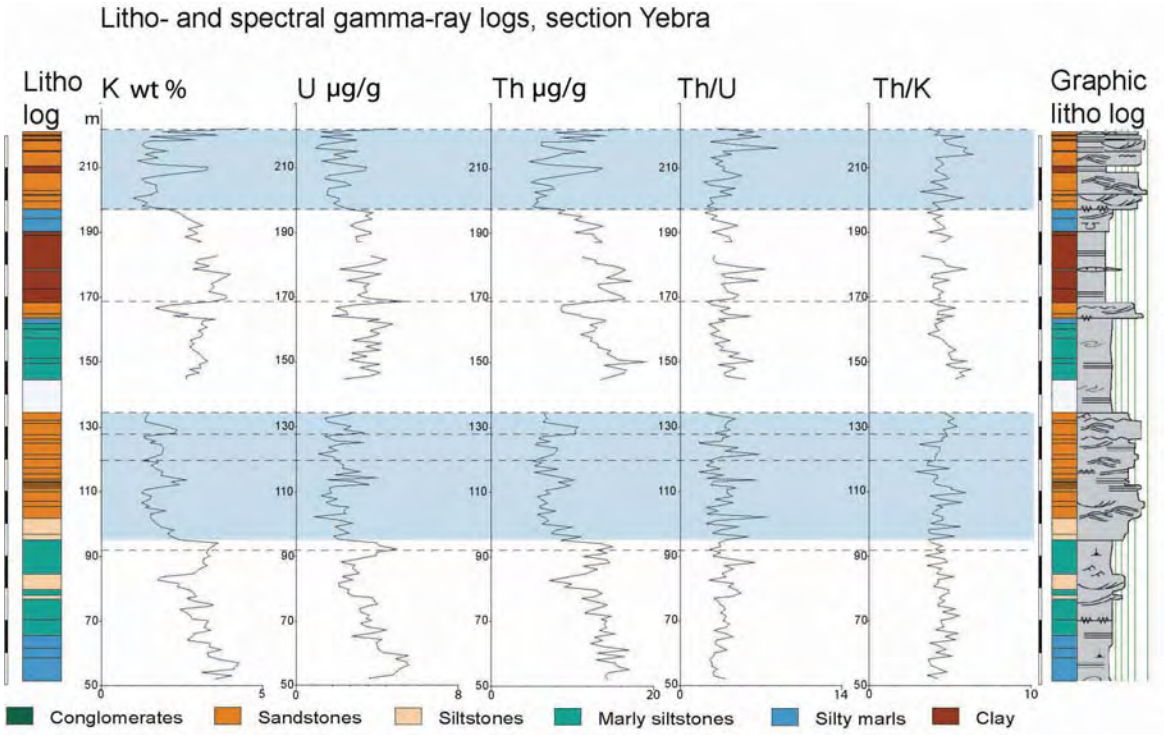

Fig. 5.3: Lithology, spectral gamma ray logs, and graphic log of the profile Yebra (cp. Fig. 5.1 for location and Fig. 5.15 for signatures). Inaccessible parts of the section, where GR data could not be collected, are shown as gaps in the log. Spectral gamma ray logs display the content of natural radioactivity contributed by potassium (K wt. %), uranium (U µg/g), and thorium (Th µg/g). The graphs show both sudden and gradational transitions from mudstone to sandstone and vice versa.

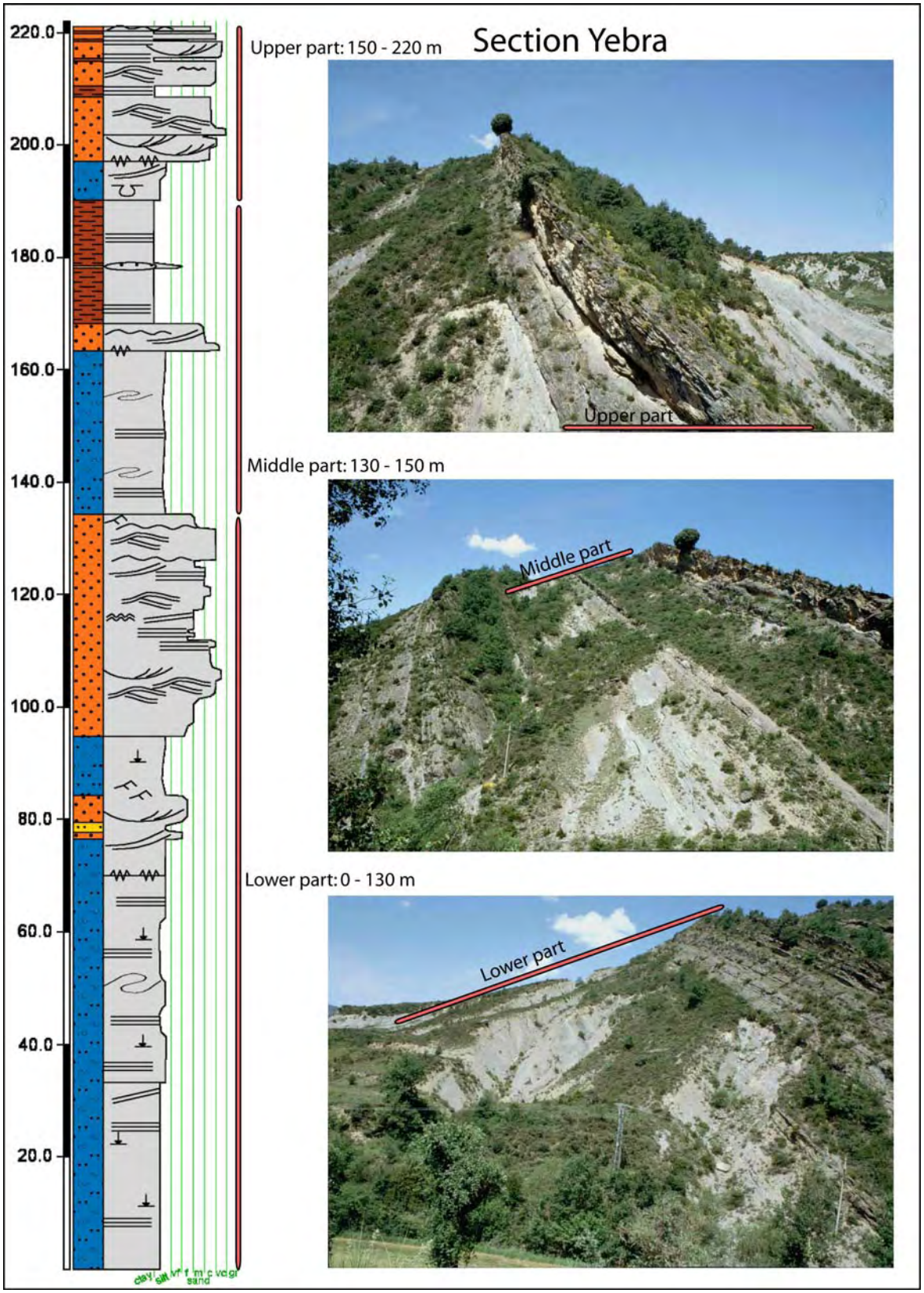

Fig. 5.4: Illustrated overview of the section Yebra (cp. Fig. 5.15 for signatures). Well-exposed fine- to coarse-grained siliciclastic rocks containing a large spectrum of facies types and facies associations observed in the SSt-Succession. For more detailed explanations and illustrations of distinct facies types and facies associations see text below.

5.3 Sedimentary facies

Individual facies types and according facies associations form the basic data set for this study. They are used both as building blocks for the depositional model and as tool for proofing and demonstrating the applicability of the different methods applied. In Chapter 3 gamma ray logs and lithological facies pattern were considered and how they can be used as interpretative devices to deduce indications on depositional environments from data sets as exemplified in Figs. 5.3 and 5.4. Figure 5.3 shows a summary lithological profile and spectral gamma ray logs of section Yebra (cp. Figs. 5.1, 5.2) as well as a graphic to visualize grain size distribution. With the presented methods an extensive pool of data could be acquired, which enabled to resolve the depositional facies of the SSt-Succession in order to develop a depositional model. The main issue of the following sections is to give a review of the analysed litho- and biofacies, facies architecture, and gamma ray characteristics of the SSt-Succession, to set the basis for the interpretation of the depositional environment and the corresponding depositional model.

5.4 Facies types revealed by standard facies analysis

The SSt-Succession exposes a series of coarsening-upward cycles as can be seen in Fig. 5.4. The displayed profile exemplary illustrates a vertical section through the succession that commonly can be divided into a lower, middle, and upper part. Therein, observed lithologies comprise a large spectrum of facies types, reaching from mudrocks to fine-grained marls, siltstones and sandstones, up to pebble-sized conglomerates. The description of the observed sedimentary rock types is mainly based on the classification given by Tucker (1996), (Fig. 5.5). For a quick review of the extensive data set an easy handling was attempted to achieve. A more detailed description of each individual facies type (FT), therefore, was outlined in note form and displayed in a chart, which can be found attached to the Appendix (Tab. B1, Appendix). For purposes of clarity it was abandoned to itemize within this chapter each single facies type that was analysed but rather focus was placed on the most common and meaningful features that can be observed within the SSt-Succession. Adequate facies types were picked and briefly described below, accompanied by a synoptical table (Tab. 5.1) of the complete account, summarizing the main facies types.

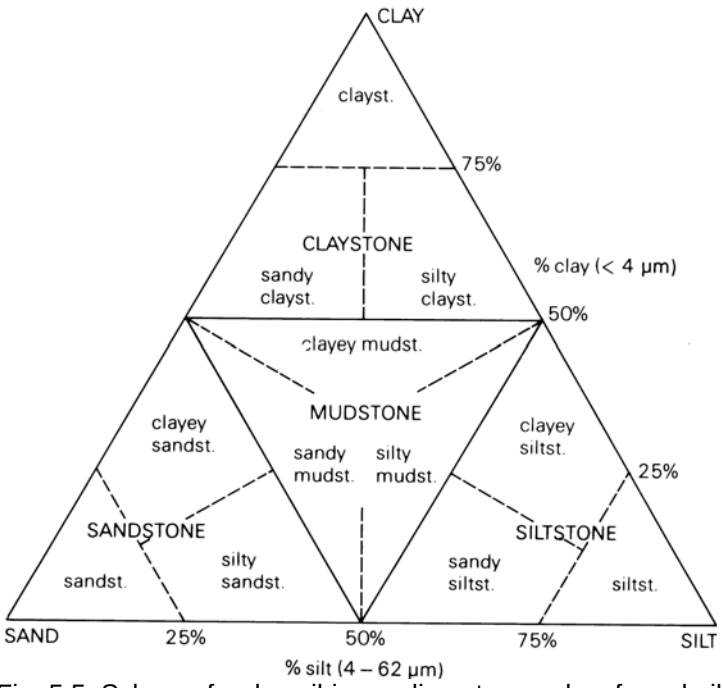

Fig. 5.5: Scheme for describing sedimentary rocks of sand-silt-clay grain sizes (Tucker 1996)

5.4.1 Mudrocks

After Tucker (1996) the term mudrock is a general expression for sediments composed chiefly of silt-sized (4-62 µm) and clay-sized (< 4 µm) particles. Shales and mudstones belong to the mudrocks. Shales are characterized by their fissile appearance (ability to split into thin sheets), while mudstones are non-fissile and mainly have a blocky to massive texture (Tucker 1996). Mudstones and shales form the finest fraction within the SSt deposits. They occur predominantly in the middle to upper part of the succession, and are enclosed by more coarse-grained deposits. The following variations were distinguished (cp. Plate A):

- Fine laminated mud- to claystones (FT-0a),
- Shale, alternating mudstones with variable content of silt-sized particles (FT-0b),
- Shale, alternating mudstones with variable content of silt- to sand-sized particles (FT-0b*),
- Silty mudstones with medium to high carbonate content (FT-0c).

The mudstones FT-0a and FT-0c (Plate A, 1/2/4) are of minor thickness and mainly appear as single layers or thin horizons within sandstone and marl successions. Facies type FT-0b and FT-0b*, however, build up more extensive successions; although the

individual layers are fairly thin, they form alternating successions up to several metres, composed of stacked mud- and siltstone layers with variable content of coarser material.

FT-0b: Shale, alternating mudstones with variable content of silt-sized particles:

The alternating shale succession is composed of claystones, silty claystones, and siltstone beds. Nodules of iron carbonates as well as pyrite occur. The succession forms coarsening- or fining-upward cycles. They show lamination to thin bedding, caused by material changes or changes in colour (grey, brown, green, reddish and yellow). Mudstones form thin layers of some millimetres, while horizons with an increased content of silt-sized particles reach thicknesses of centimetre to decimetre scale, locally showing flaser bedding and load casts (Plate A, 3).

Horizons dominated by clay minerals, predominantly are fossil free, only some plant and fossil fragments and isolated Foraminifera (*Nummulites*) and bivalves (oysters) were observed; bioturbation is rare to abundant, often concentrated within some highly burrowed horizons. The more coarse-grained beds show a slightly higher fossil content, esp. coarser plant fragments. Plant debris locally is replaced by pyrite.

Although single mudstone layers are fairly thin, the complete shale succession reaches thicknesses of several metres to decametres. The alternating cycles indicate a depositional setting with reduced to very low energy conditions, periodically interrupted by an increase in energy and coarser grain sized input.

FT-0b: Shale, alternating mudstones with variable content of silt- to sand-sized particles:*

Facies type FT-0b* is similar to FT-0b, but shows grain sizes up to fine sand grade, and generally displays a more massive texture of the individual beds. As described above, these beds are exposed within an alternating succession of several metres to decametres, showing lamination but also further sedimentary structures like: scour-, flute-, groove- and toolmarks, current ripples, load casts, slumping, ripped-up clasts and shill horizons (Plate A, 5a-c).

The fossil content changes from sparse to abundant, comprising plant and fossil fragments, tests of Foraminifera (*Nummulites*) and bivalves (oysters) and bioclasts in general. With skeletal material concentrated in some horizons (e.g. shill horizons).

From the grain sizes of this facies type either a protected (low energetic) or more distal environment can be deduced, allowing the fine-grained material to settle from suspension. As the observed sedimentary structures arise from current activities a more distal setting was supposed, with sedimentation from turbiditic currents.

Plate A: Characteristics of facies type, FT-0

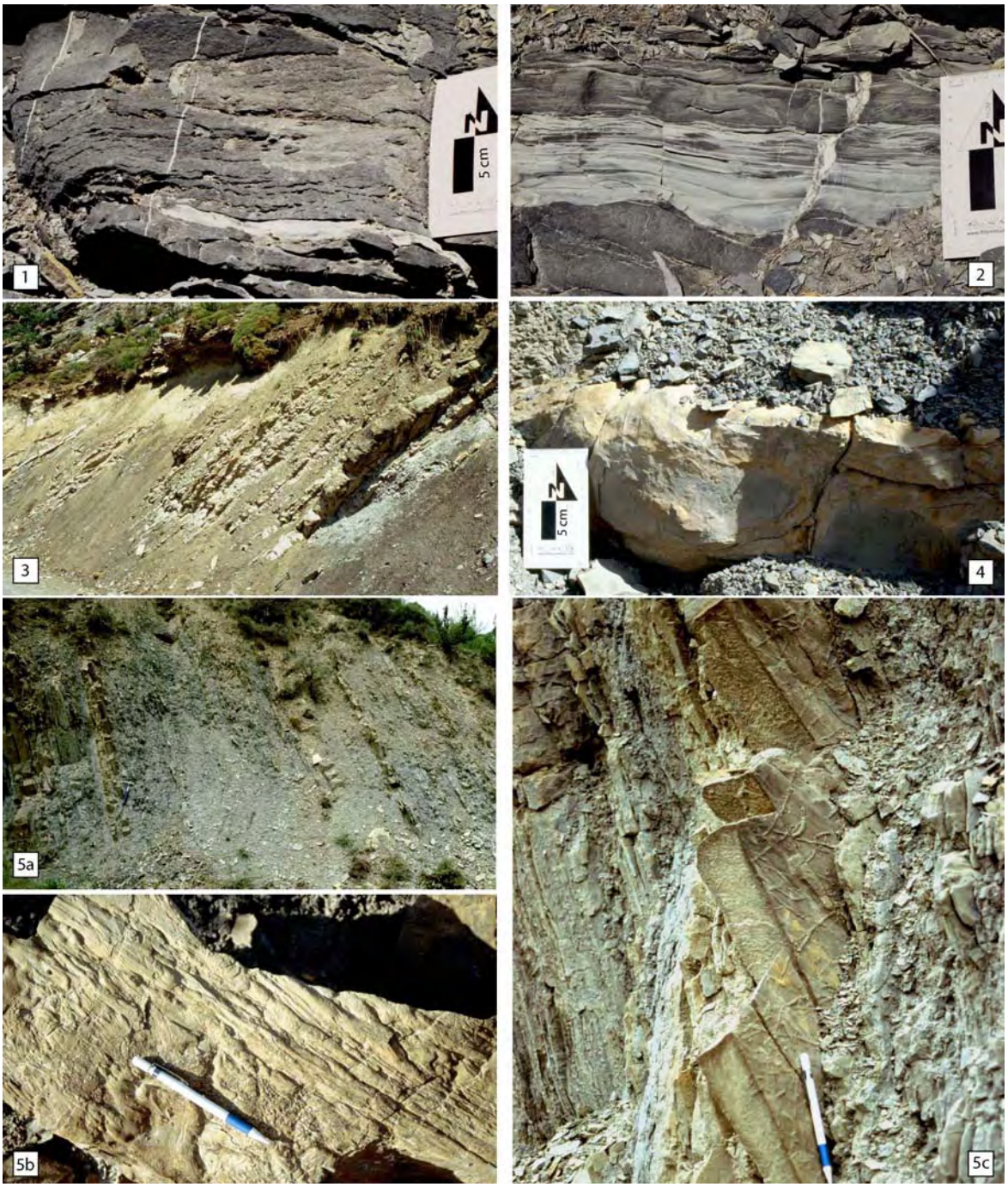

Plate A: Lithology, sedimentary structures, and successions of facies type, FT-0, as exposed in the field: 1) Thin, detached mudstone layer (FT-0a) within coarse-grained sandstones (FT-2d*); 2) Mudstone horizon (~8 cm) within coarse-grained sandstones (FT-2d*) showing lenticular bedding toward top – sandstone-lenses of FT-2d*; 3) shale succession (~15 m) of alternating mudstones with variable content of silt-sized particles and thin siltstone beds (FT-0b); 4) silty mudstone pillow with medium to high carbonate content (FT-0c); 5a) turbiditic shale succession of FT-0b* (~ 20 m), alternating mudstones with silt-, and sandstone beds showing erosional structures on their lower surface; 5b) flute marks preserved as flute moulds on the lower surface of a sandstone bed of FT-0b*; 5c) groove marks on the lower surface of a siliciclastic turbidite, and some bigger flute marks in the upper part of the picture.

5.4.2 Marls – siltstones

Following the classification proposed e.g. by Blatt (1982), and Tucker (1996), marls are defined as calcareous mudrocks, and, therefore, together with the siltstones, would belong to the mudrocks as well. In the context of this study, however, it was more suggestive to group and describe them separately, as they show several similarities within the examined sections. Within the SSt-Succession marls and marly deposits mostly form thick successions, build up by several coarsening-upward cycles. On the basis of varying grain sizes, mineralogical composition, and fossil content nine subtypes were distinguished (cp. Plate B):

- Marls to silty marls with increasing grain sizes and increasing content of silt-, and sand-sized particles (FT-1a/-1b/-1c),
- Silty marls to marly siltstones with increasing fossil content (FT-1d/-1e/-1e*/-1e**),
- Glauconitic siltstones with marl intercalations and changing glauconite, and fossil content (FT-1E/-1E*).

From afar, the successions of FT-1a to FT-1e** are very similar except of the increasing bed thicknesses (Plate B, 1/2). But a closer look reveals some striking differences; the most noticeable one is the abundant amount of fossils occurring within FT-1e* and FT-1e**, and the increased glauconite content of FT-1E and FT-1E*. The latter facies types, however, are restricted to exposures of the southern limb, and also show major differences in their fossil content.

FT-1e and FT-1e**: Fossiliferous marly siltstones:*

The lithology is mainly composed of marls and medium to coarse silt-sized quartz, with varying content of marls and silt-sized particles. Mica and glauconite can be observed, whereas micas are much more common and coarser-graded than glauconite, which usually is fine dispersed through the rock. Calcareous, limonite, and pyritic nodules locally were observed as well. Pyrite also occurs as mineralization filling vugs of fossil tests, as predominantly seen in Foraminifera (Plate B, 3-6)

The beds show thicknesses from decimetre to metre scale, whereas weathering features and intense bioturbation often obscure bedding. Load structures and slumping can be observed, as well as sharp- or even erosive-based beds.

In layers, plant fragments occur in large amounts, commonly they are millimetre sized but also coarser fragments of several centimetres can be found. Foraminifera (*Nummulites*, *Globotruncana*), bivalves, and gastropods, as well as fossil fragments in general are common, whereas *Nummulites* vary in size, from few millimetres up to two centimetres

diameter. The fossil content is quite high and locally even rock forming, whereas Foraminifera (esp. *Nummulites*) compose the predominant part (Plate B, 6).

Increased content of coarser grain sizes (compared to FT1a to FT1d) and large amounts of fossils and plant fragments indicate some current activities. Slumping and load structures argue for (rapid) sedimentation on an unconsolidated sloping base.

FT-1E and FT-1E: Glauconite bearing (fossiliferous) siltstones:*

The siltstones to marly siltstones of FT-1E/-1E* are exposed as consolidated to massive beds forming extending ridges along the southern limb. The bedding is decimetre to metre scale, but comparable to other sub-types of the FT-1 group, primary structures are masked by weathering features and/or bioturbation. Marls, silt-sized quartz, feldspar and micas prevail, and glauconite can be observed in varying amount throughout this facies type. Although glauconite was observed in almost all lithologies of the SSt-Succession, even as detrital component in some conglomerates, it is particularly noticeable for the facies types of the southern limb (namely FT-1E/-1E*/-2A/-2A*/-2B/-2B*) as it occurs more frequently therein. The enrichment of glauconite in some horizons, gives a greenish colour to the rocks, which could even be classified as greensands depending on the amount and appearance (granules) of the authigenic glauconite.

The fossil content of FT-1E is remarkable as well, and pronounced within subtype FT-1E*. Apart from bioturbation, plant and fossil fragments, varying amounts of shells and tests of Foraminifera (esp. *Nummulites*), bivalves (esp. oyster), and echinoids can be observed. Some layers are characterized by an abundant amount of *Nummulites*, but even more striking are beds with an enrichment of oysters. In some horizons, they predominate, forming oyster reef structures in association with a minor content of other fossils.

As primary structures are absent, masked respectively, grain size, glauconite and fossil content are the available indicator for an environment allocation. Hence, subsidiary current activities of more distal environments from coastal/fluvial influences were assumed.

Plate B: Characteristics of facies type, FT-1

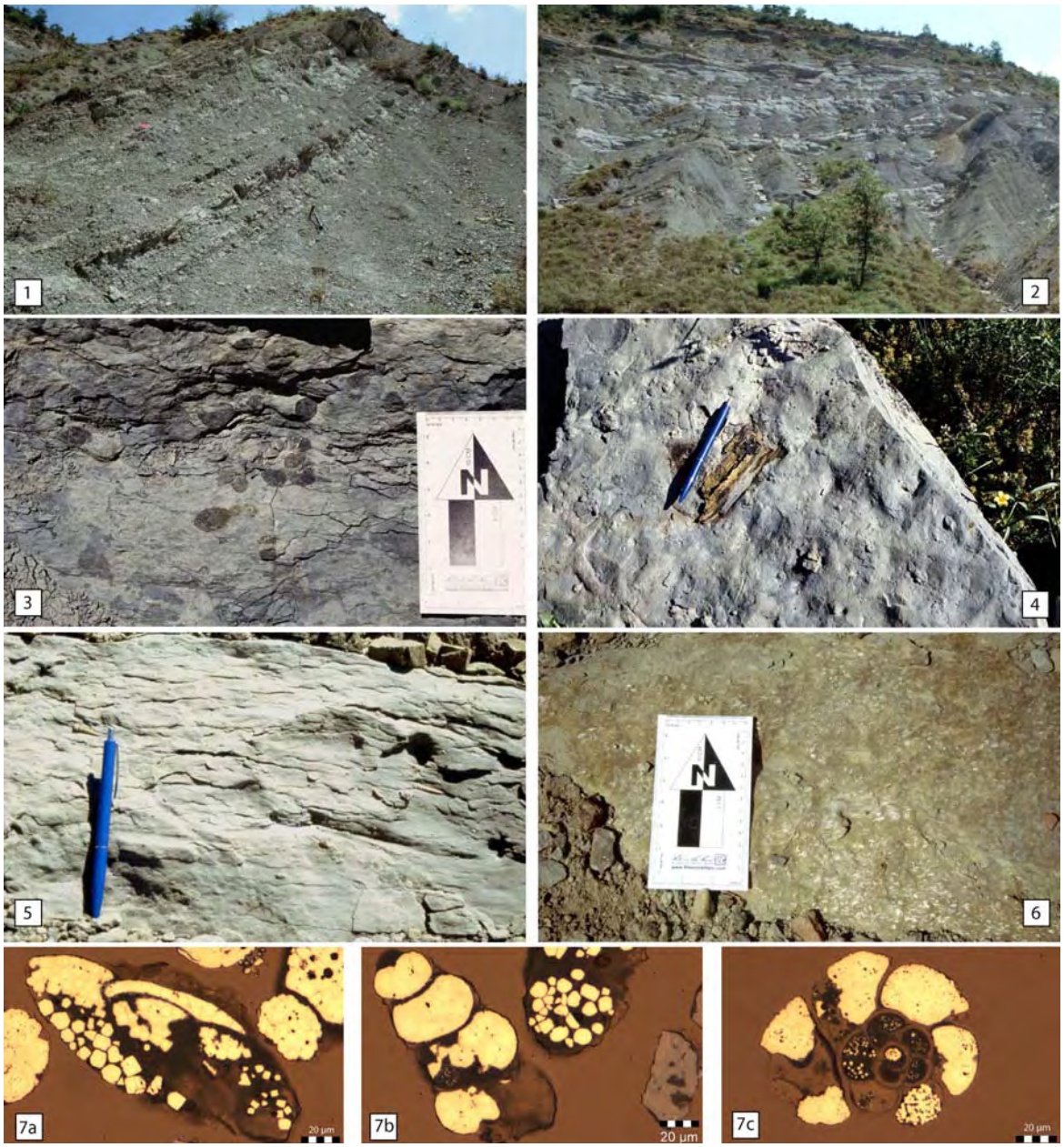

Plate B: Lithology, fossil content, and successions of facies type, FT-1, as exposed in the field: 1) Coarsening-upward successions of (FT-1a/b, Hammer for scale); 2) coarsening-upward succession with increased content of coarse grained material (FT-1c/d/e); 3) bioturbation in marly sediments of FT-1e, obscuring any primary structures, burrows penetrating into underlying layers were filled by slightly coarser sediment (scale ~14 cm); 4) bioturbated marly siltstone, with crawling traces, and large amounts of fossil and plant debris (FT-1e**); 5) fossiliferous marly siltstones with tests of gastropods (probably *Littorina* and *Loxonema*); 6) marly siltstones, almost entirely made up by Foraminifera (*Nummulites*), with individual tests up to 2 cm, and beds reaching thicknesses of 5 metres and more (FT-1e*); 7a-c) pyritized microfossils; Foraminifera of the order Rotaliida (most likely *Elphidium*, *Uvigerina*, and *Globotruncana*).

5.4.3 Sandstones

Sandstones form the most diverse lithology exposed within the SSt-Succession, comprising a number of facies type variations. They cover all grain sizes and show a wide diversity of sedimentary structures, with varying fossil content. Fine- to coarse-grained litharenites up to lithic microconglomerates, composed of quartz, feldspar, lithic fragments, micas, clay minerals, iron oxides, pyrite, locally glauconite and opaque minerals occur (cp. Plate C).

FT-2a: Fine- to medium-grained sandstones:

This facies type is predominantly composed of fine- to medium-grained litharenites, with pyrite, opaque minerals, and glauconite occurring. The occurring sub-types, mainly differ in their kind of sorting and bedding features.

In general, FT-2a shows well-consolidated beds of some decimetre to metre, locally with thin clayey to marly layers interbedded (Plate A, 1&2). The sedimentary structures comprise: planar bedding, low angel trough to hummocky and swaly cross-stratification, often accompanied by undulating to wavy surfaces. Especially within sub-type FT-2a* bidirectional stratification as well as starved ripples, and reactivation surfaces are developed (Plate C, 3&5); wave and current ripples, sometimes flaser bedding and load structures occur. The lower surfaces mainly are sharp based to erosive based, ripped up clasts, and mud chips in general occur, as well as vugs, where mud, were washed away.

Bioturbation and fossil content in general is rare, whereas the most common kind of fossils, besides some plant fragments, comprises some shells and bioclasts in general.

Grain sizes and sedimentary structures are indicating higher energy levels in a setting more proximal to the coastal area. The sediments accumulated in water depths above storm wave base, but still below fair-weather wave base and were probably only sometimes affected by tidal currents.

FT-2d: Medium- to coarse-grained sandstones:

The sandstones of FT-2d, and according sub-types, show grain sizes from medium- to coarse-grained, locally reaching up to micro-conglomerates, and are mostly well to very well sorted, except for the fossiliferous sub-type FT-2d**, which often shows bad sorting and a rusty stain on the surfaces, probably resulting from Fe-alteration of the iron-nodules.

Plate C: Characteristics of facies type, FT-2

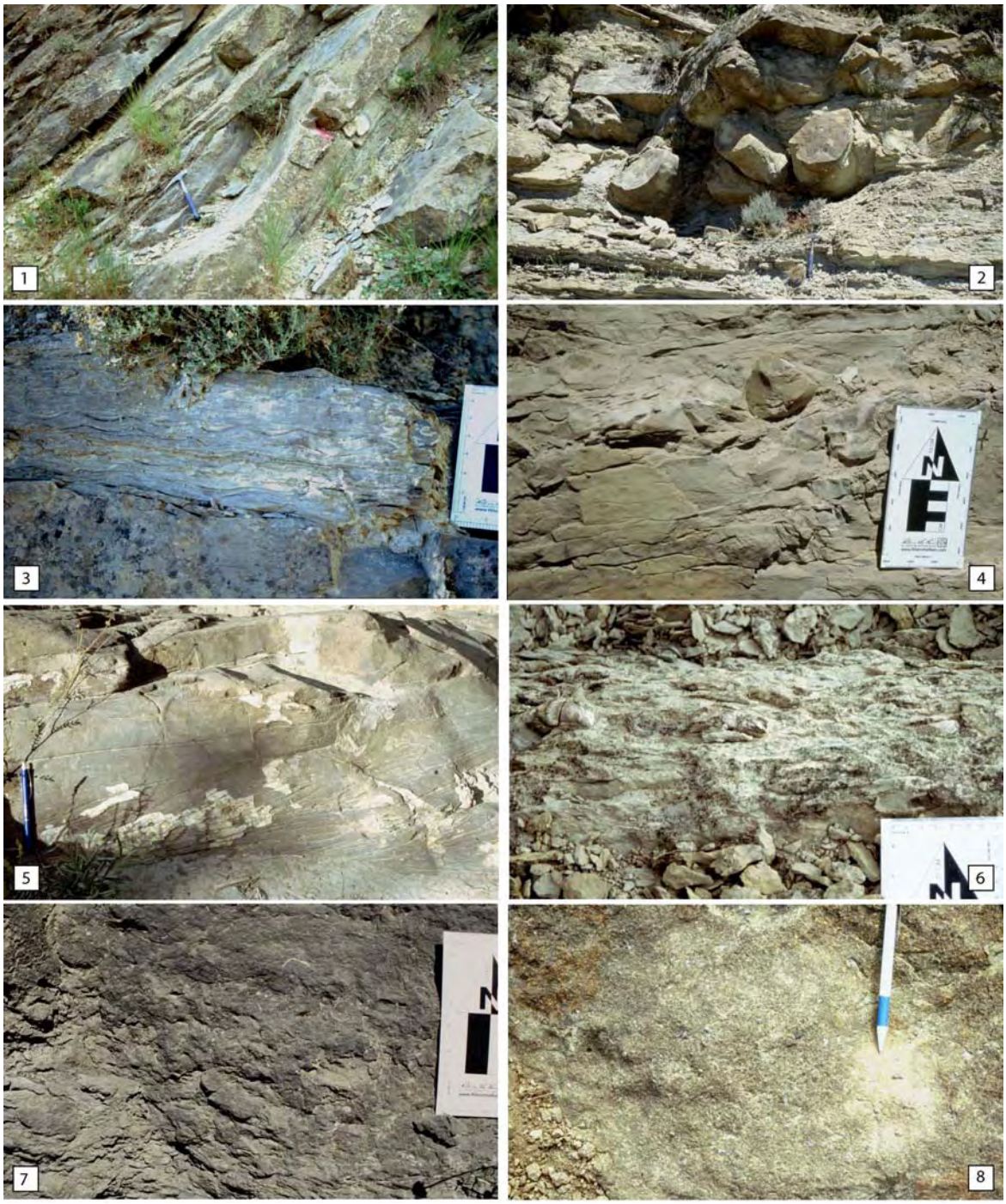

Plate C: Lithology, sedimentary structures, and fossil content of facies type, FT-2; 1) Fine- to medium-grained sandstone beds with hummocky and swaley cross stratification, and wave ripples (FT-2a/2c/2d); 2) ball- and pillow structure in sandstones of FT-2a*; structures are restricted to a well-defined horizon, overlying and underlying strata are undisturbed; 3) climbing-ripple lamination with laminae in-phase; asymmetric ripples indicate current action (FT-2a*); 4) very fine grained and well sorted sandstone with reworked mudstone clast (scale ~14 cm, FT-2a**); 5) fine- to medium-grained, well-sorted sandstone with reactivation surfaces, and sigmoidal cross stratification resulting from climbing-ripples (FT-2a*); 6) fossiliferous, fine grained sandstones, with large amounts of oysters (FT-2A*); 7) medium-grained sandstone with fossil debris, mainly shell fragments (FT-2c); 8) coarse grained fossiliferous sandstone, badly sorted with larger lithic fragments and fossil debris (FT-2d**).

In general, similar sedimentary structures as observed within FT-2a, occur, but the beds are less consolidated, and more variable in their lateral continuation. Bed thickness, in general, comprises some decimetre up to about two metre, locally with fine siliciclastic intercalations. Parallel bedding, low angle cross stratification, trough to hummocky and swaly cross stratification, and locally lateral accretion is apparent. Flaser bedding, current and oscillatory ripples, vugs, mud chips, and ripped up clasts also may occur. The lower surfaces are mainly sharp to erosive based.

Fossil content is much more divers than observed within FT-2a; and even abundant within the sub-type FT-2d**. Bivalves (oysters, *Pecten*), gastropods (*Littorina, Loxonema*), as well as echinoids, Foraminifera, and plant and fossil fragments, in general, occur. Bioturbation is mainly just moderate, some bedding surfaces, however, show large crawling structures.

The general habit of this facies type, grain sizes, sedimentary structure etc. indicates a more proximal depositional environment than FT-2a, highly influenced by fluvial currents.

5.4.4 Conglomerates

The conglomerates generally are polymict, with a matrix-supported fabric (para-conglomerates) and sub-angular to sub-rounded components (clasts, pebbles repectively). Most of the components probably are intraformational, particularly clay clasts and fragments of mudrocks and sandstones (Plate D, 2/3). But some of the lithic components might also be derived from the hinterland area outside the basin, and, therefore, be considered as extraformational clasts. The matrix is bi- to polymodal, composed of medium- to coarse-grained sandstones.

The conglomeratic beds reach thicknesses of several decimetres to some metre (~ 2 m), with surfaces often showing large scale wavy bedding (Plate D, 1/2). Planar bedding, low angle cross stratification and low angle trough cross stratification are the prevailing sedimentary structures. Within the beds mud clasts occur, but are often dissolved or washed out, that just the vugs remain. Wave ripples locally occur and large-scale undulating surfaces are developed, and impressively exposed in some areas.

In some of the conglomeratic beds, fossil shell fragments, as well as tests of bivalves (oysters*, Pecten*), gastropods (*Littorina, Loxonema*), and Foraminifera (*Nummulites*) can be observed, either in small amounts or even much more abundant.

Depending on the size of the components and the fossil content, three facies types were distinguished (cp. Plate D):

- Granulate-sized components, between ~0.5-2 cm (FT-3a),
- Pebble-sized components, up to ~10 cm (FT-3b),
- Fossiliferous type, with some variations in component size (FT-3c).

The conglomerate facies represents the most proximal deposits, highly influenced by both fluvial and shoreface currents.

Plate D: Characteristics of facies type, FT-3

Plate D: Facies type, FT-3; 1) Wave rippled surface with granulate- to pebble-sized components of facies type, FT-3a/b; 2) large scale wavy surface of FT-3a/b; 3) and 4) polymict paraconglomerates, coarse-grained sandstone matrix with components of varying size and composition (FT-3a/b).

Tab. 5.1: Synoptical table of common facies types and facies associations observed within the SSt-Succession.

Facies type	Lithology	Sedimentary structures	Paleontology, organic content
FT-0	Mudrocks Shales to mudstones, with fine-grained silt components, locally occurring as shale-siltstone- alternation with varying content of silt-sized particles and mud.	Lamination to thin bedded shales, caused by alternating material or changes in colour. Scour-, flute-, groove- and toolmarks, current ripples, load casts, slumping, ripped up clasts occur in some areas.	Sparse to abundant, plant and fossil fragments. Bivalves (oysters), Foraminifera, and bioturbation (homogenized horizons) may occur.
FT-1	Marls to Siltstones Marls with fine- to coarse-grained silt components, sand- and mudstones. Locally rich in glauconite. Increasing grain size and content of silt-, and sand-sized particles within the succession.	Successions predominantly are thin bedded with laminated to diffuse/homogenized horizons due to intense bioturbation. Undulating surfaces, slumping and load structures occur. Primary structures locally destroyed due to bioturbation. Increasing bed thicknesses within the succession often associated with a coeval coarsening-upward.	Fossil-content varies from sparse to numerous. Bioturbation is moderate to intense. Plant and fossil fragments may occur. Determined fossil content: Foraminifera (esp. *Nummulite*s, varying in size from µm-scale up to 2 cm in diameter, and globigerina), bivalves (esp. oyster), echinoids and gastropods. Enrichment of *Nummulites* in some horizons, up to more than 90% of bulk.
FT-1	Siltstones Siltstones with iron-minerals and glauconite.	Consolidated to massive, bedding decimetre to metre. Primary structures masked by weathering features and/or bioturbation.	Bioturbated, locally plant and fossil fragments. Determined fossil content: Foraminifera (esp. *Nummulites*), bivalves (esp. oyster), echinoids. Enrichment of oysters in some horizons, together with minor content of other fossils, forming oyster reef structures. Glauconite rich sitstones, and oyster-reefs, predominantly occur on the southern limb.
FT-2	Sandstones: Fine- to medium-grained Fine- to medium-grained litharenites with pyrite. Moderate to very well sorted. Some variants are rich in glauconite.	Bedding massive to consolidate, some decimetre to metre, locally clayey to marly layers. Planar bedding, low angel trough to hummocky and swaly cross-stratification, also bidirectional stratification may be developed, undulating to wavy surfaces, wave and current ripples, sometimes flaser bedding and load structures occur, sharp based surfaces, often erosive based, ripped-up clasts, and mud chips in general, as well as vugs, where the mud is washed away.	Foraminifera (*Nummulites*), fossil and plant fragments may occur. The more fossiliferous type predominantly shows: echinoids and bivalves (oysters); some Foraminifera (*Nummulites, Globotruncana*), and bioclasts in general. The fossiliferous type predominantly is composed of oysters, indicating the appearance of an oyster-bank-assemblage. This type predominantly is observed on the southern limb, as well as the glauconite-rich variants. Bioturbation reaches from bare to intense (e.g. skolithos, ophiomorpha). Skolithos and echinoid often are observed in glauconite-rich rocks
FT-2	Sandstones: Medium- to coarse grained Medium- to coarse-grained, locally up to micro-conglomerates. Predominantly well to very well sorted, except for the fossiliferous variant	Decimetre to metre thick beds, laterally variable, locally with fine siliciclastic intercalations, parallel bedding locally up to lamination, low angle cross stratification, trough- to hummocky- and swaly cross stratification, sometimes lateral accretion. Flaser bedding, current and oscillatory ripples, vugs, mud	Bivalves (oysters, *Pecten*), gastropods (*Littorina, Loxonema*), and shells in general, echinoids, Foraminifera, plant and fossil fragments. Moderate bioturbation.

		chips, ripped up clasts also may occur. Sharp based surfaces, locally erosive based,	
FT-2	Sandstones: Coarse grained Mostly coarse-grained up to microcongomeratic litharenites, lithic to clay pebbles, Fe-nodules, clay clasts. Locally high mud content.	Beds of some decimetre up to metre, undulating to wavy surfaces, low angle cross stratification, swaly cross stratification, mud drapes to locally flaser bedding, lateral accretion.	Locally high organic content: Plant and fossil fragments, Foraminifera (*Nummuliten*, *Globigerina*), bivalves (oysters, *Pecten*, shells and filaments), gastropods (*Littorina, Loxonema*), echinoids. Highly bioturbated, big burrows.
FT-3	Conglomerates Polymict para-conglomerates, with sub-angular to sub-rounded components, intra- and extraformational. Bi- to polymodal matrix of medium- to coarse grained sandstones	Decimetre to metre thick beds, planar bedding as well as planar to low angle trough cross stratification. Large scale undulating surfaces and wave ripples. Mud clasts, drapes and vugs. Three sub-types: Granulate-sized components (~ 0.5 – 2 cm), Pebble-sized components (up to ~ 10 cm), Fossiliferous, varying component size.	Fossil fragments, bivalves (shells, oysters, *Pecten*), gastropods (*Littorina, Loxonema*), Foraminifera (*Nummulites*).

5.5 Facies Indications revealed from gamma ray spectrometry

Along the two limbs of the Basa Anticline spectral gamma ray logs were recorded within selected profiles of the SSt-Succession (Fig. 5.1). The resulting GR logs display some variations in element distribution across the vertical sections, as can be seen in Figure 5.3. Owing to the fact that standard measurements revealed a general drift of the portable GR-320*enviSpec*, the obtained data set was standardized on the basis of analogue laboratory measurement (Tab. 5.2), (cp. Chapter 4).

Tab. 5.2: Computed correction factor for potassium (K), thorium (Th), and uranium (U), obtained from outcrop and laboratory analogue measurement (GR-320*enviSpec*, Canberra-Spec) on SSt-samples from the Jaca Basin. Given are mean values with standard deviation.

	Mean GR-320	Mean Canberra	Deviation
K [wt. %]	1.83 ± 0.17	0.79 ± 0.04	54 ± 10 %
Th [µg/g]	10.77 ± 0.84	3.50 ± 0.12	68 ± 6 %
U [µg/g]	2.49 ± 0.71	1.38 ± 0.05	38 ± 17 %

To analyse and interpret the characteristics of the three radioactive isotopes (K, Th, U), and corresponding log pattern, in a robust manner, the data set of each profile has been screened in several ways. Element data and element ratios were plotted for each profile both on cross plots and on vertical logs to derive indications on lithology and facies. To compute and visualize the total gamma ray flux, which is not supported by the Explore4-software, the unit of radioelement concentration (ur), defined by the International Atomic Energy Agency (IAEA 1976), was calculated:

$$ur = 2.6 \times K\ (wt.\ \%) + 1 \times U\ (\mu g/g) + 0.47 \times Th\ (\mu g/g)$$

The corresponding vertical logs in the following are termed as UR log. Based on the obtained data set different trends and log pattern could be distinguished. A review of the general gamma ray log trends in the SSt-Succession is given below, followed by an evaluation of developed gamma ray log shapes, and examination of element distribution within the successions.

5.5.1 General trends of spectral gamma ray profiles

The deposits of the SSt-Succession show some significant differences in their gamma ray log response, especially regarding the distinct exposure sites of the northern and the southern limb. Although the overall gamma ray response is slightly higher on the southern limb, the spectral GR data of the occurring rock types reveal similar isotope concentrations for both sites (Tabs. 5.3a/b).

Tab. 5.3a: Mean values of potassium (K), thorium (Th), and uranium (U), and mean total values (UR) measured in the SSt-Succession of the northern exposures (Std = standard deviation of repeated measurements + standard deviation of correction factor: 10 % K, 6 % Th, 17 % U); corrected according to Tab. 5.2.

	Mean K [wt. %]	*Std*	*Mean Th [µg/g]*	*Std*	*Mean U [µg/g]*	*Std*	*Mean UR*	*Std*
Mudstone	1.41	0.21	5.08	0.58	2.20	0.53	8.24	1.69
Marls-Siltstone	1.26	0.30	4.74	0.76	2.26	0.78	7.75	2.89
Siltstone-Marls	1.29	0.27	5.24	0.75	2.27	0.64	8.07	2.47
Siltstone	1.03	0.28	4.18	0.75	1.83	0.57	6.46	2.48
Sandstone	0.83	0.14	3.28	0.44	1.59	0.49	5.28	1.40
Total	1.16	0.24	4.50	0.66	2.03	0.53	7.16	2.18

Tab. 5.3b: Mean values of potassium (K), thorium (Th), and uranium (U), and mean total values (UR) measured in the SSt-Succession of the southern exposures; (Std = standard deviation of repeated measurements + standard deviation of correction factor: 10 % K, 6 % Th, 17 % U); corrected according to Tab. 5.2.

	Mean K [wt. %]	*Std*	*Mean Th [µg/g]*	*Std*	*Mean U [µg/g]*	*Std*	*Mean UR*	*Std*
Mudstone	1.24	0.13	5.47	0.33	2.17	0.37	7.94	0.85
Marls-Siltstone	1.21	0.23	5.12	1.19	2.35	0.60	7.89	2.21
Siltstone-Marls	1.23	0.27	5.31	0.54	2.20	0.69	7.89	2.38
Siltstone	1.08	0.17	4.86	0.52	2.06	0.46	7.14	1.43
Sandstone	1.03	0.15	4.40	0.59	1.87	0.52	6.59	1.63
Total	1.16	0.19	5.03	0.63	2.13	0.53	7.49	1.69

Across both exposure sites and within individual successions, however, a large spread of K, Th, and U values, as well as similar ranges in the element concentration can be recognized (Figs. 5.7 and 5.9). Along the entire sections a general upward decrease in gamma radiation can be observed, which is more pronounced in sections of the northern limb, accompanied by punctuated peaks. The southern successions display more uniform logs, with a subtle trend of upward decreasing gamma radiation, which are also marked

by well-defined peaks. As peaks usually correlate with a sudden change in rock composition, indicating a modification of sedimentary facies and grain size, they can be used to separate distinct facies groups, or units within a succession. Associated gamma ray log shapes that are developed across most of the examined sections, in turn can be used to determine grain size trends, giving some hints on the energy, and thus the depositional facies.

5.5.2 Gamma ray log shapes

Referring to the application techniques outlined in Chapter 3.2, the recorded sections of the SSt-Succession were screened for principal (funnel, bell, cylinder) and subordinate (bow, serrated) log shapes, as illustrated in Fig. 5.6. Within the examined successions all types of log shapes are developed, whereas funnel, and bell shapes prevail. In general individual trends are more pronounced within the sections of the northern limb, showing well-developed funnel shapes, while in the southern sections individual trends are developed more faintly. Observed log trends along the northern and the southern exposures of the SSt-Succession are illustrated in Fig. 5.7.

As already denoted, *funnel shapes* are one of the prevailing motifs within the SSt-Succession, and are well developed within the northern outcrops. Funnel shapes, in general, display a progressive upward decrease in gamma reading, and can be referred to a gradual upward change in clay mineral content (Rider 2004). Such cleaning-up trends are either caused by a progressive change in lithology, or a gradual change in the proportions of thinly interbedded units below the resolution of the logging tool (Emery & Myers 1996). Within the sections of the northern limb, funnel shape motifs are best developed in the western sections, i.e. Latás, Isún and Yebra. Towards the east, the cleaning-up trend is still present, but not as clearly expressed anymore. Distinct funnel shapes are barely recognizable, the trends rather seam to interfere with each other, especially within section Fanlillo. On the southern limb, funnel shapes are less pronounced. In contrast to the observations of the northern limb, funnel shapes seem to be more ‘prominent’ in the eastern corner, i.e. sections Sabiñánigo Alto, and Sasal, with the latter showing a stacked pattern of successive funnel shapes, while Jarlata shows just a slightly developed trend. In shallow marine settings, funnel shapes can be related to an upward transition from shale-rich to shale-free lithologies, caused by an increase in depositional energy. Shallowing-upward and coarsening-upward of the succession usually are coupled to funnel shapes, pointing to gradually increasing depositional energies, respectively (Emery & Myers 1996).

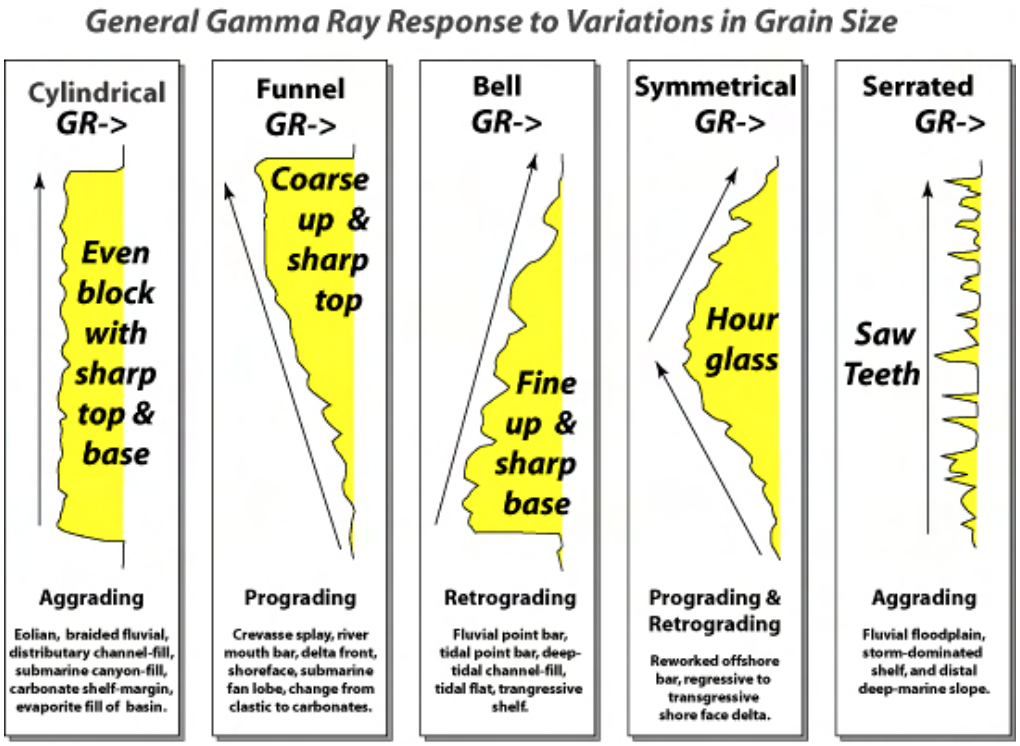

Fig. 5.6: Gamma ray logs track the upward change in clay mineral content, resulting in general log shapes/trends that can be recognized within well log curve; cylinder, funnel, and bell form the principal log shapes, while symmetrical (bow) and serrated logs represent in-between trends (source: Kendall 2003).

Bell shapes result from a progressive upward increase in gamma reading, and can be recognized in the middle and uppermost part of the northern sections. In the middle part of sections Latás and Fanlillo, subordinate bell shapes can be observed, while more pronounced shapes are developed in sections Isún and Sobás. Within the sections of the southern exposures, bell shapes are rare or just weakly developed, as for example in the middle to upper part of sections Sabiñánigo Alto and Frauca. Bell shapes generally are related to a gradual upward change in clay mineral content, resulting in a 'dirtying-up' trend of the succession. Such trends indicate a decrease in depositional energy, and can be referred to lithology changes (e.g. from sand to shale), or to upward thinning sand beds that merge into a thinly interbedded sand/shale unit (Emery & Myers 1996). There are several possibilities of interpreting such dirtying-, or fining-up trends, as listed in Fig. 5.6. According to the general position of the SSt-Succession within the Jaca Basin and also of the individual trends within the SSt-Succession, the deposits can be assigned to a shallow marine environment.

Cylinder shapes usually are characterized by sharp based units of low gamma radiation, set within a higher gamma background unit; whereas the internal gamma reading of the cylinder shape is relatively constant (Emery & Myers 1996). In the examined SSt-Succession, cylinder shapes are moderately developed. In the upper part of Sobás, a

cylinder shape can be recognized and also section Isún, and Navasa on the southern limb reveal such a trend. But to prevent an over-interpretation of the gamma ray logs, such 'weak' trends are considered with care. Abrupt changes between the contrasting log units (high to low counts and vice versa) indicate sudden changes in depositional energies. Such log trends are predominant in fluvial channel sands, turbidites, aeolian sands, and evaporites (Kendall 2003). In the case of section Sobás (Fig 5.7), for example, channel deposits are most likely, due to the position within the section.

In addition to the principle gamma ray log shapes, described above, two in-between trends, shapes respectively, can be recognized. Mainly within the southern exposures, *bow shaped* (symmetrical) gamma ray logs can be observed. They display a gradual decrease with a subsequent gradual increase in gamma response, whereas no sharp break is developed between the two trends. Section Jarlata, for example shows such a bow shape; although developed just moderately, the symmetry is well-defined. In a much smaller scale, bow shapes are developed in section Frauca, and Sabiñánigo Alto; whereas at least the latter will be treated with care regarding the interpretation, as the log shape is very ambiguous. As illustrated in Fig. 5.6, bow log shapes usually result from progradation and retrogration of clastic sediments in a basinal setting (Kendall 2003), representing larger scale depositional mechanisms.

Some more *serrated or irregular log shapes* within the successions lack a systematic character, e.g. section Frauca. They correspond to aggradation of shales or silty lithologies and can occur in various settings, representing e.g. shelf, deep water, or muddy alluvial overbank facies (Cant 1992).

From the observed log shapes, which give hints on coarsening- and fining-upward succession, progradation and retrogradation respectively, a depositional setting subjected to changes in current energies and sedimentary material can be deduced. The occurrence of bell and funnel log shapes adjacent to each other, as e.g. in section Latás and Sobás, indicates a rapid shifting of depositional energies within 'short' time intervals. This points to a shallow marine setting, affected by coastal/fluvial currents. The sections of the northern limb, in general, reveal a progradational pattern, which seems to have its correlative continuation in the southern exposures, where according upward successions are developed more moderately, e.g. stacked pattern of section Sasal.

Total gamma ray flux and equivalent log shapes recognized within the SSt-Succesion provide a rough framework of facies distribution and give first hints on the depositional character of the examined system. Further analyses of the GR data will be used to get a better resolution of the depositional setting.

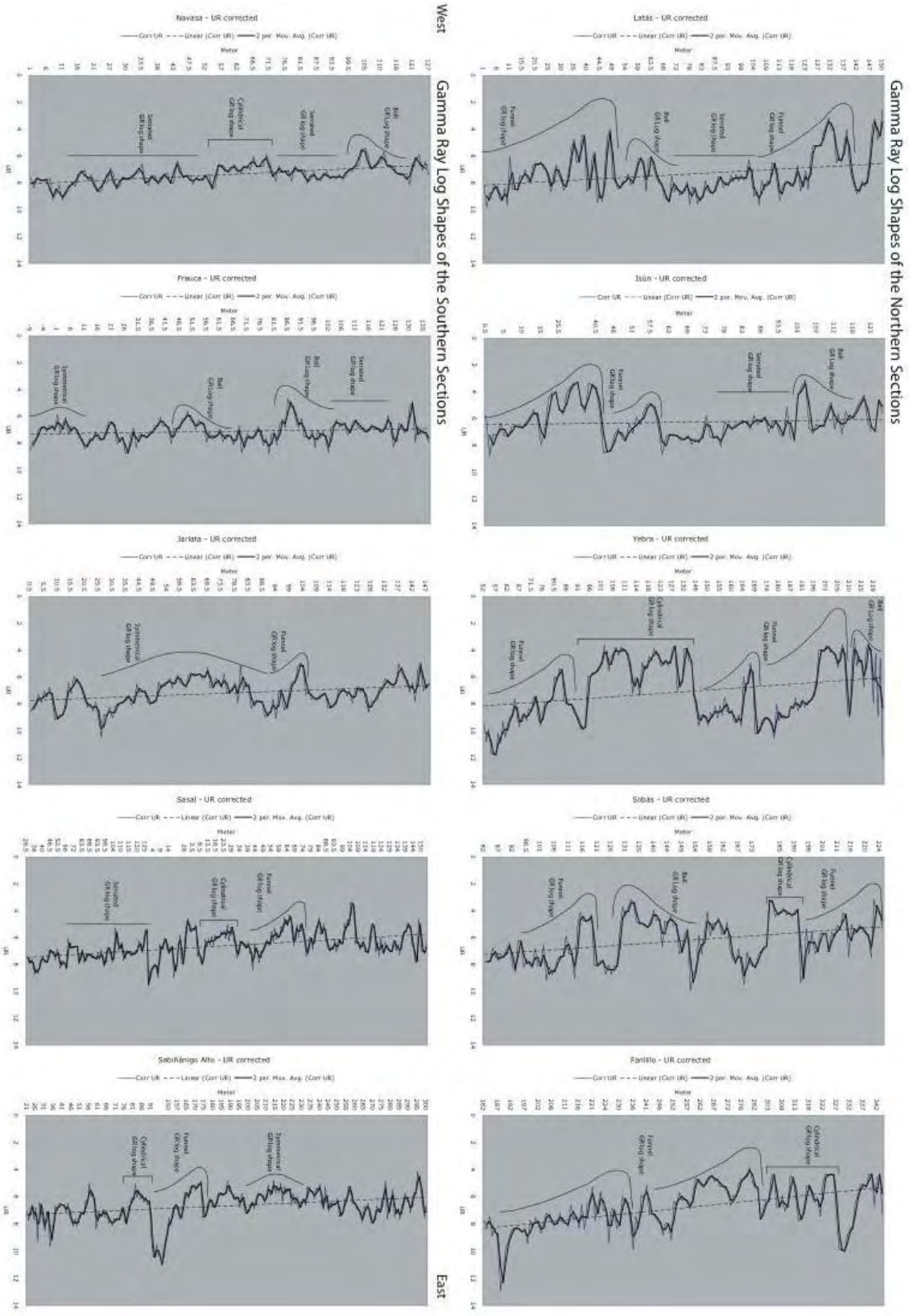

Fig. 5.7: Gamma ray logs of the northern and the southern limb (cp. Fig. 5.1 for location), displayed are UR logs, giving the total natural radioactivity. To even sharp peaks, arising from spacing between measuring points, an average curve is drawn. Dotted line indicates decrease in gamma radiation. Observed log shapes comprise: Funnel, bell, and cylinder shapes, as well as symmetrical (bow), and serrated shapes; see text for details. Enlarged illustration is given in Appendix B.

5.5.3 Element ratios

Screening element distributions and corresponding element ratios for indicative patterns provide a useful application to refine the preliminary interpretations obtained from log shape interpretations (Tabs. 5.4a,b). Element ratios, thereby, are of particular interest, as they have much more significance regarding the depositional facies than distinct element concentrations solely. Furthermore, distinct values of K, U, and Th recorded by the portable gamma ray spectrometer are more sensitive to irregularities in the measured rock surface, while the calculated ratios remain unaffected (Hampson 2005). For each processed vertical section Th/U, and Th/K logs were plotted, as well as Th/K cross plots to compare ratios, examine distinct log pattern and to reveal significant deviations from 'normal' trends. Selected logs and cross plots are displayed within this section, while an enlarged and more comprehensive illustration of GR logs abd cross plots is given in Appendix B.

Tab. 5.4a: Mean element ratios with standard deviation (Std) of the northern exposures.

	Mean Th/K	*Std*	*Mean Th/U*	*Std*	*Mean K/U*	*Std*
Mudstone	3.61	0.78	2.31	1.1	0.65	0.73
Marls-Siltstone	3.77	1.06	2.1	1.53	0.56	1.08
Siltstone-Marls	4.07	1.02	2.31	1.39	0.57	0.91
Siltstone	4.06	1.02	2.29	1.31	0.57	0.84
Sandstone	3.96	0.57	2.07	0.92	0.53	0.62
Total	3.9	0.89	2.22	1.25	0.58	0.83

Tab. 5.4b: Mean element ratios with standard deviation (Std) of the southern exposures.

	Mean Th/K	*Std*	*Mean Th/U*	*Std*	*Mean K/U*	*Std*
Mudstone	4.42	0.46	2.53	0.7	0.58	0.5
Marls-Siltstone	4.24	1.41	2.18	1.79	0.52	0.83
Siltstone-Marls	4.32	0.81	2.42	1.23	0.56	0.95
Siltstone	4.5	0.68	2.36	0.97	0.53	0.62
Sandstone	4.28	0.73	2.36	1.11	0.56	0.67
Total	4.36	0.82	2.37	1.16	0.55	0.71

Th/K cross plots

Following the approach, proposed by Quirein et al. (1982), Th/K cross plots were used as an indicator on clay mineral composition of the investigated succession (cp. Chapter 3, Fig. 3.4). Being aware of the limitations that might arise from counting statistics and analytical precision, discussed in Chapter 4, the calculated GR data were analyzed for general trends as well as for significant deviations from 'normal' values. The total (UR) GR logs already uncovered some different vertical trends within sections of the northern

and southern exposures (Fig. 5.7). From adequate cross plots of thorium against potassium further differences can be revealed (Fig. 5.8a/b). The values of the northern limb cover a much wider range, showing a kind of alignment that extends parallel above the illite field. The values of the southern limb, however, accumulate much closer to each other and do not show such a consistent pattern. More suggestive than a sheer cross plot, however, is to refine the cross plot by taking information on the lithologies into account. As proposed e.g. by Rider (2004), this semi quantitative approach enables a more reliable evaluation of dominant clay mineral and detrital mineral contents of a facies on the basis of Th/K ratio. 'Normal' Th/K ratios for sandstones, as e.g. given by Rider (2004), commonly range at about 4-6; whereas higher ratios, Th/K > 6, are attributed to Th enrichment due to heavy mineral concentrations. Siliciclastic mudrocks are also characterized by Th/K ratios within a range of 4-6, whereas major deviations are evoked by certain clay mineral abundances: a kaolinite dominated suite is shifting the ratios towards higher values, while an illite dominated suite produces lower values (Hampson 2005).

As evaluated in Chapter 4, the data set obtained from outcrop measurements using the portable GR-320 device, show a drift towards higher values, with a deviation between 38 and 68 % (Tab 5.2). The corrected values for sandstones and mudrocks exposed in the SSt-Successions of the northern limb are in intermediate array of the Th/K cross plot, given by Quirein et al. (1982). The values scatter around 4, and are partially in the 'normal' range or slightly below, whereas the successions of the southern limb show Th/K ratios above 4. Higher Th/K ratios in shales and siltstones are indicative for marine facies, dominated by kaolinite and illite, with some chlorite, smectite and mixed layer clays (Rider 2004). In the cross plot of Quirein et al. (1982), the calculated values plot in the field for 'mixed layer clays' (Fig. 5.8). The elevated Th/K ratios of siltstones in the southern sections predominantly can be referred to an increased concentration of Th bearing phases, like chlorite, kaolinite, or heavy minerals, while lower ratios for sandstones indicate the influence of observed glauconite. An increased glauconite content, as observed from field investigations and thin sections, and described by Puigdefàbregas (1975), cannot directly be detected on the basis of this cross plot. But this does not necessarily exclude the occurrence of glauconite, as polymineral phases were analysed, where mineral phases with higher Th concentrations obscure potential 'glauconite signals', as it is assumed to be the case especially for sandstones of the southern sections.

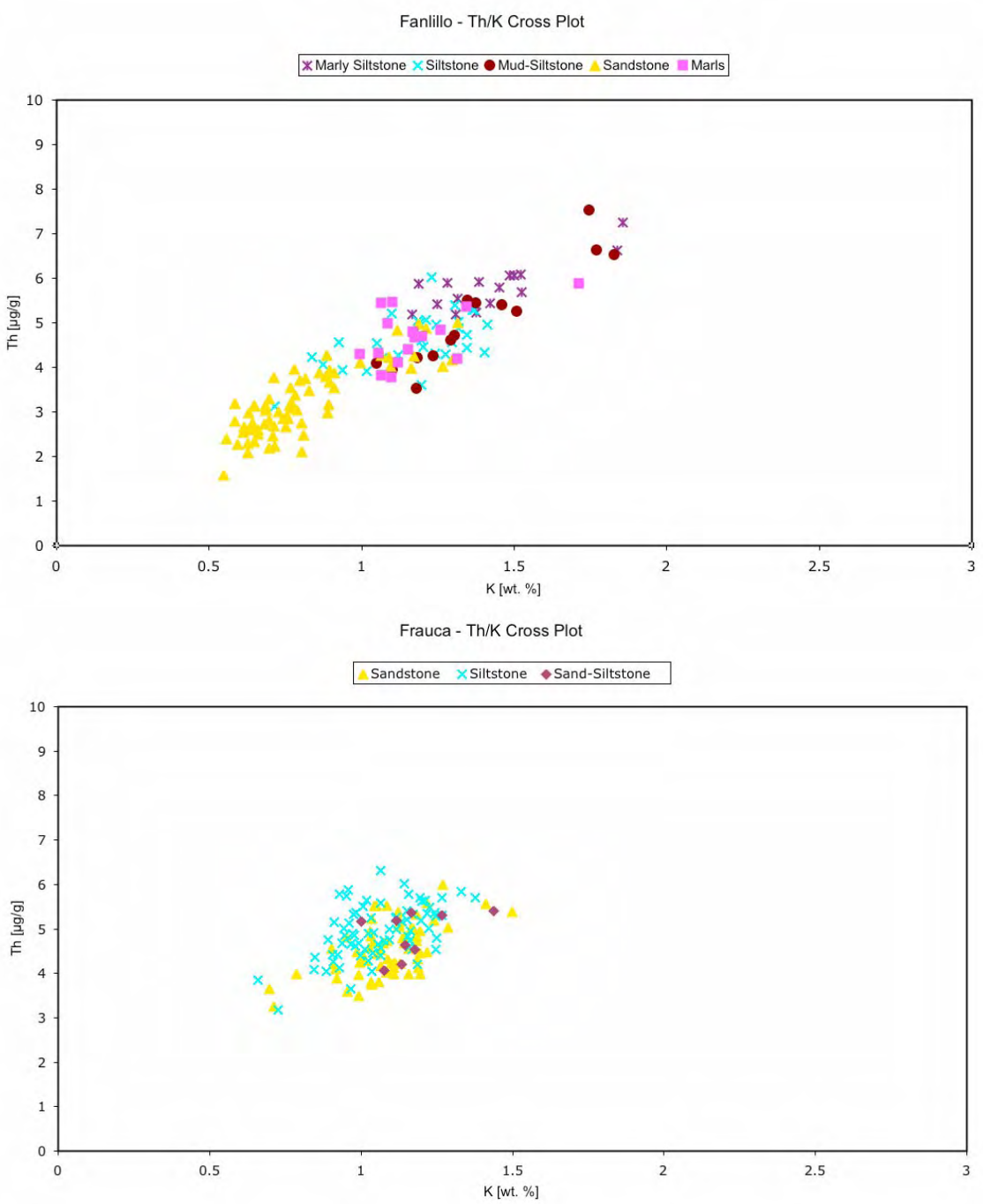

Fig. 5.8a: Th/K cross plots of the northern (Fanlillo) and the southern (Frauca) limb, showing distinct pattern in their distribution. Values of the northern sections plot roughly along a line, while for the southern sections they accumulate much closer.

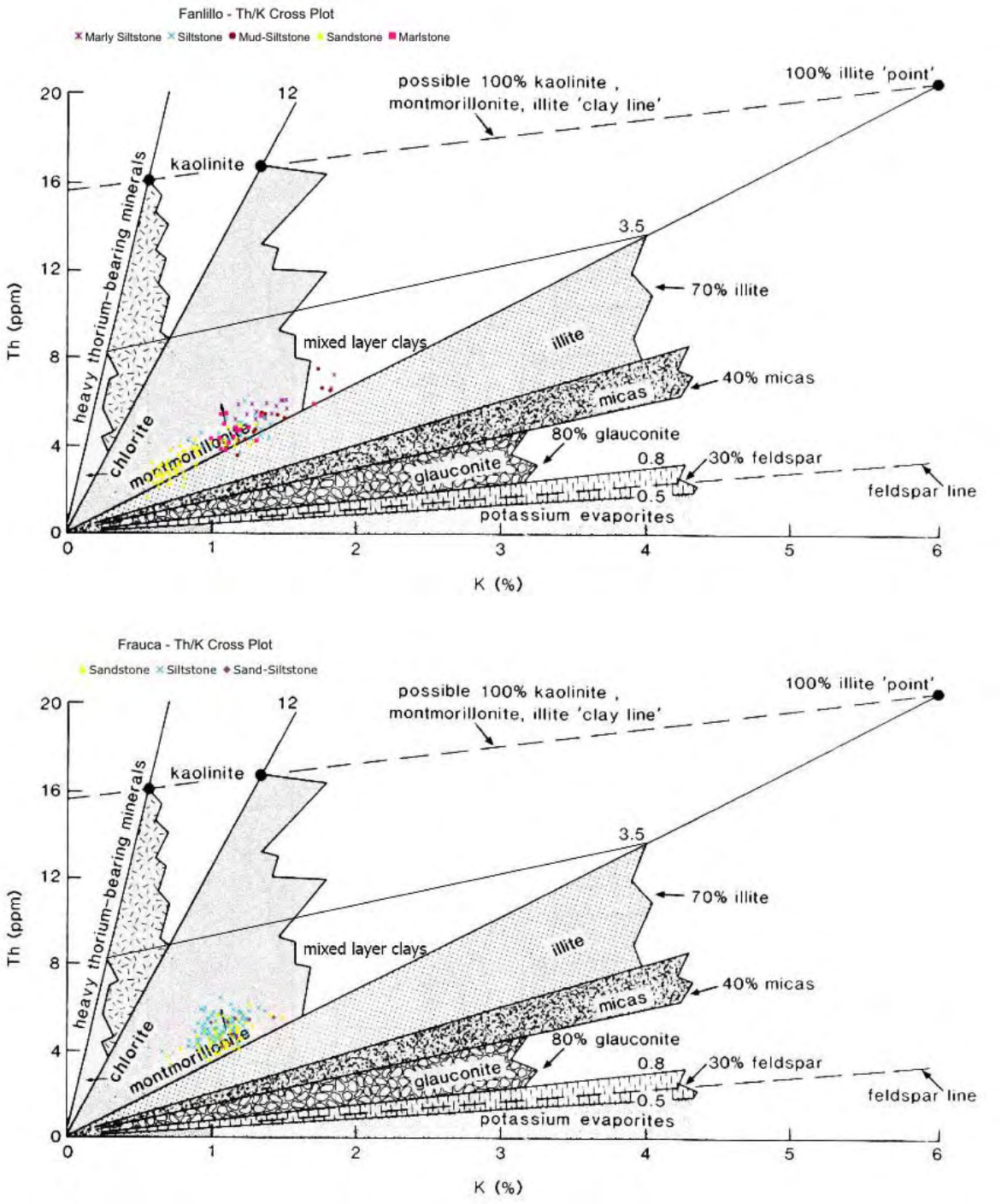

Fig. 5.8b: Th, and K values of section Fanlillo and Frauca plotted in the Th/K cross plot of Quirein at al. (1982). Th/K ratios predominantly plot in the mixed layer field. Fanlillo shows good discrimination between distinct lithologies, with clay mineral dominated rocks, plotting at higher Th and K values, while sandstones display lower values. Th/K values of section Frauca accumulate much closer, scattering slightly above the illite field.

Mean K, and U values are very similar for both exposure sites (Tabs. 5.3a/b), resulting in similar K/U ratios. The lower Th/K ratios of the northern successions are assigned to the occurrence of K-feldspar, with some horizons, e.g. in section Latás (40 m to 45.5 m),

revealing sandstones with an increased potassium content (Fig. 5.8), pointing to an increased K-feldspar content. Within some sandstone bedsets, however, elevated Th/K ratios can be revealed from the cross plots as well as from equivalent logs, which indicates enrichment in heavy mineral concentration.

Th/K and Th/U logs

For the examination of the evolution of a depositional system in time, vertical logs of isotope ratios (e.g. Th/K and Th/U ratios) are more indicative than their equivalent cross plots. Therefore, Th/K and Th/U logs of the SSt-Succession were scrutinized (Fig. 5.8). Some general trends that were already displayed by the total gamma ray flux (UR log) can also be observed in the mean Th/K and Th/U ratios. A general pattern of higher Th/K and Th/U ratios can be recognized for the southern exposures (Tabs. 5.4a/b), which is assigned to elevated Th concentrations within the southern exposures. Although the overall values for Th/K and Th/U ratios are higher on the southern limb, ultimate logs show very distinct pattern, as highest ratios are recorded for bedsets of the northern exposures (Fig. 5.9). From Th/K ratios proximal-distal indications can be revealed, as e.g. described by Parkinson (1996), there appears to be a close correspondence between elevated Th/K ratios and units interpreted as proximal from independent sedimentological facies analyses. The upward changes of the Th/K logs display a stacked pattern, indicating several progradational cycles with a general progradational character of the depositional system. This observation confirms the interpretation already deduced from the GR log shapes. Equivalent progradational Th/K stacking patterns are developed across both exposure sites, but are more pronounced within the northern successions, with the highest values recorded in the uppermost bedsets of section Latás (Fig. 5.9).

Th/U ratios provide further indications on the depositional environment. Because uranium has a marine affinity and thorium a continental affinity, the relative influence of marine to continental settings can be constrained from their element ratio (e.g. Adams & Weaver 1958). ‘Normal’ Th/U ratios range from 3-6, while higher values indicate more continental environments, lower ratios marine environments respectively (Rider 2004). For both exposure sites of the SSt-Succession, Th/U values scatter between 2 and 3. They are just within, or slightly below the ‘normal’ range respectively, generally pointing to a marine environment, with minor continental influences. Individual profiles, however, show differentiated Th/U curves, with distinct peaks of increased Th/U ratios. Gamma ray logs of sections Isún, Navasa, and Sasal for example (Fig. 5.9), show marked raises in their Th/U ratios (> 7). This might either point to an increased continental influence, or to an increased heavy mineral content, accumulated for example in lag deposits. Low to very low ratios, like in the middle part of section Fanlillo (Fig. 5.8), imply a general marine

environment with an increased uranium concentration, where continental influences are suppressed or are of minor importance. Horizons with more punctuated low Th/U ratios, e.g. section Sobás can be interpreted to represent condensed horizons, where organic material, and thus uranium was enriched (Rider 2004).

Due to the high mobility of uranium, the application of Th/U ratio is extremely difficult, and environmental indications should not be over interpreted, or based on the Th/U ratios, solely. In combination with total gamma ray flux, element distribution, and further element ratios, however, they provide meaningful indications on the depositional setting.

From GR log shapes and vertical Th/K stacking pattern a progradational depositional system can be deduced. Abrupt changes in vertical stacking patterns and log shapes, furthermore, point to a depositional environment controlled by changing current activities. This is the case e.g. within shallow marine costal settings, which can be confirmed by locally very high Th/U ratios indicate a periodic increase in continental influence, as well as from increased K-feldspar concentrations, revealed from Th/K cross plots.

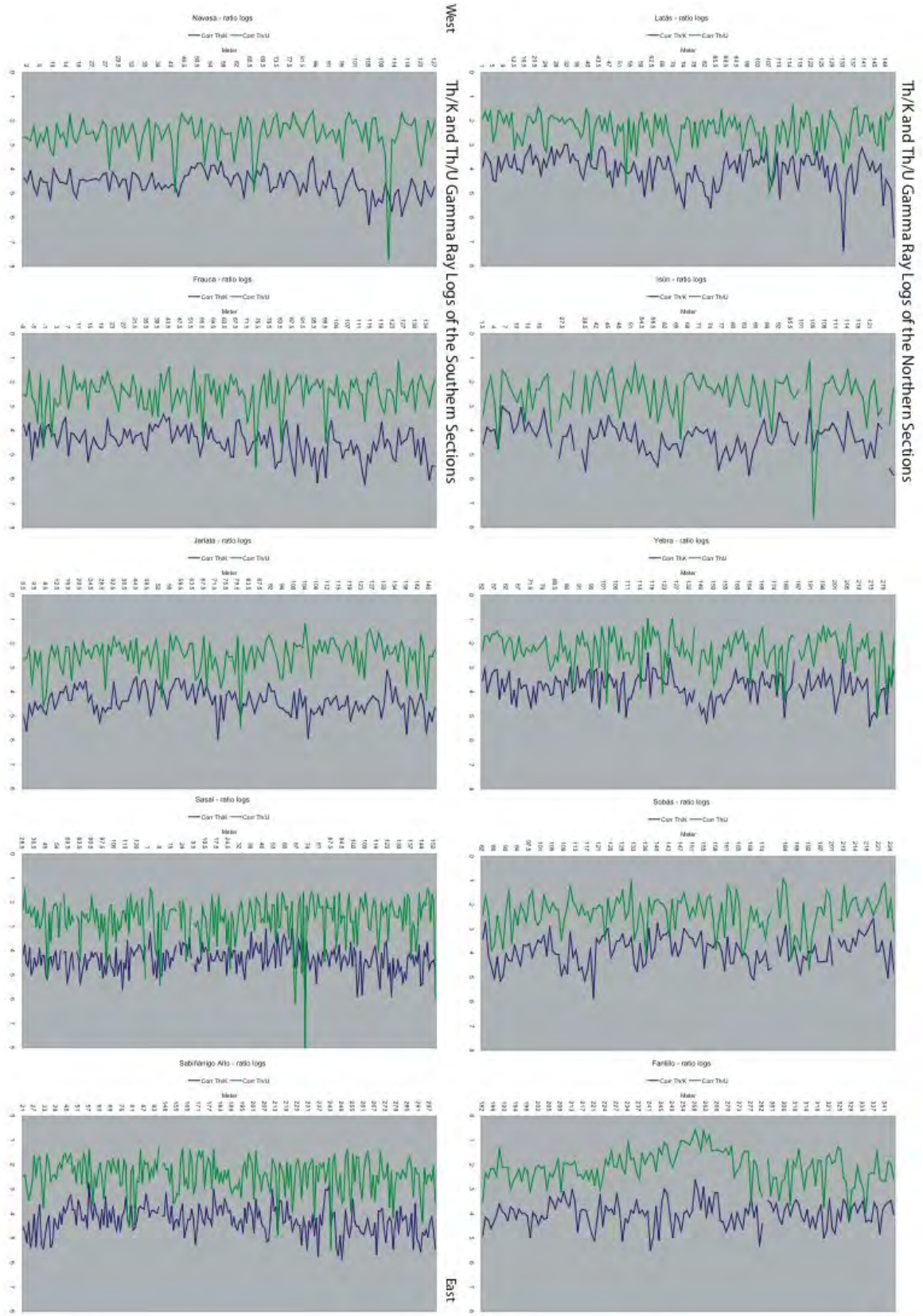

Fig. 5.9: Th/K and Th/U logs of the northern and southern sections. Vertical stacked pattern of Th/K ratios reveal progradation cycles within the SSt-Succession. Elevated Th/K ratios point to proximal depositional environments. Th/U ratios show indications of marine and continental influences, with increased values suggesting continental influence, while low values argue for marine conditions. Enlarged illustration is given in Appendix B.

5.6 Facies associations revealed within the SSt-Succession

The integrated use of different methods for analysing the sedimentary facies of the SSt-Succession positively improved the process of identifying and understanding depositional features within the succession. Using standard lithological profiles and spectral gamma ray logs helped to decipher distinct facies types and to get an impression of the ancient depositional environment. This in turn enabled to establish according facies associations and to look for a facies model, linking the observed facies pattern and features. On the basis of field observations, standard profiles, and spectral gamma ray logs, 21 facies associations were grouped, enabling to constrain the depositional setting.

As revealed from vertical sections, both standard profiles and GR logs, several coarsening-up sequences can be observed within the SSt-Succession, indicating a progradational character of the depositional environment. Grain sizes, log patterns, fossil contents and sedimentary structures point to a setting that comprises deep to shallow marine environments, and is controlled by contrasting depositional energies. Energetic conditions, thereby, vary within short intervals, resulting in a facies shift that can be observed both in vertical and lateral extension. Periodically intercalated successions with sharp bed boundaries and a subsequent fining-up trend, for example, point to abrupt changes in current activities, which can be referred to fluvial influences, while herringbone cross stratification and mud drapes are distinctive for tidal currents. The facies, and log pattern described in the sections above best match the characteristics of a deltaic environment as illustrated in the facies model of Fig. 5.10.

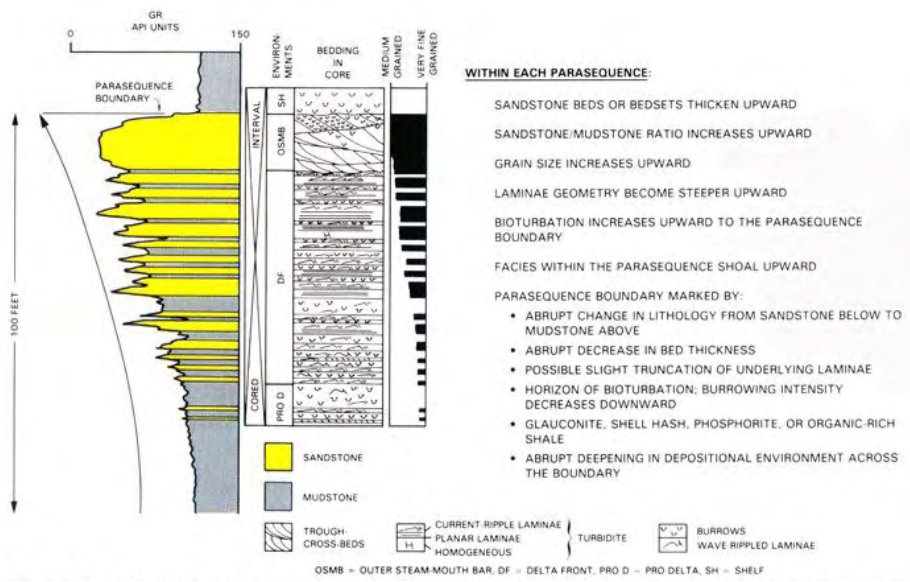

Fig. 5.10: Deltaic facies model; displaying a typical coarsening-upward succession with characteristic sedimentary structures that occur within deltaic environments (after Van Wagoner et al. 1990).

A distinctive feature of deltaic settings is their progradational character, displaying a stacked pattern of coarsening-upward cycles. Due to their intermediate position, where the river enters the ocean, deltas commonly show transitional, and highly variable depositional environments that are affected by both continental and marine conditions (Einsele 2000). Owing to the processes of redistribution, deposition, and reworking a permanent reconfiguration and relocation of distinct sub-environments takes place, resulting in the wide variety of observed facies types and a lateral and vertical facies shift of environmental units. The established facies associations, which are composed of one or several facies types, are indicative for distinct depositional environments, as they display the interaction of diverse processes.

5.7 Depositional environments of the SSt-Succession

As the final step of the facies analysis the features of the established facies associations were examined and interpreted with respect of their depositional environment. Some general aspects regarding deltaic environments, their components, occurring sub-environments and major acting processes are listed in Tab. 5.3 and schematically summarized in Figure 5.11. Adequate key features of the most common facies associations and assigned depositional environments of the SSt-Succession are reviewed and portrayed below. While a detailed description of all facies associations, with including facies types is outlined in note form and attached to the Appendix (Tab. B2).

Tab. 5.3: Main depositional environments and associated sub-environments of deltaic settings, their location and dominating processes, summarized after Coleman & Prior (1981), Bhattacharya & Walker (1992), Galloway (1996), Boggs (2001).

Delta Environments – Sub-Environments – Facies			***Relative Location***	***Dominating Processes***
Subaerial component:	Upper delta plain	Distributary channels Lacustrine delta-fill and flood-plain deposits	Above high-tide level	Fluvial processes dominate
	Lower delta plain	Crevasse splay/subdelta Marsh/swamp/lake Interdistributary embayment	Between low-tide mark and the upper limit of tidal influence; exposed during low tide but covered by water during high tide	Fluvial and marine processes
Subaqueous delta plain	Delta front	Channel mouth bar, Delta front sheet: Beach ridge, Tidal sand flat, Tidal sand ridge or shoal Natural levees, inter-distributary bays, bay fills (crevasse splays), marshes, and swamps	Uppermost part of the subaqueous delta plain, seaward of the lower delta plain, below low-tide water level water depths down to 10m	Fluvial and marine processes
	Prodelta, or Prodelta slope	Subaqueous slump deposits: Mainly fine material, locally extensive bioturbation	Remaining seaward part of the subaqueous delta	Marine processes dominate

5.7.1 Delta plain environments

The delta plain is the low area behind the shoreline, just above the high water mark, overlying the older shoreface and delta front deposits (Coe 2003). Two key depositional environments, fluvial channel deposits with associated overbank fines, and interdistributary bay deposits, are preserved from the Sabiñánigo Delta plain (Fig. 5.11).

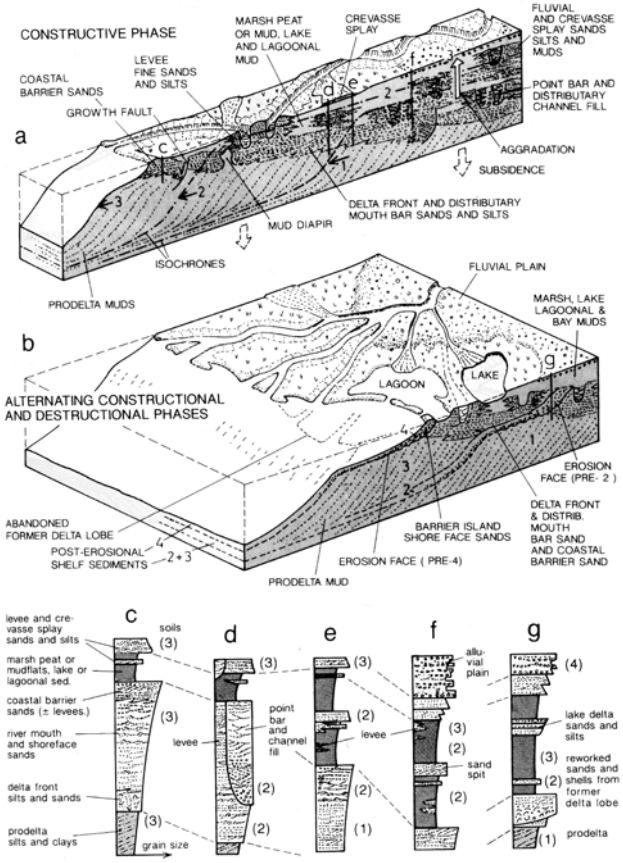

Channel Facies:

Fig. 5.11: Schematized illustration of typical features occurring within delta environments, left-hand (Einsele 2000); and some common sedimentary structures of the channel facies observed in the SSt-Succession, right-hand, top: Sharp based channel facies with mud chips; bottom: Landward accreting sandstones and associated clayey overbank fines.

Channel deposits

The distributary channel deposits represent the uppermost part of the Sabiñánigo Delta and are composed of individual fining-upward successions with thicknesses of some metres (1-5 m). Various depositional features that can be observed within the analyzed successions are indicative for fluvial processes, i.e.: lateral accretion surfaces, erosional based sandbodies, and poorly sorted rocks, reaching from pebble-sized conglomerates to sand- and siltstones with mud fragments or even mudstone layers on top (FA16/17/20). The GR logs show a bell shape pattern of according successions like in the uppermost part section Yebra, as well as low Th/K ratios (e.g. Latás, Sobás). The lower boundaries,

i.e. erosional base of channel deposits are characterized by high total GR response and high Th/K ratios (e.g. Latás). An associated increase in Th concentration can be referred to an enrichment of heavy minerals in lag deposits.

In most cases, channel structures are coupled with clayey overbank fines (FA19), or interdistributary bay deposits (FA14). If fluvial influences of a distributary channel arm cease, and the channel is deprived of an active influx of sediments, it will successively be refilled (Coleman 1982). The deposits are composed of poorly sorted sandstones and siltstones containing an abundance of transported organic debris as observed within FA10, and well exposed in section Yebra. Such channel abandonment may have several reasons, like changing upstream conditions, delta-lobe switching, or just accidental by blocking log-jams. In the lower part of abandoned delta lobes oysters tend to settle down, forming biohermal structures (FA10).

Bay deposits

Interdistributary bays and bay deposits generally represent areas of open water within the active delta, that are partially or completely surrounded by marsh or distributary levees, and are often connected to open sea by small tidal channels (Coleman & Prior 1981). The mainly fine-grained sediments settle down from suspension and build up a silty mudstone facies, typical for depositional environments protected from strong hydrodynamic energy (FT0b). The individual shales and mudstone layers of the bay deposits are fairly thin, mostly ranging from a few cm to some dm. Due to repeated filling an alternating shale succession of mudstones with variable content of coarser component build-up, reaching thicknesses of several metres to decametres. Flood events, and changing hinterland conditions periodically cause crevasse splays to spill over or break through natural levees, delivering coarse-grained channel sediments into the bay area. They are exposed as erosive-based beds within the bay deposits (FA11). This completes the typical interdistributary bay-fill succession; composed of stacked coarsening- and fining-upward series that reach thicknesses up to 15 m and more (FA14). This stacked pattern can also be observed in the GR log, with high total values (UR, total GR response) for the shale succession, and interbedded horizons of low reading, indicating the deposition of intercalated siltstone to sandstone horizons (e.g. section Yebra). Due to the progradational character of deltaic system, distributary channels successively build seaward, cut into bay areas, bifurcate and form interdistributary bays in-between (FA10, 11, 14). Depending on the course of individual distributary channels, areas with minor influence of distributary discharge form successions mostly composed of alternating silts and muds, as coarse-grained input is limited. Where distinct channel arms loose their progradational character as discussed above, it will successively be filled, representing a

fining-upward succession (FA12). Faunal associations, like small oyster bioherms (FA10) might settle down, indicating a shallow marine environment of brackish water (Coleman & Prior 1981).

Facies associations of delta plain environments are only found on the northern limb in the upper part of the Sabiñánigo Delta complex and are capped by a ravinement surface (FA18), which marks the top of the whole succession.

5.7.2 Delta front environments

Distributary mouth bars and delta front sheet sands form the depositional sediment bodies, accumulating at the seaward toe of distributary channels. When entering the marine realm, the river looses its current energies either gradually or fairly rapid, depending on the dominating current activities, i.e. fluvial, tidal, or wave dominated processes. Shoaling, therefore, is a direct consequence of a decrease in velocity and thus, reduction in carrying power of the stream, leading to extremely high accumulation rates in delta front environments (Coleman 1982). The prevailing current patterns are decisive for the formation of mouth bars and sheet sands, which show distinct sedimentary facies pattern. This in turn allows evaluating probable basinal processes. From the deposits of the SSt-Succession, for example, strong evidence for acting wave and tidal currents can be derived (Fig. 5.12).

Distributary mouth bars

The mouth bar deposits of the SSt-Succession are exposed within several coarsening-upward successions that are composed of fine- to coarse-grained sandstones with intercalated siltstones, and/or silty claystone beds. Most of the distributary mouth bars were subjected to constant reworking processes as can be concluded from their textural maturity, expressed by fairly clean and well-sorted sandstones. The reworking by either wave or tide action resulted in the formation of some characteristic sedimentary structures appearing within the SSt-Succession (cp. Reineck & Singh 1980). The observed deposits of FA5 and FA6 were subjected to pronounced wave-influence. Hummocky and swaly cross-stratified sandstones predominantly express the successions of FA5. Whereas the more tide-influenced deposits of FA6 show claystone horizons, as well as mud drapes and thin lamination, locally reactivation surfaces occur within cross-stratified horizons (FA6). The mouthbar deposits show an overall coarsening-upward trend, which records the progradation of the SSt-Succession. This is also reflected by their GR logs, which show elevated element ratios (Th/U and Th/K). Mouth bar deposits in section Yebra, for example, trace this progradational pattern by increased Th/K values, whereas the total GR response is low with horizons of increased radioactivity in-between.

Vertical Profile Yebra
Lower – Middle Part

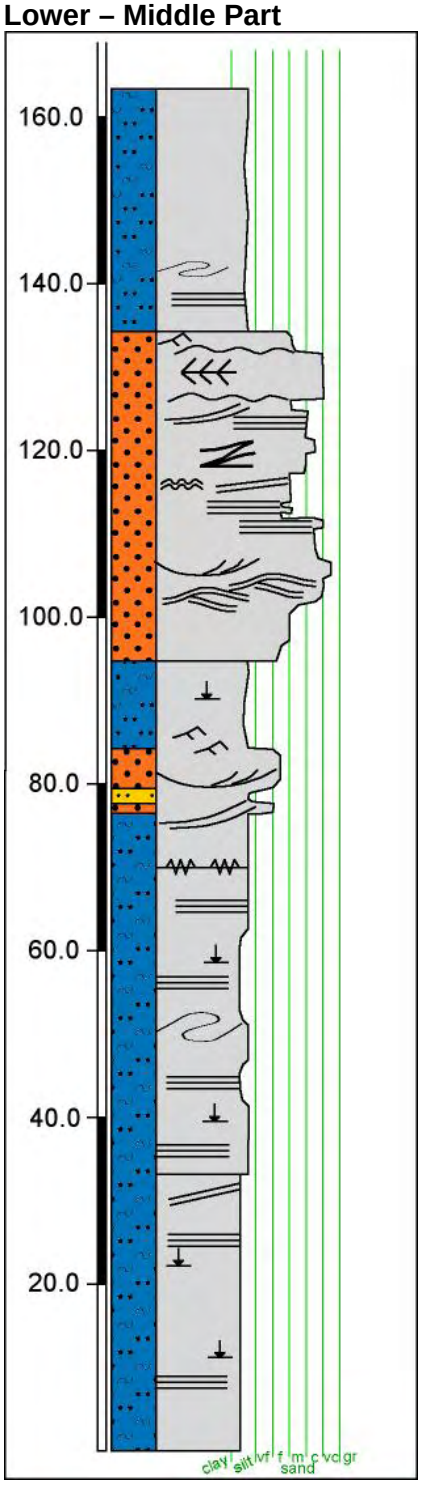

Delta Front Environments

Tidal Bar Facies

Delta Front Sandstone Bodies

Mouth Bar Facies

Fig. 5.12: Vertical profile of section Yebra, comprising lower and middle part, with delta front environments reaching from 95 m-135 m, left-hand; and some field-impressions to the right. Top: Tidal bar facies with herring bone cross stratified sandstones; middle: Succession of delta front deposits, as exposed at section Yebra (sandstone bedsets ~25 m); bottom: Mouth bar facies with hummocky and swaly cross stratified sandstones.

The latter can either be referred to heavy mineral enrichment, but more likely represent clay-dominated horizons within the succession, as Th, K, and U concentrations increase. While for heavy mineral enrichment a more pronounced elevation in Th concentration should be visible. The individual sandstone beds reflect a stronger impact of current energies with an active sediment distribution, while siltstones, and fine-grained sandstone beds indicate periods of reduced depositional energy. A brackish environment evolves due to an increase in muddy fresh water inflow. This can be deduced from both lithology and low degree of bioturbation, as bottom-dwelling fauna does not favour these brackish conditions. The minor fossil content in general argues for inconsistent environmental conditions, affected by changes in hydrodynamic energies, variable salinity, and opaqueness of the water column (Reineck & Singh 1980).

Delta front sheet sands and tidal ridges

The delta front sheet sands commonly are made up of reworked delta front silt and sand that are mainly derived from the distributary mouth bars. Due to remobilization and redistribution by persisting wave action the sediments accumulate to continuous beach ridges (Coleman & Prior 1981). Consequently the sedimentary structures predominantly display wave-dominated depositional processes, such as wave ripples and hummocky cross-stratification and sparse fauna contents (FA8).

Where tidal currents are dominant, tidal sand flats or ridges build up. Mud-draped ripples, rhythmically laminated heterolithic deposits, bidirectional cross-bedding and reactivation surfaces can be observed (Fig. 5.12), which are, according to e.g. Coe (2003), typical sedimentological features, indicative of tidal processes. As a result of the lower wave energy the sand bodies are often poorly sorted, with mudstone horizons on top (FA7). The log pattern of delta front sheet sands and tidal ridges within the SSt-Succession lack a distinct pattern. The thin mudstone horizons, deposited during low tide, are beyond the resolution of the portable gamma ray spectrometer, resulting in compound values of log responses.

The deposits of the delta front environment (FA5, FA6, FA7, FA8) are only observed within the exposures of the northern limb and tend to be most common in the intermediate part of the vertical successions but also occur within the upper part.

5.7.3 Prodelta – offshore environments

Distal bars and connected prodelta facies form the basal portion of the active prograding delta, and represent the lateral continuation of distributary mouth bars, and delta front sand bodies in general. Their facies predominantly is composed of fine-grained

siliciclastic deposits, settled from suspension, and reveal high lateral continuity and low lithologic variation (Coleman 1982). Owing to variable environmental conditions that were affecting the basin deposits of the Sabiñánigo Delta several sub-environments can be distinguished, whereas gravitational transport processes pose the main controlling factor on the sedimentary pattern of deeper marine environments.

Upper prodelta – distal bar

The prodelta areas of the Sabiñánigo Delta show a general coarsening-upward trend, merging into mouth bar deposits of the delta front environment. Depending on the depositional energies and sediment input the prodelta sediments show either a gradual coarsening-upward succession, composed of several smaller coarsening-upward cycles. Or, they show a more irregular coarsening-upward succession with intercalations of erosive, coarse-grained bedsets. Prodelta successions with gradually increasing grain sizes, indicate steady sedimentation and continuous progradation of the upper prodelta (FA3), while intercalations of erosive, coarse-grained bedsets, reflect episodes of increased current activities, caused by river floods, or distal bar sedimentation (FA4), (Fig. 5.13).

The facies association FA3 is composed of individual coarsening-upward successions from marls to fine-grained sandstones, showing slumping, load structures and often a high fossil content (*Nummulites*). The more homogenous deposits of facies associations FA3*, thereby, accumulated in an area dominated by minor hydrodynamic energy, providing calm conditions as required for the growth of biohermal structures (mainly build up by oysters) and according fossil-assemblages. The general upward increase in grain size is also displayed by the total gamma ray response, showing a funnel shaped pattern. In section Yebra, distal bar deposits are characterized by a pronounced decrease in rocks radioactivity, and an associated increase in Th/K, and Th/U ratios, indicating continental influence and a progradation of the system. According log pattern can also be observed within facies associations of the southern limb, although they are often more faintly developed.

Facies association FA4 is comparable to FA3 but indicates episodic increasing energy conditions, as erosive-based horizons of coarse-grained sandstones occur within a succession of finer-grained siliciclastics.

Upper prodelta and distal bar deposits of FA3 and FA4 are more likely to be found on the northern limb, whereas the facies associations FA3* are widespread on the southern limb.

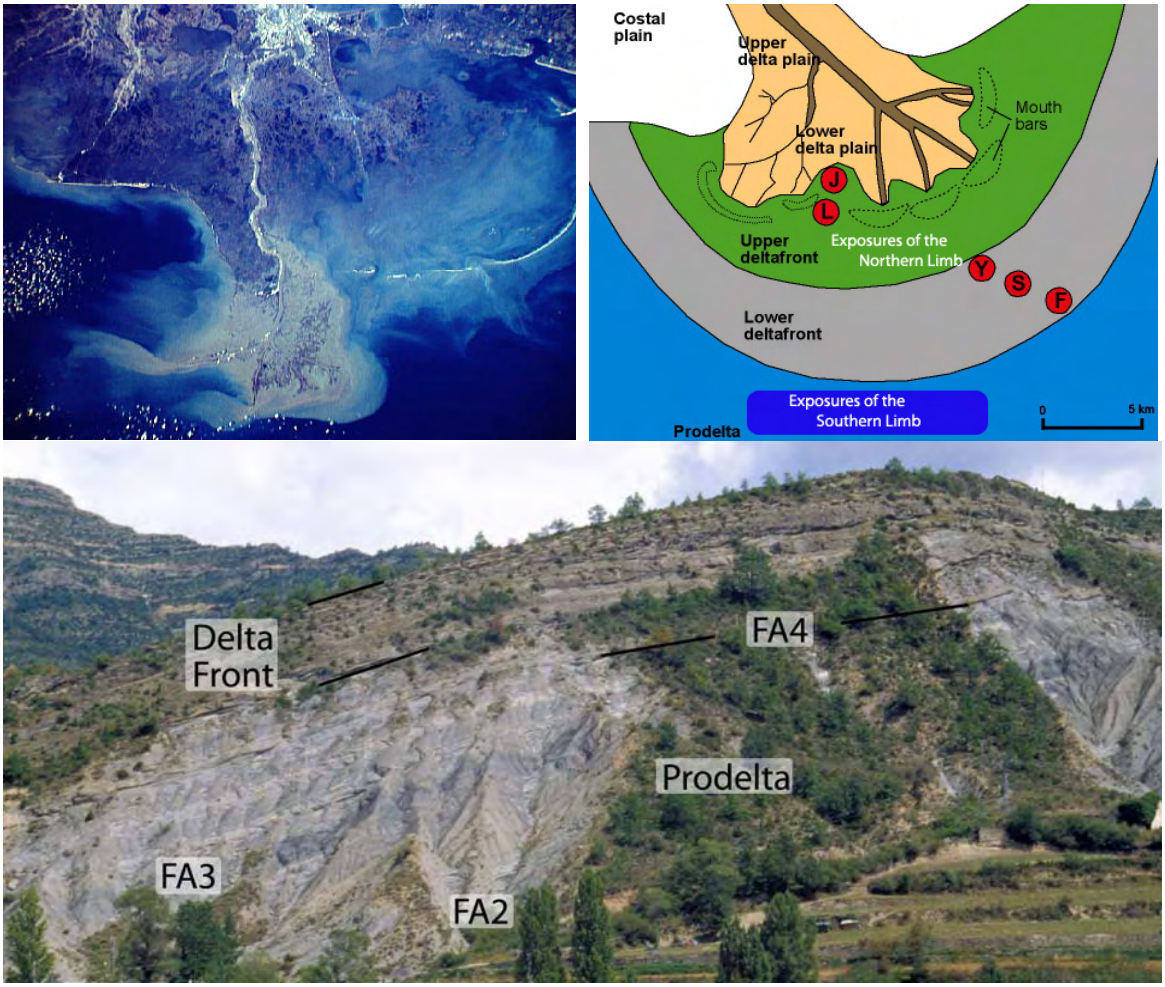

Fig. 5.13: Features and environments occurring within a deltaic system. Lefthand top: Active Mississippi-Delta with visible plume of water and suspended sediment carried out into the basin due to density-differences of river water and seawater (source: http://earth.rice.edu); righthand top: Schematized facies distribution with deltaic sub-environments and proposed relative location of analyzed sections; L: Latás, F: Fanlillo, I: Isún, S: Sobás, Y: Yebra, (modified after Nichols 1999). c) Example of a vertical succession displaying the prodelta, distal bar, and delta front deposits of the Sabiñánigo Delta.

Offshore – lower prodelta

The lowermost or offshore part of the SSt-Succession refers to the Larrés Marls (Fig. 5.14), (see Chapter 2) and consists of thick marly deposits with individual, slightly coarsening-upward successions and intercalated horizons of glauconite-bearing sandy carbonates, which mostly appear as detached ball-and-pillow structures. The rocks are blue-grey to grey, friable, with locally intense bioturbation. Load structures and slumping are common features whereas kinds of cross-stratification are observed very rarely (FA1). Foraminifera (*Nummulites*) and echinoids represent most of the appearing fossil content, apart from some bivalves, gastropods and shell fragments testifying an open marine depositional setting.

Fig. 5.14: General view of the lower part of the SSt-Succession, with the Larrés Marls gradually merging into the deposits of the Sabiñánigo Sandstones.

The Larrés Marls gradually merge into the transitional deposits of the SSt-Succession, also made up of a thick pile of successive marls, reaching locally up to 200 m and more (FA2). These deposits are mostly composed of individual coarsening-upward successions of some metres to decametres, with increasing silt- and sandstone content towards the top. Locally horizons or lenses of silt- and/or sandstones occur. Load structures and slumping again rank among the common features, as well as locally intense bioturbation, and the fossil record consisting predominantly of Foraminifera (*Nummulites*), echinoids, some bivalves, gastropods and plant-remains. In some parts of the lower prodelta, coarser-grained sediments occur that can be ascribed to gravity currents, activated by periodic flood events or turbiditic currents; locally upper parts (B-E) of the Bouma Sequence are preserved (FA0).

The facies association FA0 is rather infrequent and mainly limited to the southern limb, whereas FA1, FA2, appear throughout the succession, both at the northern and southern limb of the Basa Anticline, forming a typical ‘badlands topography’ (Fig. 5.14) as they weather fairly easy.

From the facies analysis a dynamic depositional setting can be deduced for the SSt-Succession, displaying a variety of different deltaic sub-environments, as illustrated in Fig. 5.15. The sedimentary structures indicate a deltaic environment that was influenced by tidal currents and wave activities. According sedimentary structures are more pronounced in the northern exposures. The southern exposures reveal more distal depositional environments, as sketched in Fig. 5.13, resulting in a reduced fluvial impact on sedimentation processes and sedimentary pattern. This displays the vertical and lateral distribution of facies within the deltaic setting and provides the basic ‘building blocks’ that

are necessary for the reconstruction of an adequate depositional model for the SSt-Succession.

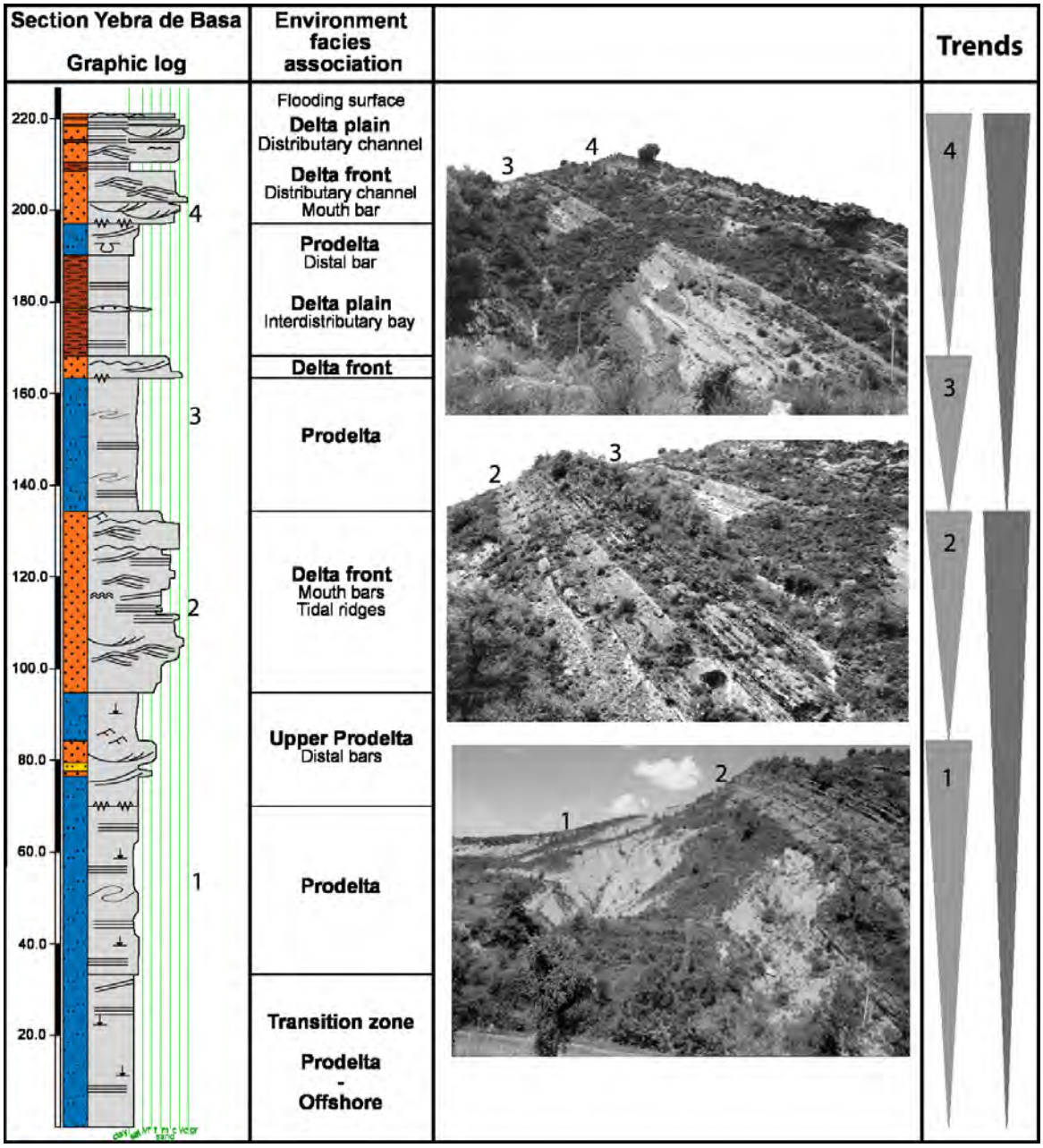

Fig. 5.15: Synthetic profile based on the vertical section of Yebra de Basa and Javierre; illustrated are the successive facies associations and assigned sub-environments as occurring within the studied successions of the Sabiñánigo Delta complex.

Chapter 6 – Previous Sedimentary Overburden

6.1 Introduction

For this study low-temperature thermochronology was used to evaluate the maximum/minimum thickness of the previous sedimentary overburden that was covering the Sabiñánigo Sandstone (SSt) Succession under investigation. The sedimentary succession atop the SSt-Succession nowadays reveals a thickness of about 1300 m, but according to estimations published e.g. by Puigdefàbregas (1975), and Hogan & Burbank (1996), the former basin fillings reached thicknesses of more than 5 km of foreland strata. This in turn would have a strong impact on the processes that affected the deposits of the Jaca Basin, e.g. diagenesis, compaction, initial thickness, and subsidence. The apatite (U-Th)/He thermochronometer was chosen as an appropriate method to unravel the denudation history of the Jaca Basin.

Published studies of low-temperature thermochronology in the Pyrenean area, e.g. by Yelland (1990), Vergés et al. (1995), Morris et al. (1998), Fitzgerald et al. (1999), Shoemaker (2000), and Sinclair et al. (2005), mainly concentrate on the Eastern and Central Pyrenees. Focus, thereby, is placed on issues related to the ECORS transect and the Axial Zone (cp. Fig. 2.1, Chapter 2), predominantly constrained by apatite and zircon fission-track dating. Thermochronological data sets for the southern foreland basins, however, are rare or even lacking. Therefore, (U-Th)/He analysis were accomplished within the framework of this study, to determine the thermal influence prevailing within the sedimentary successions under investigation. The evaluation of the current temperature range that affected the rocks of the SSt-Succession was estimated to be a critical point to i) quantify the sedimentary overburden covering the SSt-Succession, i.e. evaluate the thickness of the sedimentary pile within the eastern Jaca Basin, and, therefore, to ii) consider values of subsidence and erosion, and to iii) determine probable temperature derived effects of diagenetic processes that might have had substantial effects on the rocks of the SSt-Succession and thus the validity of the gamma ray investigations.

Together with the fission-track (FT), and $^{40}Ar/^{39}Ar$ dating methods, the (U-Th)/He method constitutes one of the main thermochronological methods that are commonly used to constrain thermal histories at temperatures below approximately 300-550 °C. All of these three methods are based on the production of isotopes or radiation damages, caused by nuclear decay and the thermally controlled retention of these decay products. Radioisotopic production decreases exponentially with time but is predictable and otherwise steady, which gives the thermochronometer the ability to keep time. The

thermal sensitivity of these radioisotopic clocks means that they provide information about the cooling history of rock (Reiners & Brandon 2006). Applying low-temperature thermochronology, therefore, allows to constrain the temperature history of rocks in the upper crust.

A more detailed description of the basic applications and analytical principles of the (U-Th)/He method was already given in Chapter 3, with an account of the preparation and analysis processes of (U-Th)/He-samples in general and the studied samples in particular. In the following, a brief introduction to previous studies on low-temperature thermochronology studies within the Southern Pyrenees will be given, followed by an examination of the processed (U-Th)/He analyses within the working area.

6.1.1 Previous studies

In the Pyrenean area, apatite FT analyses show the onset of exhumation around 50 Ma as a result of the continental plate convergence between Iberia and Eurasia (Fitzgerald et al. 1999). Accommodation of convergence took place along pre-existing structures in the Hercynian basement, giving rise to a double-wedge orogen, the Pyrenean Mountains. Synorogenic erosion amounts up to ~15 km in the Axial Zones during the Eocene. Exhumation is described as being relatively uniform across the Pyrenees for the Eocene, but higher on the southern flank of the Axial Zone during the Oligocene. This is attributed to a change of convergence and subsequent accommodation within the Pyrenean double wedge. FT data of Yelland (1990), modelled by Morris et al. (1998), suggest that discharge of sediment to the south of the Pyrenees (Ebro Basin) was 1.5 to 2.8 greater than to the north (Aquitane Basin). Miocene to present-day denudation (postorogeny) is estimated to be approximately 2-3 km (Fitzgerald et al. 1999).

6.2 (U-Th)/He analyses in the Eastern Jaca Basin

6.2.1 Sampling and sample preparation

During fieldwork 20 bedrock samples, each of 2-5 kg, were collected to extract heavy mineral concentrates for low-temperature thermochronological analysis. Rock samples comprise fine- to coarse-grained siliciclastic rocks, and were taken from outcrops within the SSt-Succession, covering both limbs of the Basa Anticline, and from overlying strata. For the latter a vertical section of about 1600 m thickness was sampled, comprising a complete succession from the base of the SSt-Succession to the top of the continental Santa Orosía Fan, which forms the uppermost deposits of the Eastern Jaca Basin. This allowed processing a more comprehensive data set of the upper Jaca Basin infill. The sample localities are illustrated in Fig. 6.1.

The sample preparation was performed according to the description given in Chapter 3, whereas for the samples of the Jaca Basin, the selection of suitable apatite grains (free of inclusions, at least 60 µm in diameter, and of good shape) generally was problematic. The apatite grains often showed some degree of rounding, abrasion and broken crystals due to the experienced transportation processes. Fluid inclusions were also quite common in the majority of the occurring apatite crystals. Another difficulty was the grain size, therefore, some samples could not be analysed, as the apatite grains did not match the required minimum size of at least 60 µm.

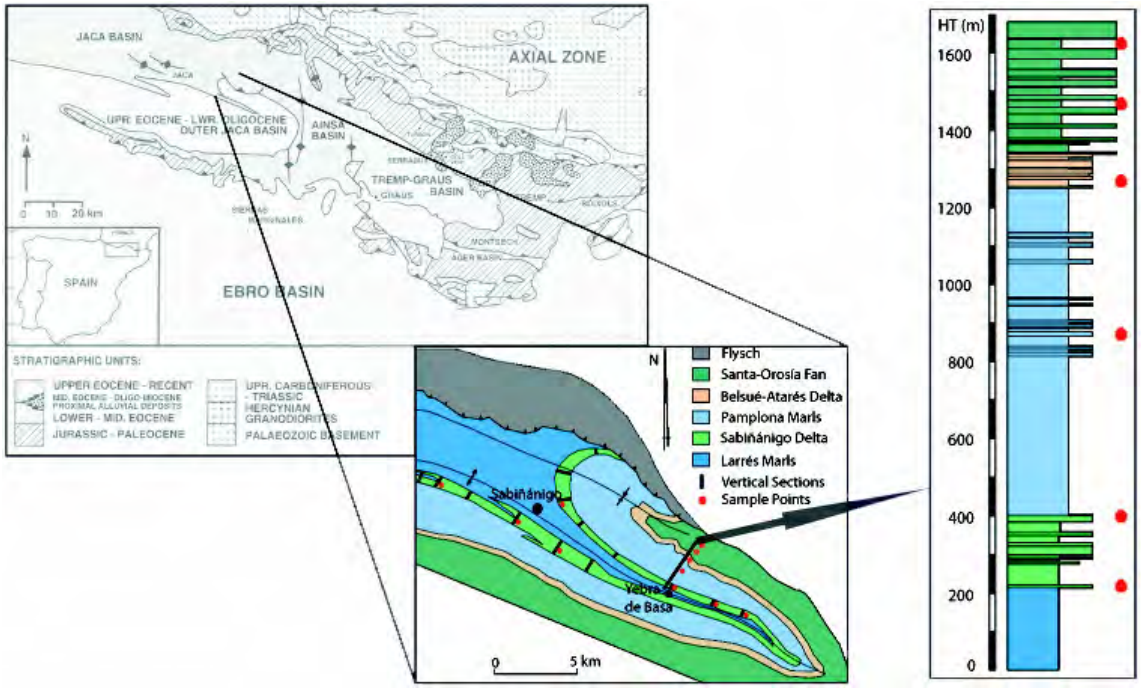

Fig. 6.1: Geological map of the studying site (modified after Vincent & Elliott 1997, Remacha 1998, Puigdefàbregas 1975) with sample localities and processed vertical section covering the strata from upper Larrés Marls up to Santa Orosía deposits; sample points are plotted next to the vertical section, (modified after Hogan and Burbank 1996).

The selected grains for analysis were, therefore, carefully inspected and from each sample at least two apatite crystals were picked, measured, digitally photographed and afterwards loaded into 1 mm uranium free Pt-foil tubes and ‘wrapped’ to Pt-packages (Mitchell & Reiners 2003, Data repository). The Pt-packages were loaded into a sample holder for the He extraction and further analytical measurements as described by House et al. (2000).

6.3 Results

From the described localities (Fig. 6.1) samples were taken to obtain a comprehensive data set spanning the upper part of the basin infill, whereas from 18 samples detrital apatites could be separated and measured by applying the (U-Th)/He dating technique.

Referring to the present strata thickness exposed in the eastern Jaca Basin, and assuming a geothermal gradient of ~30 °C/km, the expected (U-Th)/He ages should not be resetted, i.e. ages older than 36 Myr. should result (Fig. 6.2); owing to the fact, that the closure temperature of the apatite (U-Th)/He system is set to a range between 55-80 °C (Farley 2000). But, if there was a sedimentary column of more than 2000 m covering the rocks of SSt-Succession for a time span of ~10 Myr, corresponding indications will be revealed by the performed (U-Th)/He analyses. Furthermore, the yielded (U-Th)/He data set provides basic parameters concerning the thermal history of the eastern Jaca Basin, and, therefore is of great importance for further investigations within the Jaca Basin.

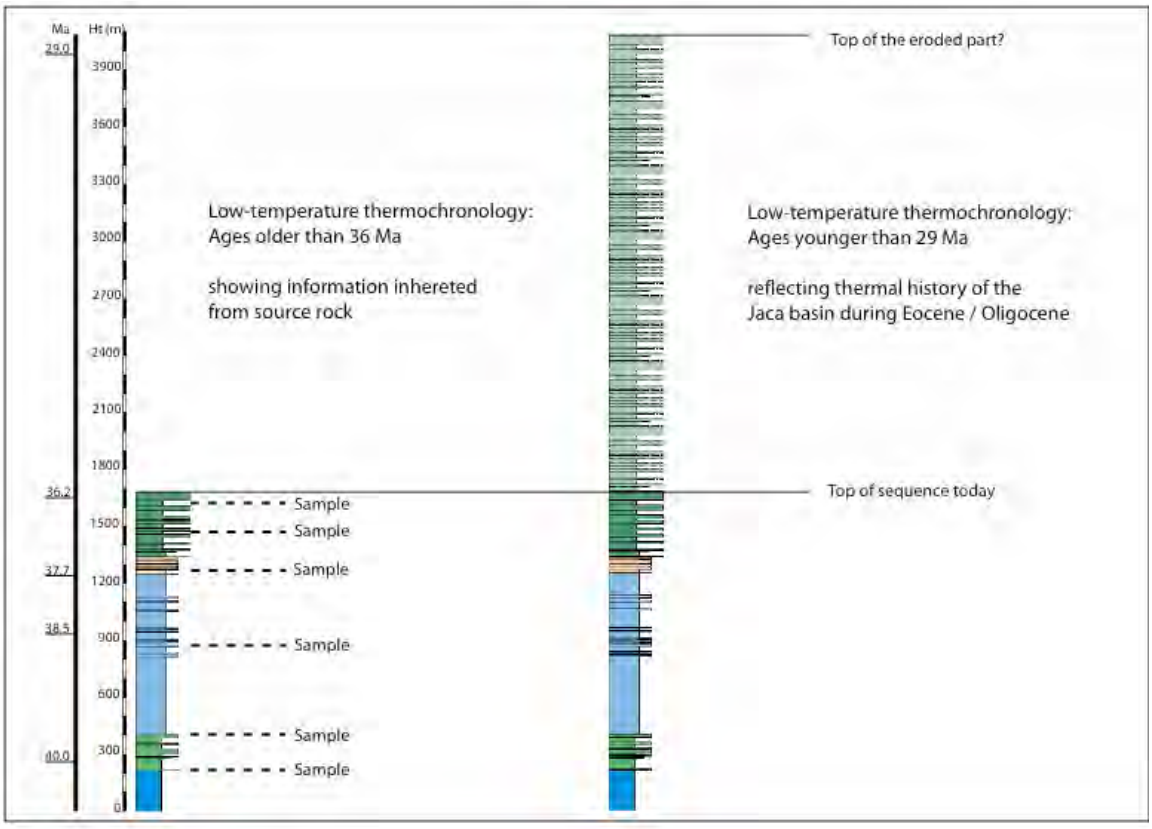

Fig. 6.2: Left-hand: Vertical section of Yebra (~1600 m thickness), including the strata of the upper Larrés Marls up to the Santa Orosía Fan deposits; right-hand: synthetic section of proposed former strata, with an eroded overburden of about 2000 m thickness, for legend cp. Fig. 6.1. Assuming a geothermal gradient of ~30 °C/Km, the deepest sample would have reached temperatures of less then 50 °C.

6.3.1 (U-Th)/He ages of the Eastern Jaca Basin

The obtained (U-Th)/He ages range from ~6.5 Ma to ~78 Ma (cp. Appendix C and Fig. 6.3 below), displaying a wide spread of ages, which have to be assessed with respect to methodological restrictions. The most common problems that arise from the applied method are linked to the apatite crystals and their inclusions (cp. Chapter 3.2.4). Mineral inclusions in apatite, therefore, are a potential source of error in determining apatite (U-Th)/He ages, especially if they are very small (< 5 µm) and difficult to detect. This explains the age spread of the (U-Th)/He ages from the samples of the SSt-Succession, and the stratigraphically younger strata, as it cannot be excluded that apatite grains with tiny mineral inclusions have been used for the (U-Th)/He analytical procedure.

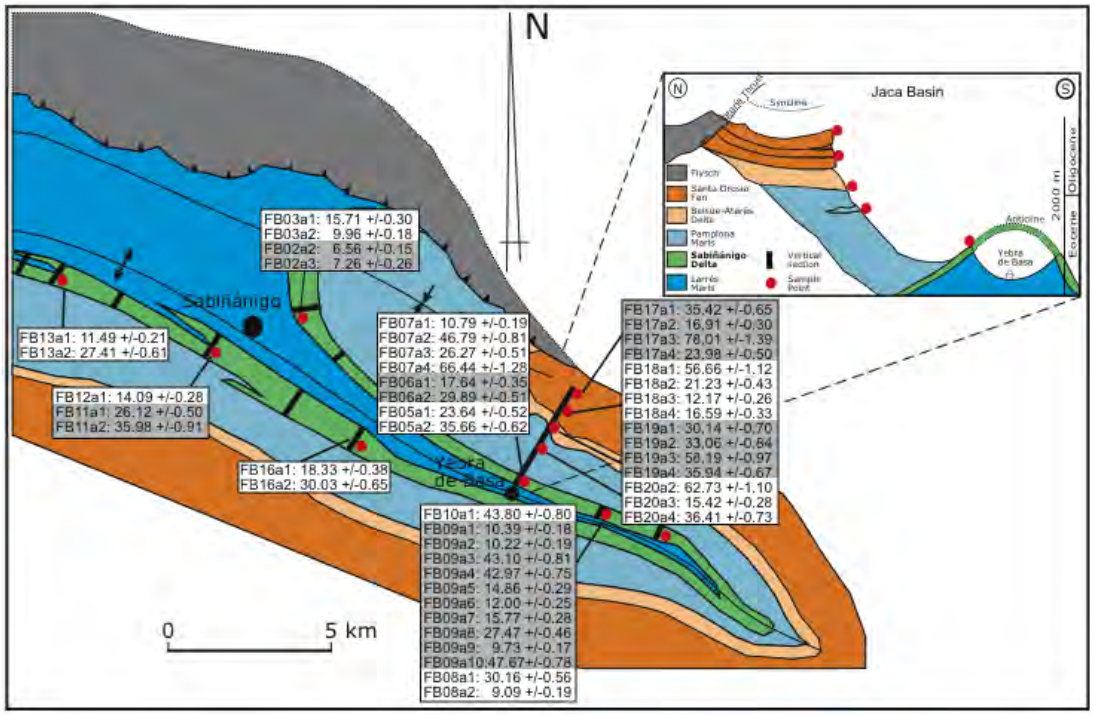

Fig. 6.3: Geological map of the working area (modified after Puigdefàbregas 1975) with location of vertical sections, sample points, and corresponding (U-Th)/He ages.

6.3.2 Interpretation

The revealed (U-Th)/He ages do not indicate formation (stratigraphic) ages, but rather cooling ages. The young ages obtained by the dating process, indicate a complete reset of the (U-Th)/He system. The more if these ages would correspond to inclusion-bearing apatites, as they generally reveal older ages than their 'true' (U-Th)/He ages (cp. Chapter 3.2.4). The samples of the overlying strata, however, show older ages, and indicate a partial resetting. This corresponds to the general pattern of low-temperature thermochronology, which displays a cooling of the rocks, given by increasing ages towards the top, as lower temperatures are affecting the thermochronometer. Assuming a

thermal gradient of 30 °C/km in late Paleogene to Neogene time, a sediment load of ~2-3 km on top of the Oligocene sediment succession would explain the partially to complete resetting of the (U-Th)/He system. Furthermore, some of the obtained (U-Th)/He ages are clustering around ages of ~10 Ma, which match the Miocene tectonic pulse (e.g. Vergés 2002); and tie up to similar observations, which were achieved by Fitzgerald et al. (1999) from fission-track ages of the Pyrenean Axial Zone. This leads to the conclusion that the post orogenic uplift of the central part of the Pyrenees also significantly affected the southern foreland basin.

6.4 Discussion

Although low-temperature thermochronology enables constraining the temperature history of rocks in the upper crust it does not provide any information about the nature of the processes that cause, respectively, caused the temperature changes. Therefore, the obtained data need to be interpreted in the context of the geological background of the investigated area, accompanied by a critical evaluation of the data, as the analytical difficulties and errors involved within this method may influence the geological interpretation rigorously (leading in the worst case to a misinterpretation of the geological history).

In the course of the analytical processing of the samples from the Jaca Basin, U and Th bearing inclusions occurring within the apatite crystals were found to pose a potential source of error in determining apatite (U-Th)/He ages. The high U and Th contents of these phases, predominantly zircon and/or monazite, will lead to an increased ^{4}He in the apatite, originating from alpha decay of the inclusions. But the major problem is associated to the chemical behaviour of the U and Th bearing mineral inclusions and the analytical procedure involved to this method, requiring the dissolution of the apatite grains to determine their U and Th concentration. While the acid used (HNO_3) is appropriate to dissolve apatite and monazite grains it is not able to dissolve zircon or non-phosphate minerals. This in turn can lead to apparently unsupported He, as He determination of such grains by laser and noble gas mass spectrometry will reveal He concentrations of both apatite and inclusions, whereas the U and Th values will be lower than the actual ones, as only the apatite phase was dissolved and analysed. This leads to lower U and Th values relative to the determined He concentration and, therefore, the calculated age would be older than the true age. This is a general problem, arising from small (< 5 µm) inclusions high in U and Th content, as it is often the case for zircon and monazite, and which may be difficult or even impossible to detect by the stereo-zoom microscope (for further reading see also Farley & Stockli 2002, Reiners & Brandon 2006, Vermeesch et al. 2006).

Chapter 7 – Depositional Model of the Sabiñánigo Sandstone Succession

So far different types of data sets were acquired, supplying the individual building blocks that are necessary for the aimed deposition model. On the way to a conclusive representation of the evolution of the SSt-Succession in time and space, three intermediate invention steps have been worked out:

i) To reveal the lateral progression of the SSt-Succession, the facies distribution across the system was studied, using lateral transects that were established by correlating the distinct standard lithological profiles in the field, both for the northern and the southern limb.

ii) For the same purpose, the gamma ray log response across the system was examined and correlated, resulting in a second set of lateral transects.

iii) To get a reference point between the distinct lateral transects each of the four transects was scrutinized for chronological horizons and sequences, to evaluate their sequence stratigraphic meaning, and enable a link-up of the transects.

7.1 Facies distribution across the system

Lateral cross-sections, both for the northern and the southern limb were generated to examine the defined facies types and corresponding facies associations in their lateral continuation. Correct correlation of stratigraphic units is a crucial step in generating reliable cross-sections, therefore, tracing horizons between distinct vertical profiles were walked out in the field, allowing to generate time calibrated lateral transects along the two limbs of the Basa Anticline (Fig. 7.1). To reconstruct the depositional architecture and to reveal the lateral progression of the SSt-Succession, the lithofacies, facies successions, and tracing horizons (i.e. concept of timelines, cp. Chapter 3) were used and examined along both limbs.

Fig. 7.1: Cut-out of the northern transect, showing successions of the lower part with a sheet-like geometry and continuous surfaces that can be traced over the entire distance, as illustrated by two horizons (lowermost corresponds to Horizon BA at the base of Unit B).

7.1.1 Depositional successions along the northern cross-section

The northern transect, or cross-section respectively, strikes approximately NW-SE. It spans ~12 km, and comprises the vertical sections between Larrede in the west and Fanlillo in the east (Fig. 7.2). Within the cross-section diverse key horizons and marker beds can be followed over large distances. They predominantly display recurring erosional events that were affecting the environment during delta evolution. Equivalent surfaces can be observed throughout the sections, displaying distinct progradational steps within the deltaic successions. In the following, the lateral evolution of occurring facies units, exposed along the northern transect will be highlighted; and their bounding surfaces will be described, with an outline of their characteristic features, thereafter, given in Table 7.1.

Unit NT-A

The lowermost part of the cross-section is composed of an interval of blue-grey marly deposits with varying content of silt- and clay-sized particles, and an overall coarsening-upward trend (FA1, FA2, FA3). They represent the offshore to lower prodelta component of the succession and are very uniformly developed throughout the studying area. At the eastern margin (section Fanlillo) of the cross-section, some intercalations of siltstones to fine-grained sandstone beds can be observed, indicative of first distal bar deposits (FA4). Towards the western portion of the cross-section, a slightly decrease in grain size is recorded, with very fine-grained intercalations of clay beds with a turbiditic character exposed in the section of Larrede (FA0).

Horizon BA represents the boundary between Unit NT-A and Unit NT-B. This horizon can be recognized in the eastern part of the cross-section, where it separates offshore and prodelta facies of Unit NT-A from overlying sandstones of Unit NT-B. In this area, it corresponds to the base of an erosive sandstone succession that indicates the appearance of first coarser-grained deposits. Between Fanlillo and San Roman, horizon BA can be followed over ~ 4 km along the cross-section, until it merges into fine-grained deposits west of Yebra de Basa without any traceable characteristics.

Unit NT-B

Unit NT-B is composed of marly siltstones and interbedded silt- to sandstones, whereas the sandstones are exposed in the eastern part of the cross-section. They represent erosional based distal bar deposits (FA4) that pass upwards and eastwards into distributary mouth bar deposits (FA6, FA13). At the easternmost termination (section Fanlillo) the succession reaches thicknesses of ~20 m with distal bar deposits at the base, grading upward into distributary mouth bar deposits. Towards the west, however, a

facies shift with an associated decrease in grain size and thickness can be observed. At Yebra the deposits are expressed as distal bars that finally merge into upper prodelta marls between Yebra and San Roman (FA2, FA3, FA4). At the westernmost portion, at section Larrede, turbiditic deposits of FA0 are exposed.

Horizon BC represents the top of Unit NT-B. It is clearly expressed in the eastern part of the cross-section, especially in section Fanlillo and Yebra, where fine-grained marly deposits transgressively overlay sandstones. West of section Yebra Horizon BC vanishes and is not traceable anymore.

Tab. 7.1: Outline of tracing horizons, their characteristic features and enclosed facies units within the northern cross-section; from base (Unit A) to top (Unit J).

Unit	*Traced Horizons – Characteristics*	
	RAV	Ravinement surface exposed along the cross-section; top of SSt-Succession; overlain by Pamplona marls.
NT-J		
	IJ	Bounding surface, leading over to uppermost coarse-grained succession of erosional based sandstones and conglomerates; prominent surface, traceable along cross-section.
NT-I		
	HI	Bounding surface, notifying lithology change; observable throughout the cross-section, most striking in area of San Roman and Yebra, less striking onwards E and W.
NT-H		
	GH	Maximum flooding surface; erosive based silt-/sandstone beds; visible along cross-section, but lacking outstanding characteristics.
NT-G	NUM	Nummulite-beds: Marls to siltstones, very high fossil content, mainly *Nummulites*, recognizable in profiles due to characteristic weathering behaviours; limited physical tracing, thus minor sequence-stratigraphic meaning, as isochronity not testified.
	FG	Marine flooding surface; terminates first coarsening-up cycle east of Isún; prominent surface between San Roman and Fanlillo, incrementally vanishes towards the west.
NT-F		
	EF	Transgressive surface, capping first coarsening-up cycle west of Isún; traceable throughout the cross-section; less striking quality east of Isún.
NT-E		
	DE	Striking surfaces in section Latás, Isún and San Roman, visible towards east, less prominent towards west.
NT-D		
	CD	Erosive base of coarse-grained delta front deposits, traceable throughout the cross-section.
NT-C		
	BC	Transgressive top of Unit NT-B; exposed between Fanlillo and Yebra, where marls overlay sandstones; vanishes west of Yebra.
NT-B		
	BA	Erosive base of sandstone succession; indicates first coarser-grained deposits; traceable ~4 km along eastern part, merges into fine-grained deposits west of Yebra.
NT-A		
		Gradational transition from substrata.

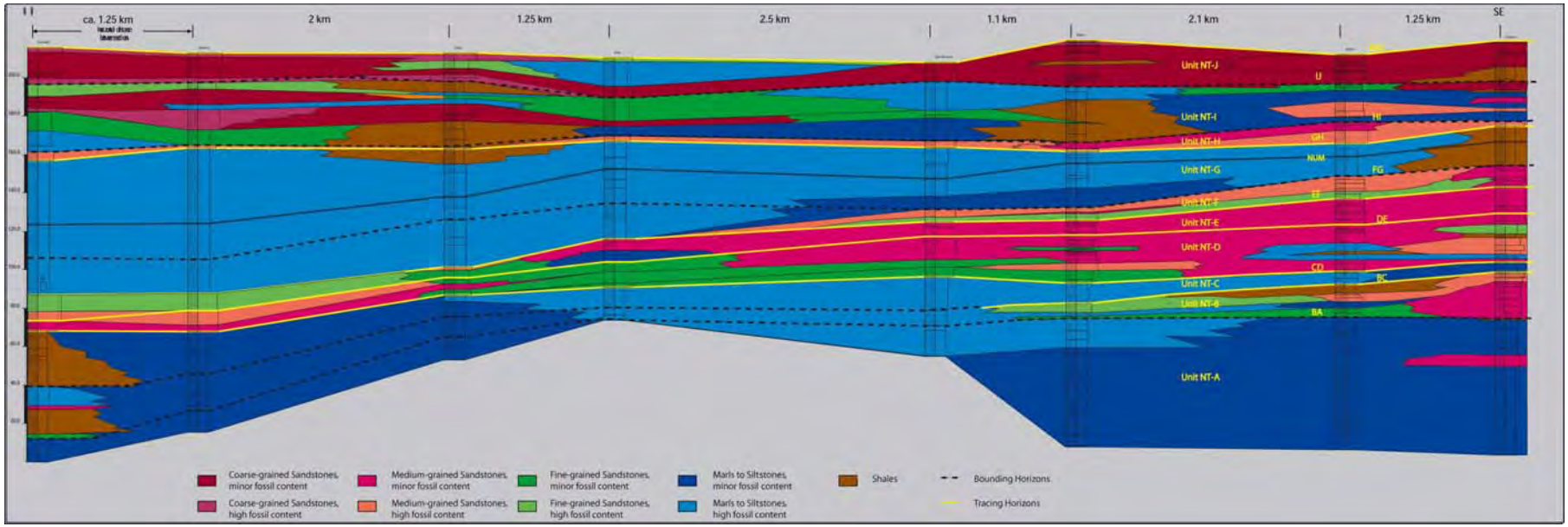

Fig. 7.2: Cross-section oft the northern limb of the Basa Anticline, displaying facies distribution. The resulting transect is based on the correlation between eight lithological profiles, from Larrede (NW) to Fanlillo (ESE), and shows a NW-SE directed trend. Tracing horizons and lithofacies distribution reveal large scale sedimentary geometries along the transect, as well as lateral and vertical stacking pattern with associated facies transitions, indicating a progradational pattern of a deltaic system, whereas changes in the direction of progradation can be deduced. Up to horizon DE the system was delivered from an eastern source area, while the following successions reveal deposition from a northern source area; (see text for details and Fig. 5.1, Chapter 5 for location of vertical sections). An enlarged illustration is given in Appendix D.

Unit NT-C

Unit C represents lower to upper prodelta facies and is composed of shales, marls. and marly siltstones with varying fossil content. Offshore to lower prodelta deposits with a turbiditic character are exposed in section Larrede (FA0), where Unit NT-C reaches thicknesses of ~30 m. Towards Fanlillo a gradual facies shift to upper prodelta deposits with a thickness of ~10 m can be observed (FA2, FA3). In general, the successions of Unit NT-C are comparable to Unit NT-A but show slightly coarser grain sizes and a higher fossil content, mainly composed of Foraminifera, echinoids and molluscs. Locally embedded horizons with an increased content of silt- to sand-sized particles occur, pointing to a progradation of delta front deposits. In the western part of the cross-section, a gradual transition from Unit NT-A to Unit NT-B, and Unit NT-C is exposed, with no marker horizon developed in between. Towards the eastern corner, however, striking horizons clearly are separating the three units, which is a further hint on the progradational character of the deltaic system.

Horizon CD marks the end of the upper prodelta marls and the onset of silt- to sandstone deposits. It is evolved as an erosional base of coarse-grained sandstones, progressively overlying prodelta facies. This tracing-horizon forms a conspicuous unconformity between Unit C and D and marks a key surface of the delta evolution.

Unit NT-D

Unit D forms a striking succession along the cross-section, consisting of silt- to sandstone beds that locally exhibit some fine-grained intercalation of clayey horizons. An overall coarsening-upward trend is displayed within Unit NT-D, whereas a westward decrease in grain size and thickness is recorded. The succession shows delta front sub-environments, predominantly expressed by distal bar and distributary mouthbar deposits, locally influenced by tidal currents or pronounced wave activities (FA5, FA6, FA7). In the eastern branch of the cross-section, the deposits of Unit NT-D are ascribed to hummocky and trough cross-stratified sandstones of distributary mouth bar beds that gradually pass westward (Larrede-Javierre) and downward into distal bar and submarine channel sedimentation (FA13, FA4).

Horizon DE forms a prominent surface of distal bar to mouth bar deposits in the sections of Latás, Isún and San Roman, that can be followed towards the east but looses its outstanding characteristics towards the west.

Unit NT-E

Between Fanlillo and Isún Unit NT-E is build up by distributary mouth bar beds that show tidal and wave influence sedimentation (FA6, FA8). The mouth bar facies is mainly composed of amalgamated hummocky cross-stratified sandstone beds, locally showing features of strong tidal influence, merging upward into trough cross-stratified sandstone beds with fine-grained intercalations and clayey horizons. In their western continuation, the bedsets merge into distal bar and submarine channel facies (FA4, FA13). Individual beds are characterized by erosional surfaces, inverse gradation, and different kinds of erosional pattern, like scour marks and groove casts (FA 13, section Larrede).

Horizon EF corresponds to the top of the first coarsening-upward cycle within the vertical sections west of Isún. In this western part of the cross-section, Horizon EF is marked by fine clastic sedimentation, transgressively overlying coarse-grained sandstones. This prominent horizon can be traced throughout the cross-section but towards the east it loses its main attributes and is enclosed in a succession of mouth bar deposits.

Unit NT-F

Along Horizon EF a facies shift from coarse-grained mouth bar deposits in section Fanlillo (FA8), to progressively deeper marine facies of prodelta sediments with turbiditic character in section Larrede can be observed (FA0, FA2, FA3). In the western corner, trough cross-stratified sandstone beds with fine-grained intercalations form the major part of the succession; bidirectional cross-stratification as well as an increased fossil content can be observed especially within the upper parts of the succession. The mouth bars and associated bay deposits of (FA10, FA11) plunge westward, where they interfinger with fine-grained fossiliferous prodelta deposits (west of Isún). The top of the sandstone units is bounded by a flooding surface, followed by marly siltstones.

Horizon FG forms a flooding surface that terminates the first coarsening-upward cycle in the eastern part of the cross-section. The surface can be easily traced between Fanlillo and San Roman, where fine-grained marly deposits transgressively overlie it. Towards the west, however, it incrementally vanishes within prodelta deposits, becoming very difficult to detect by physical or optical tracing methods.

Unit NT-G

The deposits of Unit F are unconformable overlain by fine-grained successions of Unit NT-G, which reach considerable thicknesses in the western sections (~50 m) and progressively thin towards the east (~20 m). These remarkable changes in thickness are coming along with a facies shift from clayey bay deposits in the eastern part of the cross-

section to prodelta marls and siltstones in the western part (FA3, FA4, FA12). Marly deposits dominate Unit NT-G, displaying several coarsening-upward successions and an upward increase in the proportion of siltstone beds. The successions predominantly are characterized by a high fossil content, mainly composed of Foraminifera, echinoids, molluscs, and fragments of plant remains; in some beds biogenic and/or organic matter becomes enriched, locally resulting in rock forming 'nummulite-beds' (FT-1e**).

The 'nummulite-beds' represent a characteristic feature of Unit G and can be observed throughout the cross-section. Marly siltstones to silty marls with an abundant fossil content build the framework of this succession, whereas *Nummulites* locally become rock forming. These fossiliferous bedsets reach thicknesses up to 10 m, and often reveal a gradation of their biogenic components. In most vertical profiles of the northern cross-section, this horizon exhibits recognizable surfaces that can be identified by its particular weathering behaviours. Physical tracing, however, was limited by the morphology, and optical tracing using photo panels also remains a difficult task. In a sequence-stratigraphic context, the NUM-horizon, therefore, cannot be regarded as a real tracing horizon as its isochronity could not be proven.

Horizon GH represents a maximum flooding surface (mfs) separating the deposits of Unit G and Unit H. This surface denotes the deposition of coarser material and locally is expressed by well-defined sharp boundaries, mainly where channel deposits cut into fine-grained deposits of Unit G. Horizon GH is detectable along the cross-section, but lacks major characteristics.

Unit NT-H

Unit NT-H is represented by a thin succession of fine- to coarse-grained sediments, erosively overlying Unit NT-G. An accumulation of coarser sediment load within an environment of fine-grained siliciclastics is recorded for Unit NT-H. Sharp based, trough cross-stratified silt- and sandstone beds with clayey intercalations, ripped-up clasts, and bioclasts are exposed in the eastern part (Yebra, Sobás, Fanlillo). In the westernmost section Larrede, mouth bar deposits (FA5) crop out, passing into distal bar deposits towards section Isún (FA4). The deposits of Unit NT-H indicate a renewed shallowing of the depositional setting, whereas the depositional pattern of the system cannot be clearly deduced by the bedsets alone. Considering the overlying successions, however, a southward directed progradation can be assumed, with the deposits of Fanlillo now representing the distal portion of the northern profiles. Thus mouth bar sediments of Larrede are laterally interfingering with distal bar deposits of Isún, while the bulk of the sediment load is by-passing and accumulating in more distal areas (Yebra – Fanlillo).

Horizon HI displays an abrupt change in lithology, leading from coarse-grained sediments of Unit H over to more fine-grained and muddy deposits of Unit NT-I. This surface is traceable throughout the cross-section, and is most apparent in the area of San Roman and Yebra de Basa, while towards the east and west the horizon becomes less striking.

Unit NT-I

Along the cross-section Unit NT-I exhibits a particularly heterogenic composition, reaching from muddy bay deposits to coarse-grained channel and mouth bar successions. The coarsest grain sizes can be observed in the western corner of the cross-section, where coarse-grained channel deposits and fine-grained interdistributary bay are exposed (FA14, FA16). In their lateral continuation, towards east, the channel bedsets get thinner, accompanied by a gradual facies shift to finer grain sizes. In the central part, fine-grained bay deposits prevail (FA11, FA14, FA15), while in the eastern profiles (Sobás, Fanlillo), medium-grained channel deposits are exposed within fine-grained interdistributary bay deposits (FA13, FA14). Along the transect Unit NT-I reveals both gradational and abrupt facies transitions: In their lateral continuation, most of the erosive-based channel beds shift into finer-grained sandstone facies, to finally grade into bay deposits. The vertical transition, however, exhibits distinct surfaces between coarse- and fine-grained deposits. Fine-grained, muddy bay deposits also form the cover of Unit NT-I, and erosively are capped by coarse-grained deposits again.

Horizon IJ marks the onset of the uppermost coarse-grained succession of the Sabiñánigo Delta complex. It can be traced physically and optically along the cross-section, defining the transition from fine- to coarse-grained deposits. Horizon IJ predominantly exposes erosional based sandstone and conglomerate beds, but in some parts just a subtle transition can be recorded.

Unit NT-J

The deposits of unit NT-J are composed of an alternation of amalgamated hummocky and trough cross-stratified sandstone beds and intercalated horizons of clayey deposits; with the coarse-grained bedset, erosively overlying the deposits of Unit NT-G. In the western part of the cross-section, pebble-, to granulate-sized conglomeratic facies is exposed (FA20), shifting eastward to pebbly sandstone units (FA16), and coarse-grained sandstones east of Latás (FA17). Locally lateral accretion can be observed within the amalgamated channel succession, as well as an erosive base, as the distinct channel deposits cut into underlying deposits. In their lateral continuation, the channel fillings interfinger with bay sediments (FA14), while the vertical succession consists of alternating

channel and overbank deposits (FA19). A ravinement surface (FA18) and subsequent marly deposits cap the complete deltaic succession.

Horizon RAV marks the top of the Sabiñánigo Delta complex, and is represented by a ravinement surface that caps the succession and can be observed along the cross-section. It shows a condensed horizon, locally developed as a hardground; in the western corner coarse-grained sandstones build up the matrix, containing pebble-sized lithoclasts and clay nodules as well as many fossils, while glauconite-bearing middle- to fine-grained sandstones with clay pebbles and nodules are exposed in the eastern continuation. In general a very high fossil content, and its nodulous appearance characterize this horizon.

Interpretation of the northern cross-section

Within the **northern cross-section** the deposits of the SSt-Succession show an overall shallowing upward trend that is composed of several small-scale coarsening-upward cycles. Inferred from observed depositional successions, lateral facies transitions and vertical stacking patterns, two major building blocks can be distinguished within the northern transect.

The **lower part** reaches from the basis up to Horizon EF, whereas the included Units A to E reveal a general coarsening-upward trend with low-angle foresets dipping towards west, rarely exceeding 1°; except for areas where gravitation mass movements, slumping, occurred. The successions show a progradational stacking pattern and are composed of sedimentary facies, displaying delta front to prodelta and offshore deposits. In the eastern corner of the cross-section, a thick sedimentary pile of predominantly sand-sized deposits is exposed, made up by mouth bar, and distal bar sediments (Unit NT-B, NT-D and NT-E). Their beds progressively build out and thin towards NW, i.e. basinward, where they finally merge into marly prodelta facies. Prodelta and offshore deposits of Unit NT-A and NT-C in contrast are thinning landward (SE), where they interfinger with more proximal delta sediments.

Horizon EF terminates the lower part with a transgressive surface, indicating the onset of the next coarsening-upward succession.

The **upper part** is composed of Units NT-F to NT-J, representing delta plain, delta front, and upper prodelta depositional environments. The succession is bounded by a ravinement surface (RAV) on top that caps the most proximal deposits of the Sabiñánigo Delta, i.e. of the delta plain. Conglomeratic distributary channel fillings form the uppermost components of the delta plain. In the northwestern sections (Larrede, Javierre) coarsest grain sizes and bed thicknesses can be observed, gradually decreasing in a south-eastward direction. Channel sedimentation, embayments, and prodelta are the most

common deposits within the upper part of the northern cross-section, whereas distributary mouth bar, and distal bar deposits occur only to a minor degree. Coarse-grained sandstones to pebble-sized conglomeratic beds are exposed in the western edge of the transect, while the eastern area reveals predominantly finer-grained deposits with clayey and sand-sized successions. Decreasing grain sizes and bed thickness are among the most striking features along the cross-section, accompanied by changing fossil contents and sedimentary structures shifting in general from planar to trough and hummocky cross-stratification. This indicates a facies transition from northwest to southeast. Upper and middle delta plain channel deposits in the western part gradually pass into lower delta plain and bar deposits in the eastern area. This corresponds to the general observation of eastward prograding facies belts within the upper part of the northern cross-section, which is underlined by large-scale geometries that can locally be identified, showing dip-directions to the east.

7.1.2 Depositional successions along the southern cross-section

The southern transect represents a part of a wide-stretched and straight-lined ridge that can be followed over more than 30 km from Orús up to Jaca. The ridge is striking E-W and exhibits two geomorphologic rises, that are most pronounced in the vicinity of Sabiñánigo (Fig. 7.3).

Fig. 7.3: Picture of the southern ridge, view from Sabiñánigo towards east; note the two geomorphologic heights with depression in-between. Exposures of the northern limb, to the left in the background.

In their westward continuation, both rises are starting to plunge slightly, but with distinct progress. The northern rise loses its striking characteristics already west of Sasal and almost disappears in the area of Frauca, while the southern rise is more stable in its westward continuation and dips shallowly near Jaca. This phenomenon is referred to the very steep dipping, locally overturned strata and the fact, that very fine-grained and soft

sediments compose the depositional successions in-between the two heights. As the enclosed soft sediments are much more susceptible to weathering and subsequent erosion, the present morphology evolved. Some restricting conditions regarding the examination of the southern cross-section result from that morphology. Associated weathering and erosion features obscure sedimentary structures and large-scale geometries across the southern transect, which locally hampered detailed analysis with respect to facies composition and sedimentary structures. On the other hand, however, weathering and erosion effects shaped some striking surfaces, horizons, and bed-successions (Fig. 7.4). Even if they are not necessarily equated to marker horizons like flooding surfaces, they, nevertheless represent a framework of timelines and form good criteria for correlation.

A cross-section through the Sabiñánigo Sandstones exposed along the southern limb of the Basa Anticline was generated, spanning ~14 km, from section Ulle at the western edge towards section Allué in the east (Fig. 7.5). Equivalent to the procedure accomplished for the northern cross-section, facies pattern and depositional features of the southern cross-section will be characterized and described in the following. An outline of defined facies units, and characteristic features of their bounding surfaces is given in Table 7.2.

Fig. 7.4: Exposure photograph demonstrating the outstanding character of distinct surfaces, that were walked out in the field to and used for correlation; view towards north.

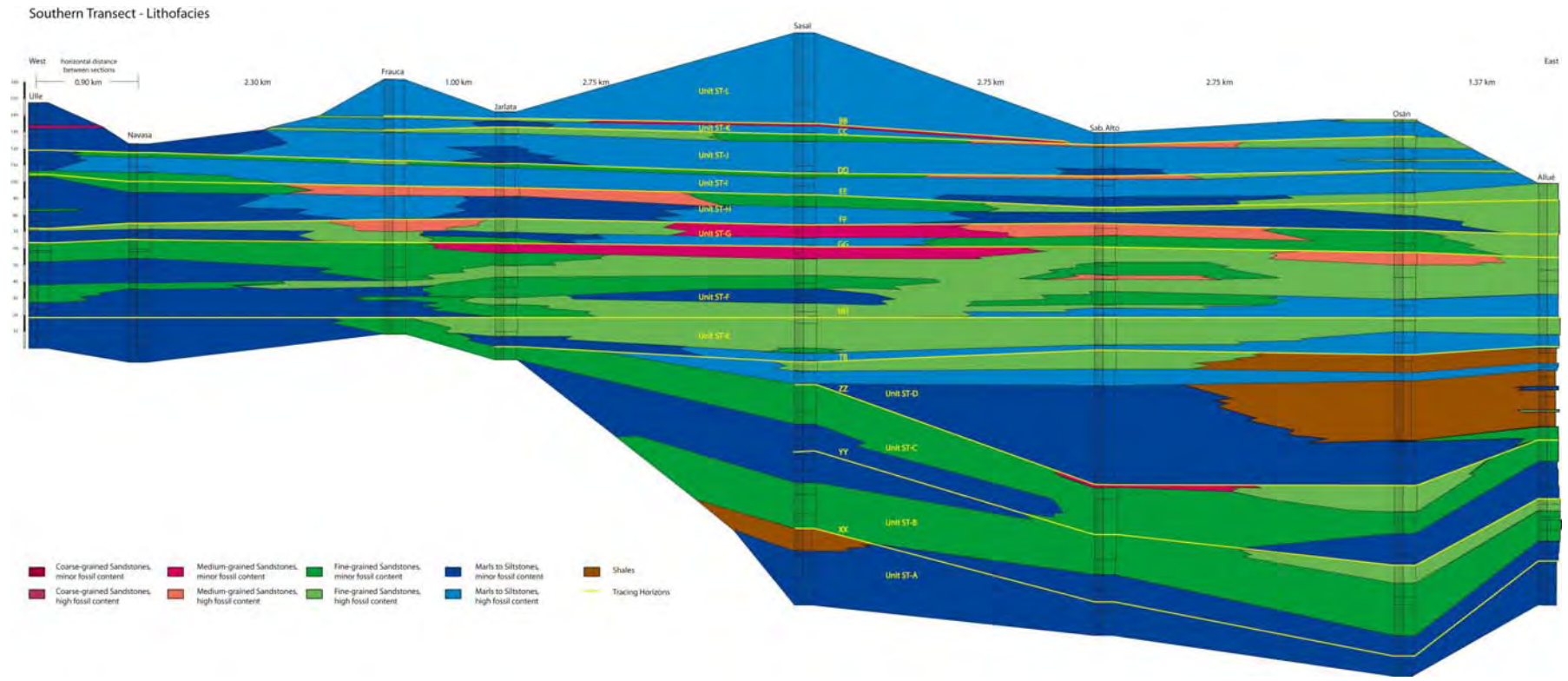

Fig. 7.5: Cross-section through the southern limb of the Basa Anticline, comprising eight vertical profiles from Ulle in the west towards Allué in the east. The section is trending E-W and is composed of several facies units, revealing lateral and vertical facies transitions. Large scale sedimentary geometries along the transect and facies distribution indicate a depositional system with changes in progradation direction between Unit ST-C and Unit ST-D. The facies represent the distal continuation of the northern cross-section; (see text for details and Fig. 5.1, Chapter 5 for location of vertical sections). An enlarged illustration is given in Appendix D.

Unit ST-A

Like the lowermost part of the northern cross-section, Unit ST-A also gradationally emerges from underlying strata of the lower Larrés Marls by forming a series of grey to blue-grey marly deposits with varying content of silt-, and clay-sized particles (FA1, FA2). In some parts, the deposits are almost homogenized by bottom dwelling organisms with some echinoids, Foraminifera and molluscs present. Generally, unit ST-A is build up by several slightly coarsening-upward successions with an insignificant visible fossil content and a subtle coarsening-upward trend. Between Sabiñánigo and Allué the succession is very consistent and can be correlated straightforward. Towards Sasal, however, shale intercalations with a turbiditic character appear in the upper part of Unit ST-A (FA0). In lateral continuation, west of Sasal, the shales pass over into the deposits of the underlying Larrés Marls without any distinctive feature. The series of Unit ST-A are referred to open marine depositional conditions without major dynamic processes present.

Horizon XX exhibits a visible surface with a sharp contact, separating Unit ST-A from the overlying Unit ST-B. In the easternmost part of the cross-section, between Allué and Sabiñánigo Alto, Horizon XX can be traced physically. Towards the west it can be followed up to Sasal by optical tracing until it finally vanishes between Sasal and Jarlata.

Unit ST-B

Marly siltstones and glauconitic silt- to fine-grained sandstones are the major lithologies of this unit ($FA2_S$). In some areas, fossiliferous silt- to fine-grained sandstone beds crop out, predominantly containing echinoids and oysters. The latter locally appearing in abundant amounts building up oyster-bank assemblages ($FA3_S$, FA9). The siltstone and sandstone beds are laterally very consistent, extending over long distances, whereas the fossiliferous horizons are of limited lateral and vertical distribution, subsequently passing into sandstones with minor fossil content.

A general increase of coarse-grained material is recorded within Unit ST-B, indicating a gradual shift towards shallower water depths and thus a transition from offshore to prodelta environments.

Horizon YY represents the top of Unit ST-B that can be traced between Allué and Sasal. It shows a transgressive character in the easternmost sections, while west of Sabiñánigo coarse-grained deposits accumulate on top. This characteristic is accompanied by a facies shift from fossiliferous sandstone beds to sandstones with minor fossil content and finally marly siltstones that can be monitored from Allué towards west, until the horizon recedes west of Sasal and vanishes west of Sasal like Horizon XX does.

Unit ST-C

Throughout the complete unit a coarsening-upward trend can be observed, reaching from silty marls to marly siltstones and fine-grained sandstones ($FA2_S$, $FA3_S$,). The deposits often contain glauconite and locally exhibit carbonaceous concretions of varying size, 2-50 cm in diameter (FA1). Towards the east (Sabiñánigo Alto) sandstones of medium grain sizes are exposed, laterally merging into fossiliferous bedsets that are locally (e.g. at Osán) composed of large amounts of oyster shells ($FA4_S$, FA9). Unit ST-C represents the uppermost part of the northern crest and transgressively is overlain by marly deposits. Analogue to the underlying units, Unit ST-C diminishes west of Sasal, and merges into fine-grained marly deposits that are comparable to the transgressive marls capping Unit ST-C.

Horizon ZZ exhibits a pronounced transgressive surface that corresponds to the top of the northern crest, or rise respectively, and terminates the described coarsening-upward succession. The overlying strata are composed of fine-grained marls, forming a depression between the two enclosing rises. Owing to different weathering and erosion susceptibility of the two rock types, the tracing Horizon ZZ emerges as a striking surface that can be observed along the cross-section until it loses its striking feature between Sasal and Jarlata.

Unit ST-D

Unit ST-D predominantly is composed of recessively weathering silty marls, that shape the series between the more weathering resistant successions of the enclosing crests. At the eastern corner of the cross-section, turbiditic series are exposed within the core (FA0), merging towards the west into marly deposits that crop out within the vertical section of Sabiñánigo Alto (FA2, $FA2_S$). In this section, Unit ST-D exhibits a thick pile of silty marls, showing several slightly coarsening-upward successions, passing at the top into fossiliferous marls and sandstones. The lateral continuation of Unit ST-D is very limited, showing maximum thicknesses at Sabiñánigo Alto and Osán (~80 m) that gradually decrease towards east. In the western prolongation, the successions are thinning more quickly, with reduced thicknesses of ~20 m already recorded at section Sasal (~20 m). The developed cross-section reveals a trough-shaped geometry, where unit ST-D accumulated. The successions are bounded by a maximum flooding surface, their correlative conformity respectively.

Horizon TB forms a correlative conformity of a maximum flooding surface; terminating the transgressive part and indicating renewed sedimentation of coarser grained material. Horizon TB represents the top of the embedded Unit ST-D, and the base of the southern

crest. It can be followed from Allué at the eastern corner of the cross-section to Jarlata, and disappears further to the west.

Unit ST-E

Unit ST-E embodies the lowermost succession of the southern rise, extending throughout the cross-section without major changes in sedimentary thickness between Allué (E) and Jarlata (W). Towards Frauca Unit ST-E still is very consistent in its upper part, the lower successions, however, cannot be defined clearly as Horizon TB is not exposed in this area. In their lateral continuation, west of Frauca a progressive decrease in grain sizes can be recorded. Unit ST-E exhibits a general facies shift along the cross-section, reaching from fossiliferous silt- to sandstones in the eastern area towards sandstones and silty marls with minor fossil content in the western part ($FA2_S$, $FA3_S$, FA9). Echinoids, Foraminifera and molluscs form the major part of the fossiliferous components, locally thick oyster-bank assemblages occurring. The observed facies shift with decreasing grain sizes denotes a deepening along Unit ST-E.

Horizon HH shows a well-shaped bed boundary and marks the top of Unit ST-E and predominantly is overlain by finer-grained deposits. Although the surface does not show significant characteristic features it provides a good tracing-horizon that can be followed either physically or optically along the cross-section.

Unit ST-F

Glauconite-bearing fine- to medium-grained sandstones of varying fossil content, exposed within several coarsening-upward successions, build the major part of this unit ($FA3_S$, $FA4_S$, FA9, $FA10_S$). Siltstones and marly siltstones locally are interbedded at the base of coarsening-upward successions ($FA2_S$). The lateral continuation of Unit ST-F is fairly uniform. Subtle changes in sedimentary thickness are developed, as well as remote facies transitions, shifting from sandstone dominated deposits in the eastern and central part of the transect to predominantly marly deposits at its western corner. An alternating fossil content, which is still mainly composed of echinoids and oysters, with some Foraminifera, is recorded along the unit, whereas oyster-bank assemblages cover larger areas compared to the underlying units.

The uppermost part of Unit ST-F forms a protrusive horizon of several metre thickness. Apart from minor changes in grain size (fine to medium), and fossil content, it exhibits a uniform sediment bank, composed of compact sandstones that can be followed along the transect.

Horizon GG represents the bounding surface of a striking sandstone bed that can be followed along the cross-section.

Unit ST-G

Unit ST-G is very similar to Unit ST-F, and shows a coarsening-upward succession of glauconite-bearing siltstone and sandstone banks, with some marly siltstone beds at the base ($FA2_S$, $FA3_S$, $FA4_S$, FA9, $FA10_S$). The fossil content again shows some variability in its amount, and mainly consists of echinoids, molluscs and Foraminifera, with some oyster-bank assemblages occurring locally. The lateral continuation of Unit ST-G is uniform, with the top evolved as a prominent sandstone bed, extending along the cross-section (Fig. 7.8). As mentioned earlier, the successions of the southern cross-section are very uniform with minor changes of sedimentary facies, along the successions. Across the successions, however, a gradual shift towards finer grain sizes can be monitored in a westward direction, accompanied by a gentle but continuous withering of striking features.

Horizon FF has a transgressive character and is overlain by fine-grained deposits of the following coarsening-up cycle. Horizon FF corresponds to the top of a prominent sandstone bed and exhibits a well-defined surface that can be traced across the transect, but loses some of its striking character in its westward continuation.

Unit ST-H

Horizon FF is pursued by a series of fine-grained marly siltstones, which are composed of several coarsening-upward successions that finally pass into sandstone deposits ($FA2_S$, $FA3_S$, $FA4_S$, FA9, $FA10_S$). Although an overall coarsening-upward trend is displayed within this unit a general increase of fine-grained sediment can be recorded, which is accompanied by a decline of oyster-bank assemblages, but raised occurrence of echinoids. The top of Unit ST-H is composed of massive sandstones, forming a uniform and outstanding horizon with a thickness of about 5 m, extending along the cross-section (Fig. 7.8).

Horizon EE is defined by the same characteristics as Horizon FF. In most parts of the cross-section, it is overlain by fine-grained marly siltstones, indicating a transgressive trend of the system. Horizon EE represents the surface of the uppermost and outstanding sandstone bank of Unit ST-H and can be followed along the cross-section. Subordinate facies transitions, referring to minor changes in fossil content and grain sizes are recorded alongside the surface.

Unit ST-I

The general trend of declining grain sizes, as denoted by the deposits of unit ST-H is continued within the successions of Unit ST-I. An overall coarsening-upward succession is exposed, commencing with fine-grained deposits and capped by a protrusive sandstone bed, which spans along the cross-section ($FA2_S$, $FA3_S$, FA9, $FA10_S$). The proportion of fine-grained marly and silty deposits is prevailing, while sandstones are only present within the uppermost part of Unit ST-I. Particularly within the fine-grained deposits an increased fossil content, mainly composed of echinoids, Foraminifera and tests of some bivalves can be observed, whereas the sandstone-beds exhibit more shell fragments and bioclasts in general.

Horizon DD forms the bounding surface of the covering sandstone bed. It is transgressively overlain by fine-grained marls, and can be traced throughout the cross-section.

Unit ST-J

Analogous to the underlying units a general decrease in grain size is recorded accompanied by a shift in fossil content, and fossil assemblage. Echinoids and Foraminifera are prevailing, while large oyster-bank deposits are rare; toward the westernmost corner of the cross-section, a general decline in fossil content can be observed. Marly siltstones transgressively overlie Horizon GG, and build up the major part of Unit ST-J ($FA2_S$). Fine- to medium-grained sandstone bedsets with comparable minor thicknesses are developed in the uppermost part of Unit ST-J ($FA3_S$, FA9, $FA10_S$). They exhibit uniform beds with an extensive and pronounced character that can be followed along the cross-section.

Horizon CC forms the boundary between the top of Unit ST-J and the overlying marly deposits. It can be referred to the outstanding surface of the uppermost sandstone bed of Unit ST-J, and represents the uppermost tracing horizon spanning the entire cross-section.

Unit ST-K

A series of marly siltstones to silty marls with a reduced thickness is overlying Horizon CC and is covered at its top by a thin but striking sandstone bank ($FA2_S$, $FA3_S$, $FA4_S$). The sandstones locally show increased amounts of fossil tests, bivalves, Foraminifera, and echinoids are the major components. Unit ST-K extends from section Ulle to Sabiñánigo Alto, but is not exposed as good as the underlying units. The covering sandstone bed can be traced between Frauca and Sasal, in its eastern and western continuation; however, it

gradually loses its outstanding character, until it finally merges with under- and overlying fine-grained deposits.

Horizon BB represents the uppermost tracing surface of the southern cross-section and corresponds to the top of the bounding sandstone bed of Unit ST-J. Horizon BB can be followed from Frauca to Sasal until it vanishes towards east and west.

Unit ST-L

The uppermost part of the complete succession is composed of marly siltstones to silty marls, containing some echinoids, molluscs and Foraminifera tests, whereas sedimentary structures or distinct facies patterns are obscured by intense weathering ($FA2_S$). Locally a thick sedimentary pile is build up, gradually passing into the deposits of the Pamplona Marls, which form the overlying strata of the Sabiñánigo Delta complex.

Tab. 7. 2: Outline of tracing horizons, their characteristic features and enclosed facies units within the southern cross-section; from base (Unit ST-A) to top (Unit ST-K).

Unit	*Traced Horizons – Characteristics*	
ST-K		
	BB	Bounding surface of outstanding sandstone bed; uppermost tracing horizon of the cross-section, exposed from Frauca to Sasal.
ST-J		
	CC	Bounding surface of prominent sandstone bed; uppermost tracing horizon spanning the entire cross-section.
ST-I		
	DD	Transgressive surface of striking sandstone bed; traceable throughout transect.
ST-H		
	EE	Bounding surface with transgressive character; top of outstanding sandstone bed; traceable throughout the cross-section.
ST-G		
	FF	Bounding surface with transgressive character; top of prominent sandstone bed, exhibits striking surface traceable across the transect.
ST-F		
	GG	Bounding surface of striking sandstone bed developed throughout the cross-section.
ST-E		
	HH	Bounding surface of Unit ST-E, exposed along the cross-section.
ST-D		
	TB	Correlative conformity of a maximum flooding surface; base of southern crest; traceable from Allué to Jarlata; exhibits facies transition from turbiditic deposits to fossiliferous sandstones (E–W).
ST-C		
	ZZ	Transgressive surface, terminating first coarsening-up cycle; top of northern crest; striking surface along the cross-section up to Sasal.
ST-B		
	YY	Bounding surface of Unit ST-B; partly transgressive character with facies transition along surface; traceable between Allué and Sasal; merges into marly siltstones.
ST-A		
	XX	Bounding surface with sharp contact, separating Unit ST-A from Unit ST-B; exposed from Allué to Sasal, vanishes between Sasal and Jarlata. Gradational transition from substrata.

Interpretation of the southern cross-section

The southern transect displays a limited facies-variety that is mainly composed of upper to lower prodelta environments and transitional offshore sedimentation. Comparable to the northern cross-section, several small-scaled coarsening-upward cycles can be observed within the southern cross-section. The described morphologic features and the general homogeneity of occurring facies complicate the determination of specific depositional pattern and progradational sequences of the southern transect, as distinctive surfaces are obscured.

On the basis of defined units, associated facies transitions, and recognized stacking pattern, four building blocks were distinguished within the southern cross-section.

Block ST-1 comprises the Units ST-A, ST-B and ST-C that are exposed within two faint coarsening-upward successions. The successions represent lower prodelta, to transitional offshore facies, whereas lateral and vertical facies transition is mainly characterized by changing fossil contents. Fossiliferous bedsets generally prevail in the eastern part of the cross-section, where they form the uppermost horizons of each coarsening-upward succession. In their western continuation, they show a decreasing fossil content and a general shift to deeper water facies. From the cross-section a trough shaped large-scale geometry of this block can be observed.

Block ST-2 is build up by a single unit, i.e. Unit ST-D, with thick deeper marine series overlying the successions of Block ST-1. The deposits laterally grade from turbiditic series in the eastern corner of the cross-section to marly siltstones in the western continuation, where they finally vanish. A general coarsening-upward trend with a transgressive character distinguishes Block ST-2.

Block ST-3 includes the Units ST-E, ST-F, and ST-G, and displays several coarsening-upward successions within an overall coarsening-upward trend. The lateral reach of this building block is very uniform, with a general although just faintly developed lateral facies transition, ranging from sandstones to marl dominated deposition towards the west of the transect. Within the successions of this block a slightly decreasing fossil content both upward and westward can be recognized. A striking sandstone bank of Unit ST-G (Horizon FF) represents the uppermost part, followed by recessively weathering marly deposits, which expose a transgressive character.

Block ST-4 covers the remaining part of the southern cross-section (Unit ST-H to Unit ST-L) and shows an alternating succession predominantly composed of marls and embedded sandstone banks. Equivalent to building block three, the lateral facies distribution of block four is very consistent, with minor changes in sedimentary facies or

thickness. Towards the top, however, both the proportion and thickness of the enclosed sandstone beds is decreasing, while the marly deposits vertically pass into the overlying Pamplona marls without any significant boundary surface exposed, as it is realized within the northern cross-section by the ravinement surface.

7.2 Gamma ray log response across the system

A second set of lateral transects was accomplished by correlating vertical gamma ray logs processed along both limbs of the Basa Anticline. Therefore, the logs were scrutinized for the presence of key surfaces (marker horizons) that commonly reveal distinct features in their spectral gamma log (cp. Tab. 3.4, Chapter 3). Marker horizons like flooding surfaces (UR-log and Th/K-log) and transgressive surfaces (abrupt GR response) were used. Some marker horizons can be correlated throughout the logs, while other striking horizons are well developed within one edge of the cross-section but hardly can be identified in all logs. In these cases, pattern matching (log-shapes, Th/K ratios) poses a helpful technique to fill the gaps, and to review and refine the correlation obtained by marker horizons (cp. Chapter 3.2.2).

7.2.1 Gamma ray log response across the northern transect

The log-based cross-section of the northern limb comprises the vertical sections of Latás, Isún, Yebra, Sobás, and Fanlillo (cp. Fig 7.2). On the basis of defined marker horizons and general log trends (log shapes), already described in Chapter 5, a log-based cross-section of the northern limb was generated (Fig. 7.6). Therein, two parts can be distinguished, composed of seven vertical cycles (‘*log units’*), which display differences between sandstone and mudrock dominated lithologies, whereas each ‘log unit’ is bounded by a horizon with a diagnostic peak pattern (Tab. 7.3).

A general upward decrease in gamma ray response marks the ‘log units’, indicating an upward increase in the sandstone/mudstone ratio. Across the transect progressive changes within the ‘log units’ can be recognized, allowing to differentiate between a lower and an upper part. The **lower part** is composed of LogU-N1, LogU-N2, and LogU-N3, whereas LogU-N1 is only partly developed in section Fanlillo and Yebra. LogU-N2 shows decreasing vertical extension from east to west, whereas the funnel shape shows a well-developed ‘nose’ (low UR values) in sections Fanlillo, Sobás, and Yebra, while towards west this pattern disappears. LogU-N3 shows changing vertical thicknesses that are generally decreasing toward west associated with more serrated log shapes. The following ‘log units’ of the **upper part**, however, show decreasing vertical dimensions from west to east, and also the log shapes are loosing their striking features towards east. LogU-N3, for example, is ~40 m thick in section Latás, and ~5 m at section Fanlillo, and

LogU-N4 shows a funnel shape with a well-developed and thick upper part in sections Latás and Yebra, disappearing eastward.

Upward decreasing GR response and lateral changing log shapes indicate a progradational character of the system. This coincides with the pattern already observed in the lithological cross-sections, as well as the change in progradational direction, which can be assumed to cause the described changes between the lower and the upper part.

Tab. 7.3: 'Log units' and bounding horizons observed within the northern cross-section by log shapes and diagnostic log pattern.

Log unit	*Bounding Horizon*	*Log Shapes - Diagnostic Pattern*
LogU-N7		Bell shape, uppermost 'log unit', only partly present
	N-6	Marked change in K and Th response
LogU-N6		Funnel log shapes
	N-5	Change from low UR and high Th/K to high UR and low Th/K
LogU-N5		Serrated and cylinder log shapes
	N-4	UR-, and U-peak, low Th/U values
LogU-N4		Symmetrical and funnel log shapes prevail
	N-3	Abrupt change in GR response
LogU-N3		Cylindrical log shapes prevail
	N-2sb	Striking horizon within LogU-N3, showing GR-spike
	N-2	Change from low UR and high Th/K to high UR and low Th/K
LogU-N2		Funnel shape, coarsening-up cycle, mostly with sharp top
	N-1	UR-, and U-peak, low Th/U values
LogU-N1		Marked change in K and Th response. Best developed in section Fanlillo, moderate in section Yebra

7.2.2 Gamma ray log response across the southern transect

The log-based cross-section of the southern limb includes the vertical sections of Navasa, Frauca, Jarlata, Sasal, and Sabiñánigo Alto (cp. Fig 7.2). The generation of the southern cross-section (Fig. 7.6) is also based on defined marker horizons and general log trends as already described. A lower and an upper part can be distinguished, composed of three and four vertical cycles ('*log units'*) that are bounded by diagnostic horizons (Tab. 7.4).

The 'log units' of the southern cross-section reveals a stacked pattern of coarsening-upward successions. The lower part, composed of LogU-S1 and LogU-S2, is present only in section Sabiñánigo Alto and Sasal. Two coarsening-upward cycles can be recognized, which are more pronounced in the east (Sabiñánigo Alto) while they are developed more weakly in section Sasal. A corresponding pattern can be observed for the first unit of the

upper part, LogU-S3, which also shows decreasing GR response from east to west. This indicates a progradation of the system in a westward direction. The following 'log units' display stacked coarsening-upward cycles, with a decreasing sandstone/mudrock ratio towards the top (increasing GR response). The described 'noses' nicely display the occurrence of coarser grained horizons within the succession and can be assigned to the sandstone beds observed in the field and described in the lithological transect. The upper part in general indicates an aggradational to progradational system, gradually passing into deeper marine depositional environments, which matches the pattern revealed from the lithological transect.

Tab. 7.4: 'Log units' and bounding horizons observed within the southern cross-section by log shapes and diagnostic log pattern.

Log unit	*Bounding Horizon*	*Log Shapes - Diagnostic Pattern*
LogU-S7		Funnel log shape from E to W
	S-6	Change from low UR and high Th/K to high UR and low Th/K
LogU-S6		Funnel log shape from E to W
	S-5	Abrupt response in GR values
LogU-S5		Varying log shapes, symmetrical and stacked pattern of funnel log shapes prevail. Pronounced decrease of GR log response at the top, well developed 'nose' (low GR response).
	S-5sb	Depicted sequence boundary, minor GR peak
	S-4	Minor GR and U peak, low Th/U
LogU-S4		Symmetrical log shapes prevail, faint GR log response
	S-3	Change from low UR and high Th/K to high UR and low Th/K
LogU-S3		Funnel log shape with well-developed sharp top
	S-2mfs	Horizon within LogU-S3, characterized by GR and U peak, and low Th/U
	S-2ts	Horizon within LogU-S3, showing abrupt GR response
	S-2	High GR response, GR spike
LogU-S2		Funnel log shape with well-developed sharp top
	S-1	Change from low UR and high Th/K to high UR and low Th/K
LogU-S1		Major funnel log shape, composed of several smaller coarsening-up cycles

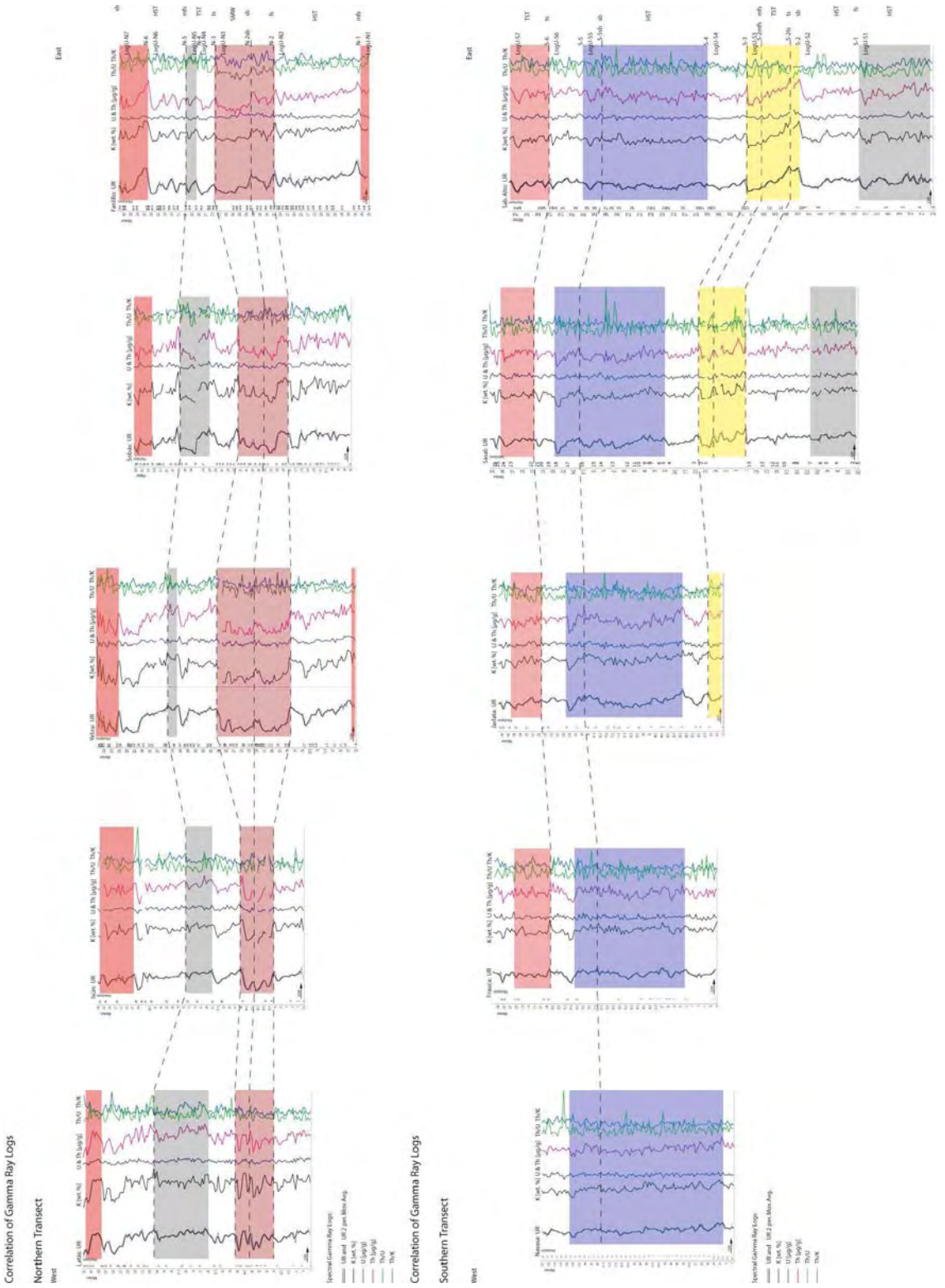

Fig. 7.6: Log-based cross-sections of the northern and the southern limb, with vertical stacking pattern and marker horizons. Up to 7 vertical 'log units', bounded by key surfaces that are detectable by their characteristic gamma ray log response (see text for details). Maximum flooding surface, mfs: tot GR-peak (UR-log), U-peak, low Th/U; flooding surface, fs: change from low tot GR and high Th/K to high tot GR and low Th/K; transgressive surface, ts: abrupt response; sequence boundary, sb: GR-peak and location within succession. Cp. Appendix D for enlarged illustration.

7.3 Chronological sequences of the Sabiñánigo Sandstone Succession

To decipher chronological sequences and horizons within the SSt-Successions the presented lithofacies and log-based cross-sections were screened for chronological evidences and matched, resulting in a condensed and sequence stratigraphically interpreted cross-section for each limb.

7.3.1 Chronological sequences along the northern cross-section

On the basis of the information obtained from the lithological and the log-based cross-section two sequences were distinguished that are subdivided by a variety of key surfaces (Fig. 7.7).

The **first sequence** comprises the Units NT-A up to NT-D, as well as LogU-N2 and lower part of LogU-N3, and reveals a progradational character, proceeding from SE to NW as observed in both cross-sections. The sequence is bounded by horizon DE that forms a striking surface throughout the northern cross-section, or horizon N-2sb, respectively, which can be identified by a GR spike and its position within the succession. As this surface shows an erosional character, but lacks evidence of a forced regression, it is assigned to a Type 2 unconformity (sb2). Two genetically linked depositional systems of an early and a late Highstand Systems Tract (HST), with associated erosion, flooding, and maximum flooding surfaces can be distinguished within the first sequence. The maximum flooding surface (mfs, N-1) forms the lower boundary of the first progradational sequence of the SSt-Succession, and can be identified within the log-based cross-section by its gamma ray response (UR an U peak, low Th/U). The early and the late HST are separated by a flooding surface (fs, Horizon CD and N-2) and capped by the erosional Type 2 sequence boundary (sb2), equivalent to Horizon DE and N-2sb.

The **second sequence** comprises the Units NT-F up to NT-J, upper part of LogU-N3 up to LogU-7, respectively. At its base it is bounded by the erosional horizon DE, N-2sb, respectively, while a ravinement surface (RAV) forms the uppermost boundary, terminating the entire SSt-Sequences. Three systems tracts build the second sequence, which shows a backstepping pattern at its base (Units NT-E up to NT-G, upper part of LogU-N3 up to LogU-N5), followed by a progradation of the system (Unit NT-H, NT-J, LogU-6, LogU-N7)). Unit NT-E and upper part of LogU-N3 are referred to a falling stage, or Shelf Margin Wedge systems tract (SMW) respectively, that is terminated by the transgressive surface (ts). The transgressive surface reveals a good marker horizon, as it was physically traced in the field (tracing Horizon EF). It can be followed across the entire distance of the lithological cross-section, as well as of the log-based cross-section, because of its abrupt GR log response (N-4).

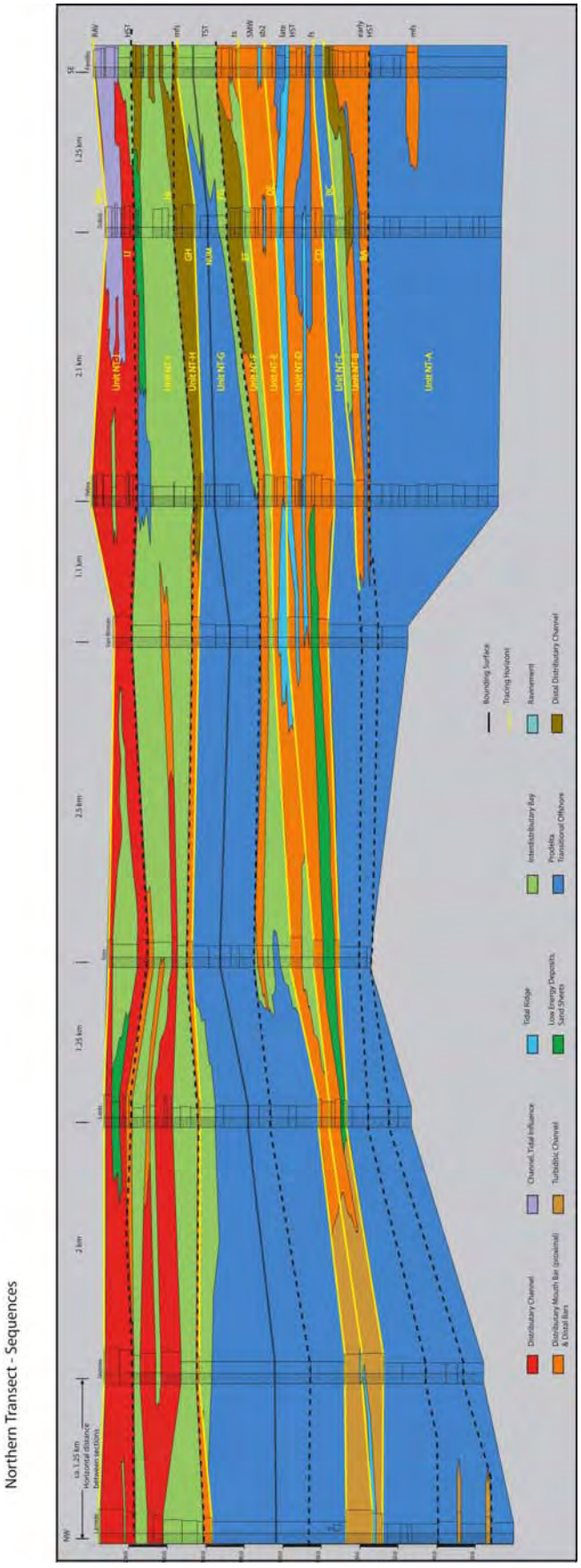

Fig. 7.7: Sequence stratigraphic interpretation of the cross-section from the northern limb of the Basa Anticline, based on Fig. 7.2. The section exhibits a progradational stacking pattern, with two sequences composed of several systems tracts. The first sequence, up to sequence boundary sb2 (horizon DE), represents an underfilled basin stage, while the second sequence, sb2 up to RAV, displays an overfilled basin stage of an almost complete delta sequence, that is capped by a ravinement surface. See Appendix D for enlarged illustration and text for further details.

A Transgressive Systems Tract (TST) that shows a retrogradational pattern (Unit NT-F, NT-G, and LogU-N4, LogU-5) overlies the SMW. The TST is bounded by a maximum flooding surface (GH, N-5), which is followed by the subsequent coarsening, i.e. shallowing-upward cycle of the HST. It includes the Units NT-H up to NT-J, LogU-N6 and LogU-N7, respectively, and is characterized by an eastward directed progradation of the system. The transgressive surface (RAV), which is equivalent to the top of the deltaic system, indicates a base level rise and associated diachronous subaqueous erosion.

7.3.2 Chronological sequences along the southern cross-section

Owing to the lithological and the log-based cross-section, three sequences were distinguished within the southern cross-section, subdivided by corresponding key surfaces (Fig. 7.8).

The **first sequence** comprises the Units ST-A up to ST-C, as well as LogU-S1 and LogU-S2, representing a HST with a progradational pattern from east to west. The capping sequence boundary forms a prominent surface that can easily be recognized in the field (trace Horizon ZZ), and by a GR spike in its log pattern (S-1). The **second sequence** starts with a TST and is composed of Units ST-D up to ST-H, LogU-3, LogU-4, and most of LogU5. The transgressive surface of the TST is developed only in the eastern corner of the cross-section as a marking surface in the field, but can be recognized by an abrupt GR log response (S-2ts). The TST (Unit ST-D, and lower part of LogU-S3) is capped by a mfs that can be identified in the log-based cross-section by a GR and U peak with associated low Th/U values (S-2mfs). The subsequent HST is composed of stacked parasequences, revealing an aggradational to progradational pattern. It includes the Units ST-E to ST-G, as well as the upper part of LogU-S3, LogU-S4 and most of LogU-S5. The sequence boundary, terminating the second sequence can be traced throughout the lithological cross-section (trace Horizon FF), but is more difficult to depict in the log-based cross-section, as a diagnostic GR response is difficult to identify. Nonetheless, as the sequence boundary is located between mfs and the subsequent ts, horizon S-5mfs is assumed to represent the sequence boundary. The **third sequence** comprises the overlying Units ST-H up to ST-L, and the uppermost part of LogU-5 up to LogU-7. Within this TST a transgressive surface is developed that can be followed throughout both cross-sections (trace Horizon EE, and S-5). The TST shows a retrogradational parasequence pattern, revealing a deepening of the depositional environment. The third sequence might already display the deposits of the Pamplona Marls, or a gradual transition from the SSt-Succession into the overlying Pamplona Marls. For the northern cross-section a discrete boundary, marking the onset of the Pamplona Marls sedimentation is given by the ravinement surface. As such a distinctive boundary is lacking within the SSt-Successions

of the southern exposures, a definite allocation of the onset remains difficult as long as no reference point is given, allowing a link-up between the northern and the southern exposures.

7.4 Depositional model of the Sabiñánigo Sandstone Succession

The integration of both correlation techniques provides detailed insights on the depositional geometries and stratal relations within the SSt-Succession of both limbs and allows reconstructing the delta evolution. Furthermore, as this approach is based on isochronous surfaces, instead of diachronous lithostratigraphic correlation horizons, a time calibrated genetic model could be developed, not just for each limb but for the entire Sabiñánigo Delta system, as marker horizons could be unravelled enabling to link up the northern and the southern exposures.

7.4.1 Sedimentary evolution of the Sabiñánigo Sandstone Succession

Two major coarsening-upward cycles characterize the entire SSt-Succession, representing two progradational sequences that are composed of several smaller parasequences. Owing to large scale geometries and facies transitions a westward oriented progradation is assumed for the first progradational sequence, with the source area located to the east. Most likely the Boltaña Anticline acted as major source area, as it was emerging coevally to the evolution of the Sabiñánigo Delta complex.

The westward, i.e. seaward progradation is demonstrated by continuous outbuilding of depositional strata proceeding over a maximum flooding surface. Distal bar deposits that successively are overlain by distributary mouth bar deposits represent first coarse-grained input from SE. This progradational pattern results from relative sea level rise accompanied by high sedimentation rates (e.g. Van Wagoner 1990). This leads to the deposition of a regressive sedimentary system, as sediment accumulation rates were exceeding the rate of relative sea level rise. The very first progradational successions observed within the Sabiñánigo Delta are related to a Highstand Systems Tract (HST). In its proximal position (northern limb), the HST is characterized by a slow rise of relative sea level (early HST), followed by a slow fall, which caused the formation of a flooding surface (fs), and renewed progradation of the late HST. Within the northern cross-section fossiliferous bedsets are characteristic for the fs (CD), which marks the bounding surface between the early and late HST. Corresponding fossiliferous bedsets can also be observed in the distal continuation of Horizon YY. Moreover, the flooding surface is characterized by the presence of radioactive and organic rich mudrocks, and glauconite, resulting in a diagnostic GR response recorded within both limbs and thus, providing a further link-up between the proximal and distal part.

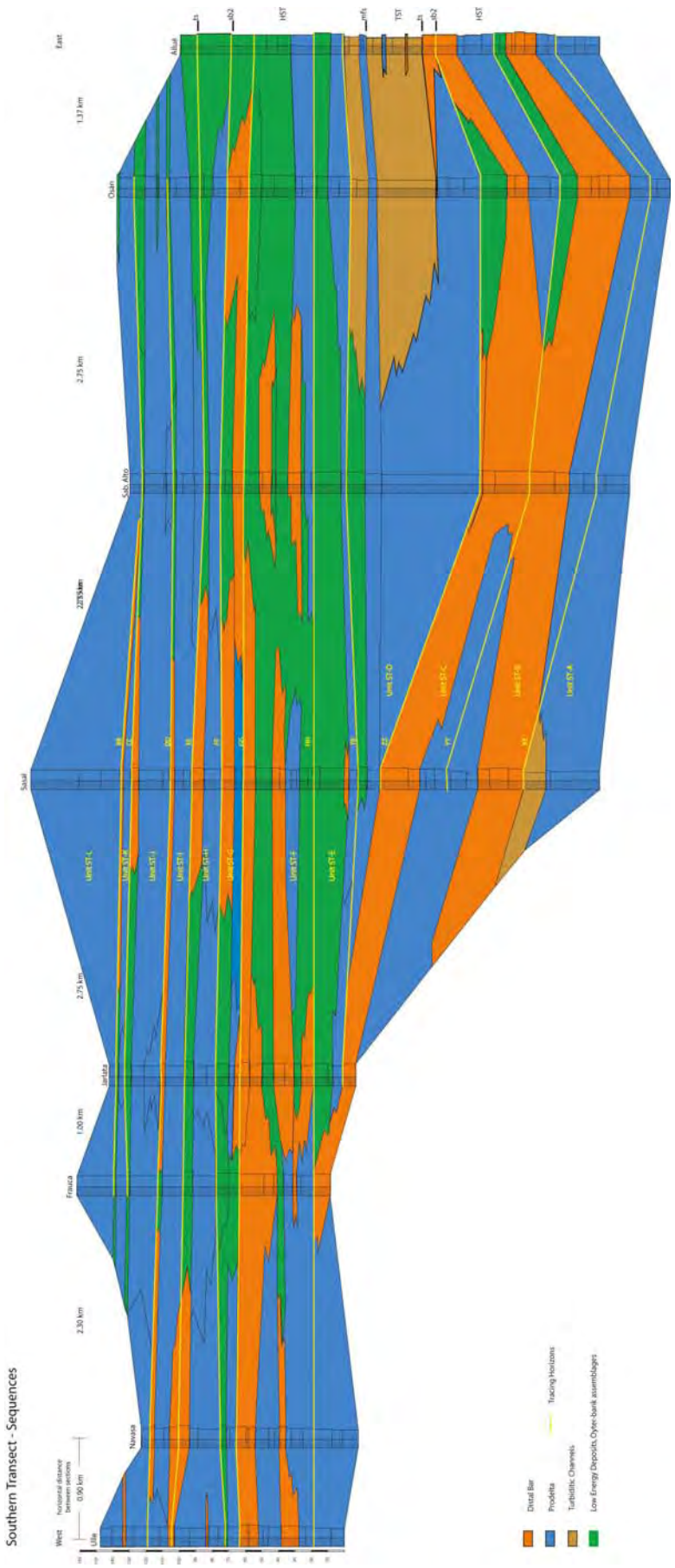

Fig. 7.8: Sequence stratigraphic interpretation of the cross-section from the southern limb of the Basa Anticline, based on Fig 7.5. The section exhibits a progradational stacking pattern, with three major sequences, representing the proximal depositional environment of the northern limb. See Appendix D for enlarged illustration and text for details.

The flooding surface forms the base over which the successions of the late HST progressively build out basinward, forming smooth downlap structures that are capped by a Type 2 sequence boundary (ZZ, DE, N-2sb, S-2). The first regressive sequence of the SSt-Succession, displays an incomplete deltaic sequence, reaching from offshore transition to distributary mouth bar deposits, without any indication for delta plain sedimentation. The abundant occurrence of hummocky cross-stratified bars with starved ripples within the bar deposits of the proximal portion, indicates high energy conditions of a wave dominated deltaic setting with periodic storm events. A minor tide influence can be revealed from mud-drapes, planar lamination and bidirectional cross-stratification.

The progradational pattern of the first sequence is followed by a retrogradational parasequence, inducing the subsequent depositional sequence, which is characterized by some major differences compared to the first sequence. From observed facies transitions and stacking patterns a change in progradation direction can be deduced. The lower portions of the cross-sections represent a section that is oriented sub-parallel to transport and deposition direction; while the upper portion shows a section oblique to progradation, which in this case proceeds from NNW to SSE. The changed progradation, and thus, transport direction, is referred to changing conditions in the hinterland, with a source area situated towards the north. The Axial Zone most likely acted as source area, because of tectonic pulses that affected this area, followed by rapid uplift of the orogene (Fitzgerald et al. 1999). This in turn, also influenced the Jaca Basin, which still was in an active piggyback basin stage and affected by thrust sheet emplacement (Puigdefàbregas and Souquet 1986). Thus, the Axial Zone as major source area replaced the Boltaña Anticline. As revealed from facies composition, the northern limb of the Basa Anticline generally exposes the proximal portion of the deltaic system, while the southern limb represents more distal depositional environments. Considering the location of the vertical profiles in relation to the trend of the anticline, the vertical profile of section Allué, thereby, roughly represents the basinward continuation of profile Latás.

In the proximal portion of the delta, within the northern limb of the Basa Anticline, a SMW forms the lowermost systems tract of the following depositional sequence. It is associated with the sb2 and a relative low position in sea level. The SMW shows a backstepping pattern of retrogradational to aggradational parasequences with onlapping clinoforms. They are capped by a transgressive surface (EF), leading to the subsequent TST, which onlaps and retrogradates across the transgressive surface. In their landward portion, the parasequences of the TST, therefore, onlap the sequence boundary, while the more distal deposits show downlapping geometries. The top is formed by a maximum flooding surface (mfs), over which the HST progrades and agrades. In the uppermost sequence of

the Sabiñánigo Delta, the HST is characterized by several agradational and progradational parasequences, gradually filling the basin, until a major transgression terminates the deltaic deposition, under formation of a ravinement surface (RAV).

Therefore, two basin stages can be distinguished within the Sabiñánigo Delta complex: An underfilled basin stage that is represented by the first progradational sequence, and the following overfilled basin stage of the upper part. The overfilled basin stage demonstrates an almost complete deltaic sequence, reaching from prodelta to delta plain sedimentation, and is capped by a transgressive surface. The ravinement horizon is continuously exposed across the northern exposure site and has its correlative unconformity in the distal setting, represented by the sequence boundary (FF), that separates the Sabiñánigo Sandstone Succession, i.e. Sabiñánigo Delta, from the Pamplona Marls.

7.5 Process Response System: Sabiñánigo Delta evolution – Pyrenean orogeny

Previous works on the deposits of the Jaca Basin in general, and the SSt-Sequence in particular missed to reveal the sequence stratigraphic significance of the entire SSt-Sequence, as no connecting marker horizons are exposed. As mentioned earlier, the SSt-Sequence takes over a challenging position within the Jaca Basin, as it forms the transitional part from deep marine to continental deposition, promising to reveal some insights on the depositional processes affecting the Jaca Basin. The sedimentary evolution of the Sabiñánigo Delta reflects a coupled delta and basin stage development. From facies transition and large-scale sedimentary geometries, as apparent within the lateral transects, changing depositional conditions can be deduced.

The SSt-Succession displays an evolution from an underfilled basin stage in lower part of the delta complex to an overfilled basin stage in upper part, associated with changes in the depositional character. The orientation of sediment transport and deposition was forced to shift from a westward directed progradation of the system to a southward directed progradation, as can be drawn from grain size distribution and clast composition and rounding. Coarsest grain sizes up to coarse-grained sandstones, within the first depositional sequence are observed, in the eastern corner of the cross-sections, while the upper depositional sequence reveals coarsest grain sizes, up to pebble-sized conglomerates in the north-western corner of the studying site. This progradation change, from a WSW- to an ESE-ward direction is referred to changing source area dynamics that are mainly driven by tectonic processes of the emerging Boltaña Anticline and renewed tectonic pulses in the Pyrenean orogeny. The latter caused the uplift of the Axial Zone, which replaced the Boltaña Anticline as dominating source area. The two depositional

basin stages, stored within the sedimentary deposits of the SSt-Succession, reflect these dynamics: During the first sequence, the delta was not able to fully develop, but rather had to adopt to changing depositional conditions and basin configurations, which resulted in the first sequence, displayed by the underfilled basin stage. During this time, east-west directed tectonic processes and new-orientations in basin configuration, still affected the Pyrenean realm (Vergés et al. 2002), resulting in major influences on depositional systems, as demonstrated by the Sabiñánigo Delta. The second stage of the Sabiñánigo Delta evolution, however, denotes that tectonic dynamics and reconfigurations settled to a more stable level, with major pulses coming from the central part of Pyrenean orogeny. Therefore, mainly regional tectonic processes within the sedimentary basin are responsible for the development of the two sequences. The individual parasequences of distinct systems tracts, however, display further mechanism causing changes in the depositional character, and are ascribed to changed sediment supply and delta-lobe switching. This indeed also can be triggered by tectonic processes in the hinterland, but reflects climatic changes and the course of individual distributaries as well.

Chapter 8 – Conclusion

The appearance, configuration and evolution of a depositional environment are highly influenced by the prevalent sedimentary processes. In general, specific depositional processes generate sedimentary successions with characteristic properties, like textures, structures, bedding features, etc. These characteristics reflect the conditions that were active during sedimentation within a given environment and its surrounding areas (Boggs 2001).

This study utilizes different techniques to characterize the sedimentary succession of the Sabiñánigo Sandstones. It considers gamma ray logs together with standard lithological profiles. In addition, to constrain the sedimentary overburden, covering the SSt-Sequence, low-temperature thermochronology has been applied. Lithofacies, facies successions, and physically traced sediment surfaces were used to compile lateral cross-sections and to reconstruct the depositional architecture and evolution of the Sabiñánigo Delta. Based on this framework of timelines, stratal terminations and trans-/regressive facies trends were identified within the sedimentary successions, and visualized by three sets of lateral cross-sections. The integration of various data sets enabled to develop a depositional model of the SSt-Succession and to investigate its evolution within a time calibrated framework, comprising the entire sequence. This was used to understand the genesis of the deltaic deposits of the SSt-Succession and to develop a picture of how sedimentation was affected by the Jaca Basin evolution. In general, this exemplifies how the sedimentary infill of an actively moving piggyback basin was investigated, and how different techniques were used to constrain the acting processes that were affecting the depositional environment and subsequently the evolution of a sedimentary system.

From facies analysis a dynamic depositional setting was deduced for the SSt-Succession, displaying a variety of different deltaic subenvironments. The sedimentary structures indicate a deltaic environment that was influenced by tidal currents and wave activities. Accordant sedimentary structures are more pronounced in the northern exposures. The southern exposures reveal more distal depositional environments, resulting in a reduced fluvial impact on sedimentation processes and sedimentary patterns. In general, two progradational sequences were observed within the Sabiñánigo Delta, revealing different progradational patterns. While the first sequence shows progradation roughly from E to W, the second sequence shows progradation from the north. For the lower sequence the Boltaña Anticline most likely acted as source area, while the upper part predominantly was shed from the Axial Zone in the north, which was affected by a renewed tectonic pulse. This was deduced from progradational patterns and grain size distribution, as the

upper sequence shows coarsest grain sizes in the north-western portion of the cross-section, gradually decreasing towards east. In addition, the components of the conglomeratic bedsets show subangular rounded clasts, which presume a more remote source area, than the Boltaña Anticline.

Thus, the main driving mechanisms causing the deposition of the major progradational sequences are of tectonic origin and connected to the loction of the Jaca Basin within an active foreland basin setting. The development of individual systems tracts and parasequences, however, reflect depositional mechanisms that are triggered by more internal processes. Especially within the upper sequence facies transitions reveal a pattern pointing to facies transitions between different delta lobes. Climatic influences pose a further controlling parameter triggering the evolution of the delta parasequences. But to reveal this, more detailed investigations on organic material need to be done, while detailed provenance analyses might help to decipher the main source areas.

With this study a solid time calibrated framework is provided for further analyses within the Jaca Basin and neighbouring basin. As could be demonstrated spectral gamma ray data provide a powerful tool to construct and extend a high-resolution sequence stratigraphic framework through siliciclastic strata that are difficult to subdivide on the basis of standard facies analyses alone. However, to achieve a definite interpretation, it is essential to have a sound understanding of the lithofacies and the general stratigraphic position of the investigated successions within the basin. Nonetheless, this study suggests that spectral gamma ray logs remain underutilized as a sedimentological and stratigraphic tool both in outcrop and subsurface geology. Further research should concentrate on micropaleontological and palecological studies to reveal a better timeframe and to elucidate climatic impact on the depositional environment of the SSt-Succession.

References

Adams, J. A. S., Weaver, E. (1958). "Thorium to uranium ratios as indicators of sedimentary process: example of concept of geochemical facies." AAPG Bulletin 42: 387-430.

Ahmadi, Z. M., Coe, A.L. (1998). Methods for simulating natural gamma ray and density wireline logs from measurements on outcrop exposures and samples: examples from the Upper Jurassic, England. Core-Log Integration. P. K. Harvey, Lovell, M.A., Geol. Soc. London Spec. Publ. 136: 65-80.

Aitken, J. F., Howell, J.A. (1996). High resolution sequence stratigraphy: innovations, applications and future prospects. High Resolution Sequence Stratigraphy: Innovations and Applications. J. F. Aitken, Howell, J.A. London, Geological Society Special Publication. 104: 1-9.

Allen, P. A., Allen, J.R. (1990). "Basin Analysis Principles and Applications." 451 pp.

Anastasio, D. J. (1992). Structural evolution of the external Sierra, southern Pyrenees, Spain. Structural geology of fold and thrust belts. S. F. Mitra, G.W., Johns Hopkins Univ. Press, Baltimore, MD, United States (USA): 239-251.

Andeweg, B. (2002). Cenozoic tectonic evolution of the Iberian Peninsula, causes and effects of changing stress fields PhD Thesis. Amsterdam, Vrije Universiteit: 178 pp.

Arbués, P., Marzo, M., Muñoz, J.A. (2003). Anatomy and evolution of the Ainsa Slope Complex and its constituent turbidite elements; field trip proposal, GGAC, Grup de Geodinàmica i Anàlisi de Conques, http://www.ub.es/ggac/research/ainsa/ainsa.htm.

Arenas, C. e. a. (2001). "Ebro basin continental sedimentation associated with late compressional Pyrenean tectonics (north-eastern Iberia): controls on basin margin fans and fluvial systems." Basin Research 13: 65-89.

Asquith, G., Krygowski, D. (2004). Gamma Ray. Basic Well Log Analysis. G. Asquith, Krygowski, D., AAPG Methods in Exploration. 16: 31-35.

Barnolas, A., Gil-Peña, I. (2001). "Ejemplos de relleno sedimentario multiepisódico en una cuenca de antepaís fragmentada: La Cuenca Surpirenaica." Boletin Geologico y Minero 112(3): 17-38.

Barnolas, A., Pujalte, V. (2004). La Cordillera Pirenaica. Geología de España. J. A. Vera. Madrid, SGE-IGME: 890 pp.

Baum, G. R., Vail, P.R. (1988). Sequence Stratigraphic concepts applied to Paleogene outcrops, Gulf and Atlantic basins. Sea-Level changes: an integrated approach. C. K. e. a. Wilgus, Soc. Econ. Paleon. and Min. Spec. Publ. 42: 309-327.

Bentham, P. A. e. a. (1992). "Temporal and spatial controls on the alluvial architecture of an axial drainage system: late Eocene Escanilla Formation, southern Pyrenean foreland basin, Spain." Basin Research 4: 335-352.

Bernet, M., Garver, J.I. (2005). Fission-track analysis of detrital zircon. Low-temperature thermochronology: Techniques, interpretations, and applications, Reviews in Mineralogy and Geochemistry. P. W. Reiners, Ehlers, T.A. 58: 205-237.

Bhattacharya, J. P., Walker, R.G. (1992). Deltas. Facies Models: Response to Sea Level Change. R. G. Walker, James, N.P., Geological Association of Canada: 157-177.

Blatt, H. (1982). Sedimentary Petrology. San Francisco, W.H. Freeman and Company: 564 pp.

Blum, J. D. (1995). Isotope Decay Data. Global Earth Physics, A handbook of Physical Constant. T. J. Ahrens, A.G.U.: 271-282.

Boggs, S. J. (2001). Principles of Sedimentology and Stratigraphy, 3rd ed. Englewood Cliffs, New Jersey, Prentice Hall: 726 pp.

Bourrouilh, e. a. (2004). Western Pyrenees fold- and thrust belt: Geodynamics, sedimentation and plate boundary reconstruction from rifting to inversion. Field Trip Guide Book - B16. 32nd International Geological Congress, 2004. L. e. a. Guerrieri. Florence, Italy, APAT, Italian Agency for Environment Protection and Technical Service. B16: 64 pp.

Busby, C. J., Ingersoll, R.V. (eds.) (1995). Tectonics of sedimentary basins. Cambridge, Blackwell Scientific publications: 579 pp.

Camara, P. and J. Klimowitz (1985). "Interpretacion geodinamica de la vertiente Centro-Occidental Surpirenaica (Cuencas de Jaca y Tremp). Geodynamic interpretation of the west-central slope of the southern Pyreenees; Jaca and Tremp basins." Estudios Geologicos (Madrid) 41(5-6): 391-404.

Cant, D. J. (1992). Subsurface facies analysis. Facies Models. R. G. Walker, James, N.P. Sherbrooke, Quebec: 27-47.

Capote, R. e. a. (2002). Alpine tectonics I: the Alpine system north of the Betic Cordillera. The geology of Spain. W. Gibbons, Morena, T. London, Geological Society: 649 pp.

Catuneanu, O. (2002). "Sequence stratigraphy of clastic systems: concepts, merits, and pitfalls." Journal of African Earth Sciences 35: 1-43.

Catuneanu, O. (2006). Principles of sequence stratigraphy. Oxford, Elsevier: 375 pp.

Coe, A. L., et al. (2003). The Sedimentary Record of Sea-Level Change. Cambridge, UK, Cambridge University Press, June 2003: 288 pp.

Coleman, J. M., Prior, D.B. (1981). Deltaic environments of deposition. Sandstone depositional environments. P. A. Scholle, Spaering, D., AAPG. Mem. 31: 139-178.

Coleman, J. M., Prior, D.B. (1982). Deltas, Processes of Deposition and Models of Exploration. Boston, USA, IHRDC, International Human Resources Development Corporation: 124 pp.

Coney, P. J., J. A. Munoz, et al. (1996). "Syntectonic burial and post-tectonic exhumation of the southern Pyrenees foreland fold-thrust belt." Journal of the Geological Society of London 153(1): 9-16.

Davies, S. J., Elliott, T. (1996). Spectral gamma ray characterization on high resolution sequence stratigraphy: examples from Upper Carboniferous fluvio-deltaic systems, County Clare, Ireland. High resolution sequence stratigraphy: Innovations and applications. J. A. Howell, Aitken, J.F., Geological Society Special Publications. 104: 25-35.

Dodson, M. H. (1973). "Closure temperature in cooling geochronological and petrological systems." Contrib. Mineral. Petrol. 40: 259-274.

Donelick, R. A., O'Sullivan, P.B., Ketcham, R.A. (2005). Apatite fission-track analysis. Low-temperature thermochronology: Techniques, interpretations, and applications, Reviews in Mineralogy and Geochemistry. P. W. Reiners, Ehlers, T.A. 58: 49-94.

Doveton, J. H. (1992). "Geological application of wireline logs - a synopsis of developments and trends." Log Analyst 33(3): 286-303.

Doveton, J. H., Merriam, D.F. (2004). "Borehole petrophysical chemostratigraphy of Pennsylvanian black shales in the Kansas subsurface." Chemical Geology 206: 249-258.

Dunai, T. J. (2005). Forward modeling and interpretation of (U-Th)/He ages. Low-temperature thermochronology: Techniques, interpretations, and applications, Reviews in Mineralogy and Geochemistry. P. W. Reiners, Ehlers, T.A. 58: 259-274.

ECORS, P. T. (1988). The ECORS deep reflection seismic survey across the Pyrenees. Nature. 331: 508-510.

Ehlers, T. A., Farly, K.A. (2003). "Apatite (U-Th)/He thermochronometry: methods and applications to problems in tectonic and surface processes." Earth and Planetary Science Letters 206: 1-14.

Einsele, G. (2000). Sedimentary Basins. Evolution, Facies, and Sediment Budget , 2nd ed. Heidelberg, Springer-Verlag: 792 pp.

Ellis, D. V. (1987). Well logging for earth scientists. Amsterdam, Elsevier: 532 pp.

Emery, D., Myers, K.J. (1996). Sequence Stratigraphy. Sequence Stratigraphy. D. Emery, Myers, K.J. Cambridge, Massachusetts, USA, Blackwell Science, Inc.: 297 pp.

Exploranium, R. D. S. (2000). GR-320 Portable Gamma Ray Spectrometer users manual: 70 pp.

Farley, K. A., Wolf, R.A., Silver, L.T. (1996). "The effects of long alpha-stopping distances on (U-Th)/He ages." Geochimica at Cosmochimica Acta 60(21): 4223-4229.

Farley, K. A. (2000). "Helium diffusion from apatite: General behavior as illustrated by Durango fluorapatite." Journal of Geophysical Research 105(B2): 2903-2914.

Farley, K. A. (2002). "(U–Th)/He Dating: Techniques, Calibrations and Applications. in: Noble Gases in Geochemistry and Cosmochemistry. D. Porcelli, C. J. Ballentine and R. Wieler, ." Reviews in Mineralogy and Geochemistry. 47: 819-844.

Farley, K. A., Kohn, B.P., Pillans, B. (2002). "The effects of secular disequilibrium on (U^Th)/He systematics and dating of Quaternary volcanic zircon and apatite." Earth and Planetary letters 201: 117-125.

Fernández, O. e. a. (2004). "Three-dimensional reconstruction of geological surfaces: An example of growth strata and turbidite systems from the Aínsa basin (Pyrenees, Spain)." AAPG Bulletin 88(8): 1049-1068.

Fitzgerald, P. G., et al. (1999). "Asymmetric exhumation across the Pyrenean orogen: implications for the tectonic evolution of a collisional orogen." Earth and Planetary Science Letters 173: 157-170.

Friend, P. F. e. a. (1996). Evolution of the central part of the northern Ebro basin margin, as indicated by ist Tertiary fluvial sedimentary infill. Tertiary basins of Spain - the stratigrafic record of crustal kinematics. P. F. Friend, Cambridge University Press.

Galloway, W. E. (1975). Process framework for describing the morphologic and stratigraphic evolution of deltaic depositional systems. Deltas. B. M.L. Houston, Geological Society: 87-98.

Galloway, W. E., Hobday, D.K. (1983). Terrigenous clastic depositional systems. New York, Springer-Verlag: 423 pp.

Galloway, W. E. (1989). "Genetic stratigraphic sequences in basin analysis I: architecture and genesis of flooding-surface bounded depositional units." AAPG Bulletin 73(2): 125-142.

Garwin, L. (1985). Fission track dating and tectonics in the eastern Pyrenees, Ph.D. thesis. Camebridge, UK, Cambridge University: 320 pp.

Hampson, G. J. e. a. (2005). "Use of spectral gamma-ray data to refine subsurface fluvial stratigraphy: late Cretaceous strata in the Book Cliffs, Utah, USA." Journal of the Geological Society, London 162: 603-621.

Haq, B. U., Hardenbol, J., Vail, P.R. (1988). Mesozoic and Cenozoic chronostratigraphy and cycles of sea-level change. Sea-level changes: an integrated approach. C. K. e. a. Wilgus, SEPM Special Publication. 42: 71-108.

Harrison, T. M., Zeitler, P. K. (2005). Fundamentals of noble gas thermochronometry. Low-temperature thermochronology: Techniques, interpretations, and applications, Reviews in Mineralogy and Geochemistry. P. W. Reiners, Ehlers, T.A. 58: 123-149.

Hodges, K. V. (2003). Geochronology and thermochronology in orogenic systems. Treatise on Geochemistry. K. K. Turekian, Holland, H.D. Oxford, UK, Elsevier: 263-92.

Hogan, P. J., Burbank, D.W. (1996). Evolution of the Jaca piggyback basin and emergence of the External Sierra, southern Pyrenees. Tertiary basins of Spain - the stratigrafic record of crustal kinematics. P. F. Friend: 153-160.

Holl, J. E., Anastasio, D.J. (1995). "Kinematics around a large-scale oblique ramp, southern Pyrenees, Spain." Tectonics 14(5): 1368-1379.

Hourigan, J. K., Reiners P.W., Brandon M.T. (2005). "U-Th zonation dependent alpha-ejection correction in (U-Th)/He chronometry." Geochimica et Cosmochimica Acta 69: 3349-3365.

House, M. A., Farley, K.A., Stockli, D. (2000). "Helium chronometry of apatite and titanite using Nd-YAG laser heating." Earth and Planetary Science Letters 183: 365-368.

Howell, J. A., Aitken, J.F., (1996). High resolution sequence stratigraphy: Innovations, applications and future prospects. High resolution sequence stratigraphy: Innovations and applications. J. A. Howell, Aitken, J.F.,, Geological Society Special Publications. 104: 1-9.

Hurst, A., Lovell, M.A., Morton, A.C. (1990). Natural gamma-ray spectrometry in hydrocarbon-bearing sandstones from the Norwegian Continental Shelf. Geological Applications of Wireline Logs. A. Hurst, Lovell, M.A., Morton, A.C., Geol. Soc. London Spec. Publ. 48: 211-222.

IAEA, I. A. E. A. (1976). Radiometric Reporting Methods and Calibration in Uranium Exploration. Technical Reports Series. IAEA. Vienna, IAEA. 174.

Integrated Ocean Drilling Program, I.-U. (2003-2006). Application of gamma ray logs. http://iodp.ldeo.columbia.edu/TOOLS_LABS/LEGACY/Pat/text.html.

Jordan, D. W. e. a. (1993). "Gamma-ray logging of outcrops by a truck-mounetd sonde." Bull. Am. Assoc. Pet. Geol. 77: 118-123.

Juez-Larre , J. (2003). Late Paleozoic tectonothermal evolution of the northeastern margin of Iberia, assessed by fission-track and (U-Th)/He analysis. A case history from the Catalan Coastal Ranges. PhD thesis. Amsterdam, Vrije Universiteit: 200 pp.

Kalchgruber, R. (2002). Alpha-Al2O3:C als Dosimeter zur Bestimmung der Dosisleistung bei der Lumineszenzdatierung. Naturwissenschaftlich - Mathermatische Gesamtfakultät. Heidelberg, Ruprecht Karls Universität: 146 pp.

Kendall, C. (2003). Use of well logs for sequence stratigraphic interpretation of the subsurface. USC Sequence Stratigraphy Web. http://strata.geol.sc.edu/index.html, University of South Carolina.

Kendall, C. (2005). Use of well logs for sequence stratigraphic interpretation of the subsurface. USC Sequence Stratigraphy Web. http://strata.geol.sc.edu/index.html, University of South Carolina.

Klein, C., Hurlbut, C.S. (1993). Manual of Mineralogy. a. J. D. D. Ed. New York, USA, John Wiley & Sons, INC: 681pp.

Kohn, B. P. e. a. (2005). Visualizing thermotectonic and denudation histories using apatite fission track thermochronology. Low-temperature thermochronology: Techniques, interpretations, and applications, Reviews in Mineralogy and Geochemistry. P. W. Reiners, Ehlers, T.A. 58: 527-565.

Labaume, P., M. Séguret, et al. (1985). "Evolution of a turbiditic foreland basin and analogy with an accretionary prism; example of the Eocene South-Pyrenean Basin." Tectonics 4(7): 661-685.

Lafont, F. (1994). Influences relatives de la subsidence et de l'eustatisme sur la localisation et la geometrie des reservoirs d'un systeme deltaique; exemple de l'Eocene du bassin de Jaca, Pyrenees espagnoles. Relative influence of subsidence and eustacy on the localization and geometry of deltaic reservoirs; example of the Eocene of the Jaca Basin, Spanish Pyrenees. Memoires de Geosciences Rennes. 54: 264 pp.

Leeder, M. (1999). Sedimentology and Sedimentary Basins: from turbulence to tectonics: 592 pp.

Lippolt, H. J. e. a. (1994). "(Uranium + thorium)/helium dating of apatite: experience with samples from different geochemical environments." Chemical Geology (Isotope Geoscience Section) 112: 179-191.

López-Blanco, M., Marzo, M., Muñoz, J.A. (2003). "Low-amplitude, synsedimentary folding of a deltaic complex: Roda Sandstone (lower Eocene), South-Pyrenean Foreland Basin." Basin Research 15: 73-95.

Løvborg, L., Wollenberg, H., Sorensen, P., Hansen, J. (1971). "Field determination of uranium and thorium by gamma ray spectrometry, exemplified by measurements in the llimaussaq alkaline intrusion, South Greenland." Economic Geology 66: 368-384.

Luthi, S. M. (2001). Geological well logs: their use in reservoir modeling. Berlin, Springer-Verlag: 373 pp.

Marzo, M. e. a. (1998). "Sedimentation and tectonics; case studies from Paleogene, continental to deep water sequences of the South Pyrenean foreland basin (NE Spain)."

Medjadj, F. (1985). Une zone de confluence deltaique en domaine compressif: Le delta paleogene de Jaca dans le secteur de Sabiñánigo. Geologie de matieres premieres minerales et energetique. Pau, Université de Pau: 421 pp.

Meesters A.G.C.A., D. T. J. (2002a). "Solving the production-diffusion equation for finite diffusion domains of various shapes Part I. Implications for low-temperature (U-Th)/He thermochronology." Chemical Geology 186: 333-344.

Meesters A.G.C.A., D. T. J. (2002b). "Solving the production-diffusion equation for finite diffusion domains of various shapes Part II. Application to cases with -ejection and nonhomogeneous distribution of the source." Chemical Geology 186: 347-363.

Miall, A. D. (1997). The Geology of Stratigraphic Sequences. Berlin, Springer-Verlag,: 433 pp.

Middleton, G. V. (1978). Facies. Encyclopedia of sedimentology. R. W. Fairbridge, Bourgeois, J. Stroudsburg, Pennsylvania, Dowden, Hutchinson and Ross. 323-325.

Mitchell, S. G., Reiners, P.W. (2003). "Influence of wildfires on apatite and zircon (U-Th)/He ages." Geology 31(12): 1025-1028.

Mitchum, J., R.M. (1977). Seismic Stratigraphy and Global Changes of Sea Level: Part 1. Glossary of Terms used in Seismic Stratigraphy. Seismic startigraphy-applications to hydrocarbon exploration. C. E. Payton, AAPG Memoir. 26: 205-212.

Mitchum, R. M., Vail, P.R., Thompson, S. (1977). Seismic stratigraphy and global changes of sea level, Part 2: the depositional sequence as a basic unit for stratigraphic analysis. Seismic stratigraphy applications to hydrocarbon exploration. C. E. Payton, AAPG Memoir. 26: 53-62.

Morris, R. G., Sinclair, H.D., Yelland, A.J. (1998). "Exhumation of the Pyrenean orogene: implications for sediment discharge." Basin Research 10(1): 69-85.

Muñoz, J. A. (1992). Evolution of a continental collision belt; ECORS-Pyrenees crustal balanced cross-section. Thrust Tectonics. K. R. McClay: 235-246.

Muñoz, J. A. (2003). The Pyrenees - structure and modelling of an orogene, GGAC, Grup de Geodinàmica i Anàlisi de Conques.

Mutti, E., Séguret, M., Sgavetti, M. (1988). Sedimentation and deformation in the Tertiary sequences of the Southern Pyrenees , Field Guidebook. American Association of Petroleum Geologists Mediterranean Basins Conference. 7: 169 pp.

Myers, K. J., Wignall, P.B. (1987). Understanding Jurassic organic-rich mudrocks - new concepts using gamma-ray spectrometry and palaeoecology: Examples from the Kimmeridge Clay of Dorset and the Jet Rock of Yorkshire. Marine Clastic Sedimentology. J. K. Leggett, Zuffa, G.G.: 172-189.

Nichols, G. (1999). Sedimentology and Stratigraphy. London, Blackwell Science: 368 pp.

Ori, G. G., Friend, P.F. (1984). "Sedimentary basins formed and carried piggyback on active thrust sheets." Geology 12: 475-478.

Parkinson, D. N. (1996). Gamma -ray spectrometry as a tool for stratigraphical interpretation: examples from the western European Lower Jurassic. Sequence Stratigraphy in British Geology. S. P. Hesselbro, Parkinson, D.N., Geol. Soc. London Spec. Publ. 103: 231-255.

Posamentier, H. W., Vail, P.R. (1988). Eustatic controls on clastic deposition II sequence and systems tract models. Sea-Level Changes: An Integrated Approach. C. K. e. a. Wilgus, SEPM Special Publications. 42: 125-154.

Posamentier, H. W., Jervey, M.T., Vail, P.R. (1988). Sea-level changes: an integrated approach: Society of Economic Paleontologists and Mineralogists Special Publication. C. K. e. a. Wilgus. 42: 109-124.

Postma, G. and J. H. ten Veen (1999). "Astronomically and tectonically linked variations in gamma-ray intensity in late Miocene hemipelagic successions of the Eastern Mediterranean Basin." Sedimentary Geology 128(1-2): 1-12.

Puigdefàbregas, C. T. (1975). "La sedimentación molásica en la cuenca de Jaca." Monografias del Instituto Pirenaicos 104: 188 pp.

Puigdefàbregas, C. T., J. A. Munoz, et al. (1986). Thrust belt development in the eastern Pyrenees and related depositional sequences in the southern foreland basin. Thrust belt development in the eastern Pyrenees and related depositional sequences in the southern foreland basin, Special Publication of the International Association of Sedimentologists. P. A. Allen, Homewood, P. 8: 229-246.

Quirein, J. A., et al. (1982). "Combined natural gamma ray spectral/litho-density measurements applied to complex lithologies." SPE 11143: 1-14.

Ravenhurst, C. E., Donelick, R.A. (1992). Fission track thermochronology. Short course handbook on low temperature thermochronology. M. Zentilli, Reynolds, P.H. Wolfsville, Novia scotia, Mineralogical association of Canada. 20: 21-42.

Readig, H. G., Levell, B.K. (1996). Clastic Coasts. Sedimentary Environments: Processes, Facies and Stratigraphy. H. G. Reading. Oxford, Blackwell Science: 154-231.

Reineck, H. E., Singh, I.B. (1980). Depositional sedimentary environments with references to terrigenous clastics, 2nd ed. Berlin, Springer Verlag: 549 pp.

Reiners, P. W., Farley, K.A. (2001). "Influence of crystal size on apatite (U-Th)/He thermochronology: An example from the Bighorn Mountains, Wyoming." Earth and Planetary Science Letters 188: 413-420.

Reiners, P. W. (2002). "(U-Th)/He chronometry experiences a renaissance." Eos 83: 21-27.

Reiners, P. W., Ehlers, T.A, (2005). Low-temperature thermochronology: Techniques, interpretations, and applications. Low-temperature thermochronology: Techniques, interpretations, and applications, Reviews in Mineralogy and Geochemistry. P. W. Reiners, Ehlers, T.A. 58: v-ix.

Reiners, P. W., Brandon, M.T. (2006). "Using thermochronology to understand orogenic erosion." Annu. Rev. Earth Planet. Sci. 34: 419-466.

Reiners, P. W., Nicolescu, S. (2006). Measurement of parent nuclides for (U-Th)/He chronometry by solution sector ICP-MS, ARHDL Report 1., http://www.geo.arizona.edu/%7Ereiners/arhdl/arhdl.htm.

Remacha, E., P. Arbues, et al. (1987). "Precisiones sobre los limites de la secuencia deposicional de Jaca; evolucion de los facies desde la base de la secuencia hasta el techo de la Arenisca de Sabinanigo. Data on the limits of depositional sequences of Jaca; evolution of facies from the the base of the sequence to the top of the Sabinanigo Sandstone." Boletin Geologico y Minero 98(2): 40-48.

Rider, M. H. (1990). Gamma-ray log shape used as a facies indicator: critical analysis of an oversimplified methodology. Geological Applications of Wireline Logs. A. Hurst, Lovell, M.A., Morton, A.C., Geol. Soc. London Spec. Publ. 48: 27-37.

Rider, M. H. (2004). The Geological Interpretation of Well Logs, 2nd ed. Caithness, Whittles Publishing: 280 pp.

Rosell, J., Puigdefàbregas, C. (1975). Evolution du Bassin paléogène sud-Pyrénéen; Sedimentary evolution of the paleogene South Pyrenean Basin. IX me Congrès international de Sédimentologie, Nice 1975: 1-33.

Schellart, W. P. (2002). "Alpine deformation at the western termination of the Axial Zone, Southern Pyrenees. In: Rosenbaum, G. and Lister, G.S. 2002. Reconstruction of the Alpine Himalayan Orogen." Journal of the Virtual Explorer 8: 35-55.

Schlumberger, L. (1972). Log Interpretation, Vol. 1, Principles. The gamma ray log, Schlumberger, Ltd.: 57-59.

Schlumberger, L. (2006). Schlumberger Oilfield Glossary, http://www.slb.com/.

Schnyder, J., et al. (2006). "Conjunctive use of spectral gamma-ray logs and clay mineralogy in defining late Jurassic - early Cretaceous palaeoclimate change (Dorset, U.K.)." Palaeogeography, Palaeoclimatology, Palaeoecology 229(4): 303-320.

Scotese, C. R. (2003). Paleomap Project, www.scotese.com.

Séguret, M. (1972). Etude Tectonique des Nappes et Séries Décollées de la Partie Centrale du Versant Sud des Pyrénées. Caractère Sysédimentaire, Role de la

Compression de la Gravité. Sér. Géol. Str. Montpellier, France, Univ. Sci. Techn. Languedoc. 2: 155 pp.

Selley, R. C. (1998). Elements of Petroleum Geology. San Diego, Academic Press: 470 pp.

Serra, O., Sulpice, L. (1975). "Sedimentological analysis of shale-sand series from well logs." Transactions of the SPWLA 16th Annual Logging Symposium, paper W.

Shoemaker, S. J. (2000). "The exhumation history of the Pyrenees using detrital fission track thermochronology." http://idol.union.edu/~garverj/FT/shoemaker/Shoemaker.htm.

Sinclair, H. D. (1997). "Tectonostratigraphic model for underfilled peripheral foreland basins: An Alpine perspective." GSA Bulletin 109(3): 324-346.

Slatt, R. M., et al. (1992). Outcrop gamma ray logging to improve understanding of subsurface well log correlations. Geological applications of wireline logs II. A. Hurst, Griffiths, C.M., Worthington, P.F., Geol. Soc. Spec. Publ. 65: 3-19.

Sloss, L. L., Krumbein, W.C., Dapples, E.C. (1949). "Integrated facies analysis." Geol. Soc. America Mem. 39: 91-124.

Soler, S. M., Puigdefàbregas, T.C. (1970). "Líneas generales de la geología del alto aragón occidental." Pirineos 96: 5-20.

Stockli, D. F. (2005). Application of low-temperature thermochronometry to extensional tectonic settings. Low-temperature thermochronology: Techniques, interpretations, and applications, Reviews in Mineralogy and Geochemistry. P. W. Reiners, Ehlers, T.A,. 58: 411-448.

Tagami, T., O'Sullivan, P.B. (2005). Fundamentals of fission-track thermochronology. Low-temperature thermochronology: Techniques, interpretations, and applications, Reviews in Mineralogy and Geochemistry. P. W. Reiners, Ehlers, T.A,. 58: 19-47.

Teixell, A. (1996). "The Anso transect of the southern Pyrenees; basement and cover thrust geometries." Journal of the Geological Society of London 153(2): 301-310.

Teixell, A. (1998). "Crustal structure and orogenic material budget in the west central Pyrenees." Tectonics 17(3): 395-406.

Teixell, A. (2000). "Geotectónica de los Pirineos." Investigación y Ciencia 288: 54-65.

Tucker, M. E. (1996). Sedimentary rocks in the field. Chichester, John Wiley & Sons: 153 pp.

Turner, J. P. (1990). "Structural and stratigraphic evolution of the West Jaca thrust-top basin, Spanish Pyrenees." Journal of the Geological Society of London 147(1): 177-184.

Turner, J. P. and P. L. Hancock (1990). "Thrust systems of the Southwest Pyrenees and their control over basin subsidence." Geological Magazine 127(5): 383-392.

USGS, U. S. G. S. (2007). U.S. Geological Survey Geocheimical Reference Materials and Certificates. http://minerals.cr.usgs.gov/geo_chem_stand/index.html.

Vail, P. R. e. a. (1977). Seismic stratigraphy and global changes of sea level. Seismic stratigraphy, Applications to hydrocarbon exploration, AAPG Mem. C. E. Payton, AAPG Mem. 26: 49-212.

Van Wagoner, e. a. (1988). An overview of the fundamentals of sequence stratigraphy and key definitions. Sea-level Changes An Integrated Approach. C. K. e. a. Wilgus, Society of Economic Petrologists and Mineralogists, Special Publication. 43: 38-45.

Van Wagoner, J. C., Mitchum, R.M., Campion, K.M., and Rahmanian, V.D. (1990). Siliciclastic sequence stratigraphy in well logs, cores and outcrops: Concepts for high-resolution correlation of time and facies. AAPG Methods in Exploration Series. 7: 1-55.

Vera, J. A. (2004). Geología de España. J. A. Vera. Madrid, Instituto Geologico y Minero Espana: 890 pp.

Vergés, J., et al. (1995). "Eastern Pyrenees and related foreland basins; pre-, syn- and post-collisional crustal-scale cross-sections." Marine and Petroleum Geology 12(8): 903-915.

Vergés, J., J. A. Munoz, et al. (1992). South Pyrenean fold-and-thrust belt; role of foreland evaporitic levels in thrust geometry. Thrust tectonics. K. R. McClay. London, Chapman and Hall: 255-264.

Vergés, J. e. a. (2002). "The Pyrenean orogen: pre-, syn-, and post-collisional evolution." Journal of the Virtual Explorer 8: 57-76.

Vermeesch, P. e. a. (2006). "Alpha-Emitting mineral inclusions in apatite, their effect on (U-Th)/He ages, and how to reduce it." Geochimica et Cosmochimica Acta 71(7): 1737-1746.

Wagner, G. A., Van den Haute, P. (1992). Fission Track-Dating. Dordrecht, Kluwer Academic Publishers: 285 pp.

Wagner, G. A. (1998). Age determination of young rocks and artifacts. Physical and chemical clocks in Quaternary
Geology and Archaeology. Heidelberg, Springer Verlag Heidelberg.

Walker, R. G. (1992). Facies models and modern stratigraphic concepts. Facies Models: Response to Sea Level Change. R. G. Walker, James, N.P., Geological Association of Canada: 1-14.

Warnock, A. C. e. a. (1997). "An evaluation of low-temperature apatite U-Th/He thermochronometry." Geochimica at Cosmochimica Acta 61(24): 5371-5377.

Wheeler, H. E. (1958). "Time Stratigraphy." AAPG Bulletin 42(5): 1047-1063.

Wheeler, H. E. (1959). "Stratigraphic units in space and time." Am. Jour. Sci. 257: 692-706.

Wolf, R. A., Farley K.A., Silver L.T. (1996). "Helium diffusion and low-temperature thermochronometry of apatite." Geochimica et Cosmochimica Acta 60(21): 4231-4240.

Wolf, R. A., Farley, K.A., Kass, D.M. (1998). "Modeling of the temperature sensitivity of the apatite (U–Th)He thermochronometer." Chemical Geology 148: 105-114.

Yelland, A. J. (1990). Fission track thermotectonics in the Pyrenean Orogen. Proceedings of the 6th international fission track dating workshop. S. A. Durrani, Benton, E.V. 17: 293-299.

Zeitler, P. K. e. a. (1987). "U-Th-He dating of apatite: A potential thermochronometer." Geochimica et Cosmochimica Acta 51: 2865-2868.

Ziegler, P. A., Bertotti, G., Cloetingh, S. (2002). Dynamic processes controlling foreland development - the role of mechanical (de)coupling of orogenic wedges and forelands. Continental collision and the tectono-sedimentary evolution of forelands. G. Bertotti, Schulmann, K., Cloetingh, S., EGU. Stephan Mueller Spec. Publ. Series: 17-56.

Hiermit erkläre ich, dass ich die vorliegende Dissertationsarbeit selbst verfasst und mich dabei keiner anderen als der von mir ausdrücklich bezeichneten Quellen und Hilfen bedient habe.

Ich erkläre, dass ich an keiner anderen Stelle ein Prüfungsverfahren beantragt bzw. die Dissertation in dieser oder anderer Form bereits anderweitig als Prüfungsarbeit verwendet oder einer anderen Fakultät als Dissertation vorgelegt habe.

Heidelberg, den 08. November 2007

Friederike U. Bauer